On the Influence of Trimethylamine-N-oxide (TMAO) and Pressure on Hydrophobic Interactions

submitted in fulfillment of the requirements for the degree of doctor rerum naturalium
(Dr. rer. nat.)
Dissertation by Angelina Folberth, M.Sc.

Examiner: Prof. Dr. Nico van der Vegt
Co-Examiner: Prof. Dr. Florian Müller-Plathe
Darmstadt 2022

TECHNISCHE UNIVERSITÄT DARMSTADT

Chemistry Department
Eduard-Zintl Institut für Anorganische und Physikalische Chemie
Computational Physical Chemistry

Angelina Folberth, M.Sc.
from Limburg a.d. Lahn

On the Influence of Trimethylamine-N-oxide (TMAO) and Pressure on Hydrophobic Interactions
Über den Einfluss von Trimethylamin-N-oxid (TMAO) und Druck auf hydrophobe Interaktionen

Darmstadt, Technische Universität Darmstadt
Date of submission: 09.08.2022
Date of oral exam: 26.09.2022

1. Gutachten: Prof. Nico van der Vegt
2. Gutachten: Prof. Florian Müller-Plathe

Veröffentlicht im Jahr 2022 auf TUprints
E-Publishing-Service der TU Darmstadt
http://tuprints.ulb.tu-darmstadt.de
tuprints@ulb.tu-darmstadt.de

Erklärungen

§8 Abs. 1 lit. c der Promotionsordnung der TU Darmstadt
Ich versichere hiermit, dass die elektronische Version meiner Dissertation mit der schriftlichen Version übereinstimmt und für die Durchführung des Promotionsverfahrens vorliegt.

§8 Abs. 1 lit. d der Promotionsordnung der TU Darmstadt
Ich versichere hiermit, dass zu einem vorherigen Zeitpunkt noch keine Promotion versucht wurde und zu keinem früheren Zeitpunkt an einer in- oder ausländischen Hochschule eingereicht wurde. In diesem Fall sind nähere Angaben über Zeitpunkt, Hochschule, Dissertationsthema und Ergebnis dieses Versuchs mitzuteilen.

§9 Abs. 1 der Promotionsordnung der TU Darmstadt
Ich versichere hiermit, dass die vorliegende Dissertation selbstständig und nur unter Verwendung der angegebenen Quellen verfasst wurde.

§9 Abs. 2 der Promotionsordnung der TU Darmstadt
Die Arbeit hat bisher noch nicht zu Prüfungszwecken gedient.

Darmstadt, der

Angelina Folberth

Acknowledgement

When I started the preparation for my Abitur, I would have never thought that I would one day make it this far. Nevertheless, I could have never done it without the support of many people.

I hereby would like to thank Prof. Dr. Nico van der Vegt for his guidance throughout the thesis. Nico always provided the freedom to work on my own scientific projects and thereby grow as a scientist, but he was always open for many fruitful discussions, giving insight that I might have overlooked otherwise and providing suggestions for advancing the project.
I am also grateful to Prof. Dr. Florian Müller-Plathe for examining the thesis and giving feedback in group seminars.

I thank Dr. Jan Heyda and Jakub Polák for a successful collaboration and allowing me insights into the experimental part of solvation chemistry by welcoming me in their lab.

I would also like to express my appreciation to my colleagues, who have been in the group over the years. Marvin, Viktor and Moritz always gave support when there where problems with programming or the computer software. Also, many thanks to Francisco and Divya, who have introduced me to Molecular Dynamics Simulations, making it so exciting that I wanted to stay and solve scientific questions with it. I am happy that I was able to collaborate with Swami and I am thankful for his continuous support, advice and his patience in reading my article drafts and thesis. I am sure that he will be a great supervisor for his own students.

Furthermore I would also like to thank my close friends, which I have made in kindergarden, school, university and the group. Vishal, Swami, Alissa, Paula, Paul and Thomas always gave me great support and where there when I needed to vent and give me renewed motivation.

Many thanks to my family. My cousin Raphael, who has been there when I had any questions regarding programming and my uncle Ingo, who has always helped me out. I am deeply grateful for their support and seeing the pride in my grandparents eyes always motivated me to go even further. Lastly, I would like to thank my mother. Not only is she my greatest role model and I hope that one day I can become as kind, fierce and loving as her, but she also supported me through the hardest time. I know that she would do everything for me and hope she knows that I would do the same for her. This thesis is dedicated to her.

Abstract

Osmolytes are small organic molecules that influence the protein folding equilibrium and biomolecular condensates formed by liquid-liquid phase separation (LLPS). Thereby they can protect the cell from extracellular stress in the form of other molecules or external variables like pressure, temperature and pH, allowing life to flourish at extreme conditions. Trimethylamine-N-oxide (TMAO) is one such osmolyte, which has been studied due to its presence in deep sea organisms living in high pressure environments. Experimentally, it has been found that TMAO can counteract pressure denaturation and the disappearance of LLPS, both crucial in the functioning of the cell. However, there is still no consensus on the molecular mechanism governing the stabilising effect of TMAO and it is still highly controversial in the sense that it is not clear which interactions are responsible for TMAOs stabilising ability. Protein interactions can be manifold, ranging from electrostatic interactions (salt bridge formation between charged side chains), polar interactions, like hydrogen bonds, and hydrophobic interactions. Furthermore, the reason why TMAO is called a “piezolyte”, an osmolyte specialized in its pressure counteracting ability, and whether it is even distinct from other osmolytes at all is unsure.

This work focuses on hydrophobic interactions, which are one of the main driving forces for protein folding and biocondensate formation. It proposes molecular mechanisms on the cumulative effect of TMAO and temperature, pressure or molecule size on hydrophobic interactions and hydrophobic hydration. For these studies a combination of structural analysis of the solvent and cosolute distribution, thermodynamic data and statistical mechanics analysis was used. Lastly, the folding equilibrium of a miniprotein has been analyzed to transfer the knowledge gained with hydrophobic molecules to a more complex system.

A major problem of computational studies on TMAO effects is the existence of several force fields, which often can not reproduce experimental properties. The results in this work showed that the force field used is capable to capture the general experimentally observed trend of preferential TMAO binding to a small peptide. It is shown that preferential TMAO binding depends on temperature, solute size and charge state (protonation state) of the solute and its functional groups. Generally, the presence of charged groups contribute to TMAO depletion. TMAO is depleted (lowers the solubility of the solute) from small non-polar solutes at low temperatures and switches to preferential binding (increases the solubility of the solute) upon increasing the temperature. Furthermore, TMAO is depleted from small repulsive solutes at all temperatures, but

preferentially binds to large repulsive solutes at ambient temperatures. For small solutes TMAO increases hydrophobic interactions independent of preferential TMAO binding, proving that TMAO can increase solute aggregation not only through a depletion mechanism, as is usually proposed in the literature for the stabilising TMAO effect, but also through preferential binding. Intriguingly, preferential TMAO binding to large repulsive solutes drives solute association through a surfactant-like mechanism, dominating at low TMAO concentrations. This leads to a non-monotonic trend in its effect on the association of non-polar solutes, as the contribution of attractive interactions drive solute dissociation, driving the equilibrium to the dissociated state at high TMAO concentrations. Furthermore, this non-monotonic trend prevails at high pressure, but the stabilising TMAO effect of the associated state is enhanced. This effect is due to the enhancement of the TMAO dipole moment upon pressure increase. Force fields which do not take this into account do not exhibit this effect. Thus, in the case of hydrophobic interactions TMAOs piezolytic abilities are caused by its increased dipole moment. Lastly, a protein having hydrophobic, charged and polar interactions was simulated. It has been shown that hydrophobic and electrostatic interactions are strengthened by the presence of TMAO. Additionally, the protein looses protein-solvent hydrogen bonds in the TMAO mixture compared to the pure water case. This destabilizes both the folded and unfolded protein state, but more so the unfolded state as it has a higher solvent accessible surface area. As a result, TMAO drives protein folding due to the loss of favorable protein-solvent hydrogen bonds.

This thesis extends the current knowledge of TMAO effects on hydrophobic interactions. Furthermore, it takes collective effects into account, enhancing the knowledge across the temperature-pressure plane and adding knowledge about other functional group effects. Several stabilising effects of TMAO on hydrophobic interactions and protein folding have been discovered, serving to understand the manifold interactions of TMAO with more complex molecules. These findings can be used for a general understanding of cosolute effects on the polymer collapse equilibrium, protein folding equilibrium and the formation of biocondesates via liquid-liquid phase separation (LLPS).

Zusammenfassung

Osmolyte sind kleine organische Moleküle, welche das Faltungsgleichgewicht von Proteinen und die Bildung biomolekularer Kondensate durch liquid-liquid phase separation (LLPS) beeinflussen. Dadurch können sie Zellen von extrazellulärem Stress durch andere Moleküle oder externen Variablen wie Druck, Temperatur und pH schützen und erlauben das Gedeihen von Leben unter extremen Konditionen. Trimethylamine-N-oxide (TMAO) ist ein solcher Osmolyt, der wegen seiner Präsenz in Tiefseeorganismen, welche unter Hochdruckkonditionen leben, untersucht wird. Experimentell wurde gefunden, dass TMAO der Proteindenaturierung durch Druck und der Auflösung von LLPS, beide zentral für die Funktionen der Zelle, entgegenwirken kann. Trotzdem gibt es keinen Konsensus über den molekularen Mechanismus des stabilisierenden Effekts von TMAO und ein möglicher Mechanismus wird weiterhin stark diskutiert in dem Sinne, dass nicht klar ist, welche Interaktionen für TMAOs stabilisierende Fähigkeit verantwortlich sind. Es gibt viele Arten der Proteininteraktionen, von elektrostatischen Interaktionen (Salzbrückenformation zwischen geladenen Seitenketten), polare Interaktionen wie Wasserstoffbrücken, zu hydrophoben Interaktionen. Des Weiteren ist der Grund, weshalb TMAO ein “Piezolyt”, ein Osmolyt spezialisiert in der Fähigkeit Druck entgegenzuwirken, genannt wird und ob es sich von anderen Osmolyten unterscheidet, nicht klar.

Diese Arbeit fokussiert sich auf hydrophobe Interaktionen, welche eine der Haupttriebkräfte für Proteinfaltung und die Formation von Biokondensaten sind. Es werden molekulare Mechnismen über den kumulativen Effekt von TMAO und Temperatur, Druck oder Molekülgröße auf hydrophobe Interaktionen und hydrophobe Hydratation vorgeschlagen. Für diese Studien wurde eine Kombination von strukturellen Analysen der Lösungsmittel und Co-lösungsmittelverteilung, thermodynamische Analysen und statistische Mechanik Analysen genutzt. Zuletzt wurde das Faltungsgleichgewicht eines Mini-proteins analysiert, um das Wissen, welches mit hydrophoben Molekülen erhalten wurde, auf komplexere Systeme zu transferieren.

Ein Hauptproblem computergestützter Studien des TMAO Effekts ist die Existenz mehrerer Kraftfelder, welche oft nicht die experimentellen Eigenschaften reproduzieren können. Die Resultate in dieser Arbeit haben gezeigt, dass das hier genutzte Kraftfeld fähig ist die generellen Trends für das präferenzielle Binden, welche in Experimenten gesehen wurden, nachzubilden. Es wurde gezeigt, dass das präferenzielle Binden von TMAO von der Temperatur, Molekülgröße und Ladungszustand (Protonierungszustand) des gelösten Stoffes und seiner funktionellen Gruppen abhängt. Generell tragen die Präsenz von geladenen Gruppen zur Abstoßung von TMAO bei. TMAO wird abgestoßen (reduziert die Löslichkeit) von kleinen nicht-polaren gelösten Stoffen bei niedriger Temperatur und wechselt zum präferenziellen Binden (erhöht Löslichkeit) bei Erhöhung der Temperatur. Des Weiteren ist TMAO abgestoßen von kleinen repulsiven Molekülen bei allen Temperaturen, bindet jedoch an große repulsive Moleküle bei Raumtemperatur. TMAO erhöht hydrophobe Interaktionen von kleinen Molekülen unabhängig des präferenziellen Bindens. Dies beweist, dass TMAO die Aggre-

gation von gelösten Stoffen nicht nur durch dessen Abstoßung von den Stoffen, wie normalerweise vorgeschlagen, sondern auch durch präferenzielles Binden fördern kann. Faszinierenderweise führt präferenzielles Binden von TMAO an große repulsive gelöste Stoffe zur Assoziation dieser durch einen surfactant-like mechanism, welcher bei niedrigen TMAO Konzentration den Effekt auf die Assoziation nicht-polarer Moleküle dominiert. Dies führt zu einem nicht-monotonen Trend des TMAO Effekts auf die Assoziation nicht-polarer Stoffe, da attraktive Interaktionen die Dissoziation unterstützen, was das Gleichgewicht zum dissoziierten Zustand bei hohen TMAO Konzentrationen verschiebt. Des Weiteren ist dieser nicht-monotone Trend auch bei hohem Druck vorhanden, aber der stabilisierende TMAO Effekt ist erhöht. Dies geschieht durch den erhöhten TMAO Dipol bei hohem Druck. Kraftfelder, die dies nicht einfangen, zeigen den beschriebenen Effekt auf die Assoziation gelöster Stoffe nicht. Daher führt bei hydrophoben Interaktionen der erhöhte TMAO Dipol zu dem Piezolyt-Effekt. Zuletzt wurde ein Protein mit hydrophoben, elektrostatischen und polaren Interaktionen simuliert. Es wurde gezeigt, dass hydrophobe und elektrostatische Interaktionen durch die Präsenz von TMAO erhöht werden. Außerdem verliert das Protein Protein-Lösungsmittel Wasserstoffbrücken in der TMAO Lösung im Vergleich zur Lösung mit purem Wasser. Dies destabilisiert sowohl den gefalteten als auch den entfalteten Proteinzustand, jedoch mehr den entfalteten Zustand durch seine größere Fläche, welche dem Lösungsmittel zugänglich ist. Dadurch führt TMAO zur Proteinfaltung durch den Verlust günstiger Protein-Lösungsmittel Wasserstoffbrücken.

Diese Thesis erweitert das momentane Wissen des TMAO Effekts auf hydrophobe Interaktionen. Außerdem werden kollektive Effekte betrachtet, was zur Erweiterung des Wissens in der gesamten Temperatur-Druck Ebene führt und auch das Wissen zu weiteren funktionellen Gruppen erweitert. Mehrere stabilisierende Effekte von TMAO auf hydrophobe Interaktionen und Proteinfaltung wurden entdeckt, was zu einer tiefen Erfassung der vielfältigen Interaktionen mit komplexeren Molekülen führt. Diese Erkenntnisse nutzen dem generellen Verständnis der Effekte von Co-lösungsmitteln auf das Kollapsgleichgewicht von Polymeren, das Faltungsgleichgewicht von Proteinen und die Bildung von Biokondensaten durch liquid-liquid phase separation (LLPS).

Contents

Nomenclature

Abbrevations

Acronym	Description
∞	reference to quasi-infinite chain
F	Folded protein state
NpT	isothermal-isobaric ensemble
+–	zwitterionic end groups
0–	charged C-terminus
00	neutral termini
A	Associated state
AA	Alchemical Analysis
Ala	alanine
Amber	Assisted Model Building with Energy Refinement
$COO^{—}$	deprotonated carboxyl group
COOH	carboxyl group
D	Dissociated state
Elec	Electrostatic interactions
ELP	elastine-like-peptide
FEP	Free Energy Perturbation

FF	force field
G	glycine
Gromacs	GROningen MAchine for Chemical Simulations
H-Atom	hydrogen atom
LINCS	LINear Constraint Solver
LJ	Lennard-Jones
LLPS	Liquid-liquid phase separation
MD	Molecular Dynamics
NaOH	sodium hydroxide
NH_2	primary amide group
NH_3^+	protonated primary amide group
P	proline
pAla	penta-alanine
PME	Particle Mesh Ewald
PMF	Potential of Mean Force
PNiPAM	poly(N-isopropylacrylamide)
pSer	penta-serine
rdf	radial distribution function
S	Solubility
SASA	solvent accessible surface area
Ser	serine
SPC/E	extended simple point charge water model
TBA	Tert-butyl-alcohol
TI	Thermodynamic Integration

TIP4P/2005	four-site water model, optimized in 2005
TMAO	Trimethylamine-N-oxid
TPI	Test Particle Insertion
U	Unfolded protein state
V	valine
vdW	van der Waals interactions
vdW,A	cohesive interactions/attractive van der Waals interactions
vdW,R	Repulsive van der Waals interactions
WCA	Weeks-Chandler-Andersen Potential
WHAM	Weighted Histogram Analysis Method
X-mer	chain consisting of X monomer units

Constants

Symbol	Description	Unit
π	3.1416	
k_B	Boltzmann constant: $1.380 \cdot 10^{-23}$	J K^{-1}
R	gas constant (8.314)	J K^{-1} mol^{-1}

Mathematical Symbols

Symbol	Description	Unit
α	soft-core α parameter	
$\Delta\Delta G$	Relative (with respect to pure water) solvation free energy	kJ mol^{-1}
$\delta\psi_A$	$= \psi_A - \langle\psi_A\rangle$	kJ mol^{-1}
ΔG	Gibbs Free Energy Difference	kJ mol^{-1}

ΔG_{Elec}	Free energy associated with introducing electrostatic interactions	kJ mol^{-1}
ΔG_{R}	Reversible work of cavity formation	kJ mol^{-1}
$\Delta G_{\mathrm{vdW,A}}$	Free energy associated with introducing attractive van der Waals interactions	kJ mol^{-1}
$\Delta G_{\mathrm{vdW,R}}$	Free energy associated with introducing repulsive van der Waals interactions	kJ mol^{-1}
$\Delta N(r)$	mean number of solvent/cosolute molecules at distance r	
ΔN_i	Excess Number of particles around particle i	
Δt	Time step	fs
ΔV	Volume difference/Volume in bin	nm^3
ϵ	depth of Lennard Jones potential	kJ mol^{-1}
ϵ_0	electric constant	mol e^2 kJ^{-1} nm^{-1}
ϵ_r	relative dielectric constant	
Γ	Preferential Binding Coefficient	
γ	surface tension	mN m^{-1}
κ_T	compressibility for pressure coupling	bar^{-1}
Λ	momentum partition function	
λ	Values to indicate simulation windows for FEP/TI	
μ_{cav}	Reversible work of cavity creation	kJ mol^{-1}
ϕ_0	minimum of the proper dihedral potential	deg
Ψ	Angle	
ψ	Lennard Jones potential	kJ mol^{-1}

ψ_A	Attractive part of the Lennard Jones potential	kJ mol^{-1}
ψ_R	Repulsive part of the LJ potential (WCA potential)	kJ mol^{-1}
ρ_3	Molar cosolute concentration	mol L^{-1}
σ	Distance at which Lennard-Jones potential becomes 0	nm
τ_P	time constant for pressure coupling	ps
τ_T	time constant for temperature coupling	ps
θ	angle (between solute atom/N(TMAO) and N(TMAO)/(O(TMAO)))	
θ^0_{ijk}	minimum of the angle potential	rad
ξ	Collective variable for PMF calculation	
ξ_0	minimum of the improper dihedral potential	deg
a	acceleration	nm ps^{-2}
F	Force	kJ mol^{-1} nm^{-1}
F_k	Undetermined factor for umbrella sampling window k	
$g(r)$	radial distribution function as function of r	
$h(\xi)$	counts in histogram in umbrella sampling bin	
K	equilibrium constant	
k	force constant	
k_ϕ	force constant of the proper dihedral potential	kJ mol^{-1}
k_ξ	force constant of the improper dihedral potential	kJ mol^{-1} rad^{-2}
K_p	Local/Bulk Partition Coefficient	

k_s	molar Setschenow constant	L mol^{-1}
k^{θ}_{ijk}	force constant of the harmonic angle potential of atom i, j and k	kJ mol^{-1} rad^{-2}
k^{b}_{ij}	force constant of the harmonic bond potential of atom i and j	kJ mol^{-1} nm^{-2}
N_i	Number of particles in an observation volume around i for an even density distribution	
N'_i	Number of particles in an observation volume around i	
P	Probability distribution	
p	soft-core λ power	
P_{12}	Exchange probability for replica exchange	
q	tetrahedral order parameter	
q_α	partial charge of atom α	e
r	distance from solute	
r^0_{ij}	minimum of the bond potential	nm
R_c	Sphere Radius	nm
R_g	Radius of gyration	nm
s_A	fluctuation entropy	kJ mol^{-1} K^{-1}
S_{13}	cumulative stochiometry of exchange	
t	time	ps
T_0	target temperature	K
U	Potential Energy	kJ mol^{-1}
v	velocity	nm ps^{-1}
$w(\xi)$	Umbrella sampling bias	
$w(r)$	Potential of Mean force between component i and j	kJ mol^{-1}

H_2O	water	
$\Delta\mu$	transfer Gibbs energy	kJ mol^{-1}
μ	(pseudo) chemical potential	kJ mol^{-1}
A	Absorbance	
B	Number of solvent/cosolute molecules in local shell	
BAR	Bennett Acceptanc Ratio	
C	Correction Factor for Setschenow constants	
c	molar concentration	mol L^{-1}
f	electric conversion factor $f = \frac{1}{4\pi\epsilon_0} = 138.94$	kJ nm mol^{-1} e^{-2}
G	Kirkwood-Buff Integral	cm^3 mol^{-1}
H	Hamiltonian	kJ mol^{-1}
K	Kinetic Energy	kJ mol^{-1}
L	box length	nm
M	Molar Mass	g mol^{-1}
m	molal Setschenow constant	kg mol^{-1}
m	molal concentration	mol kg^{-1}
a_{cc}	activity coefficient derivative	
N	N particles	
n	cummulative number of solvent/cosolvent	
n	multiplicity	
P	Pressure/Pressure tensor component	bar
p	momentum	kg m s^{-1}
T	Temperature	K

V	Potential Energy	kJ mol^{-1}

Sub- and Superscripts

Symbol	Description
$\langle\bigcirc\rangle_0$	Average in a system without the solute
$\langle\bigcirc\rangle_1$	Average in a system with a present solute
$\langle\bigcirc\rangle$	average (mostly time)
$D \rightarrow A$	Quantity for the the association process
$\bigcirc^b$	Biased quantity in umbrella sampling
$\bigcirc^g$	in the gas phase
$\bigcirc^l$	in the liquid
$\bigcirc^{\text{local}}$	local quantity in bin
$\bigcirc^{\text{prox}}$	quantity of proximal distance
$\bigcirc^{A\rightarrow B}$	Quantity for the reaction $A \rightarrow B$
$\bigcirc^{tot}$	total
$\bigcirc_0$	in pure water
$\bigcirc_1$	water
$\bigcirc_2$	Protein/Solute
$\bigcirc_3$	cosolute
$\bigcirc_{\alpha/\beta/i/j/k}$	indices for molecule type α or β
$\bigcirc_{\text{TMAO}}$	in water/TMAO mixtures
$\bigcirc_{\text{WP}}$	water-protein
$\bigcirc_{x/y/z}$	direction in the cartesian coordinate system

1 Introduction

1 Motivation

Organisms are not only able to flourish under ambient pressure and temperatures, but also under extreme conditions. These conditions include high temperatures, for example at geysers or volcanic vents, or high pressure, like in the deep sea, which might even be the birth place of life.[1] These organisms have to adapt to these conditions, since functions in the cell get disrupted by deviations from ambient conditions. Specifically, the protein folded state structure is disrupted and liquid-liquid phase separation (LLPS) does not occur. Proteins have a native three-dimensional structure, which is necessary for it to become functional in the cell. This structure has characteristic formations, like α-helices and β-sheets. On the other hand, LLPS is the formation of membraneless organelles through the condensation of proteins and is therefore crucial in cell compartmentalization.[2] To counteract this functional loss it has, for example, been found that deep sea creatures, which live under extreme pressure conditions, have a high amount of trimethylamine-N-oxide (TMAO) in their muscle tissue.[3–5] It has therefore been proposed that TMAO may be a so-called “piezolyte”, a protecting osmolyte that is specialized in its ability to protect the protein folded state from high pressure denaturation. It may also protect the protein folded state from denaturants, like urea, that are used to counteract osmotic pressure effects.[6–8] Recently, it has also been found that TMAO may prevent the pressure-induced dissolution of domains of liquid-liquid phase separation (LLPS).[9–12] Although TMAO has been thoroughly studied in the past decade, there is still no consensus on its protein stabilisation mechanism. Therefore, in this thesis I investigate possible stabilisation mechanisms of TMAO. It is also unclear how TMAO works under the influence of other external conditions, so that we also investigate the cumulative influence of TMAO with pressure or temperature. Additionally, the question why especially this osmolyte is used by deep sea creatures to counteract pressure effects has not been

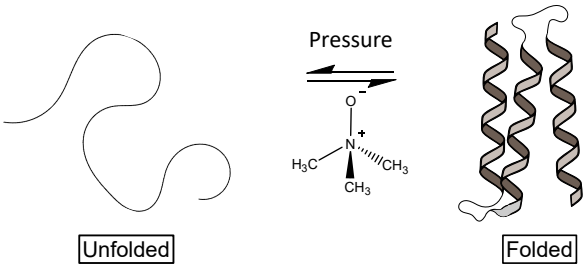

Figure 1.1: Protein folding equilibrium between the coil-like unfolded state and the folded state (here the formation and then aggregation of three α-helical protein parts)

properly addressed in earlier studies, i.e. is there something special that makes TMAO well suited to counteract pressure effects?

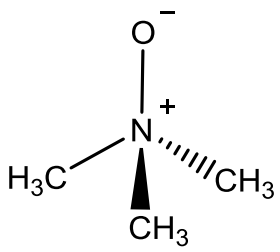

Figure 1.2: Structure of TMAO

TMAO is an amphiphilic, organic molecule. It is zwitterionic and therefore has a high dipole moment of 8.55 D in aqueous solution,[13,14] which increases even further to 8.87 D at 10 kbar.[15] The negatively charged oxygen strongly binds water molecules. Three methyl groups are bound to the positively charged nitrogen. This closeness of the charged groups and hydrophobic methyl groups leads to some unusual behavior of TMAO.

The amphiphilic nature of TMAO also leads to numerous possible interactions with different groups of proteins. Proteins are build from around 20 amino acids, which may have hydrophobic, polar, positively or negatively charged side chains. Therefore, intermolecular and intramolecular interactions of proteins can be manifold. Most commonly discussed are salt bridges, polar interactions, especially intramolecular hydrogen bonds, and hydrophobic interactions.[16–20]

An example is shown in Fig. 1.3 in the miniprotein TrpCage that forms a hydrophobic core (grey residues), a α-helix through hydrogen bonds of the protein backbone and a salt bridge (red and blue residues). In this thesis we will focus on hydrophobic interactions as it is believed to be of utmost importance for protein folding and LLPS.[21–23] In LLPS, where protein-protein interactions are very important, π-π interactions and π-cation interactions also stabilize protein aggregation,[9,23] but not much is known about TMAO interactions with those groups, so that we will focus on the first three mentioned interactions.

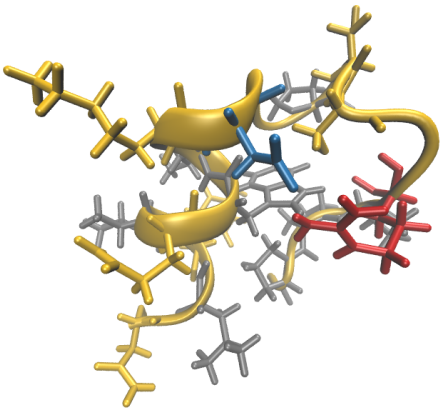

Figure 1.3: Example of a protein: TrpCage. Hydrophobic groups are shown in grey, polar groups and the backbone in yellow, positively charged groups in red and negatively charged groups in blue. TrpCage forms a small hydrophobic core and a salt bridge, visible in the closeness of the differently charged amino acids.

It is vital to realize that TMAO may interact distinctively with these different kind of groups as this gives indications about its effect on solubility of an additional solute, like a protein, and therefore solute association. However, due to its amphiphilic nature, it is not straightforward to predict the manner in which TMAO may interact with these groups.

The commonly assumed mechanism of cosolute interactions (cosolute preferential binding, see Fig. 1.4) and their effects is based on osmometry and dialysis experiments and says: cosolutes, which preferentially bind to a solute (accumulate at the solute surface) drive solute dissociation.[24–26] This is due to the maximization of the solute surface that can interact with the accumulated cosolute. On the other hand, cosolutes, which are excluded from the solute (stay away from the solute interface, which thereby is preferentially hydrated), drive solute association. This

is due to excluded volume effects, since the excluded cosolute can not occupy the volume around the solute reducing the cosolutes translational entropy. Therefore, it tries to minimize this volume, which it can do by association. Experimentally it has been shown that TMAO is depleted from the protein surface[27–30] and this has been commonly used to reason the TMAO effect on protein folding and LLPS.[9,11,31–33]

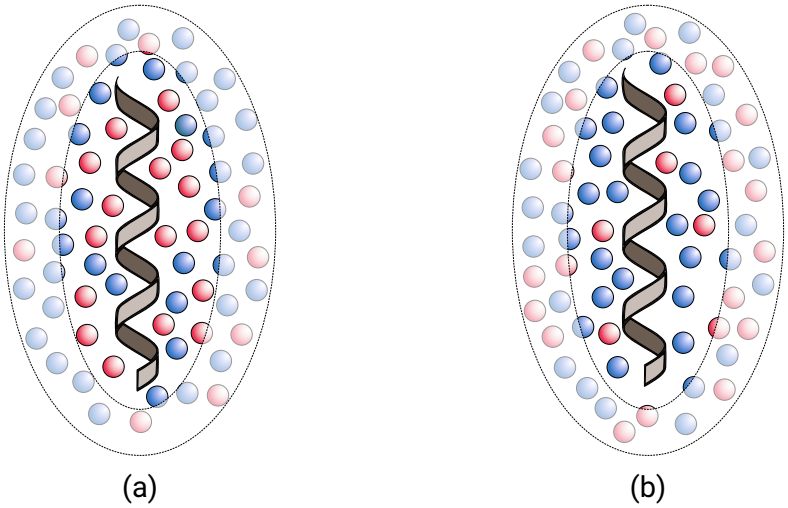

Figure 1.4: The concept of preferential binding of a cosolute shown on the example of a α-helix (shown in grey), a solute commonly used in this thesis. Cosolutes are shown as red spheres and water as blue spheres. The bulk solvent is visualized as the faded area and the solvation shell as the clearly visible area. (a) shows the accumulation (preferential binding) of the cosolute around the solute, while (b) shows the depletion (exclusion) of the cosolute.

However, in some cases it has been found that TMAO may act in a concentration dependent manner and may even act as a denaturant.[34–36] In the following paragraphs, I will summarize what is known about TMAOs interaction with these functional groups and whether this explains the protein stabilisation.

Salt Bridges The charged residue of proteins may form salt bridges, which are also thought to contribute much to the stabilisation of the protein folded state. There, negatively charged side chains, like those of aspartic and glutamic acid, and positively charged side chains, like those of arginine, histidine and lysine, strongly interact with each other through coulombic interactions, as shown in Fig. 1.3, where a salt bridge consisting of aspartic acid (negatively charged carboxyl group) and arginine (positively charged guanidinium group) is formed. TMAO is depleted from salt bridges and it has been hypothesized that the presence of TMAO stabilizes salt bridge formation in proteins.[16,17] However, in the study of Su et al. they used NaCl as a model for salt bridges[17] and it is not clear how TMAO influences a less sterically available ion pairing, which is also surrounded by other functional groups. The influence of TMAO on a charged polymer is non-monotonic and highly depends on the charge distribution.[37] An experimental study on the mixed effect of salt and osmolytes has also found that osmolytes counteract the screening effect of salt on electrostatic

interactions, enhancing them.[38] On the other hand, it has been hypothesized that TMAO may stabilize the association of polyanionic GB1 through charge screening.[39] This screening effect suggests that TMAO decreases coulombic interactions and thereby may destabilize salt bridges. Studies on the mini-protein TrpCage has found that TMAO stabilizes the single salt bridge of the protein.[16,40] However, Ganguly et al. have shown that TMAO stabilizes only the formation of one of the R2 peptide salt bridges, but destabilizes the formation of the other two.[41] Therefore, there are ambivalent results about the TMAO effect on salt bridge formation.

Polar Interactions Proteins can form hydrogen bonds. Secondary structures, like α-helices or β-sheets, are stabilized by hydrogen bonds between backbone atoms of the protein, but, aside from that, also the polar side chains can form hydrogen bonds. In Fig. 1.3 TrpCage forms a α-helix, burying the hydrogen bonds of the backbone inside the helix. The common picture of TMAO interactions with proteins is that of TMAO depletion, i.e. TMAO reduces the solubility of proteins (increases the solvation free energy/a positive transfer free energy).[9,11,31–33] Therefore, it is assumed that TMAO does not interact with the protein directly. Bolen et al. have calculated the transfer free energy of amino acids from a binary water mixture to a 1 M aqueous TMAO mixture. They assumed that the transfer free energies of different parts of molecules are additive and subtracted the transfer free energy of glycine from that of other amino acids to obtain the contribution of the side chains. Calculations of the additive transfer free energies of proteins and the contributions from protein sidechains and backbone revealed that the contribution from the backbone causes TMAO depletion, while most TMAO interactions with side chains are favorable.[26,31,42] This has since been confirmed by MD simulations.[43,44] Still, TMAO may form hydrogen bonds with polar groups of proteins, but remain net depleted. It has been shown that TMAO disrupts the hydrogen bond network around proteins, reducing water-protein hydrogen bonds.[18] This effect is bigger for the denatured state, which exposes a bigger surface to the solvent. Therefore, TMAO may shift the folding equilibrium towards the folded state by destabilising the denatured state. Another mechanism is based on the strengthening of water-water hydrogen bonds by TMAO, where protein denaturation would break these water-water hydrogen bonds due to a larger formation of protein-water hydrogen bonds.[45]

Hydrophobic Interactions Lastly, it has been found that hydrophobic interactions are a key driving force in the stabilisation of the protein folded state and protein aggregation. Upon folding, proteins bury their hydrophobic side chains in the internal part to screen them from water molecules.[21] These hydrophobic interactions are determined by short range van der Waals interactions. Therefore, increased attention has been given to the hydrophobic effect, that is the solvation of hydrophobic particles (hydrophobic hydration) and their association (hydrophobic interactions). Hydrophobic molecules are not well soluble in water.[46,47] The term hydrophobic might be misleading since there are favorable London dispersion interactions between water and hydrophobic molecules. The solvation of hydrophobic molecules is enthalpically favorable but comes with a large entropic penalty. This thermodynamic dependence is also captured in the large solvation heat capacity, a trademark for hydrophobic hydration.[48–50] Therefore, the temperature effects on the solvation of

hydrophobic molecules is of great interest. Furthermore, there is a crossover between the solvation of small and large hydrophobic solutes. Solvation of small solutes is determined by the bulk properties of the solvent and solutes like methane do not disrupt the tetrahedral order of water considerably. However, the solvation of large solutes is also determined by interfacial, that is liquid-vapor interface, properties, as part of the solvation process is the creation of a repulsive surface (see the Theory on Solvation for more information, Chap. 2.5).[51–54] The insertion of such large solutes disturbs the tetrahedral order of water molecules and may lead to unusual effects.[55,56] Hydrophobic solutes are associating in water due to the excluded volume effect. Insertion of a solute leads to volume, that can not be occupied by water molecules (excluded volume). This lowers the translational entropy of these water molecules. Solute aggregation lowers this excluded volume since the contact surface can shed its solvation shell. Thereby, aggregation increases the translational entropy of water.[57] This effect is even further enhanced by an increase in temperature. Understanding all these hydration effects is crucial in the comprehension of protein folding and LLPS as the association of their hydrophobic groups is so important in their overall folding/aggregation equilibrium. Therefore, the focus of this thesis is on TMAO effects on hydrophobic hydration and interactions. As we herein study model systems and look at their association and dissociation to get a model understanding of protein folding and aggregation, we will from hereon use the terms association and dissociation. Furthermore, we will mainly use the term cosolute when we mention osmolytes or denaturants.

The interactions of TMAO and the thereby resulting effects on hydrophobic solute interactions are much discussed and there is still no consensus on it. This may also be due to a bad representation (bad force fields) of aqueous TMAO mixtures in computer simulations, which is crucial in the description of hydrophobic hydration.[46] Model studies give ambivalent results. Early studies based on the transfer model of Bolen assumed that TMAO is also depleted from hydrophobic surfaces.[31,42] This does not take into account that the solvation effects may not be additive and solvation is often conditional, dependent on other functional groups in the vicinity of the hydrophobic groups. Based on the scaled particle theory, it is assumed that TMAO is depleted from hydrophobic surfaces due to its increase of the binary mixture density.[58,59] On the other hand, surface tension measurements revealed that TMAO decreases the surface tension and therefore accumulates at the air-water interface.[60,61] Accordingly, it can also be assumed that TMAO accumulates at large hydrophobic interfaces. Studies on protein adsorption on hydrophobic surfaces have shown that TMAO may inhibit protein adsorption by accumulating at the hydrophobic surface and thereby making it more repulsive to the protein.[62] Athawale et al. have studied the influence of TMAO on small hydrophobic solutes and a model hydrophobic polymer.[63] They have found that TMAO has a negligible effect on hydrophobic interactions, which has since also been reported in other studies on the association of small hydrophobic solutes.[64,65] Since it is usually understood that accumulation of a cosolute leads to protein denaturation and dissociation of solutes, it has also been speculated that TMAO may reduce hydrophobic interactions. This has been shown using the

mini-protein TrpCage[16] and small solutes. Recently, groups have suggested that the accumulation of TMAO may also lead to the increase of hydrophobic interactions. A joint experimental and simulation study on ELP suggested a surfactant mechanism, in which TMAO interacts stronger with the patchy surface, consisting of both hydrophobic and hydrophilic regions, of a folded protein than with the extended surface. This stronger interactions then leads to the shift of the equilibrium to the folded state.[61] Similarly, Mondal et al. showed that TMAO favors the interaction with the collapsed polystyrene compared to the extended state and thereby drives the collapse of polystyrene chains.[19] Furthermore, they showed that the folded state of TrpCage can similarly be stabilized by TMAO preferential binding.[66] Rodriguez-Ropero et al. used a model hydrophobic polymer chain to study the TMAO effect on hydrophobic interactions, but, unlike Athawale et al., they took different TMAO concentrations into account.[20] This revealed a concentration dependent effect of TMAO on the hydrophobic polymer collapse, first stabilising the globule formation at low TMAO concentrations and then destabilising it at high TMAO concentrations. This non-monotonic effect has also been observed with the relatively hydrophobic protein stem bromelain and can be well observed in the compaction and then loosing of its hydrophobic core.[36] Other studies suggested that also the chain length may play a major role in the non-monotonic TMAO effect on hydrophobic interactions.[67,68] The overall picture is rather diverse and non-conclusive. Binary solvent properties are important for the depiction of hydrophobic interaction and therefore the models (force fields) used in simulations might have added to various conclusions. Furthermore, very often only one TMAO concentration is taken into account, so that the underlying concentration dependent non-monotonic behavior may lead to wrong interpretations. The parameterization of a new force field that is able to reproduce the binary solvent properties well and also studies taking several TMAO concentrations into account should also help in getting a clearer picture.[15]

To understand the effect of TMAO on hydrophobic molecules, binary solvent studies are essential. A study using ab initio molecular dynamics (AIMD) and THz spectroscopy has found that TMAO is surrounded by water molecules, which they classified as “hydrophilic” and “hydrophobic” water.[13] “Hydrophilic” water molecules, which are three on average, are bound to the TMAO-oxygen via hydrogen bonds. These water molecules have an enhanced dipole moment and the hydrogen bonds with TMAO are so long-lived that TMAO$\cdot(H_2O)_3$ can be considered as a supermolecular solvation complex.[13,69] This is further shown when considering a very similar molecule to TMAO: tert-butyl-alcohol (TBA), which resembles TMAO apart from a hydroxyl group instead of a negatively charged oxygen and a carbon atom replacing the central nitrogen. TMAO binds water more tightly than TBA leading to TBA being an only mono-hydrated molecule.[70,71] “Hydrophobic” water molecules are those close to the TMAO methyl groups. These water molecules have slightly less hydrogen bonds with other molecules than their bulk counterparts, slower rotation dynamics and their hydrogen bonds with bulk water molecules are slightly longer. Other than that, they behave very similar to bulk water molecules.[13,72] The net effect of TMAO on the binary mixture is that of a decreased self-diffusion of water, higher density of the mixture and a slower collective dipolar reorientation due

to the big water-TMAO complexes.[71,72] TMAO is also able to interact with other osmolytes through its negatively charged oxygen. For example, it can bind urea molecules and it has been suggested that it thereby might counteract the denaturing effects of urea on protein folding.[73] Another study found that urea and TMAO form well hydrated complexes, where both form hydrogen bonds with water rather than with each other.[74]

Lastly, the question arises why it is TMAO that deep sea creatures use to counteract pressure. Most studies of TMAO effects have been conducted at ambient pressure and do not reveal any exceptional effect of TMAO, that makes it different from other osmolytes. Piezolytes, molecules that are thought to be special in their pressure counteracting ability, mostly include methylamines, but also the neurotransmitter glutamate and the amino acid derivative sarcosine, all forming zwitterionic molecules at neutral pH.[75,76] The volume difference of the associated state or dissociated state (or protein folded state and unfolded state) determines the pressure effect according to Le-Chateliers principle. Accordingly, assembly of molecules in solution increases the volume due to higher density of the hydration shell compared to the bulk solvent.[77,78] Furthermore, there may be void volumes due to packing deficits in folded/collapsed macromolecular systems.

Therefore, the effect of pressure and cosolute on a chemical equilibrium can be summed up as:

$$\mathrm{d}\Delta G_2(c_3,p) = \underbrace{\Delta\overline{V}_2\mathrm{d}p}_{(1)} \underbrace{-RT\Delta\Gamma_{23}\frac{a_{cc}}{c_3}\mathrm{d}c_3}_{(2)}$$

where ΔG_2 is the free energy difference between the folded (F) and unfolded (U) state of the protein, $\Gamma_{23} = \Gamma_{23}^U - \Gamma_{23}^F$ denotes the difference in cosolvent (e.g. TMAO) preferential binding coefficient (see Sec. 4, a measurement for TMAO accumulation or depletion) upon unfolding, $a_{cc} = \left[1 + c_3(G_{33} - G_{31})\right]^{-1}$ and G_{xy} are Kirkwood-Buff integrals (see section 3) between water (1) and cosolute (3) and the expression is always positive for stable mixtures. Based on this expression it has been proposed that these so-called "piezolytes" lower the volume difference between the associated and dissociated state, reducing the actual pressure effect on association, while other cosolutes have no such effect. However, also the second term (2) might play an important role as the pressure is increased and lead to a stronger effect of the cosolute due to changes in cosolute preferential binding to proteins. Current studies have only focused on the first (1) term and neglected the possibility of a change in cosolute effect. Adaption of organism is supposed to happen either through protein adaption, so-called piezophiles that have mutated to possess a lower volume difference between folded and unfolded states, or cosolute effect on the volume difference. Even so, the Makhatadze research group has found that proteins classified as piezophiles do not differ from non-piezophiles in their volume difference.[79] Furthermore, their study of piezolytes has shown that denaturants always increase the volume difference at the melting point, while protecting cosolutes, independent of their use as a pressure counteracting osmolyte, decrease the volume difference at the melting point. However, the measurements have been conducted at the according

melting temperatures, where the temperature difference and thermal expansion is responsible for the volume change. Therefore, a correction for the temperature dependence of the volume change shows that cosolutes do not affect the volume difference. This in turn means that the osmolyte preferential binding does not change with pressure. They concluded that neither the so-called piezophiles nor the piezolytes deserve this distinction.[80] Still, TMAO has not been a part of this study due to experimental difficulties.

Most studies on the effect of TMAO on solvation and solvent-mediated interactions have focused on the TMAO effect at ambient pressure and extrapolated these results to high pressure. Experimental studies have proven that TMAO is capable of protecting the protein folded state and LLPS against pressure effects, that is protein unfolding and formation of a single phase respectively.[9,10] However, the molecular mechanism remains unclear since these studies assume that there is no change in preferential binding of TMAO to solutes and therefore it is assumed that also at high pressure TMAO protects proteins using a depletion mechanism as suggested by the transfer model. It also remains unclear how the pressure changes TMAO interactions with apolar molecules. Some studies have addressed the issue using small nonpolar molecules like methane and neopentane. They have found that TMAO neither stabilizes the association of these molecules at low nor at high pressure. Furthermore, TMAO may even destabilize the aggregation of neopentane at high pressure, so that they concluded that the stabilising quality of TMAO may be a consequence of its interactions with polar groups.[64,65]

Therefore, the question why deep sea organism have evolved to use methylamines like TMAO for their protein protection has not been answered satisfactorily. Furthermore, the depletion mechanism, which has been assumed to be the only mechanism by which TMAO stabilizes protein folding and LLPS, has been challenged in the recent years and a deeper understanding of TMAO interactions with different protein functional groups has been looked for.[16,19,20,44,66] Our studies have focused on the effect of TMAO on hydrophobic interactions and uncovered new mechanism by which TMAO can enhance solvent-mediated interactions aside from preferential TMAO exclusion. Part of our studies focus on TMAO effects on the hydration shell of hydrophobic solutes and how binary solvent properties influence these. Another part focuses on the interplay of TMAO and pressure effect and whether TMAO has a special mechanism to counteract the reduction of solvent-mediated interactions by pressure.

2 Structure of this Thesis

We wanted to understand the TMAO effect on hydrophobic groups and thereby extend the knowledge about interactions of TMAO with hydrophobic parts of proteins and the collective effect of TMAO and other external variables like pressure and temperature. This broadens the understanding about protein and LLPS stabilisation due to the presence of TMAO by providing possible stabilisation mechanisms based on local interactions of TMAO with different functional groups of proteins. This thesis is extending the current knowledge of TMAO effects on solvent-mediated hydrophobic interactions and the interplay of this effect with increased pressure. The aim of this thesis is to understand the interactions of TMAO with hydrophobic molecules, their solvation shells and how conditions like pressure, solute size and temperature may affect it and therefore the thesis addresses these three main questions:

1. How does TMAO interact with hydrophobic molecules and influence hydrophobic interactions?

2. How do nonpolar solute size, temperature and pressure influence these interactions, since they change the solvation shell of the solute in water?

3. What contributes to the piezolytic behavior of TMAO (if it exists)? Which role does the enhanced dipole moment at high pressure play?

By including statistical mechanics and thermodynamic analysis an in depth understanding of different influences was created using molecular dynamics simulations. That is, the contributions of cohesive van der Waals interactions and repulsive van der Waals interactions on TMAO-solute interactions. Furthermore, a novel stabilisation mechanism of TMAO on hydrophobic interactions was discovered (surfactant-like mechanism, similar to the stabilisation mechanism of methanol) and it was confirmed that TMAO has piezolytic properties in the case of hydrophobic interactions, in the sense that the increasing ability to enhance hydrophobic interactions at high pressure is a result of the enhanced dipole moment. The objectives are summerized in Fig. 1.5.

The text is constructed as follows: In chapter 2 relevant basics and theories are summarized and explained. My publications are presented in chapter 3 to 7. These include:

Chapter 3

The publication in Chapter 3 includes a comparison of experimental and simulation data and data that helps to understand the second point (**2.**). We show that the effect of TMAO on penta-alanine solubility is correctly represented, although the representation is worse if both zwitterionic charges of the amino acid are used for the model. Furthermore, we show that TMAO preferential binding may depend on chain length, end group character and TMAO concentration. Even though, TMAO accumulates locally close to the peptide while remaining net depleted. This effect is independent of penta-peptide chemistry or pressure. Lastly, we see that TMAO reduces the peptide-solvent hydrogen bonds, which in the case of larger solutes may drive the collapse of the solute.

- Folberth, A.; Polák; J. Heyda, J.; van der Vegt, N. F. A; Pressure, Peptides, and a Piezolyte: Structural Analysis of the Effects of Pressure and Trimethylamine-N-oxide on the Peptide Solvation Shell. J. Phys. Chem. B, **2020**, 124(30), 6508-6519.

Chapter 4

In the publication presented in chapter 4 we investigate the interplay of temperature and TMAO effect on hydrophobic hydration and hydrophobic interactions addressing the first (**1.**) and second point (**2.**). We observe a temperature induced change of the TMAO effect on hydrophobic hydration. Namely, at low temperatures, TMAO lowers methane solubility (it is depleted from the methane surface), but at high temperatures TMAO increases methane solubility (it preferentially binds to methane). Using statistical mechanics we find that the creation of the methane cavity is opposed by TMAO at all temperatures. This is the dominant force at low temperatures. At high temperatures this excluded-volume effect is overcompensated by cohesive van der Waals interactions. Furthermore, TMAO increases hydrophobic interactions between methane molecules. Therefore, this increased effective attraction correlates with TMAO depletion at low temperatures, but with preferential TMAO binding at high temperatures.

- Folberth, A.; van der Vegt, N. F. A; Temperature Induced Change of TMAO Effects On Hydrophobic Hydration. J. Chem. Phys., **2022**, 184501

Chapter 5

Chapter 5 consists of the statistical mechanics analysis of the solvation of small and large hydrophobic molecules and its impact on the association of two large solutes addressing the first (**1.**) and second point (**2.**). We observe that the reversible work of cavity creation of large solutes is reduced due to TMAO accumulation at the repulsive solute surface. Meanwhile, TMAO is depleted from the repulsive solute-solvent interface of small solutes, increasing the reversible work of cavity creation. The solvent-mediated interactions between large repulsive molecules are enhanced by

TMAO through a surfactant-like mechanism. Upon addition of attractive interactions this is compensated by enthalpic solute-solvent interactions, leading to a net non-monotonic effect of TMAO on the association of two nonpolar solutes: At low TMAO concentrations, the association of nonpolar molecules is reinforced due to the dominating effect of the surfactant-like mechanism. At high TMAO concentrations, enthalpic solute-solvent interactions dominate, leading to a minimum of the association free energy.

- Folberth, A.; Bharadwaj, S.; van der Vegt, N. F. A; Small-to-Large Length Scale Transition of TMAO Interaction with Hydrophobic Solutes. Phys. Chem. Chem. Phys., **2022**, 24, 2080–2087

Chapter 6

The publication of chapter 6 reports the interplay of TMAO and pressure on the association of nonpolar solutes addressing the second (**2.**) and third (**3.**) question. Pressure enhances the effect of TMAO on the association, namely, the stabilising TMAO effect becomes stronger at high pressure. This is due to the enhanced dipole moment of TMAO at high pressure, which allows it to bind more water molecules. Without the enhanced dipole moment, no stabilising TMAO effect can be observed. Thus, in the case of hydrophobic interactions, TMAO acts as a piezolyte as it binds water more strongly and thereby the TMAO preferential binding to the solute changes. Therefore, we show that TMAO is capable of enhancing several interactions, which is the reason for it being such a good osmolyte.

- Folberth, A.; van der Vegt, N. F. A; A unique piezolyte mechanism of TMAO: Hydrophobic interactions under extreme pressure conditions , ,

Chapter 7

In the publication of chapter 6 we investigated the cumulative effect of temperature, pressure and TMAO concentration on the folding equilibrium of the protein TrpCage to help understand the first (**1.**) and second point (**2.**). We find that TMAO is capable to counteract the pressure effect and that it stabilizes the protein folded state across the whole temperature-pressure plane through several mechanism. TMAO enhances the salt bridge formation and hydrophobic interactions. It also reduces the amount of protein-solvent hydrogen bonds and thereby stabilizes the protein folded state.

- Folberth, A.; van der Vegt, N. F. A; Influence of TMAO and Pressure on the Folding Equilibrium of TrpCage. ,

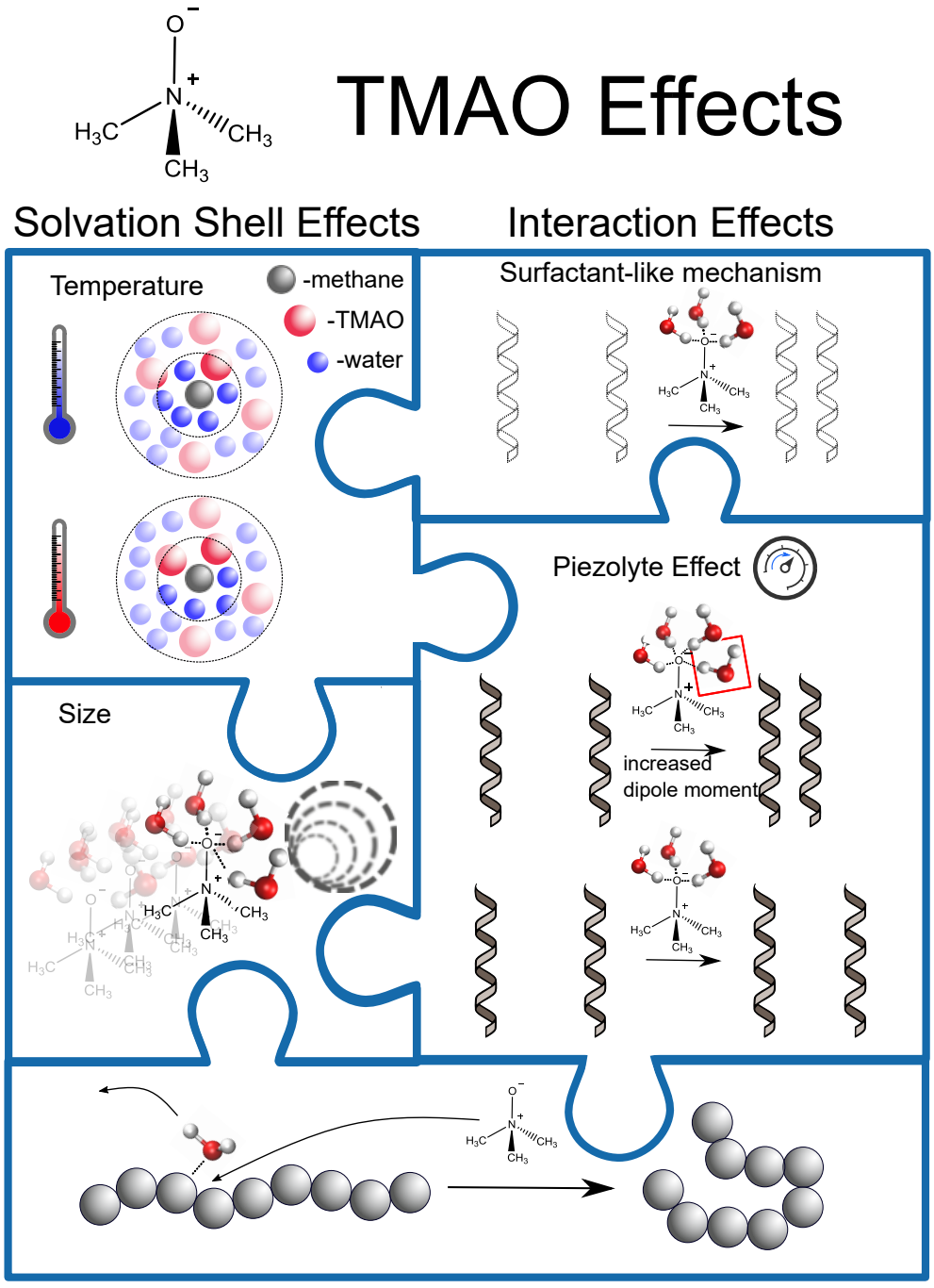

Figure 1.5: Overview of the new findings on TMAO effects in this work, which are those of the solvation shell (due to size, temperature and (not shown) pressure) and those of interaction effects, like the surfactant-like mechanism. Top left: Temperature induced change in TMAO preferential binding. Top right: Surfactant-like mechanism on helix cavities driving cavity association. Mid left: TMAO switching from depletion to preferential binding upon solute cavity size increase. Mid right: The increased dipole moment of TMAO at high pressure leads to a pressure counteracting effect. Bottom: Loss of solute-solvent hydrogen bonds due to the bulky TMAO molecules can lead to reduction of the solvent accessible surface and therefore compaction.

2 Theory

1 Computer Simulations

1.1 Historical Development of Computer Simulations

Computer simulations are used to understand and predict occurences in physical systems through mathematical models. They allow a profound analysis of phenomena by granting insight into the exact molecular occurrences and possible unphysical manipulations, which are not available in experiments.[81,82] Additionally, they can be used to aid industrial operations by saving laboratory costs, reducing time-consuming development cycles and may be more sustainable than laboratory experiments. The studied systems may be theoretical models, like Lennard-Jones liquids, but also real-world systems, like proteins or atom clusters.[83–85]

Today, the most common theoretical methods to understand physical phenomena are quantum chemistry and molecular dynamics simulations.

In 1928 there were first attempts to solve the Schrödinger equation through the use of mechanical calculators.[86] The solution to these calculations matched experimental values of simple systems, allowing a different approach than experiments to understanding physical phenomena. After the emergence of electronic computers, scientist were able to make numerical approximations to the solution of the Schrödinger equation in the mid-1950s to understand the behavior of molecules.[87–89] In the early 1970s simulation packages were available for scientists, leading to an increased use of computational chemistry to understand the structure and reactivity of molecules.[90,91]

In the 1950s Molecular dynamics (MD) simulations were invented to allow the simulation and computational analysis of bigger systems than those feasible through quantum chemistry. In MD it is assumed that the Born-Oppenheimer approximation is valid, so that only nuclear coordinates are taken into account and the Hamiltonian (equation 1) depends only on the position and momentum of the atoms.[92,93] The movements of atoms should then satisfy the laws of classical mechanics (Newtons law). We will explain the calculations done to obtain molecule trajectories in the next section.

$$H(r^N, p^N) = V(r^N) + K(p^N) \tag{1}$$

Early molecular dynamics simulations (MD) had to use extreme simplifications due to low computational resources. One of the first MD simulations was that of a nonlinear chain by Fermi et al. at the Los Alamos National Laboratory.[94] 1957 the first MD simulations of a hard sphere fluid (32 to 96 particles) was published by Berni Alder and Tom Wainwright.[95] The first simulation of a polymer (50 units) then followed as a molecule with freely jointed hard spheres was investigated.[96] Researchers have then started to use MD to calculate fluid properties, like diffusion coefficients and were able to connect their findings to experimental methods. One example is an early paper by Rahman in 1964 where they simulated liquid argon using a Lennard-Jones potential and calculated properties of interest like the radial distribution function, which can be connected to the structure factor, measured in neutron scattering experiments.[97,98] Up to then all MD simulations were conducted in the microcanonical ensemble (NVE), making the comparison to experiments difficult. One of the earliest constant temperature simulation was done in 1971 using velocity-rescaling to obtain the target temperature.[99] Other methodological advances contributed to making MD simulations more feasible and initiated the employment of simulations for realistic models of bigger sized systems.[100,101] 1971 the first simulation of liquid water was done by Rahman and Stillinger.[102] By the mid-1980s large-scale simulations were feasible. One important step of connecting MD simulations to realistic systems was the introduction of free energy perturbation methods, which provide free energies of solvation and therefore solubilities of molecules (first done with hard-sphere models).[103] 1987 free energy perturbation methods were used by Singh et al. to calculate the free energy of solvation of amino acids.[104] More realistic models were created in the 1990s as researchers and industry were able to simulate bigger and more realistic systems. With this came the use of established open source MD codes instead of own local codes, for example LAMMPS, Amber and Gromacs.[105–107]

Today we are able to simulate systems of proteins and polymers extensively to study their equilibrium properties.[108–110] Still, it is often necessary to simplify molecules through coarse graining or use of special algorithms to speed up the equilibration if bigger systems are considered. Below, I will explain the basics of MD simulations and techniques used in this thesis to obtain equilibrium properties.

1.2 Molecular Dynamics Simulations Basics

In MD quantum chemistry is used to parameterize so-called force fields. In force fields each atom has a charge, a (van der Waals) radius and a polarizability. Bonded interactions are usually described through an harmonic potential, just like angles and dihedrals. Therefore, each atom interacts through bonded interactions and non-bonded interactions (typically Lennard-Jones and coulomb interactions).[93] An example for interaction potentials V used in molecular mechanics methods is given in equation 2[111]

$$V(r_{ij}) = \underbrace{4\epsilon_{ij}\left[\left(\frac{\sigma_{ij}}{r_{ij}}\right)^{12} - \left(\frac{\sigma_{ij}}{r_{ij}}\right)^{6}\right]}_{\text{Lennard-Jones Potential}} + \underbrace{f\frac{q_i q_j}{\epsilon_r r_{ij}}}_{\text{Coulomb Potential}} + \underbrace{\frac{1}{2}k_{ij}^{b}(r_{ij} - r_{ij}^{0})^2}_{\text{Bond Potential}} + \underbrace{\frac{1}{2}k_{ijk}^{\theta}(\theta_{ijk} - \theta_{ijk}^{0})^2}_{\text{Angle Potential}} + \underbrace{k_{\phi}(1 + \cos(n\phi - \phi_0))}_{\text{Proper Dihedral Potential}} + \underbrace{\frac{1}{2}k_{\xi}(\xi_{ijkl} - \xi_0)^2}_{\text{Improper Dihedral Potential}} \quad (2)$$

ϵ depth of the potential well

σ distance at which the Lennard-Jones potential becomes 0

r_{ij} distance between molecule i and j

$f = \frac{1}{4\pi\epsilon_0} = 138.94$ the electric conversion factor

ϵ_0 electric constant

q_α partial charge of atom α

ϵ_r the relative dielectric constant

k_{ij}^{b} force constant of the harmonic bond potential of atom i and j

r_{ij}^{0} minimum of the bond potential

k_{ijk}^{θ} force constant of the harmonic angle potential between atom i, j and k

θ_{ijk}^{0} minimum of the angle potential

k_ϕ force constant of the proper dihedral potential (set of atoms being linearly connected)

ϕ_0 minimum of the proper dihedral potential

n multiplicity

k_ξ force constant of the harmonic improper dihedral potential

ξ_0 minimum of the improper dihedral potential

The first part of the Lennard-Jones potential is the Pauli-Repulsion, the second part is the London Dispersion (induced Dipole-Dipole interactions, polarizability). Bonded interactions are mostly described through harmonic potentials. Proper dihedral potentials are used to define the dihedral as per the definition of IUPAC (atoms being connected linearly).[112] Improper dihedral potentials are used to keep atoms in a plane (e.g. for aromatic molecules or to restrain structures with a double bond in their mesomeric structure). There are also other potentials which can be used. One such potential that can be used instead of Lennard-Jones interactions is the Weeks-Chandler-Andersen (WCA) potential ψ_R (equation 3), which is often used in this work.[113]

$$\psi_R = \begin{cases} 4\epsilon \left[\left(\frac{\sigma}{r}\right)^{12} - \left(\frac{\sigma}{r}\right)^{6} \right] + \epsilon, & r < 2^{1/6}\sigma \\ 0, & r \geq 2^{1/6}\sigma \end{cases} . \tag{3}$$

This is the purely repulsive version of the Lennard-Jones potential ψ, where the Lennard-Jones potential is shifted up by $+\epsilon$ and the cut off at the minimum, leading to a soft core repulsion. Figure 2.1 shows the Lennard-Jones potential and its separate repulsive and attractive contributions, as used in this thesis.

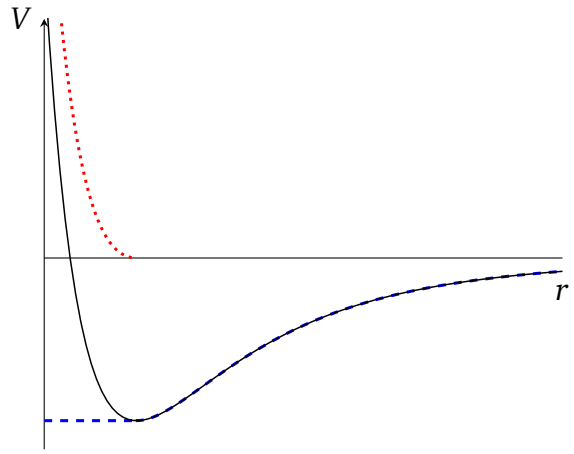

Figure 2.1: The Lennard-Jones Potential ψ (black) as a function of the distance r between atoms. The red, dotted line represents the WCA potential ψ_R (equation 3), the repulsive part of the potential. The dashed, blue line represents the attractive part ψ_A, where $\psi = \psi_A + \psi_R$.

The different contributions to the potential make up the so-called force fields. These force fields are often parameterized in ab-initio simulations and then tuned so that properties of the simulated system fit experimental values. There might also be additions to the force fields like artificial restraints of the atoms to a certain position. These are often necessary when trying to reduce some complexity of the problem or for equilibration of the system.

It is then necessary to choose the settings of the simulation. This consists of the choice of algorithms, like choosing the algorithm to calculate coulomb interactions, and the settings of the system, like ensemble type and the target temperature and pressure. Most simulations in this work

use the Berendsen thermostat and barostat for equilibration and the Nosé-Hoover thermostat and Parrinello-Rahman barostat for the production run.[114,115]

1.3 Running simulations

There are several steps in which the trajectory, which consists of all configurations of the system along a time path, is generated. MD simulations use discrete time steps Δt to form the trajectory. This time step is usually around 1-2 fs and is chosen so that the largest frequency in the system is sampled. First, the MD algorithm needs the potential interaction as a function of atom distances and positions. Then, the forces F between the atoms are calculated by taking the sum of the force between non-bonded atom pairs and the forces originating from the bonded interactions (and restraints if they are present). Newton's equation of motion is solved to calculate the atom position. Therefore, an integration method has to be used. Most often the leap-frog integrator is used, where the formula is given in the schematic. Since a discrete time step length has to be chosen, velocities, positions and accelerations a have to be approximated through a Taylor-Expansion. The output consists of atom positions, velocities v, energies, temperatures and pressure.

The MD simulation is done in the following fashion:[116,117]

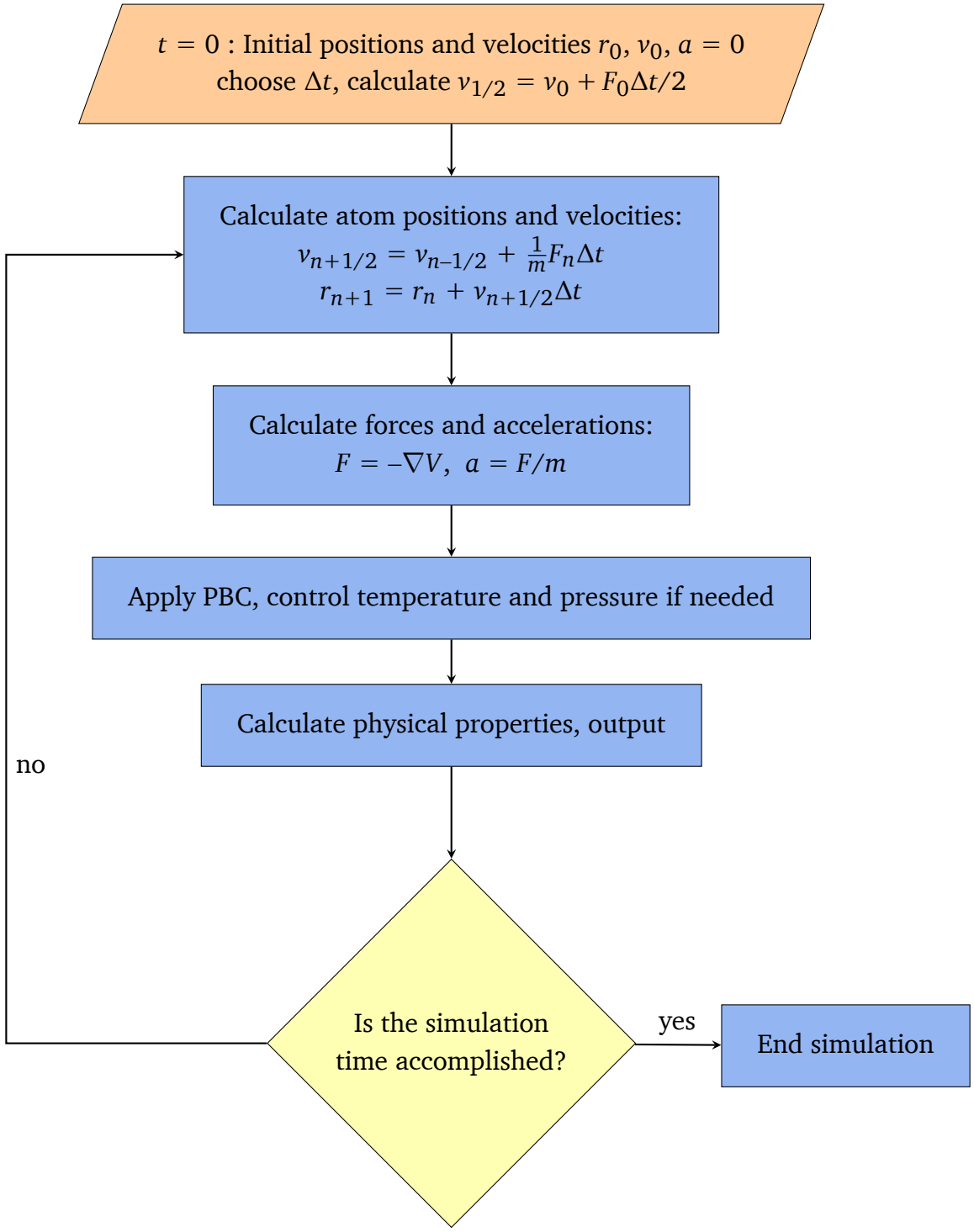

Simulations in this work usually match the following procedure:

Systems commonly have a high potential energy due to configurations where particles overlap or are very close to each other after setting them up and are not at the target temperature and pressure

yet. Thus, we first have to do an energy minimization to relax the structure. This uses the steepest descent method to find the minimum of the potential energy. The configuration is adjusted in a stepwise fashion to obtain a reasonable starting structure. The subsequent equilibration is first done restraining the solute as otherwise the system may collapse. In the first step, a constant volume-temperature simulation (*NVT* ensemble) is done to adjust the temperature. In the equilibration, first velocities are randomly generated and then the Berendsen thermostat is used to reach the target temperature by suppressing the kinetic energy fluctuations.[118]

$$\frac{\mathrm{d}T(t)}{\mathrm{d}t} = \frac{T_0 - T(t)}{\tau}$$

Here, T_0 is the target temperature and τ is the coupling parameter, which has to be set beforehand. The ensemble generated by this is not canonical[119] and therefore only used for equilibration of the system as the Berendsen thermostat is very efficient in reaching the target temperature. Subsequently, a constant pressure-temperature simulation (*NpT* ensemble) is done. The Berendsen barostat is used, which is based on the same concept as the thermostat.

For the production run the Nosé-Hoover thermostat is used to probe the correct canonical ensemble.[115] The Nosé-Hoover thermostat combined with the Parrinello-Rahman barostat achieves a realistic canonical ensemble and is therefore suited for the study of thermodynamic properties of a system.[114] Hence, it is the preferred combination in our studies.

2 Solvation

Understanding aqueous solutions of biomolecules and polymers is crucial for the comprehension of biological processes. Protein folding, liquid-liquid phase separation and thermoresponsive polymers are some of the heavily studied subject in this context, where the investigation of solvation phenomena plays an important role.[9,120–122]

The process of solvation is defined by transferring a molecule from a fixed position in the gas phase to a fixed position in the solvent, so that the translational degrees of freedom can be neglected. In a second step, the liberation process, it is allowed that the molecule can move freely in the solvent, so that it is no longer indistinguishable from other molecules of the same kind.[57]

The excess chemical potential (solvation free energy) can then be defined as

$$\mu^* = -\mathrm{k_B}T \ln\langle \exp(-\beta \Delta U) \rangle_0 \tag{4}$$

where ΔU is the energy of the interactions of the solute with its surrounding solvent molecules and the index 0 denotes that the average is taken over the solvent configurations without the solute present. To further understand the solvation process, we can split it up into a two step process:[57]

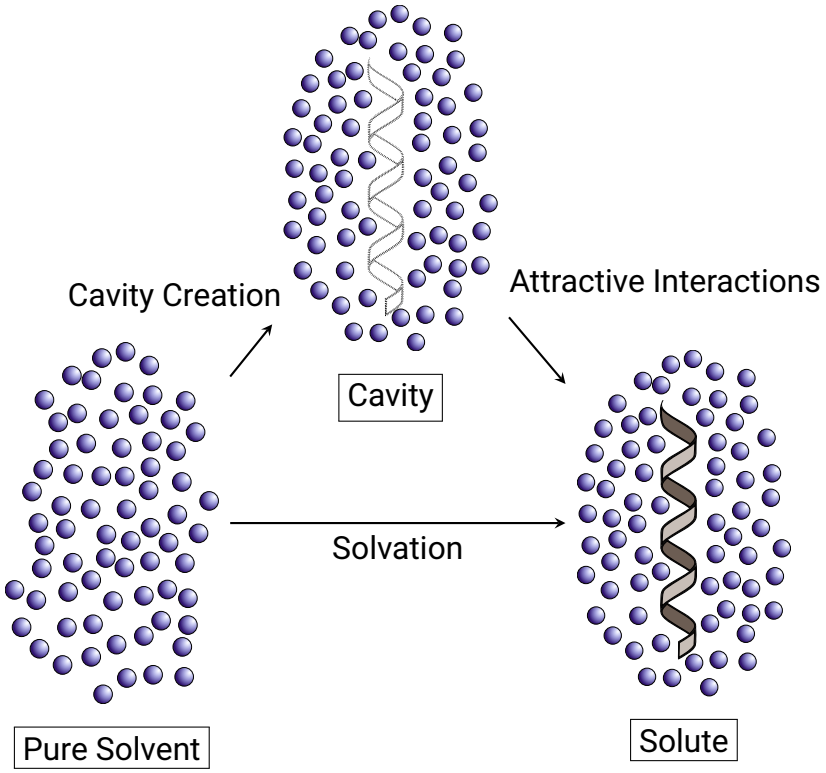

First, an empty volume, a cavity, of the same shape and size as the solute is created in the solvent. This can be regarded as the introduction of repulsive solute-solvent interactions. Solvent molecules can not access this volume anymore, reducing their translational entropy. Therefore, the reversible work of cavity creation μ_{cav} is always positive and usually contributes largely to the solvation free energy. In the case of two molecules, this contribution will lead to solvent-mediated attraction of the molecules to minimize the volume and surface area. The cavity contribution is determined by the probability of finding this empty volume in the pure solvent solution. In a subsequent step, attractive interactions are introduced, leading to two effects. Firstly, solute-solvent attractive interactions reduce the solvation free energy. Secondly, the solvent is biased to remain at the interaction sites of the solute. This bias reduces the translational entropy, increasing the solvation free energy. This component is especially important in the case of preferential binding cosolutes, where the cosolutes are biased to cluster around the solute.[44,122] The described split up of the excess chemical potential μ^* is summed up in equation 5

$$\mu^* = \langle \psi_A \rangle_1 - \mathrm{k_B}T \ln\langle e^{-\beta\psi_R}\rangle_0 + \mathrm{k_B}T \ln\langle e^{\beta\delta\psi_A}\rangle_1 = \langle \psi_A \rangle_1 + \mu_{\text{cav}} - Ts_A \tag{5}$$

where ψ_A and ψ_R are the attractive and repulsive part of the solute-solvent interactions, respectively, $\delta\psi_A = \psi_A - \langle\psi_A\rangle$ is the fluctuation in attractive energies, μ_{cav} is the cavity contribution to the excess chemical potential and s_A is termed the fluctuation entropy. Although, these components alone are very large contributions to the solvation free energy, they mostly cancel each other out, as can also

be seen in our calculations (see chapter 5). The solvation free energy is a useful tool to understand equilibria in aqueous mixtures.

The solvent induced contribution to the Gibbs enery ΔG of an equilibrium is[123]

$$\Delta G = \Delta G^l - \Delta G^g \tag{6}$$

where ΔG^l is the Gibbs energy of the equilibrium in the solvent and ΔG^g is the Gibbs energy of the equilibrium in the gas phase. Assuming that the momentum partition function Λ of each solute is independent of its surroundings we can write for the equilibrium between associated and dissociated state (A $\rightleftharpoons$ D)

$$\Delta G = (\mu_D^{*l} - \mu_D^{*g}) - (\mu_A^{*l} - \mu_A^{*g}) \tag{7}$$

$$\frac{K^l}{K^g} = \exp(-\beta(\Delta G_D - \Delta G_A)) \tag{8}$$

where μ^* is the excess chemical potential ($\mu = \mu^* + k_B T \ln \rho \Lambda^3$) of the dissociated (D) and associated (A) state in the gas phase (g) or liquid phase (l), $\beta = 1/k_B T$, K is the equilibrium constant in the gas or liquid phase and ΔG is the solvation free energy of dissociated (D) or associated state (A) (both ΔG_2 (where the index 1 is commonly used for water, 2 the solute and 3 the cosolute) and μ^* are used to express the change upon the free energy in the solvation process). Therefore, the driving force for the reaction is a function of the solvation Gibbs energies of each reactand. Thus, it is crucial to understand the solvation process of biomolecules and its components. The equilibrium constant in equation 8 is in relation to the gas phase as a reference as shown in Fig. 2.2.

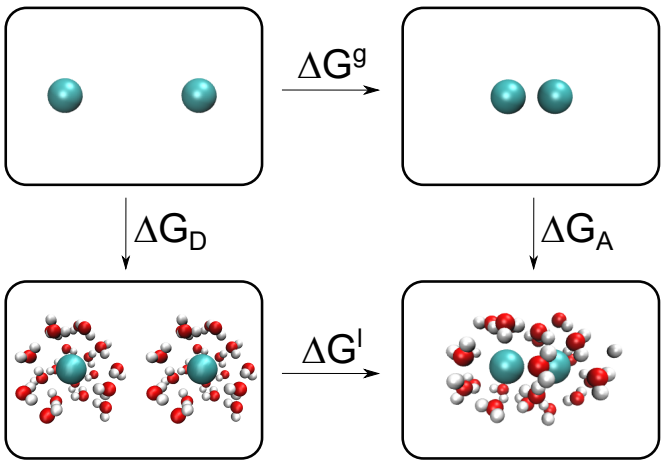

Figure 2.2: Thermodynamic cycle showing the association of two methane molecules. The relation between the free energy of association in the gas phase (ΔG^g) and in the liquid phase (ΔG^l) can be obtained through the free energy of solvation of the dissociated (ΔG_D^*) and associated (ΔG_A^*) state as shown in equation 8.

If we want to understand the influence of external stimuli on the equilibrium, we can take the pure water solvation at ambient conditions as a reference and study the influence on the equilibrium.[31] Here, we use this relation to study the influence of TMAO and pressure on solute equilibria.

3 Radial Distribution Function and Kirkwood-Buff Theory

The radial distribution function $g_{ij}(r)$ (rdf) or pair correlation function describes the relative density distribution of component i around component j as a function of the distance r from component j in a multicomponent system.

$$\rho_i(r) = \rho_i \cdot g_{ij}(r)$$

Here $\rho(r)$ is a conditional density and ρ the average bulk density of i. An rdf of 1 means that the density of the component i has reached the bulk density value and the distribution of the component i do not correlate with the existence of component j anymore. Therefore, $g_{ij}(r)$ converges to 1 for large distances as can be seen in Fig. 2.3. This convergence is only given for an open system. However, in a closed system, commonly used in MD simulations, the bulk density will be affected by the non-ideal distribution of the components and therefore the bulk will be depleted. Thus, the rdf will not converge to 1. This effect is important for the calculations of Kirkwood-Buff Integrals discussed below. An example of $g_{ij}(r)$ is given in Fig. 2.3 for the water(oxygen)-water(oxygen) pair correlation function.

The rdf shows a large first peak, showing that the density of water molecules around another molecule in the first solvation shell is increased. This density increase becomes weaker for the solvation shells which are farther away due to weaker interactions between the molecules. Water molecules are layered, so that minima occur between the peaks. Integration of the rdf gives the total number of molecules i. The rdf can also give information about thermodynamic quantities, like the compressibility (equation 12), which will be further discussed below.[57,124] Furthermore, the potential of mean force (PMF) $w(r)$, the free energy dependence on the distance r between the components i and j, can be calculated from the rdf via equation 9.[125]

$$w(r) = -\mathrm{k_B}T \ln(g_{ij}(r)) \tag{9}$$

The Kirkwood-Buff integral (KBI) G_{ij}, which is essential to Kirkwood-Buff (KB) theory, that links microscopic to macroscopic properties, can be calculated from the rdf, but is based on a derivation from Eqn. 10.

$$G_{ij} = V\left(\frac{\langle N_i N_j\rangle - \langle N_i\rangle\langle N_j\rangle}{\langle N_i\rangle\langle N_j\rangle} - \frac{\delta_{ij}}{N_i}\right) \tag{10}$$

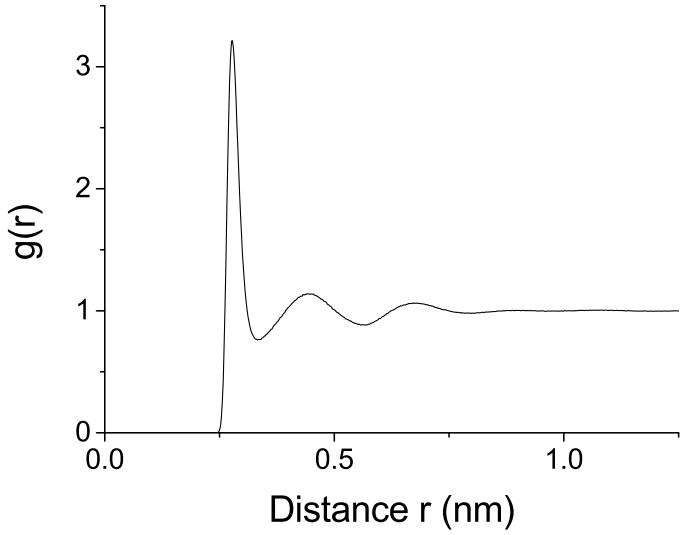

Figure 2.3: Radial distribution function g_{ij} of water(oxygen)-water(oxygen) as a function of atom distance. $g_{ij}(r) > 1$ shows a larger accumulation than in the bulk. Therefore, water shows a layered structure with a large water accumulation in the first solvation shell and then less in the solvation shells which are farther away. Inbetween the solvation shell the water density decreases below the bulk density due to packing.

The KBI is connected to the covariance of particle fluctuations and is therefore only defined in the grand canonical ensemble. This definition can be used to obtain the dependence of the chemical potential of solute (2) μ_2^* on cosolute (3) concentration c_3 through the first law of thermodynamics and the total differential of the grand canonical ensemble:[126]

$$-\beta \left(\frac{\partial \mu_2^*}{\partial c_3} \right)_{p,T} = \frac{G_{23} - G_{21}}{1 + c_3(G_{33} + G_{31})} \tag{11}$$

where $\beta = 1/k_B T$. One example of uses of KB theory is the calculation of the compressibility (equation 12).

$$RT\kappa_T = \frac{1 + c_i G_{ii} + c_j G_{jj} + c_i c_j (G_{ii} G_{jj} - G_{ij}^2)}{c_i + c_j + c_i c_j (G_{ii} + G_{jj} - 2G_{ij})} \tag{12}$$

The KBI can also be calculated from rdfs, but one has to keep in mind that this expression is also only exact if the rdf is obtained in an open system.

$$G_{ij} \int_0^\infty \mathrm{d}r \left((g_{ij}(r) - 1 \right) 4\pi r^2 \tag{13}$$

Further examples are the calculation of molar volumes and the dependence of the excess chemical potential μ^* (solvation free energy) of one component on the concentration of another compo-

nent.[126] Furthermore, KB theory can be used to give information about excess numbers.[57,124] As an example we will take a binary solution of molecular components i and j.

The number of molecules N_i in a sphere with radius R_c (∞ for an open system, in which the KBIs are defined) in a binary solution without a fixed point can be calculated through

$$N_i = \rho_i \frac{4}{3}\pi R_c^3 \tag{14}$$

$$N_j = \rho_j \frac{4}{3}\pi R_c^3 \tag{15}$$

If we put the center of the observation volume on component i as shown in Fig. 2.4 we obtain the number N_i' in the observation volume, which can be calculated from the rdf.

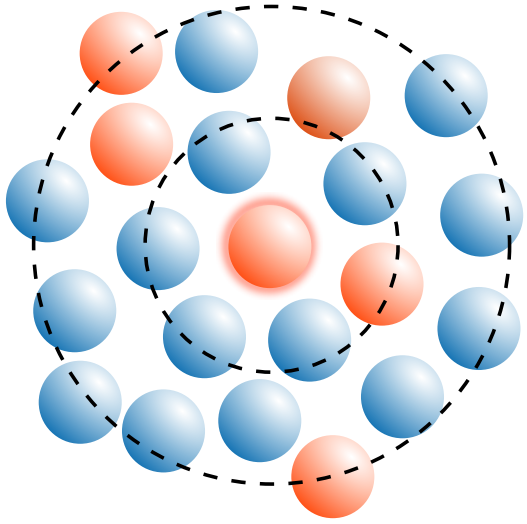

Figure 2.4: Distribution of component i in blue around a component j in orange. In this case the rdf g_{ij} would exhibit a big first peak due to the high accumulation of i around j.

$$N_i' = \int_0^{R_c} \mathrm{d}r \rho_i g_{ii}(r) 4\pi r^2 \tag{16}$$

$$N_j' = \int_0^{R_c} \mathrm{d}r \rho_j g_{ij}(r) 4\pi r^2 \tag{17}$$

The excess numbers ΔN_i and ΔN_j, which are related to the KBI, then give information about the affinity of molecules.

$$\Delta N_i = N_i' - N_i = \rho_i G_{ii} \tag{18}$$

$$\Delta N_j = N_j' - N_j = \rho_j G_{jj} \tag{19}$$

$$\Delta N_{ji} = N_j' - N_j = \rho_j G_{ji} \quad \text{with} \quad G_{ij} = G_{ji} \tag{20}$$

Additionally, the preferential binding of a cosolute to a solute in a cosolute-solvent mixture can be probed by the use of KBIs and thereby a equilibrium constant between two states determined, as is often done in our studies. The details are discussed in the next section.

4 Preferential Binding

The term preferential binding is commonly used in mixtures of a solvent and one or more cosolutes and a solute. It describes the excess of the cosolute around the solute compared to the solvent and is a thermodynamic property, which can also be understood in terms of Kirkwood-Buff theory (KB theory).[126]

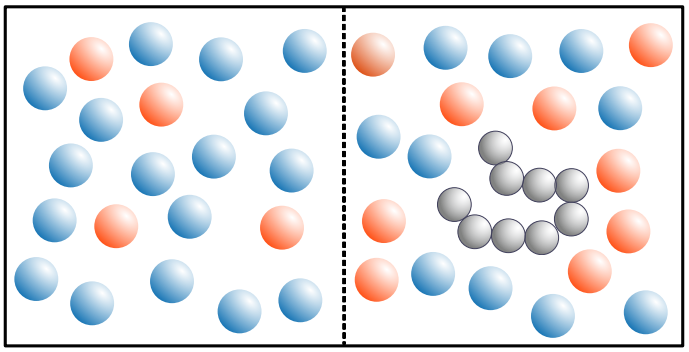

Figure 2.5: Schematic of the dialysis experiment. A solute (shown in grey) is given into one of the volume compartments separated by a semi-permeable membrane (dashed line). The cosolute (orange) and water (blue) concentration in the compartments will change due to preferential binding to the solute. This is measured in the experiment.

It can be understood by considering a dialysis experiment as seen in Fig. 2.5.[127] A volume is separated by a semi-permeable membrane, allowing water and a cosolute to pass through the membrane, but not the solute. The solute is added to one of the volume parts and the change in cosolute concentration is monitored. Taking this definition and using Schwarz's theorem the preferential binding parameter Γ_{23} is then described by

$$\Gamma_{23} = \left(\frac{\partial c_3}{\partial c_2}\right)_{p,T,\mu_3} = \left(\frac{\partial \mu_2}{\partial \mu_3}\right)_{p,T,c_2}$$

where 1 is the solvent, 2 is the solute and 3 is the cosolute, T is the temperature, and μ_i is the chemical potential of the molecule of type i.

Γ_{23} is connected to KB theory allowing conclusions about the excess of cosolutes around solutes through KBIs $G_{\alpha\beta}$, where α and β are solute, cosolute or solvent.[126]

$$\Gamma_{23} = c_3(G_{23} - G_{21}) \tag{21}$$

Here G_{23} and G_{21} are solute-cosolute and solute-water Kirkwood-Buff integrals, which are related to the radial distribution function.

$$G_{\alpha\beta} = G_{\beta\alpha} = 4\pi \int dr \left(g_{\alpha\beta}(r) - 1\right) r^2 \tag{22}$$

A positive preferential binding coefficient ($\Gamma_{23} > 0$) indicates preferential adsorption of the cosolute, while a negative preferential binding coefficient ($\Gamma_{23} < 0$) indicates the depletion of the cosolute from the solute surface (preferential hydration).

The preferential binding coefficient can be connected to the dependence of the solvation free energy ΔG of the solute on the cosolute concentration through the Wyman-Tanford relations for dilute solutions, which is applicable under fixed solute concentration c_2 in a dilute solution ($c_2 \to \infty$).[126,128,129]

$$\beta \left(\frac{\partial \Delta G}{\partial c_3}\right)_{p,T} = -\frac{\Gamma_{23}}{c_3(1 + c_3(G_{33} - G_{31}))} \tag{23}$$

where c_3 is the molar concentration of the cosolute, and p is the pressure. The term $1 + c_3(G_{33} - G_{31})$ in the denominator is always positive, if the cosolute and solvent form stable mixtures (then the Kirkwood-Buff theory can be used). Therefore, preferential adsorption ($\Gamma_{23} > 0$) of the cosolute leads to a decrease of the solvation free energy (increase in the solute solubility) with increase in cosolute concentration, while depletion of the cosolute from the solute interface ($\Gamma_{23} < 0$) leads to an increase of the solvation free energy (decrease in solute solubility) with an increase in cosolute concentration.

Consequently, the equilibrium between two states A $\rightleftharpoons$ B can be related to the difference in their preferential binding coefficients as it gives information about the free energy change of the equilibrium A $\rightleftharpoons$ B, $\Delta G^{A\to B}$, with cosolute concentration.

$$\begin{aligned} \beta \left(\frac{\partial \Delta G^{A\to B}}{\partial c_3}\right)_{p,T} &= -\frac{\Gamma_{23}^B - \Gamma_{23}^A}{c_3(1 + c_3(G_{33} - G_{31}))} \\ &= -\frac{\Delta\Gamma_{23}^{A\to B}}{c_3(1 + c_3(G_{33} - G_{31}))} \end{aligned} \tag{24}$$

The equilibrium shifts towards state B if the cosolute binds stronger to the solute in state B (or is less depleted from state B; $\Gamma_{23}^B > \Gamma_{23}^A$) and vice versa.

Commonly, the solvent is water and the solute is a protein or polymer. The preferential binding coefficient has been used to study protein folding equilibria (Folded protein $\rightleftharpoons$ Unfolded protein) and polymer collapse equilibria (Collapsed polymer $\rightleftharpoons$ Extended polymer).[61,66,130] Preferential binding/depletion and the cosolute effect on the equilibrium have been connected. In previous years the following explanation has been used to describe the effect of preferential binding on the equilibrium U $\rightleftharpoons$ F, where the equilibrium is shifted towards U if $\Delta\Gamma_{23}^{F\to U} > 0$ and vice versa: If

the cosolute accumulates around the solute it will bind stronger to the more extended surface (the unfolded protein state or extended polymer surface), since:

$$\begin{aligned} \Gamma_{23} &= n_{23}\left(1-\frac{1}{K_p}\right) \\ K_p &= \frac{\langle n_{23}\rangle}{\langle n_{21}\rangle}\cdot\frac{N_1}{N_3} \end{aligned} \tag{25}$$

where K_p is the local/bulk partition coefficient, an intensive quantity, N_i is the total number of molecules i in the system and n_i is the number of molecules i in the solute solvation shell and $\langle ...\rangle$ denotes a time average. Therefore, preferential binding should shift the equilibrium towards the unfolded (extended) state.[131,132] This argument has been used for denaturing cosolutes like urea and guanidinium chloride. In case of cosolute depletion, depletion from the unfolded (extended) state is larger (and therefore Γ_{23} more negative) to avoid protein-cosolute interactions. Therefore, depletion should shift the equilibrium towards the folded (collapsed) state.[68,133,134] However, this view has been challenged in recent years and the influence on the preferential cosolute binding is not as simple as previously believed.[19,130]

Γ_{23} can not only be determined by experiments, but also through simulations.[126] Similar to the KBI, Γ_{23} will converge for larger distances. Some assumptions have to be made to Eqn. 26 due to the use of closed systems in most MD simulations. The solute has to be at infinite dilution and since simulations are usually done at constant amount of molecules, the amount of bulk molecules have to be approximated by $N_i - n_i$, where N_i is the total number of molecules i in the system and n_i is the number of molecules i in the solute solvation shell. Therefore, Γ_{23} as a function of the proximal distance from the solute surface R is calculated by

$$\Gamma_{23}(R) = \left\langle n_{23}(R) - \frac{\rho_3}{\rho_1}\cdot n_{21}(R)\right\rangle \tag{26}$$

$$\Gamma_{23}(R) = \left\langle n_{23}(R) - \frac{N_3^{\mathrm{tot}} - n_{23}(R)}{N_1^{\mathrm{tot}} - n_{21}(R)}\cdot n_{21}(R)\right\rangle \tag{27}$$

Here, $\langle ...\rangle$ denotes a time average. The code at each time step is as follows:

```
#Proximal distance to the solute is binned into i bins.
 for current_distance_bin = 0, total_number_bins:
        number_TMAO(current_distance_bin) = 0
        number_water(current_distance_bin) = 0

#Take the oxygen atom of water as reference for counting water
 for water_oxygen_atoms = 0, total_number_water: #loop over water oxygen atoms
        smallest_distance = 300.0 #nm, very large number
```

```
        for solute_atom = 0, total_number_solute_atoms: #loop over solute atoms
                distance = pbc_distance(solute_atom, water_oxygen_atom)
                smallest distance = min(distance, smallest_distance) # The minimum
                   distance to the solute should be found at the end of the polymer
                    loop.
        bin_number = smallest_distance/bin_size # Check to which bin this water
           molecule belongs based on its distance to the solute.

        for at_distance = bin_number, total_number_bins:
                number_water(at_distance) += 1 #Add 1 to the number of water
                   molecules in this bin and all bins that are farer away from the
                   solute than this one (the number of molecules is cummulative).


#Take the nitrogen atom of TMAO as reference for counting TMAO
for TMAO_nitrogen_atoms = 0, total_number_TMAO: #loop over TMAO nitrogen atoms
        smallest_distance = 300.0 #nm, very large number
        for solute_atom = 0, total_number_solute_atoms: #loop over solute atoms
                distance = pbc_distance(solute_atom, water_oxygen_atom)
                smallest distance = min(distance, smallest_distance)
        bin_number = smallest_distance/bin_size # Check to which bin this TMAO
           molecule belongs based on its distance to the solute.


        for at_distance = bin_number, total_number_bins:
                number_TMAO(at_distance) += 1

for at_distance = 0, max_number_bins:
        Γ23(at_distance) = number_TMAO(at_distance) − (max_number_TMAO−number_TMAO(at_distance)) / (max_number_water−number_water(at_distance))
                        ·number_water(at_distance)
                  # Calculate Gamma from the formula as a function of the proximal
                     distance to the solute using the total number of TMAO and
                     water molecules and the calculated amount of TMAO and water
                     molecules in the distance bin. Average over time.
```

The preferential binding coefficient is then averaged over time and taken from the converged region (convergence signals that the threshold between bulk region and solvation shell´ has been reached). In this work, we use Γ_{23} to make prediction about ΔG and vice versa. We also try to understand whether the connection between preferential binding (depletion) and the shift of the folding/collapse equilibrium towards the unfolded/extended (folded/collapsed) state holds true as previously explained.

5 Free Energy Calculations

MD simulations are limited by the computational power. If high energy-barriers are present in the system, equilibration may not be possible in the limited simulation time (which is typically up to 1 μs). For example, the mini-protein TrpCage has a fast folding speed, so that it is used in many MD studies. Still, it folds in the μs time-scale, meaning that reaching an equilibrium distribution takes much longer than what is feasible using MD simulations.[135] Therefore, advanced sampling methods have to be used to gain informations about equilibrium distributions in MD simulations. I will describe the methods used in this thesis below.

5.1 Replica Exchange

Replica exchange is used to obtain trajectories, which follow the equilibrium distributions.[136] It combines MD simulations with a Monte Carlo methods. In replica exchange several MD simulations (replicas) are run in parallel spanning a temperature range. The simulations run independent from each other for a short time, but then an exchange attempt of the configurations between the replicas is made. This is shown in the schematic:

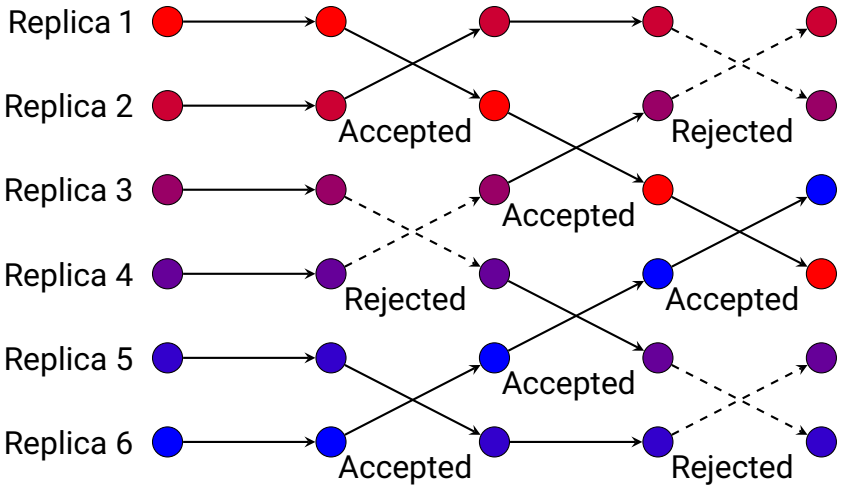

This attempt can be accepted or declined with the Metropolis criterion, which fulfills detailed balance. The acceptance probability P_{12} to exchange replica 1 and 2 is

$$P_{12} = \min(1, \exp\left(\left(\frac{1}{k_B T_1} - \frac{1}{k_B T_2}\right)(U_1 - U_2)\right) \tag{28}$$

where T_1 is the temperature of system 1, T_2 the temperature of system 2, U_1 the potential energy of system 1 and U_2 the potential energy of system 2. Therefore, if $T_1 > T_2$ and $U_2 > U_1$, then there is a guaranteed exchange. Velocities of the exchanged configurations are then scaled by $\sqrt{T_1/T_2}$

for replica 2 and vice versa for replica 1. The isobaric ensemble also contains an additional term to take volume differences into account,[137] but we will focus on the isochor example for simplicity.

Replica exchange is commonly used in protein simulation, where the folding/unfolding states are sampled across the temperatures and then made available to the other temperature replicas by exchanging configurations.

Here, we present a replica exchange study on TrpCage in chapter 7.

5.2 Free Energy Perturbation and Widom Particle Insertion

Free Energy Perturbation is used to calculate the free energy for going from state A to state B. If the phase space of system B is completely in the phase space of system A, as shown in Fig. 2.6, left side, then we only need accurate simulations of system A to get informations about occurences in state B. For example, we can conduct a simulation of water and then predict the solvation free energy of a small solute by computing the potential energy, that a solute would have if it was present in this water system. In practise, this is done by trying to insert the solute several times into different positions of a configuration at a fixed time and then averaging over the time frames. The excess chemical potential μ^* (or solvation free energy) is then calculated by:[138]

$$e^{-\beta\mu^*} = \langle e^{-\beta\Delta U} \rangle_0 \tag{29}$$

$$\mu^* = -\mathrm{k_B}T \ln \int \exp(-\beta\Delta U) P_0(\Delta U) d\Delta U \tag{30}$$

Here, $\beta = 1/\mathrm{k_B}T$, ΔU is the potential energy of the particle and the subscript 0 denotes averaging over a system of pure solvent (water). Therefore, the expression describes the potential energy of the particle if it was present in the system without the particle.

The water simulation also has to sample fluctuations, which open up space to fit the solute. It can be seen that if the particle is big and does not fit into any empty volume, insertion attempts will have only repulsive interactions, leading to the right side of the equation being 0 (very precise calculation, but wrong answer). This method is called Widom Particle Insertion and can only be used for small enough solutes. As fluctuations to create larger empty volume are not sampled well, this method may also provide wrong results for too small simulation times. This is due to bad sampling of the energy tails, which can lead to large errors as shown in Fig. 2.6.

Most often the phase spaces of A and B only partially overlap, as shown on the left side of Fig. 2.7. Therefore, other methods have to be used, where the solvation process is split into several steps and doing additional simulations of each intermediate state allows for better overlap of the phase space of adjacent systems.[139] For example, for the process of solvation it might be necessary to conduct simulations in which solute-solvent interactions are scaled between no and full interactions. The free energy of solvation is then the sum of the free energies calculated between each intermediates.

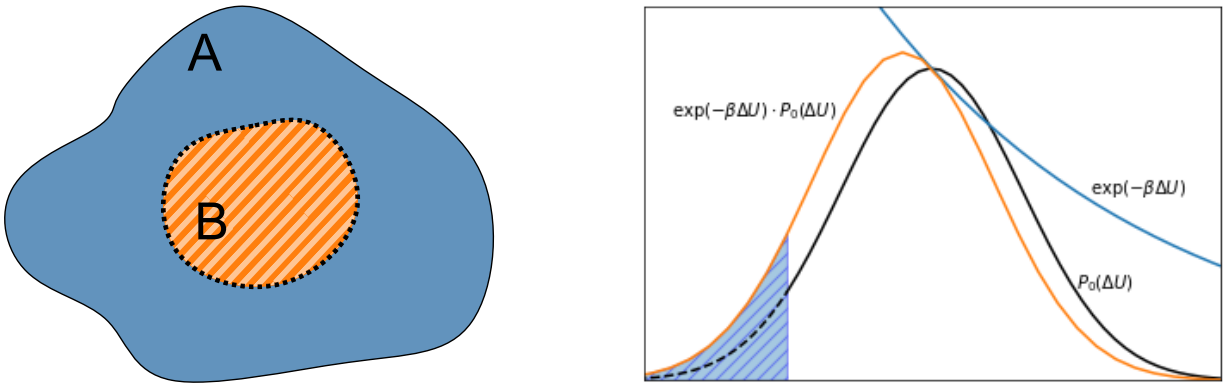

Figure 2.6: Visual representation of the free energy calculation using particle insertion. Left: The phase space of B is completely in the phase space of A, allowing a correct calculation of the free energy going from state A to B. Right: The probability distribution of the potential energy difference between state 1 and 0, obtained from sampling state 0 (pure solvent) has regions, where no sampling is achieved, here represented by the dashed part of the black line. When taking the integral of equation 30, which is the product of the exponential and the probability, a large portion of the integral is not taken into account due to the lack of sampling. This leads to errors in the calculation of the free energy.

One such method is exponential averaging, which can be used forward (sample 0, eqn. 29) or backward (sample 1, eqn. 31) to obtain the free energy to go from state 0 to 1.[140–142]

$$e^{\beta\mu^*} = \langle e^{\beta\Delta U} \rangle_1 \tag{31}$$

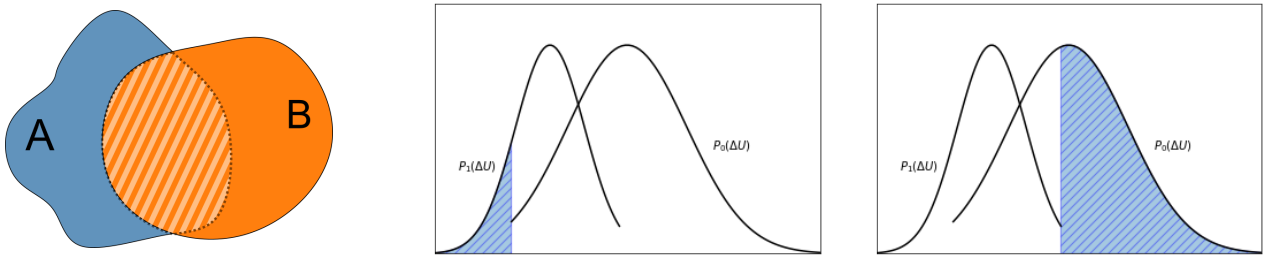

Figure 2.7: Visual representation of the free energy calculation using FEP between state 1 (A) and 0 (B), where the phase space only particlla overlaps (left) and the relative inaccurancy in the calculations. The probability distribution of the potential energy difference between state 1 and 0, obtained from sampling state 0 and state 1 respectively can not be fully sampled. When sampling from the broader distribution (P_0, middle) compared to the more narrow distribution (P_1, right) (e.g. particle insertion) it leads to smaller errors than vice versa (e.g. particle deletion).[142]

As with Widom Particle insertion, errors can occur due to bad sampling of the energy tails. This error is smaller if one chooses to use the broad distribution for the sampling as shown in Fig. 2.7. The error can also be reduced by sampling both states using a bidirectional method. This is used

in Bennetts Acceptance ratio (BAR), which will be used in this work several times.[143] BAR is the maximum likelihood estimator of the free energy for a given set of forward and reverse process (e.g. the insertion and deletion of a solute).[144] The derivation is based on minimizing the standard error and it has been proven to be superior compared to other free energy calculation methods.[145]

5.3 Thermodynamic Integration

Like FEP, thermodynamic integration (TI) is used to calculate the free energy of going from state A to state B using a scaling parameter λ, where the potential energy in the simulated system is calculated through[146]

$$U(\lambda) = U_{\mathrm{A}} + \lambda(U_{\mathrm{B}} - U_{\mathrm{A}}) \tag{32}$$

where $\lambda = 0$ corresponds to simulations of state A and $\lambda = 1$ corresponds to simulations of state B. Like in FEP, simulations of intermediate states have to be done for systems where A and B are very dissimilar. The free energy is then calculated by

$$\Delta F_{A\to B} = \int_0^1 \mathrm{d}\lambda \frac{\partial F(\lambda)}{\partial \lambda} = \int_0^1 \mathrm{d}\lambda \left\langle \frac{\partial U(\lambda)}{\partial \lambda} \right\rangle \tag{33}$$

The result can be obtained through numerical integration, so that the integration path should be as smooth as possible as shown in Fig. 2.8. Therefore, it is necessary to sample enough λ values.

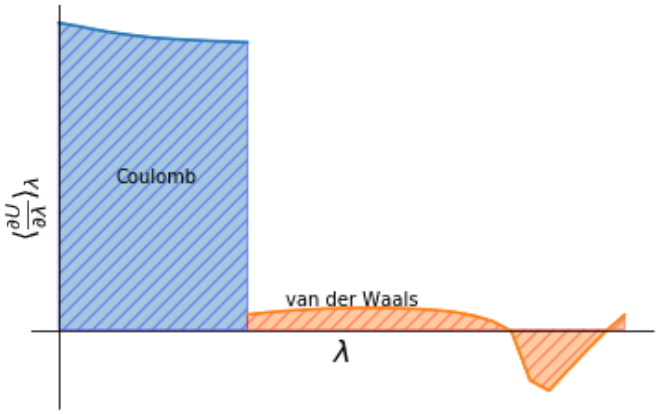

Figure 2.8: Example of thermodynamic integration. As λ increases, first coulomb interactions are turned off (blue area) and then van der Waals interactions (orange area). The integration path of the coulomb interactions is relatively smooth, but the contribution is very large (as seen from the blue area), so that small deviations may cause large errors. The van der Waals contributions are smaller than the coulomb contributions. Especially at very large λ values (where the solute is nearly not present anymore) the function shows some roughness, so that more sampling is necessary in this region.

One problem in inserting a solute into the solvent might be singularities. These appear in the first insertion windows, in which the solute will have a lot of overlaps with the present solvent. Both the Lennard-Jones potential and coulomb potential exhibit these so that convergence can only be achieved very slowly. This can be avoided by using so-called soft-core potentials, as is done in our studies.[147]

5.4 Umbrella Sampling

Umbrella sampling can be used to calculate the PMF along a certain path of the collective variable ξ, where large potential energy barriers lead to low sampling of certain states or lead to a configuration being trapped in a low energy state. This path may be the association of two molecules (ξ = distance) or the collapse of a polymer (ξ = Radius of Gyration). A bias potential $w(\xi)$ is introduced to sample all regions along the path. This bias potential is usually harmonic with a force constant k and forces ξ to be in the region of the point that should be sampled, ξ_0.[148]

$$U^B(\xi, R') = U(\xi, R') + w(\xi) \tag{34}$$

$$w(\xi) = k(\xi - \xi_0)^2 \tag{35}$$

The biased distrubtion is obtained from several simulations along the path.

$$V_{\mathrm{PMF}}(\xi) = -\mathrm{k_B}T \ln P(\xi) \tag{36}$$

$$V^b_{\mathrm{PMF}}(\xi) = -\mathrm{k_B}T \ln P^b(\xi) \tag{37}$$

$$V_{\mathrm{PMF}}(\xi) = -\mathrm{k_B}T \ln P^b(\xi) - w(\xi) + F \tag{38}$$

Here, b denotes the biased quantity, no superscript refers to the unbiased quantity, V_{PMF} is the PMF and $P(\xi)$ the distribution and F is an undetermined factor, which varies for each window. Solving the equation for $V_{\mathrm{PMF}}(\xi)$ gives the PMF. One method to analyze umbrella sampling is the weighted histogram analysis method (WHAM), which combines all windows and optimizes the estimation for F in each window iterativelly.[149,150]

$$P(\xi) = \frac{\sum_{i=1}^{N} h_i(\xi)}{\sum_{k=1}^{N} n_k \exp((F_k - U^b(\xi))/\mathrm{k_B}T)} \tag{39}$$

$$F_k = -\mathrm{k_B}T \ln \sum_{\xi} P(\xi) \exp(-w(\xi)/\mathrm{k_B}T) \tag{40}$$

Here, N is the number of umbrella windows, i and k are indices of these windows, $h(\xi)$ is the number of counts in the histogram at the bin ξ, n_k the number of data points of window k and F_k is the undetermined factor for the window k.

Some care is required as to the choice of the reaction coordinate ξ. For example, if we take the radius of gyration R_g of a polymer chain and sample low R_g values, we might only sample one globular state. The chain cannot extend and re-collapse so that we neglect the free energy contribution from other possible globular states. If there is access to a good reaction coordinate, umbrella sampling is one of the cheapest methods to obtain information about phase transitions.

Bibliography

[1] Daniel, I.; Oger, P.; Winter, R. Origins of life and biochemistry under high-pressure conditions. *Chem. Soc. Rev.* **2006**, *35*, 858–875.

[2] Wang, B.; Zhang, L.; Dai, T.; Qin, Z.; Lu, H.; Zhang, L.; Zhou, F. Liquid–liquid phase separation in human health and diseases. *Sign. Transduct. Target. Ther.* **2021**, *6*, 1–16.

[3] Yancey, P. H.; Gerringer, M. E.; Drazen, J. C.; Rowden, A. A.; Jamieson, A. Marine fish may be biochemically constrained from inhabiting the deepest ocean depths. *Proc. Natl. Acad. Sci. U.S.A.* **2014**, *111*, 4461–4465.

[4] Yancey, P. H.; Blake, W. R.; Conley, J. Unusual organic osmolytes in deep-sea animals: adaptations to hydrostatic pressure and other perturbants. *Comp. Biochem. Physiol. Part A Mol. Integr. Physiol.* **2002**, *133*, 667–676.

[5] Yancey, P. H.; Fyfe-Johnson, A. L.; Kelly, R. H.; Walker, V. P.; Auñón, M. T. Trimethylamine oxide counteracts effects of hydrostatic pressure on proteins of deep-sea teleosts. *J. Exp. Zool.* **2001**, *289*, 172–176.

[6] Julius, K.; Al-Ayoubi, S. R.; Paulus, M.; Tolan, M.; Winter, R. The effects of osmolytes and crowding on the pressure-induced dissociation and inactivation of dimeric LADH. *Phys. Chem. Chem. Phys.* **2018**, *20*, 7093–7104.

[7] Sung, H.-L.; Nesbitt, D. J. High pressure single-molecule FRET studies of the lysine riboswitch: cationic and osmolytic effects on pressure induced denaturation. *Phys. Chem. Chem. Phys.* **2020**, *22*, 15853–15866.

[8] Smolin, N.; Voloshin, V. P.; Anikeenko, A. V.; Geiger, A.; Winter, R.; Medvedev, N. N. TMAO and urea in the hydration shell of the protein SNase. *Phys. Chem. Chem. Phys.* **2017**, *19*, 6345–6357.

[9] Cinar, H.; Fetahaj, Z.; Cinar, S.; Vernon, R. M.; Chan, H. S.; Winter, R. H. A. Temperature, Hydrostatic Pressure, and Osmolyte Effects on Liquid–Liquid Phase Separation in Protein Condensates: Physical Chemistry and Biological Implications. *Chem. Eur. J.* **2019**, *25*, 13049–13069.

[10] Möller, J.; Grobelny, S.; Schulze, J.; Bieder, S.; Steffen, A.; Erlkamp, M.; Paulus, M.; Tolan, M.; Winter, R. Reentrant liquid-liquid phase separation in protein solutions at elevated hydrostatic pressures. *Phys. Rev. Lett.* **2014**, *112*, 028101.

[11] Cinar, S.; Cinar, H.; Chan, H. S.; Winter, R. Pressure-sensitive and osmolyte-modulated liquid–liquid phase separation of eye-lens γ-crystallins. *J. Am. Chem. Soc.* **2019**, *141*, 7347–7354.

[12] Cinar, H.; Winter, R. The effects of cosolutes and crowding on the kinetics of protein condensate formation based on liquid–liquid phase separation: a pressure-jump relaxation study. *Sci. Rep.* **2020**, *10*, 1–16.

[13] Imoto, S.; Forbert, H.; Marx, D. Aqueous TMAO solutions as seen by theoretical THz spectroscopy: hydrophilic versus hydrophobic water. *Phys. Chem. Chem. Phys.* **2018**, *20*, 6146–6158.

[14] Imoto, S.; Kibies, P.; Rosin, C.; Winter, R.; Kast, S. M.; Marx, D. Toward Extreme Biophysics: Deciphering the Infrared Response of Biomolecular Solutions at High Pressures. *Angew. Chem. Int. Ed.* **2016**, *55*, 9534–9538.

[15] Hölzl, C.; Kibies, P.; Imoto, S.; Frach, R.; Suladze, S.; Winter, R.; Marx, D.; Horinek, D.; Kast, S. M. Design principles for high–pressure force fields: Aqueous TMAO solutions from ambient to kilobar pressures. *J. Chem. Phys.* **2016**, *144*, 144104.

[16] Su, Z.; Mahmoudinobar, F.; Dias, C. L. Effects of Trimethylamine-*N*-oxide on the Conformation of Peptides and its Implications for Proteins. *Phys. Rev. Lett.* **2017**, *119*, 108102.

[17] Su, Z.; Ravindhran, G.; Dias, C. L. Effects of Trimethylamine-N-oxide (TMAO) on Hydrophobic and Charged Interactions. *J. Phys. Chem. B* **2018**, *122*, 5557–5566.

[18] Ma, J.; Pazos, I. M.; Gai, F. Microscopic insights into the protein-stabilizing effect of trimethylamine N-oxide (TMAO). *Proc. Natl. Acad. Sci. U.S.A.* **2014**, *111*, 8476–8481.

[19] Mondal, J.; Halverson, D.; Li, I. T.; Stirnemann, G.; Walker, G. C.; Berne, B. J. How osmolytes influence hydrophobic polymer conformations: A unified view from experiment and theory. *Proc. Natl. Acad. Sci. U.S.A.* **2015**, *112*, 9270–9275.

[20] Rodríguez-Ropero, F.; Ro tzscher, P.; van der Vegt, N. F. Comparison of different TMAO force fields and their impact on the folding equilibrium of a hydrophobic polymer. *J. Phys. Chem. B* **2016**, *120*, 8757–8767.

[21] Dill, K. A. Dominant forces in protein folding. *Biochemistry* **1990**, *29*, 7133–7155.

[22] Dannenhoffer-Lafage, T.; Best, R. B. A Data-Driven Hydrophobicity Scale for Predicting Liquid–Liquid Phase Separation of Proteins. *J. Phys. Chem. B* **2021**, *125*, 4046–4056.

[23] Dignon, G. L.; Best, R. B.; Mittal, J. Biomolecular phase separation: From molecular driving forces to macroscopic properties. *Annu. Rev. Phys. Chem.* **2020**, *71*, 53–75.

[24] Street, T. O.; Bolen, D. W.; Rose, G. D. A molecular mechanism for osmolyte-induced protein stability. *Proc. Natl. Acad. Sci. U.S.A.* **2006**, *103*, 13997–14002.

[25] Tanford, C. Protein denaturation. *Adv. Protein Chem* **1970**, *24*, 95.

[26] Liu, Y.; Bolen, D. W. The Peptide Backbone Plays a Dominant Role in Protein Stabilization by Naturally Occurring Osmolytes. *Biochemistry* **1995**, *34*, 12884–12891.

[27] Lin, T.-Y.; Timasheff, S. N. Why do some organisms use a urea-methylamine mixture as osmolyte? Thermodynamic compensation of urea and trimethylamine N-oxide interactions with protein. *Biochemistry* **1994**, *33*, 12695–12701.

[28] Courtenay, E. S.; Capp, M. W.; Anderson, C. F.; Record, M. T. Vapor Pressure Osmometry Studies of Osmolyte Protein Interactions: Implications for the Action of Osmoprotectants in Vivo and for the Interpretation of Osmotic Stress Experiments in Vitro. *Biochemistry* **2000**, *39*, 4455–4471.

[29] Hong, J.; Xiong, S. TMAO-Protein Preferential Interaction Profile Determines TMAO's Conditional In Vivo Compatibility. *Biophys. J.* **2016**, *111*, 1866 – 1875.

[30] Auton, M.; Bolen, D. W.; Rösgen, J. Structural thermodynamics of protein preferential solvation: Osmolyte solvation of proteins, aminoacids, and peptides. *Proteins: Struct. Funct. Genet.* **2008**, *73*, 802–813.

[31] Auton, M.; Rösgen, J.; Sinev, M.; Holthauzen, L. M. F.; Bolen, D. W. Osmolyte effects on protein stability and solubility: a balancing act between backbone and side-chains. *Biophys. Chem.* **2011**, *159*, 90–99.

[32] Shimizu, S.; Boon, C. L. The Kirkwood–Buff theory and the effect of cosolvents on biochemical reactions. *J. Chem. Phys.* **2004**, *121*, 9147–9155.

[33] Davis-Searles, P. R.; Saunders, A. J.; Erie, D. A.; Winzor, D. J.; Pielak, G. J. Interpreting the effects of small uncharged solutes on protein-folding equilibria. *Annu. Rev. Biophys. Biomol. Struct.* **2001**, *30*, 271–306.

[34] Chilson, O. P.; Chilson, A. E. Perturbation of folding and reassociation of lactate dehydrogenase by proline and trimethylamine oxide. *Eur. J. Biochem.* **2003**, *270*, 4823–4834.

[35] Rani, A.; Venkatesu, P. Changing relations between proteins and osmolytes: a choice of nature. *Phys. Chem. Chem. Phys.* **2018**, *20*, 20315–20333.

[36] Rani, A.; Jayaraj, A.; Jayaram, B.; Pannuru, V. Trimethylamine-N-oxide switches from stabilizing nature: A mechanistic outlook through experimental techniques and molecular dynamics simulation. *Sci. Rep.* **2016**, *6*, 1–14.

[37] Mukherjee, M.; Mondal, J. Osmolyte-Induced Collapse of a Charged Macromolecule. *J. Phys. Chem. B* **2019**, *123*, 4636–4644.

[38] Govrin, R.; Tcherner, S.; Obstbaum, T.; Sivan, U. Zwitterionic Osmolytes Resurrect Electrostatic Interactions Screened by Salt. *J. Am. Chem. Soc.* **2018**, *140*, 14206–14210.

[39] Rydeen, A. E.; Brustad, E. M.; Pielak, G. J. Osmolytes and Protein–Protein Interactions. *J. Am. Chem. Soc.* **2018**, *140*, 7441–7444.

[40] Borgohain, G.; Paul, S. Atomistic level understanding of the stabilization of protein Trp cage in denaturing and mixed osmolyte solutions. *Comput. Theor. Chem.* **2018**, *1131*, 78–89.

[41] Ganguly, P.; Boserman, P.; van der Vegt, N. F. A.; Shea, J.-E. Trimethylamine N-oxide Counteracts Urea Denaturation by Inhibiting Protein–Urea Preferential Interaction. *J. Am. Chem. Soc.* **2018**, *140*, 483–492.

[42] Auton, M.; Bolen, D. W. Predicting the energetics of osmolyte-induced protein folding/unfolding. *Proc. Natl. Acad. Sci. U.S.A.* **2005**, *102*, 15065–15068.

[43] Hu, C. Y.; Kokubo, H.; Lynch, G. C.; Bolen, D. W.; Pettitt, B. M. Backbone additivity in the transfer model of protein solvation. *Prot. Sci.* **2010**, *19*, 1011–1022.

[44] Folberth, A.; Bharadwaj, S.; van der Vegt, N. F. A. Small-to-large length scale transition of TMAO interaction with hydrophobic solutes. *Phys. Chem. Chem. Phys.* **2022**, *24*, 2080–2087.

[45] Zou, Q.; Bennion, B. J.; Daggett, V.; Murphy, K. P. The molecular mechanism of stabilization of proteins by TMAO and its ability to counteract the effects of urea. *J. Am. Chem. Soc.* **2002**, *124*, 1192–1202.

[46] Ashbaugh, H. S.; Truskett, T. M.; Debenedetti, P. G. A simple molecular thermodynamic theory of hydrophobic hydration. *J. Chem. Phys.* **2002**, *116*, 2907–2921.

[47] Blokzijl, W.; Engberts, J. B. F. N. Hydrophobic Effects. Opinions and Facts. *Angew. Chem. Int. Ed.* **1993**, *32*, 1545–1579.

[48] Widom, B.; Bhimalapuram, P.; Koga, K. The hydrophobic effect. *Phys. Chem. Chem. Phys.* **2003**, *5*, 3085–3093.

[49] Naghibi, H.; Dec, S. F.; Gill, S. J. Heat of solution of methane in water from 0 to 50.degree.C. *J. Phys. Chem.* **1986**, *90*, 4621–4623.

[50] Ben-Amotz, D.; Widom, B. Generalized solvation heat capacities. *J. Phys. Chem. B* **2006**, *110*, 19839–19849.

[51] Patel, A. J.; Varilly, P.; Chandler, D. Fluctuations of water near extended hydrophobic and hydrophilic surfaces. *J. Phys. Chem. B* **2010**, *114*, 1632–1637.

[52] Rajamani, S.; Truskett, T. M.; Garde, S. Hydrophobic hydration from small to large length-scales: Understanding and manipulating the crossover. *Proc. Natl. Acad. Sci. U.S.A.* **2005**, *102*, 9475–9480.

[53] Hillyer, M. B.; Gibb, B. C. Molecular shape and the hydrophobic effect. *Annu. Rev. Phys. Chem.* **2016**, *67*, 307–329.

[54] Berne, B. J.; Weeks, J. D.; Zhou, R. Dewetting and hydrophobic interaction in physical and biological systems. *Annu. Rev. Phys. Chem.* **2009**, *60*, 85–103.

[55] Wu, X.; Lu, W.; Streacker, L. M.; Ashbaugh, H. S.; Ben-Amotz, D. Temperature-dependent hydrophobic crossover length scale and water tetrahedral order. *J. Phys. Chem. Lett.* **2018**, *9*, 1012–1017.

[56] Rogers, B. A.; Okur, H. I.; Yan, C.; Yang, T.; Heyda, J.; Cremer, P. S. Weakly hydrated anions bind to polymers but not monomers in aqueous solutions. *Nat. Chem.* **2022**, *14*, 40–45.

[57] Ben-Naim, A. Y. *Solvation Thermodynamics*; Springer Science & Business Media, 1987.

[58] Cozzolino, S.; Oliva, R.; Graziano, G.; Del Vecchio, P. Counteraction of denaturant-induced protein unfolding is a general property of stabilizing agents. *Phys. Chem. Chem. Phys.* **2018**, *20*, 29389–29398.

[59] Vigorita, M.; Cozzolino, S.; Oliva, R.; Graziano, G.; Del Vecchio, P. Counteraction ability of TMAO toward different denaturing agents. *Biopolymers* **2018**, *109*, e23104.

[60] Sagle, L. B.; Cimatu, K.; Litosh, V. A.; Liu, Y.; Flores, S. C.; Chen, X.; Yu, B.; Cremer, P. S. Methyl Groups of Trimethylamine N-Oxide Orient Away from Hydrophobic Interfaces. *J. Am. Chem. Soc.* **2011**, *133*, 18707–18712.

[61] Liao, Y.-T.; Manson, A. C.; DeLyser, M. R.; Noid, W. G.; Cremer, P. S. Trimethylamine-N-oxide stabilizes proteins via a distinct mechanism compared with betaine and glycine. *Proc. Natl. Acad. Sci. U.S.A.* **2017**, *114*, 2479–2484.

[62] Anand, G.; Jamadagni, S. N.; Garde, S.; Belfort, G. Self-Assembly of TMAO at Hydrophobic Interfaces and Its Effect on Protein Adsorption: Insights from Experiments and Simulations. *Langmuir* **2010**, *26*, 9695–9702.

[63] Athawale, M. V.; Dordick, J. S.; Garde, S. Osmolyte Trimethylamine-N-Oxide Does Not Affect the Strength of Hydrophobic Interactions: Origin of Osmolyte Compatibility. *Biophys. J.* **2005**, *89*, 858–866.

[64] Sarma, R.; Paul, S. The effect of aqueous solutions of trimethylamine-N-oxide on pressure induced modifications of hydrophobic interactions. *J. Chem. Phys.* **2012**, *137*, 094502.

[65] Sarma, R.; Paul, S. Effect of trimethylamine-N-oxide on pressure-induced dissolution of hydrophobic solute. *J. Chem. Phys.* **2012**, *137*, 114503.

[66] Mukherjee, M.; Mondal, J. Unifying the Contrasting Mechanisms of Protein-Stabilizing Osmolytes. *J. Phys. Chem. B* **2020**, *124*, 6565–6574.

[67] Mukherjee, M.; Mondal, J. Osmolyte-induced macromolecular aggregation is length-scale dependent. *J. Phys. Chem. B* **2019**, *123*, 8697–8703.

[68] Cho, S. S.; Reddy, G.; Straub, J. E.; Thirumalai, D. Entropic stabilization of proteins by TMAO. *J. Phys. Chem. B* **2011**, *115*, 13401–13407.

[69] Oprzeska-Zingrebe, E. A.; Smiatek, J. Aqueous Mixtures of Urea and Trimethylamine-N-oxide: Evidence for Kosmotropic or Chaotropic Behavior? *J. Phys. Chem. B* **2019**, *123*, 4415–4424.

[70] Freda, M.; Onori, G.; Santucci, A. Hydrophobic hydration and hydrophobic interaction in aqueous solutions of tert-butyl alcohol and trimethylamine-N-oxide: a correlation with the effect of these two solutes on the micellization process. *Phys. Chem. Chem. Phys.* **2002**, *4*, 4979–4984.

[71] Sinibaldi, R.; Casieri, C.; Melchionna, S.; Onori, G.; Segre, A. L.; Viel, S.; Mannina, L.; De Luca, F. The Role of Water Coordination in Binary Mixtures. A Study of Two Model Amphiphilic Molecules in Aqueous Solutions by Molecular Dynamics and NMR. *J. Phys. Chem. B* **2006**, *110*, 8885–8892.

[72] Hunger, J.; Tielrooij, K.-J.; Buchner, R.; Bonn, M.; Bakker, H. J. Complex Formation in Aqueous Trimethylamine-N-oxide (TMAO) Solutions. *J. Phys. Chem. B* **2012**, *116*, 4783–4795.

[73] Zetterholm, S. G.; Verville, G. A.; Boutwell, L.; Boland, C.; Prather, J. C.; Bethea, J.; Cauley, J.; Warren, K. E.; Smith, S. A.; Magers, D. H.; Hammer, N. I. Noncovalent Interactions between Trimethylamine N-Oxide (TMAO), Urea, and Water. *J. Phys. Chem. B* **2018**, *122*, 8805–8811.

[74] Meersman, F.; Bowron, D.; Soper, A. K.; Koch, M. H. Counteraction of Urea by Trimethylamine N-Oxide Is Due to Direct Interaction. *Biophys. J.* **2009**, *97*, 2559–2566.

[75] Downing, A. B.; Wallace, G. T.; Yancey, P. H. Organic osmolytes of amphipods from littoral to hadal zones: Increases with depth in trimethylamine N-oxide, scyllo-inositol and other potential pressure counteractants. *Deep Sea Res. Part I: Oceanogr. Res. Pap.* **2018**, *138*, 1–10.

[76] Martin, D.; Bartlett, D. H.; Roberts, M. F. Solute accumulation in the deep-sea bacterium Photobacterium profundum. *Extremophiles* **2002**, *6*, 507–514.

[77] Voloshin, V. P.; Medvedev, N. N.; Smolin, N.; Geiger, A.; Winter, R. Exploring volume, compressibility and hydration changes of folded proteins upon compression. *Phys. Chem. Chem. Phys.* **2015**, *17*, 8499–8508.

[78] Del Galdo, S.; Amadei, A. The unfolding effects on the protein hydration shell and partial molar volume: a computational study. *Phys. Chem. Chem. Phys.* **2016**, *18*, 28175–28182.

[79] Avagyan, S.; Vasilchuk, D.; Makhatadze, G. I. Protein adaptation to high hydrostatic pressure: Computational analysis of the structural proteome. *Proteins* **2020**, *88*, 584–592.

[80] Papini, C. M.; Pandharipande, P. P.; Royer, C. A.; Makhatadze, G. I. Putting the Piezolyte Hypothesis under Pressure. *Biophys. J.* **2017**, *113*, 974–977.

[81] Steinbrecher, T. *Protein Ligand Interactions*; John Wiley & Sons, Ltd, 2012; Chapter 11, pp 207–236.

[82] Michel, J.; Essex, J. W. Prediction of protein–ligand binding affinity by free energy simulations: assumptions, pitfalls and expectations. *J. Comput-Aided Mol. Des.* **2010**, *24*, 639–658.

[83] ten Wolde, P. R.; Frenkel, D. Computer simulation study of gas–liquid nucleation in a Lennard-Jones system. *J. Chem. Phys.* **1998**, *109*, 9901–9918.

[84] Snow, C. D.; Zagrovic, B.; Pande, V. S. The Trp cage: folding kinetics and unfolded state topology via molecular dynamics simulations. *J. Am. Chem. Soc.* **2002**, *124*, 14548–14549.

[85] Shayeghi, A.; Götz, D.; Davis, J. B. A.; Schäfer, R.; Johnston, R. L. Pool-BCGA: a parallelised generation-free genetic algorithm for the ab initio global optimisation of nanoalloy clusters. *Phys. Chem. Chem. Phys.* **2015**, *17*, 2104–2112.

[86] Gamow, G. Zur Quantentheorie des Atomkernes. *Z. Phys.* **1928**, *51*, 204–212.

[87] Kuhn, H. Analogieversuche mit schwingenden Membranen zur Ermittlung von Elektronenzuständen in Farbstoffmolekülen mit verzweigtem Elektronengas. *Z. Elektrochem. angew. phys. Chem.* **1951**, *55*, 220–225.

[88] Kopineck, H.-J. Zweizentrenintegrale mit 2 s-und 2p-Funktionen II Ionenintegrale. *Z. für Naturforsch. A* **1951**, *6*, 177–183.

[89] Hartmann, H. *Theorie der Chemischen Bindung*; Springer, 1954; Vol. 5.

[90] Publisher's note: Sir John A. Pople, 1925–2004. *J. Comput. Chem.* **2004**, *25*, fmv–viii.

[91] Moore, E. A.; Sutcliffe, B. T.; Pakiari, A. H. In *Chemical Modelling*; Hinchliffe, A., Ed.; SPR - Chemical Modelling; The Royal Society of Chemistry, 2009; Vol. 5; pp 1–487.

[92] Maginn, E. J.; Elliott, J. R. Historical Perspective and Current Outlook for Molecular Dynamics As a Chemical Engineering Tool. *Ind. Eng. Chem. Res.* **2010**, *49*, 3059–3078.

[93] Frenkel, D.; Smit, B. *Understanding Molecular Simulation: From Algorithms to Applications*, 2nd ed.; Computational Science Series; Academic Press: San Diego, 2002; Vol. 1.

[94] Fermi, E.; Pasta, J.; Ulam, S. Studies of Nonlinear problems. *Enrico Fermi Collection* **1955**,

[95] Alder, B. J.; Wainwright, T. E. Phase Transition for a Hard Sphere System. *J. Chem. Phys.* **1957**, *27*, 1208–1209.

[96] Rapaport, D. Molecular dynamics simulation of polymer chains with excluded volume. *J. Phys. A: Math. Gen.* **1978**, *11*, L213.

[97] Rahman, A. Correlations in the motion of atoms in liquid argon. *Phys. Rev.* **1964**, *136*, A405.

[98] Yarnell, J. L.; Katz, M. J.; Wenzel, R. G.; Koenig, S. H. Structure Factor and Radial Distribution Function for Liquid Argon at 85 °K. *Phys. Rev. A* **1973**, *7*, 2130–2144.

[99] Woodcock, L.-V. Isothermal molecular dynamics calculations for liquid salts. *Chem. Phys. Lett.* **1971**, *10*, 257–261.

[100] de Leeuw, S. W.; Perram, J. W.; Smith, E. R. Simulation of electrostatic systems in periodic boundary conditions. I. Lattice sums and dielectric constants. *Proc. R. Soc. Lond. A Math. Phys. Sci.* **1980**, *373*, 27–56.

[101] Ryckaert, J.-P.; Ciccotti, G.; Berendsen, H. J. Numerical integration of the cartesian equations of motion of a system with constraints: molecular dynamics of n-alkanes. *J. Comput. Phys.* **1977**, *23*, 327–341.

[102] Stillinger, E. Molecular Dynamics Study of Liquid Water. *J. Chem. Phys* **1971**, *55*, 3336.

[103] Zwanzig, R. W. High Temperature Equation of State by a Perturbation Method. I. Nonpolar Gases. *J. Chem. Phys.* **1954**, *22*, 1420–1426.

[104] Singh, U. C.; Brown, F. K.; Bash, P. A.; Kollman, P. A. An approach to the application of free energy perturbation methods using molecular dynamics: applications to the transformations of methanol $\longrightarrow$ ethane, oxonium $\longrightarrow$ ammonium, glycine $\longrightarrow$ alanine, and alanine $\longrightarrow$ phenylalanine in aqueous solution and to $H_3O^+(H_2O)_3 \longrightarrow NH_4^+(H_2O)_3$ in the gas phase. *J. Am. Chem. Soc.* **1987**, *109*, 1607–1614.

[105] Bekker, H.; Berendsen, H.; Dijkstra, E.; Achterop, S.; Vondrumen, R.; van der Spoel, D.; Sijbers, A.; Keegstra, H.; Renardus, M. GROMACS - A PARALLEL COMPUTER FOR MOLECULAR-DYNAMICS SIMULATIONS. Physics Computing '92. 1993; pp 252–256, 4th International Conference on Computational Physics (PC 92) ; Conference date: 24-08-1992 Through 28-08-1992.

[106] Salomon-Ferrer, R.; Case, D. A.; Walker, R. C. An overview of the Amber biomolecular simulation package. *WIREs Comput. Mol. Sci.* **2013**, *3*, 198–210.

[107] Plimpton, S. Fast Parallel Algorithms for Short-Range Molecular Dynamics. *J. Comput. Phys.* **1995**, *117*, 1–19.

[108] Levitt, M. A simplified representation of protein conformations for rapid simulation of protein folding. *J. Mol. Biol.* **1976**, *104*, 59–107.

[109] Karplus, M.; Kuriyan, J. Molecular dynamics and protein function. *Proc. Natl. Acad. Sci. U.S.A.* **2005**, *102*, 6679–6685.

[110] Zimmerman, M. I. *et al.* SARS-CoV-2 simulations go exascale to predict dramatic spike opening and cryptic pockets across the proteome. *Nat. Chem.* **2021**, *13*, 651–659.

[111] Kast, K. M.; Brickmann, J.; Kast, S. M.; Berry, R. S. Binary Phases of Aliphatic N-Oxides and Water: Force Field Development and Molecular Dynamics Simulation. *J. Phys. Chem. A* **2003**, *107*, 5342–5351.

[112] Moss, G. P. Basic terminology of stereochemistry (IUPAC Recommendations 1996). *Pure Appl. Chem.* **1996**, *68*, 2193–2222.

[113] Weeks, J. D.; Chandler, D.; Andersen, H. C. Role of Repulsive Forces in Determining the Equilibrium Structure of Simple Liquids. *J. Chem. Phys.* **1971**, *54*, 5237–5247.

[114] Parrinello, M.; Rahman, A. Polymorphic transitions in single crystals: A new molecular dynamics method. *J. Appl. Phys.* **1981**, *52*, 7182–7190.

[115] Nosé, S. A molecular dynamics method for simulations in the canonical ensemble. *Mol. Phys.* **1984**, *52*, 255–268.

[116] Cuendet, M. A.; van Gunsteren, W. F. On the calculation of velocity-dependent properties in molecular dynamics simulations using the leapfrog integration algorithm. *J. Chem. Phys.* **2007**, *127*, 184102.

[117] Young, P. MS Windows NT The leapfrog method and other "symplectic" algorithms for integrating Newton's laws of motion. Accessed: 2021-12-07.

[118] Berendsen, H. J.; Postma, J. P.; Van Gunsteren, W. F.; DiNola, A.; Haak, J. R. Molecular dynamics with coupling to an external bath. *J. Chem. Phys.* **1984**, *81*, 3684–3690.

[119] Morishita, T. Fluctuation formulas in molecular-dynamics simulations with the weak coupling heat bath. *J. Chem. Phys.* **2000**, *113*, 2976–2982.

[120] Baldwin, R. L.; Rose, G. D. How the hydrophobic factor drives protein folding. *Proc. Natl. Acad. Sci. U.S.A.* **2016**, *113*, 12462–12466.

[121] Kauzmann, W. In *Some Factors in the Interpretation of Protein Denaturation11The preparation of this article has been assisted by a grant from the National Science Foundation.*; Anfinsen, C., Anson, M., Bailey, K., Edsall, J. T., Eds.; Advances in Protein Chemistry; Academic Press, 1959; Vol. 14; pp 1–63.

[122] Rodríguez-Ropero, F.; van der Vegt, N. F. A. On the urea induced hydrophobic collapse of a water soluble polymer. *Phys. Chem. Chem. Phys.* **2015**, *17*, 8491–8498.

[123] Ben-Naim, A. *Molecular Theory of Water and Aqueous Solutions*; World Scientific Publishing Company, 2011.

[124] Ben-Naim, A. *Molecular theory of solutions*; Oxford University Press, 2006.

[125] Koga, K.; Yamamoto, N. Hydrophobicity Varying with Temperature, Pressure, and Salt Concentration. *J. Phys. Chem. B* **2018**, *122*, 3655–3665.

[126] Pierce, V.; Kang, M.; Aburi, M.; Weerasinghe, S.; Smith, P. E. Recent Applications of Kirkwood–Buff Theory to Biological Systems. *Cell Biochem. Biophys.* **2008**, *50*, 1–22.

[127] Timasheff, S. N. Protein-solvent preferential interactions, protein hydration, and the modulation of biochemical reactions by solvent components. *Proc. Natl. Acad. Sci. U.S.A.* **2002**, *99*, 9721–9726.

[128] Wyman, J. Linked Functions and Reciprocal Effects in Hemoglobin: A Second Look. *Adv. Prot. Chem.* **1964**, *19*, 223 – 286.

[129] Tanford, C. Extension of the theory of linked functions to incorporate the effects of protein hydration. *J. Mol. Biol.* **1969**, *39*, 539–544.

[130] Nayar, D.; Folberth, A.; van der Vegt, N. F. A. Molecular origin of urea driven hydrophobic polymer collapse and unfolding depending on side chain chemistry. *Phys. Chem. Chem. Phys.* **2017**, *19*, 18156–18161.

[131] Timasheff, S. N. Water as ligand: preferential binding and exclusion of denaturants in protein unfolding. *Biochemistry* **1992**, *31*, 9857–9864.

[132] Canchi, D. R.; Paschek, D.; García, A. E. Equilibrium Study of Protein Denaturation by Urea. *J. Am. Chem. Soc.* **2010**, *132*, 2338–2344.

[133] Bolen, D. W.; Rose, G. D. Structure and Energetics of the Hydrogen-Bonded Backbone in Protein Folding. *Annu. Rev. Biochem.* **2008**, *77*, 339–362.

[134] Chalikian, T. V. Excluded volume contribution to cosolvent-mediated modulation of macromolecular folding and binding reactions. *Biophys. Chem.* **2016**, *209*, 1 – 8.

[135] Byrne, A.; Williams, D. V.; Barua, B.; Hagen, S. J.; Kier, B. L.; Andersen, N. H. Folding Dynamics and Pathways of the Trp-Cage Miniproteins. *Biochemistry* **2014**, *53*, 6011–6021.

[136] Sugita, Y.; Okamoto, Y. Replica-exchange molecular dynamics method for protein folding. *Chem. Phys. Lett.* **1999**, *314*, 141–151.

[137] Okabe, T.; Kawata, M.; Okamoto, Y.; Mikami, M. Replica-exchange Monte Carlo method for the isobaric–isothermal ensemble. *Chem. Phys. Lett.* **2001**, *335*, 435–439.

[138] Widom, B. Potential-distribution theory and the statistical mechanics of fluids. *J. Phys. Chem.* **1982**, *86*, 869–872.

[139] Klimovich, P. V.; Shirts, M. R.; Mobley, D. L. Guidelines for the analysis of free energy calculations. *J. Comput. Aided Mol. Des.* **2015**, *29*, 397–411.

[140] Widom, B. Some Topics in the Theory of Fluids. *J. Chem. Phys.* **1963**, *39*, 2808–2812.

[141] Shing, K.; Gubbins, K. The chemical potential in dense fluids and fluid mixtures via computer simulation. *Mol. Phys.* **1982**, *46*, 1109–1128.

[142] Lu, N.; Kofke, D. A. Accuracy of free-energy perturbation calculations in molecular simulation. I. Modeling. *J. Chem. Phys.* **2001**, *114*, 7303–7311.

[143] Bennett, C. H. Efficient estimation of free energy differences from Monte Carlo data. *J. Comput. Phys.* **1976**, *22*, 245–268.

[144] Shirts, M. R.; Bair, E.; Hooker, G.; Pande, V. S. Equilibrium Free Energies from Nonequilibrium Measurements Using Maximum-Likelihood Methods. *Phys. Rev. Lett.* **2003**, *91*, 140601.

[145] Shirts, M. R.; Pande, V. S. Comparison of efficiency and bias of free energies computed by exponential averaging, the Bennett acceptance ratio, and thermodynamic integration. *J. Chem. Phys.* **2005**, *122*, 144107.

[146] Straatsma, T. P.; McCammon, J. A. Multiconfiguration thermodynamic integration. *J. Chem. Phys.* **1991**, *95*, 1175–1188.

[147] Pitera, J. W.; van Gunsteren, W. F. A Comparison of Non-Bonded Scaling Approaches for Free Energy Calculations. *Mol. Simul.* **2002**, *28*, 45–65.

[148] Kästner, J. Umbrella sampling. *WIREs Comput. Mol. Sci.* **2011**, *1*, 932–942.

[149] Kumar, S.; Rosenberg, J. M.; Bouzida, D.; Swendsen, R. H.; Kollman, P. A. THE weighted histogram analysis method for free-energy calculations on biomolecules. I. The method. *J. Comput. Chem.* **1992**, *13*, 1011–1021.

[150] Meng, Y.; Roux, B. Efficient Determination of Free Energy Landscapes in Multiple Dimensions from Biased Umbrella Sampling Simulations Using Linear Regression. *J. Chem. Theory Comput.* **2015**, *11*, 3523–3529.

[151] Nayar, D.; van der Vegt, N. F. A. Cosolvent Effects on Polymer Hydration Drive Hydrophobic Collapse. *J. Phys. Chem. B* **2018**, *122*, 3587–3595.

[152] Markthaler, D.; Zeman, J.; Baz, J.; Smiatek, J.; Hansen, N. Validation of Trimethylamine-N-oxide (TMAO) Force Fields Based on Thermophysical Properties of Aqueous TMAO Solutions. *J. Phys. Chem. B* **2017**, *121*, 10674–10688.

[153] Imoto, S.; Forbert, H.; Marx, D. Water structure and solvation of osmolytes at high hydrostatic pressure: pure water and TMAO solutions at 10 kbar versus 1 bar. *Phys. Chem. Chem. Phys.* **2015**, *17*, 24224–24237.

[154] Schneck, E.; Horinek, D.; Netz, R. R. Insight into the Molecular Mechanisms of Protein Stabilizing Osmolytes from Global Force-Field Variations. *J. Phys. Chem. B* **2013**, *117*, 8310–8321.

[155] Abascal, J. L. F.; Vega, C. A general purpose model for the condensed phases of water: TIP4P/2005. *J. Chem. Phys.* **2005**, *123*, 234505.

[156] Kirkwood, J. G.; Buff, F. P. The Statistical Mechanical Theory of Solutions. I. *J. Chem. Phys.* **1951**, *19*, 774–777.

[157] Ganguly, P.; van der Vegt, N. F. A. Convergence of Sampling Kirkwood–Buff Integrals of Aqueous Solutions with Molecular Dynamics Simulations. *J. Chem. Theory Comput.* **2013**, *9*, 1347–1355.

[158] Krüger, P.; Schnell, S. K.; Bedeaux, D.; Kjelstrup, S.; Vlugt, T. J. H.; Simon, J.-M. Kirkwood–Buff Integrals for Finite Volumes. *J. Phys. Chem. Lett.* **2013**, *4*, 235–238.

[159] Milzetti, J.; Nayar, D.; van der Vegt, N. F. A. Convergence of Kirkwood–Buff Integrals of Ideal and Nonideal Aqueous Solutions Using Molecular Dynamics Simulations. *J. Phys. Chem. B* **2018**, *122*, 5515–5526.

[160] Bruce, E. E.; Bui, P. T.; Rogers, B. A.; Cremer, P. S.; van der Vegt, N. F. A. Nonadditive Ion Effects Drive Both Collapse and Swelling of Thermoresponsive Polymers in Water. *J. Am. Chem. Soc.* **2019**, *141*, 6609–6616.

[161] Bharadwaj, S.; Nayar, D.; Dalgicdir, C.; van der Vegt, N. F. A cosolvent surfactant mechanism affects polymer collapse in miscible good solvents. *Comm. Chem.* **2020**, *3*, 1–7.

[162] Mozhaev, V. V.; Heremans, K.; Frank, J.; Masson, P.; Balny, C. High pressure effects on protein structure and function. *Proteins* **1996**, *24*, 81–91.

[163] Hajari, T.; van der Vegt, N. F. A. Peptide Backbone Effect on Hydration Free Energies of Amino Acid Side Chains. *J. Phys. Chem. B* **2014**, *118*, 13162–13168.

[164] Xi, E.; Venkateshwaran, V.; Li, L.; Rego, N.; Patel, A. J.; Garde, S. Hydrophobicity of proteins and nanostructured solutes is governed by topographical and chemical context. *Proc. Natl. Acad. Sci. U.S.A.* **2017**, *114*, 13345–13350.

[165] Moore, F., Gordon Cramming more components onto integrated circuits. *Electronics* **1965**, *38*.

[166] Yancey, P. H.; Somero, G. N. Counteraction of urea destabilization of protein structure by methylamine osmoregulatory compounds of elasmobranch fishes. *Biochem. J.* **1979**, *183*, 317–323.

[167] Yancey, P. H.; Clark, M. E.; Hand, S. C.; Bowlus, R. D.; Somero, G. N. Living with Water Stress: Evolution of Osmolyte Systems. *Science* **1982**, *217*, 1214–1222.

[168] Ganguly, P.; Hajari, T.; Shea, J.-E.; van der Vegt, N. F. A. Mutual Exclusion of Urea and Trimethylamine N-Oxide from Amino Acids in Mixed Solvent Environment. *J. Phys. Chem. Lett.* **2015**, *6*, 581–585.

[169] Ganguly, P.; Polák, J.; van der Vegt, N. F. A.; Heyda, J.; Shea, J.-E. Protein Stability in TMAO and Mixed Urea–TMAO Solutions. *J. Phys. Chem. B* **2020**, *124*, 6181–6197.

3 Pressure, Peptides, and a Piezolyte: Structural Analysis of the Effects of Pressure and Trimethylamine-N-oxide on the Peptide Solvation Shell

This chapter to and is reproduced with permission from

Reprinted with permission from: Folberth, A.; Polák; J. Heyda, J.; van der Vegt, N. F. A; Pressure, Peptides, and a Piezolyte: Structural Analysis of the Effects of Pressure and Trimethylamine-N-oxide on the Peptide Solvation Shell. J. Phys. Chem. B, **2020***, 124(30), 6508-6519. Copyright 2020 American Chemical Society*

Abstract

The osmolyte trimethylamine-N-oxide (TMAO) is able to increase the thermodynamic stability of folded proteins, counteracting pressure denaturation. Herein, we report experimental solubility data on penta-alanine (pAla) in aqueous TMAO solutions (at pH=7 and pH=13) together with molecular simulation data for pAla, penta-serine (pSer) and an elastin-like peptide (ELP) sequence (VPGVG) under varying pH and pressure conditions. The effect of the peptide end groups on TMAO-peptide interactions is investigated by comparing the solvation of zwitterionic and negatively charged pentamers with the solvation of pentamers with charge-neutral C- and N-termini and linear, virtually infinite, peptide chains stretched across the periodic boundaries of the simulation cell. The experiments and simulations consistently show that TMAO is net-depleted from the pAla-water interface, but a local accumulation of TMAO is observed just outside the first hydration shell of the peptide. While the same observations are also made in the simulations of the zwitterionic pentamers (Ala, Ser, ELP) and virtually-infinite peptide chains (Ala, ELP), weak preferential binding of TMAO is instead observed for pAla with neutral end groups at 1 M TMAO concentration and for an ELP pentamer with capped, neutral end groups at 0.55 M TMAO concentration studied in previous work (Y.-T. Liao et al. *Proc. Natl. Acad. Sci. USA*, 2017, **114**, 2479-2484). The above observations, made at 1 bar ambient pressure, remain qualitatively unchanged at 500 bar and 2 kbar. Local accumulation of TMAO correlates with a reduction in the total number of peptide-solvent hydrogen bonds, independent of the peptide's primary sequence and the applied pressure. By weak-

ening water hydrogen bonds with the protein backbone TMAO indirectly contributes to stabilizing internal hydrogen bonds in proteins, thus providing a protein stabilization mechanism beyond net depletion.

1 Introduction

Trimethylamine-N-oxide (TMAO) is able to counteract the denaturation of proteins due to hydrostatic pressure in biological systems.[1–3] The role of TMAO stands out since the amount of TMAO in muscle tissue of deep sea fish increases with the depth of the catch and thus with higher pressure. Therefore, TMAO is often called a piezolyte due to its ability to counteract detrimental pressure effects on proteins.[4] In contrast, other protecting osmolytes like glycine have been shown to fail to maintain enzyme activity at high pressure.[1] Various experimental and theoretical studies have been conducted, but a universally accepted picture of the molecular mechanism with which TMAO protects proteins from denaturation remains elusive.[5–12]

Most experimental studies report that TMAO acts through a depletion mechanism, in which it is preferentially excluded from the protein-water interface.[10,11,13–16] This agrees with measurements on amino acids and few proteins at ambient pressure[17–22] and was used in the development of the group transfer model to predict the stabilizing effect of osmolytes on proteins.[23–25] Furthermore, spectroscopical and thermodynamic studies on binary and ternary systems attributed the depletion mechanism to strong TMAO-water interactions.[11,26–28] As computer simulations provide a direct way towards the molecular level detail and can overcome experimental difficulties, such as high pressure measurements, they are often used to investigate TMAO-peptide interactions. Although molecular dynamics (MD) simulation studies could therefore help with giving insight into the TMAO-protein interactions, the results remain elusive as both preferential TMAO binding and TMAO depletion were reported.[5,6,8,9,12,29–32] This fact, and the missing connection between simulation and experiment to validate TMAO force fields in ternary systems,[33,34] adds to the uncertainty about whether there exists a general mechanism of protein stabilization due to direct or indirect interactions of TMAO.

Furthermore, the peptide chemistry, TMAO concentration, and pressure might influence the preferential binding and stabilizing nature of TMAO. It has been reported that TMAO may act differently based on the hydrophobicity of the solute.[7,10,29,35] For instance, Su et al. described in a MD simulation study that TMAO acts as a denaturant for very hydrophobic parts of proteins while stabilizing salt bridges,[7,35,36] but pointed out that this is only one possible mechanism as interactions with the backbone may not be neglected. That salt bridges alone cannot explain the stabilization of compact protein and polymer states is consistent with TMAOs ability to stabilize the more compact state for macromolecules like poly(N-isopropylacrylamide) (PNiPAM) and an elastin-like protein (ELP, sequence: VPGVG) lacking groups that can form salt bridges.[5,8] In case of ELP, Liao et al. reported that TMAO preferentially binds to the protein and suggested a mechanism in which TMAO acts as a surfactant for the heterogenous surface of folded proteins.[8] Therefore, it is not straightforward

to see how a change in peptide chemistry changes TMAO interactions.
Additionally, most studies report that TMAO acts concentration independently as a stabilizing osmolyte,[13,14,37] while a recent experimental study revealed that TMAO denatures the enzyme stem bromelain at concentrations higher than 1.5 M.[38] Moreover, a study with a hydrophobic polymer revealed that TMAO may have denaturing abilities at concentrations higher than 1 M.[29,34] It is unknown why these concentration effects play a role in some systems, but not in others.
Lastly, although the counteracting effect of TMAO against pressure denaturation is often mentioned, most simulation studies consider TMAO effects at ambient pressure.[6–9,12] TMAO changes its interaction with water, forming more hydrogen bonds when pressure is increased,[39] which in turn might change its interaction with proteins. Accordingly, the preferential binding and the mechanism with which TMAO stabilizes proteins may change at high pressure.
Herein, we aim to provide insight in interaction mechanism of TMAO with short peptides. Therefore, we chose a pentapeptide for which the preferential binding coefficient can be measured experimentally. We compare the experiments to simulations and study how a variation in concentration, peptide chemistry and pressure affects the preferential binding and the solvation shell structure around the peptides.

2 Methods and Simulation Details

2.1 Experimental Methods

Chemicals

penta-Alanine (pAla) was purchased from Bachem, TMAO dihydrate from Thermo Fisher Scientific (>98%) and NaOH from Penta (p.a.). All chemicals were used without further purification. The distilled water, used as the solvent, was purified using mili-Q-ultra-pure water system from Millipore.

Methods

The relative solubility of pAla in TMAO solutions was determined for two states of pAla. For the anionic state, turbidimetry titrations at pH=13.5 and ambient temperature were performed, while the solubility of the zwitterionic state was probed by UV-spectroscopy at neutral pH and ambient temperature[40].

Solubility of the pAla anion in TMAO solutions

The solution of NaOH was prepared with a concentration appropriate to a pH of 13.5. Aproximately 20 mg of pAla were disolved by adding the NaOH solution until it became clear (see figure 3.8). In order to avoid systematic errors from over-titration, two different approaches were applied. In the first approach, solid TMAO was added directly into the solution until it became cloudy. This cloudy solution was then titrated by the NaOH solution in form of 8 to 3 drops (depending on the intensity of turbidity) in 15 minute intervals, until the solution became clear. During

titration, the solution was periodicaly weigthed after each NaOH or TMAO addition to calculate the exact composition of the solution and to determine the pAla solubility. An illustrative example of this titration protocol is provided in figure 3.8. In the second approach the titrations were performed with highly concentrated solution of TMAO (around 9.5 mol kg^{-1}) by 5 drops in 15 minute intervals, until the solution became cloudy (which was visually detected, the cloudiness of the pAla solution at different TMAO concentrations is shown in figure 3.9). The salting-out constant was evaluated from the Setschenow equation (equation 5).

Solubility of the pAla zwitterion in TMAO solutions

TMAO solutions were prepared at concentrations 0.5, 1 and 2 mol kg^{-1} (pH was not adjusted). Approximately 10 mg of pAla were added to five milliliters from each TMAO solution and were stirred for five days at room temperature. Afterwards, samples were cleansed from remaining solid particles via filtration through a Newway PES Syringe Filter 25 mm/0.2 μm. Cleansed pAla in TMAO solutions were measured by UV–VIS spectrophotometry (Spectrometer Varian Cary 50 UV-Vis Spectrophotometer - Agilent) at a wavelength, which maximizes the difference between pAla and TMAO (230 nm), using distilled water as the blank.[41,42] Each solution was measured in the pure, 1:1 diluted and 1:2 diluted form. The absorbance of pAla was obtained by subtracting the absorbance of TMAO solution without pAla from the absorbance of the mixed solution with the same TMAO concentration. Employing the Lambert-Beer law, relative molar concentrations were calculated as

$$\frac{S_0}{S(\mathrm{TMAO})} = \frac{A_0}{A_2} \tag{1}$$

Here, A_0, S_0, and A_2, S(TMAO) are pAla absorbance and solubility in pure water and in the presence of TMAO respectively. Equation 1 was combined with the Setschenow equation 5 to evaluate the salting-out constant.

2.2 Simulation Details

All systems are summarised in table 3.1, where they are numbered for easier reference. Systems I and II were used to compare to the experimental findings. System I–IV and VII consist of pentamers with neutral or charged end groups. Here, pAla with neutral end groups (COOH and NH_2, System IV) was included in order to examine the effect of the end group charges on TMAO-peptide interactions independent of the role of chain length. System V and VI consisted of 15-mers, whose head and tail groups were connected through the periodic boundary conditions (quasi-infinite chain).[45] The majority of peptides in table 3.1 were studied using the Amber99sb-ildn force field.[46] The Charmm27 force field[47] was used for peptides with neutral termini since there were no parameters for neutral termini in the Amber force field. Na^+ and OH^- ion parameters were taken from the Charmm27 force field as well. We included a comparisons of the Amber and Charmm force fields for systems I and V.

The starting configuration was created by PEPFOLD3.[48] If not mentioned otherwise, the Hölzl

Table 3.1: Studied systems and their acronyms. Peptides are studied with both the Amber99sb-ildn (amber) and Charmm27 (charmm) force field (FF). The peptide state refers to the charge of the end group, where +– means zwitterionic, 0– means that the C-terminus is charged but the N-terminus is neutral, 00 means that both termini are neutral and ∞ refers to the quasi-infinite chain without end groups. Ions refers to the presence of Na^+ and OH^- in the simulation box in order to achieve pH=13

System	peptide	TMAO FF	Peptide FF	Peptide state	Ions
Ia/c	pAla	Hölzl[43]	amber/charmm	+–	no
II	pAla	Hölzl[43]	charmm	0–	yes
III	pAla	Kast[44]	amber	+–	no
IV	pAla	Hölzl[43]	charmm	00	no
Va/c	Ala	Hölzl[43]	amber/charmm	∞	no
VI	ELP	Hölzl[43]	amber	∞	no
VII	pAla, pSer, ELP	Hölzl[43]	amber	+–	no

Table 3.2: Number of water, TMAO, and ion molecules, average density $\langle\rho\rangle$ and box volume $\langle V\rangle$ for simulations of system I to VI at 1 bar pressure and 298 K. All systems contained a single peptide molecule

pH	TMAO Conc. / M	# TMAO	# water	# Na^+	# OH^-	$\langle\rho\rangle$ / kg m^{-3}	$\langle V\rangle$/ nm^3
7	1	207	10635	-	-	1001.36	344.12
	2	414	9789	-	-	1005.72	343.13
	3	620	8951	-	-	1011.15	341.91
	4	826	8148	-	-	1017.41	341.45
13	1	207	10635	22	21	1008.55	343.09
	2	414	9789	22	21	1012.67	342.19
	3	620	8951	22	21	1017.59	341.15
	4	826	8148	22	21	1023.43	340.84

force field[43] was used to describe TMAO with the TIP4P/2005 water model.[49] The Hölzl force field has been parametrised to capture the change in water-TMAO hydrogen bonds upon increasing the pressure and has been proven to work excellent for binary systems at ambient pressure (see figure 3.10 for the effect of TMAO on the surface tension of the air-water interface).[33] Although parameterized with the TIP3P water model, the combination of the Amber99sb-ildn forcefield and TIP4P/2005 water model has been proven to work well.[50] For System III the Kast force field[44] for TMAO with SPC/E water[51] and the Amber99sb-ildn force field for the protein was used. Sytems I to VI were simulated with set-ups shown in table 6.1, varying the pH and TMAO concentration. Simulations at different pressures and the comparison with different peptides (System VII) were performed with smaller set-ups, summarised in table 3.3.

All MD simulations were performed with Gromacs version 4.6.7.[52,53] LINCS[54] was used to restrain all bonds involving an H-atom. The systems were first equilibrated using the steepest descent algorithm with 50000 steps and a step size of 0.001 nm. Afterward, the systems were first equilibrated for 5 ns in a constant volume and temperature simulation using the Berendsen thermostat[55]

Table 3.3: Number of water and TMAO molecules, average density and box volume for simulations of system VII at 298 K. All systems contained a single peptide molecule

Pressure / bar	TMAO Conc. / M	# TMAO	# water	$\langle\rho\rangle$ / kg m^{-3}	$\langle$V$\rangle$/ nm^3
1	0	0	2968	999.45	89.46
	0.5	27	2860	1000.98	89.46
	1	54	2752	1002.80	89.43
	4	217	2122	1019.16	89.45
500	0	0	3036	1021.24	89.54
	0.5	27	2926	1021.99	89.55
	1	54	2817	1022.97	89.57
	4	217	2181	1035.05	89.78
2000	0	0	3206	1076.11	89.70
	0.5	27	3092	1075.36	89.73
	1	54	2979	1074.81	89.76
	4	217	2313	1076.69	89.98

(τ_T=1.0 ps, T=298 K), followed by a constant pressure-temperature simulation of another 5 ns using the Berendsen barostat (τ_P=2.0 ps, $\kappa_T = 5 \cdot 10^{-5}$ bar^{-1} ($4.5 \cdot 10^{-5}$ bar^{-1} for SPC/E water)). The time step was 2 fs. In the production run the Nose-Hoover thermostat[56] at 298 K (τ_T=1.0 ps) and the Parrinello-Rahman barostat (τ_P=2.0 ps)[57] with a compressibility of $5 \cdot 10^{-5}$ bar^{-1} ($4.5 \cdot 10^{-5}$ bar^{-1} for SPC/E water) were employed. The compressibility was set to 0 in the z-direction for the quasi-infinite chains (Systems V and VI). The neighbor list was updated every time step. Coulomb interactions were treated using particle mesh ewald (PME)[58] with a real-space cut off of 1 nm, a PME order of 4 and a grid spacing of 0.12 nm. The van der Waals interactions cut off length was 1 nm with long range dispersion corrections applied for pressure and energy. The production run of systems I–VI were done for 300 ns (1 M and 2 M TMAO) or 500 ns (3 M and 4 M TMAO). The production runs for system VII were 100 ns. In all cases, the first 5 ns were discarded for equilibration.

Gromacs tools[52,53] have been used to calculate the solvent accessible surface area (SASA) employing a probe sphere of 0.14 nm and hydrogen bonds using a cut-off angle of 30^o and a cut-off distance of 0.35 nm. Proximal radial distribution functions[59] (rdfs) have been calculated by binning the proximal distance of a solvent or TMAO molecule to the peptide and calculating the mean number of solvent or TMAO molecules, $\Delta N^{\text{prox}}(r)$, in a bin. Proximal slice volumes, $\Delta V^{\text{prox}}(r)$, have been calculated from 10 randomly chosen reference structures of the peptide. The proximal rdf is calculated according to $g^{\text{prox}}(r) = \frac{\rho(r)}{\rho^0}$ with $\rho(r) = \frac{\Delta N^{\text{prox}}(r)}{\Delta V^{\text{prox}}(r)}$ and ρ^0 the TMAO or water particle density.

3 Theory

We here derive equations which allow to relate the experimental peptide solubility changes to preferential binding parameters accessible in simulations. We use the subscripts 1, 2 and 3 to refer to the solvent (water), the peptide and the co-solute (TMAO), respectively. The chemical potential of the peptide (2) in pure water ($\mu_2(0)$) and in TMAO-water solution ($\mu_2(c_3)$) can be written as:

$$\mu_2(0) = \mu_2^{\mathrm{x}}(0) + RT \ln c_{2,0} \tag{2}$$

$$\mu_2(c_3) = \mu_2^{\mathrm{x}}(c_3) + RT \ln c_2 \tag{3}$$

where μ_2^{x} is the pseudo chemical potential as defined by Ben-Naim,[60] R is the gas constant, T the temperature, $c_{2,0}$ the molar peptide concentration in water ($c_3 = 0$) and c_2 the molar peptide concentration in the solution with TMAO. Under saturation conditions, the chemical potentials in equation 2 and 3 are equal, i.e. $\mu_2(0) = \mu_2(c_3)$, and therefore

$$\ln \left(\frac{c_{2,0}}{c_2} \right)_{\mathrm{sat}} = \frac{\Delta\mu_2^{\mathrm{x}}}{RT} \tag{4}$$

where $\Delta\mu_2^{\mathrm{x}} = \mu_2^{\mathrm{x}}(c_3) - \mu_2^{\mathrm{x}}(0)$ represents the transfer Gibbs energy of the peptide from neat water to the TMAO-water solution.
The Setschenow equation expresses equation 4 as

$$k_s \cdot c_3 = \log \left(\frac{c_{2,0}}{c_2} \right)_{\mathrm{sat}} \tag{5}$$

in which k_s is the Setschenow constant. We can therefore write

$$k_s \cdot c_3 = \frac{\Delta\mu_2^{\mathrm{x}}}{2.303\, RT} \tag{6}$$

Equation 6 is the integral form of

$$k_s = \frac{1}{2.303RT} \left(\frac{\partial\mu_2}{\partial c_3} \right)_{p,T} \tag{7}$$

Using the Wyman-Tanford / Kirkwood-Buff approach[61–63] in the dilute limit for $c_2 \to 0$, the derivative, $\left(\partial\mu_2/\partial c_3\right)_{p,T}$, can be written as

$$\left(\frac{\partial \mu_2}{\partial c_3}\right)_{p,T} = -\frac{RT\Gamma_{23}}{c_3} \cdot \frac{1}{1 + c_3(G_{33} - G_{31})} \tag{8}$$

in which Γ_{23} is the preferential binding coefficient defined as

$$\Gamma_{23} = c_3(G_{23} - G_{21}) \tag{9}$$

$G_{\alpha\beta}$ ($\alpha, \beta = 1, 2, 3$), the Kirkwood-Buff integral (KBI) for solution component pairs α and β, and the term $a_{cc} = \left[1 + c_3(G_{33} - G_{31})\right]^{-1}$ accounts for the thermodynamic nonideality of the TMAO/water binary solution. Combining equations 5, 7 and 8 yields

$$\log\left(\frac{c_{2,0}}{c_2}\right)_{\text{sat}} = -\frac{\Gamma_{23}}{2.303} \cdot \frac{1}{1 + c_3(G_{33} - G_{31})} \tag{10}$$

The quantities Γ_{23}, G_{33} and G_{31} are obtained from simulation data, and, by means of equation 10, permit to validate the simulation model against experimental data.
The preferential binding coefficient, which can be conveniently calculated from simulations using equation 11,[64,65] allows us to compare findings from simulations to experiment.

$$\Gamma_{23}(r) = \left\langle n_{23}(r) - \frac{N_3^{\text{tot}} - n_{23}(r)}{N_1^{\text{tot}} - n_{21}(r)} \cdot n_{21}(r) \right\rangle \tag{11}$$

Here $n_{2\alpha}$ denotes the cumulative number of co-solute or water molecules within a certain proximal distance, r, to the peptide and N_α^{tot} is the total number of co-solute or water molecules in the simulation box. A positive preferential binding coefficient refers to the excess of co-solute in the vicinity of the peptide relative to the bulk solution, while a negative preferential binding coefficient shows that the co-solute is depleted from the peptide solvation shell. The preferential binding coefficient, equation 11, is calculated as a function of the distance to the peptide. The limiting value of Γ_{23} is reached at the boundary between the local solvation shell of the peptide and the bulk reservoir. This value can be compared to the experimental data. The distance has been measured from the nitrogen atom of TMAO/oxygen atom of water to the closest atom of the peptide.
Similar to the preferential binding coefficient, the local/bulk partition coefficient, K_p, shows depletion or accumulation, but is an intensive quantity. It is defined according to equation 12.

$$K_p(r) = \frac{\langle n_{23}(r)\rangle}{\langle n_{21}(r)\rangle} \cdot \frac{N_1^{tot}}{N_3^{tot}} \tag{12}$$

Here, $\langle n_{2\alpha}(r)\rangle$ is the average cumulative number of α in the solvation shell around the peptide from 0 to r and N_α^{tot} is the total number of α in the box. A value of K_p larger than 1 indicates accumulation around the peptide, while a value smaller than 1 indicates depletion. The local/bulk

partition coefficient is connected to the preferential binding coefficient through equation 13 if taken at a single time frame and if the correction for the bulk depletion was not applied for the preferential binding coefficient.

$$\Gamma_{23} = n_{23}\left(1 - \frac{1}{K_p}\right) \tag{13}$$

The local/bulk partition coefficient provides information on the depletion of TMAO around the peptide, but, in contrast to the preferential binding coefficient, it cannot be related directly to thermodynamic data. As it is intensive, it is easier to converge than the preferential binding coefficient and allows smaller systems and simulation times. Furthermore, we can use an additional analysis by calculating $\langle n_{2\alpha}(r)\rangle$ within distance intervals $[r, r+dr]$, instead of taking the cumulative number of molecules of type α within $[0, r]$. The corresponding, differential, local/bulk partition coefficient will be referred to as K_p^{local}.

Additionally, we calculated the average tetrahedral order parameter as a function of the peptide distance. Usually only water oxygen atoms are taken into account. However, since TMAO and the peptide possess atoms that can form hydrogen bonds, we included, similar to Nayar et al.,[66] the nitrogen and oxygen of the peptide bond, the oxygen of the serine side chain and the oxygen of TMAO into the calculation. We used the formula of Debenedetti[67] to calculate the tetrahedral order parameter.

$$q = 1 - \frac{3}{8}\sum_{j=1}^{3}\sum_{k=j+1}^{4}\left(\cos\Psi_{jk} + \frac{1}{3}\right)^2 \tag{14}$$

Here, q is the tetrahedral order parameter. The formula takes the four closest atoms and is based on the angle Ψ_{jk}, which describes the angle between atom j, the center atom, and atom k. The tetrahedral order parameter, q , reflects correspondance of the angles to a perfect tetrahedral structure (an order parameter of 1) or a random orientation like in an ideal gas (an order parameter of 0). Here, we have analyzed the tetrahedral order parameter in bins around the peptide, since details might get lost if we average over the solvation shell.

4 Results and discussion

4.1 Preferential Binding - Experiment and Simulation

The Preferential Binding Coefficient shows that TMAO is depleted.

Figure 3.1 a) shows the pAla solubility data obtained from the experiments and simulations. The pAla solubility decreases with increasing TMAO concentration, both in the neutral and basic pH range. This implies that TMAO is depleted from the peptide-water interface (Γ_{23} is negative,

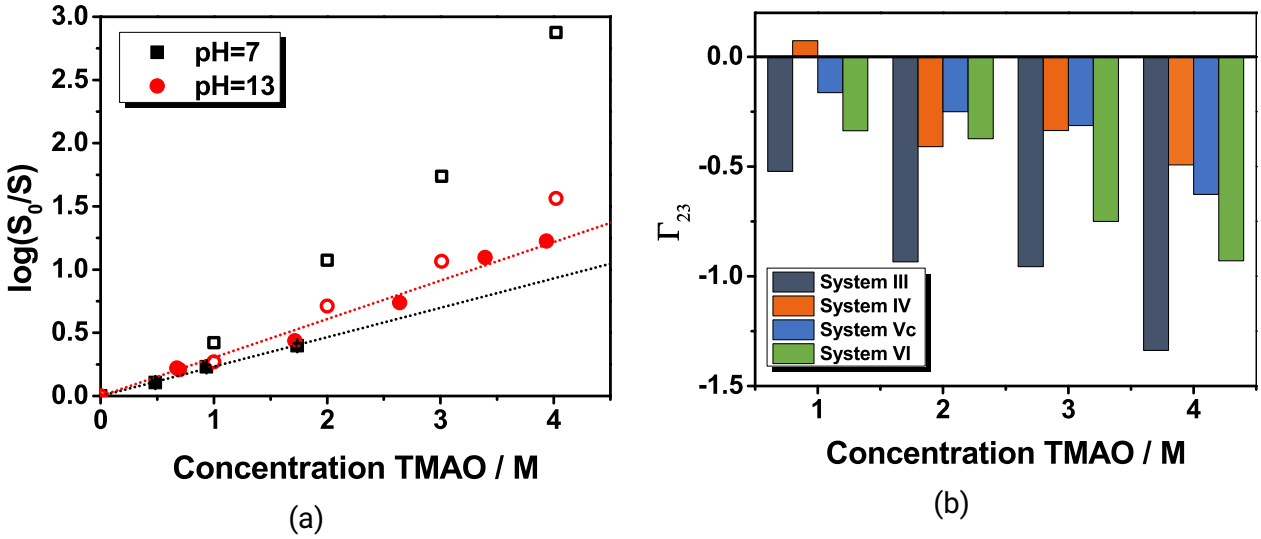

Figure 3.1: a) Setschenow graph comparing simulations (open symbols, System I and II) and experimental data (closed symbols, lines are fitted to experimental data) at pH=7 and 13. b) Comparison of preferential binding coefficients obtained from simulation when changing to the TMAO Kast force field (System III), switching the termini to neutral (System IV) or taking a quasi-infinite chain of alanine (System V) or ELP (System VI). The quasi-infinite chains have been normalised to represent the preferential binding per unit of five amino acids.

cf. equation 10). Details on the calculation of the quantities Γ_{23} and the nonideality correction $a_{cc} \equiv \left[1 + c_3(G_{33} - G_{31})\right]^{-1}$ on the right-hand-side of equation 10 are provided in the supporting information. Significantly, a_{cc} increases with increasing TMAO concentration (see table 3.5) due to a larger TMAO-water than TMAO-TMAO affinity ($G_{31} > G_{33}$). This contributes to the observed decrease in peptide solubility upon mixing the aqueous pAla solution with an increasing concentration of TMAO. We assume that the nonideality correction is similar at pH=7 and pH=13.

The simulation data at both pH values overestimate the experimental values. This is due to too strong depletion, as the non-ideality correction has been well reproduced by the Hölzl force field (see table 3.5). When fitting to the data in the TMAO concentration range of 0 to 4 M, we obtain a slope and thus the Setschenow constant (all units in L mol^{-1}) of 0.641 (0.417 with Charmm27, shown in figure 3.11) at pH=7 and of 0.370 at pH=13. The experimental value is 0.233 at pH=7 and 0.305 at pH=13. The observed TMAO depletion is independent of the protein force field, but

data obtained with the Charmm force field are closer to experimental values, hinting at better representation of TMAO-peptide interactions. Nevertheless, TMAO exclusion is overestimated by both force fields, although the trend remains correct.

Systems III–VII were studied to investigate aspects of end groups, peptide length and composition on Γ_{23}. Figure 3.1 b) shows that TMAO remains depleted from the zwitterionic peptide when the Kast force field is used (System III), but the Setschenow constant of 0.285 is closer to the experimental value at pH=7. We will continue the study with the Hölzl force field as it is derived for high pressure MD simulations. On the other hand, a peptide with neutral termini (System IV) shows slight preferential binding of TMAO at low concentration (here 1 M). If a depletion of TMAO from pAla is due to an end group effect, this effect should become smaller when the peptide becomes longer, approaching the size of proteins. Thus, an alanine-15-mer (System Vc) has been spanned over the periodic boundary conditions to obtain an quasi-infinite chain without end groups. Strong depletion can be observed for the quasi-infinite chain with the Charmm and even more with the Amber force field (figure 3.18 for both force fields). Depletion of TMAO around the quasi-infinite chain has also been reported for glycine, phenylalanine, asparagine and aspartic acid chains with the osmotic TMAO model.[30] Further simulations of a quasi-infinite ELP chain reveal that TMAO stays depleted throughout the concentration range (figure 3.1 b, System VI). This is intriguing since Liao et al. used capped, thus neutral, ELP-5-mers at low TMAO concentrations in their study.[8] Our findings suggest that the preferential adsorption in this case may have been merely a special case and cannot be used for a general mechanism, as a longer ELP chain (System VI) shows preferential exclusion and zwitterionic ELP (System VII) shows no preferential binding either (see the peptide comparison, figure 3.5).

To investigate TMAO interactions with specific groups on the peptide in more detail, we calculated the so called partial preferential binding coefficient Γ^i_{23} by considering TMAO and water molecules at the proximal distance to these groups only. That is, if a TMAO molecule is proximal to NH_3^+, it is included only in the calculation of $\Gamma_{23}^{NH_3^+}$ for this group but not in the calculation of Γ^i_{23} of any other group. Therefore, only the proximal sub-volume is used for the calculation of each Γ^i_{23} as illustrated in the inset in figure 3.2 b). Hence, Γ^i_{23} provides information on the preferential TMAO interactions with the different peptide groups. Figure 3.2 shows that there is a clear difference between the neutral and charged termini, where TMAO is depleted from charged termini but shows slight accumulation around neutral termini. This is counterintuitive since TMAO is also zwitterionic, so that it could interact with charged groups. We refer the interested reader to the SI, where other TMAO concentrations are shown (figure 3.13) and also the influence of SASA is discussed (figure 3.14, table **??**).

Our analysis points to two effects, which become operational: for small peptides TMAO is depleted due to zwitterionic end termini. When the chain becomes longer, the end group effect reduces but the increasing size of the internal chain starts to play a role. This has also been observed with glycine chains, where TMAO accumulates around small peptides, but is depleted from hexa-glycine.[6] Thus,

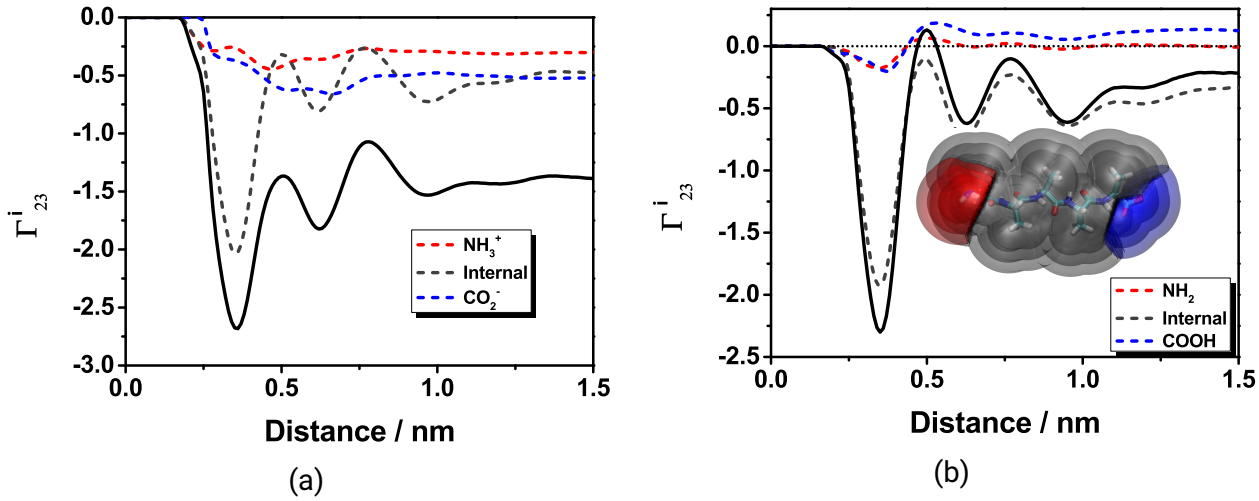

Figure 3.2: a) Partial preferential binding coefficient Γ^i_{23} for a) pAla with charged termini (zwitterionic, system Ia) b) pAla with neutral termini (system IV) at 3 M TMAO concentration. The inset shows an illustration of the proximal volume shells of pAla as used in the calculation of the partial preferential binding coefficient. The part of the molecule that does not contain the end groups is referred to as the internal part. The full preferential binding coefficient is shown as the solid line.

our simulations hint towards a general depletion of TMAO from the peptide-water interface.

TMAO accumulates locally

Although TMAO is depleted from the peptide surface, it might still be spatially enriched at larger distances. The local/bulk partition coefficient of pAla at pH=7, presented in figure 3.3 a), has been locally resolved, as shown in figure 3.3 b), to analyze these deviations. While the data in figure 3.3 a) shows that TMAO is net-depleted, it can be seen in figure 3 b) that local accumulation of TMAO occurs. A closer inspection in figure 3.4 shows that water surrounds the peptide, while TMAO stays enriched in a second solvation shell. When more TMAO accumulates at higher TMAO concentrations, few water molecules are removed from the first solvation shell, but the largest effect is visible in the second solvation shell, where water is pushed out. The accumulated TMAO molecules are mostly oriented randomly with a slightly higher probability of facing the oxygen towards the bulk or towards the peptide when it is close to the peptide as can be seen from figure 3.16. Furthermore, the proximal rdf in figure 3.4 b) shows that the water peak at 0.26 nm increases when going from 0 to 4 M TMAO and therefore the ratio of the amount of water in the solvation shell compared to the bulk increases slightly.

The local accumulation effect of TMAO is end group independent as can be seen from the local/bulk partition coefficient of the quasi-infinite polyalanine in figure 3.17.

The local/bulk partition coefficient increases at higher TMAO concentration (figure 3.3). The increase shows that water is replaced by TMAO and that the TMAO:water ratio changes in favor of TMAO. This can also be seen in the non-linear decrease of the preferential binding coefficient

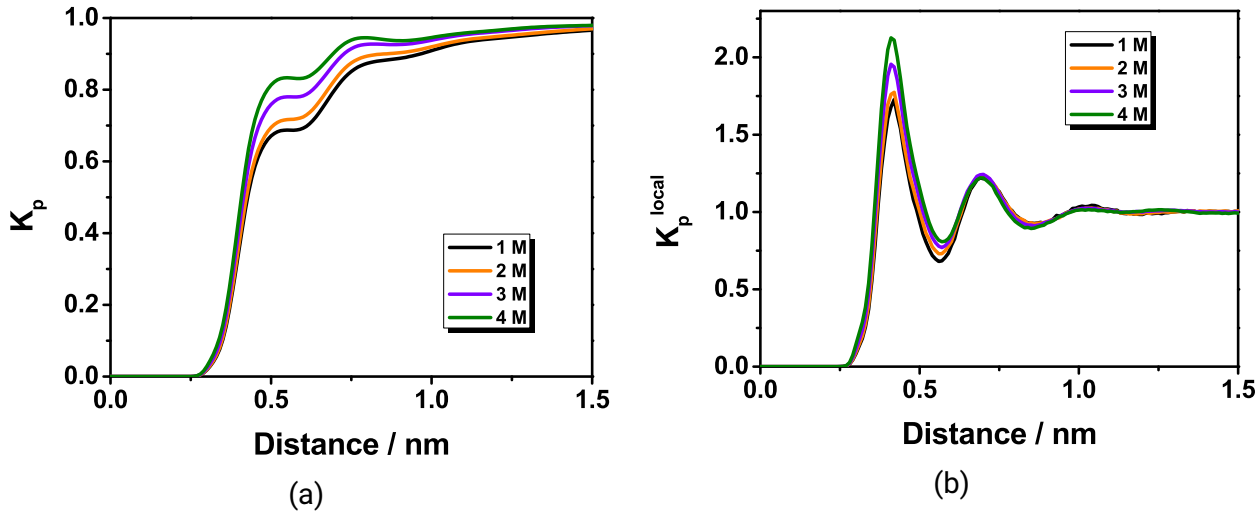

Figure 3.3: a) Local/bulk partition coefficient, K_p (Eq. 12), as a function of the proximal distance from pAla at pH=7 (System Ia) and b) K_p^{local} as a function of the proximal distance from pAla at pH=7 (System Ia).

(figure 3.12). We have also calculated the local/bulk partition coefficients via an experimental procedure and discuss it in terms of local non-ideality in the SI (figure 3.15).[68]

In conclusion, experiments have validated that TMAO is depleted from pAla. Comparison with simulations revealed a qualitatively correct representation of the depletion. The combination of the Hölzl force field with the Charmm27 force field leads to solubility predictions that are closer to experimental data than the use of the Amber force field for the peptide. Several robust and generic (force field independent) observations can be drawn from simulations: 1) The enrichment of TMAO in a second solvation shell with water molecules occupying the first solvation shell, similar to the results of Schroer et al. with PNiPAM[5] and Bruz dziak et al. with lysozyme.[22] 2) Replacing charged terminal groups of the peptide by neutral terminal groups can lead to a slight preferential TMAO binding at low concentration. 3) Although TMAO is depleted from peptides with charged end groups, simulations with a stretched, periodically replicated, peptide chain indicate that TMAO is also depleted for long chains without charged end groups. These findings have important consequences for proteins, in which end group effects are negligible and due to the importance of the internal groups TMAO remains generically net depleted. This might be the general physicochemical mechanism for protein stabilization as has been discussed before.[17–20]

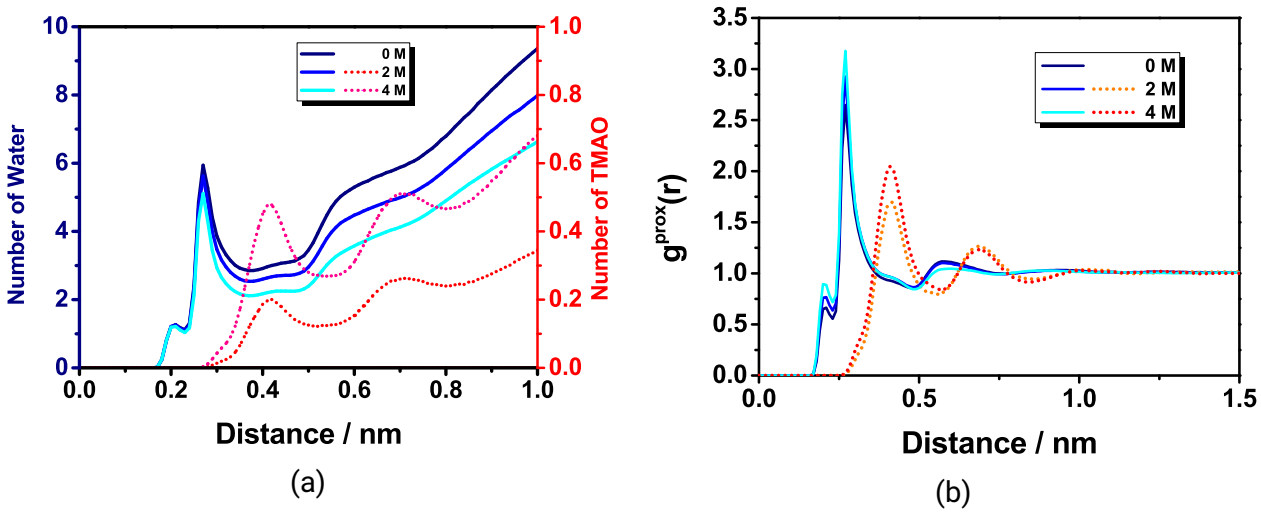

Figure 3.4: a) Local number of water (solid lines, left axis) and TMAO molecules (dashed lines, right axis) as a function of the proximal distance to the peptide and b) Proximal rdf of water (solid lines) and TMAO molecules (dashed lines) around the peptide (System Ia).

4.2 Effect of primary peptide structure

In the previous section, it has been observed that the peptide chemistry might change the depletion behavior of TMAO. Thus, simulations of hetero-peptide ELP (VPGVG) and pSer, which is more polar than pAla, are used to understand the influence of the hydrophobicity of the peptide. This is crucial since simulations of Ala-15-mers using the Netz TMAO model[45,69] and Ala-10-mers using the Kast TMAO model[7,44] revealed no impact of TMAO on the compactness of the peptide. Indeed, the influence of TMAO on hydrophobic association is controversially discussed.[7,29,34,35,70,71]

TMAO depletion is independent of the peptide structure

The local/bulk partition coefficient plotted in figure 3.5 a) shows depletion of TMAO around all three peptides. Furthermore, the accumulation of TMAO in the second solvation shell is present for all peptides, as shown in figure 3.5 b). We observe that TMAO forms hydrogen bonds with pSer, as seen in a peak at small distances (figure 3.5 b), and is less accumulated in the second solvation shell of the polar pSer. Although here we report effects of peptide polarity on TMAO interactions, it should be noted that opposite extremes with large nonpolar side chains versus charged side chains have not been considered herein. Positive preferential binding of TMAO may occur for peptide sequences with large nonpolar side chains.[7] Moreover, TMAO binding to extended hydrophobic surfaces has been reported,[10] in line with the observation of TMAO binding to hydrophobic polymers since TMAO is able to interact with these molecules through its methyl groups.[29,34] The effect of TMAO on the interaction between charged residues, was not investigated in this work. In some biomolecules, it has been reported that salt bridges play an important role in the stabilization of compact peptide structures by TMAO.[7,36,69] Nevertheless, TMAO also stabilizes the more compact structures of PNiPAM and ELP, which do not possess charged residues and thus

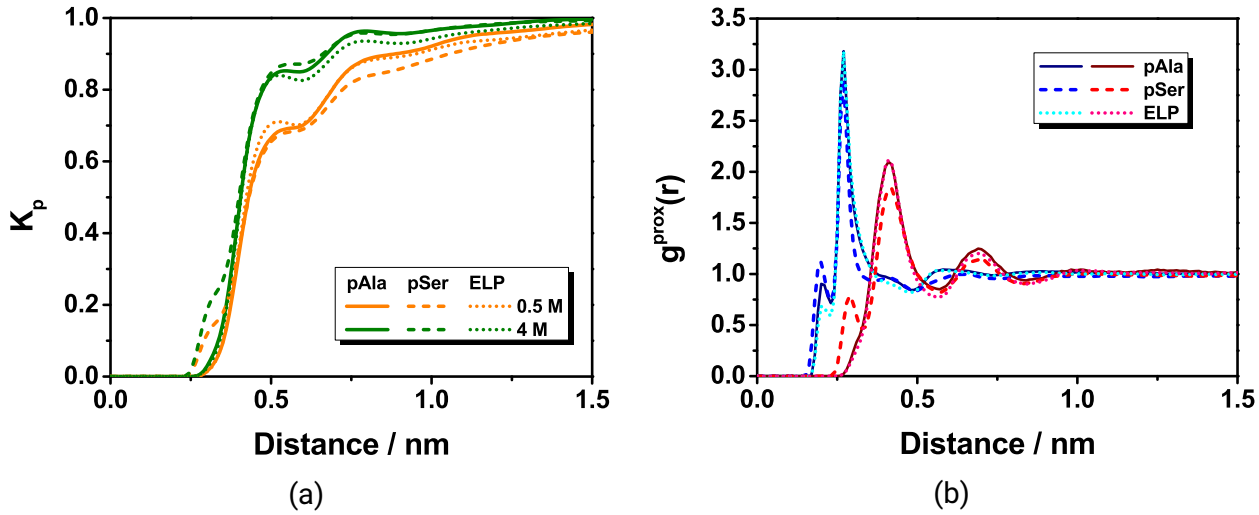

Figure 3.5: a) Local/bulk partition coefficient, K_p (Eq. 12), as a function of the proximal distance for pAla, pSer (dashed lines) and ELP (dotted lines) at pH = 7 (system VII) and b) Proximal peptide-TMAO rdf (red, taken at the nitrogen) and peptide-water rdf (blue, taken at the oxygen) (system VII).

salt bridges are absent.[5,8] Therefore, an additional mechanism of protein folded state stabilization by TMAO must be operational. Assuming the effects of extended hydrophobic surfaces facing the solvent are small for proteins with heterogenous, patchy surfaces, the observations made herein hint towards a mechanism of TMAO action, in which TMAO affects the hydration of the peptide backbone, rather than directly interacting with the backbone itself. This might explain why TMAO can act in such an independent fashion, not only when the peptide chemistry is different, but also when the pressure increases.

4.3 Effect of pressure

The chemical potential of the peptide is affected not only by the addition of osmolytes, but also by a change in pressure p. The thermodynamic relation that describes these effects on protein stability reads

$$\mathrm{d}\Delta G_2(c_3, p) = -RT\,\Delta\Gamma_{23}\frac{a_{cc}}{c_3}\mathrm{d}c_3 + \Delta\overline{V}_2\mathrm{d}p \tag{15}$$

where ΔG_2 is the free energy difference between the folded (F) and unfolded (U) state of the protein, and $\Delta\overline{V}_2 = \overline{V}_2^U - \overline{V}_2^F$ and $\Delta\Gamma_{23} = \Gamma_{23}^U - \Gamma_{23}^F$ denote the partial molar volume and difference in TMAO preferential binding coefficient upon protein unfolding, respectively. In contrast to $\overline{V_2}$, $\Delta\overline{V_2}$ is typically negative due to packing deficits in the folded protein state.[72,73] Thus, increase in pressure shifts the protein folding equilibrium towards the unfolded state. This effect can be counteracted by stabilizing osmolytes as they are usually more depleted from the unfolded state (Γ_{23}

approximately scales with the surface area).[25,74] With increasing pressure, the solvation structure around proteins and peptides changes and some osmolytes are reported to lose their protecting ability.[75] In the following section, we examine whether TMAO remains depleted from peptide surfaces also at elevated pressures. We will mostly focus on pAla as the trends remain mostly the same for all peptides. We refer the interested reader to the SI, where we present the results for pSer and ELP in more detail (figure 3.19, 3.20, 3.21 and 3.23).

TMAO remains depleted at increased pressure

The local/bulk partition coefficient plotted in figure 3.6 reveals that TMAO remains depleted when the pressure is increased, but reveals some non-linear trend with pressure. This is the most pronounced at low concentrations and seems to be stronger for the hydrophobic peptides. Moreover, local accumulation of TMAO in the second solvation shell of the peptides is pressure independent. In all cases the number of water molecules in the first solvation shell increases with increasing pressure (see also figure 3.22). While pressure has only a marginal effect on the net preferential exclusion of TMAO, peptide-water hydrogen bonding and the solvent tetrahedral order parameter may be affected by it.

Figure 3.7 a) show the number of water-peptide hydrogen bonds as a function of TMAO concentration for three different pressures. In general, with increasing TMAO concentration, the number of water-peptide hydrogen bonds is decreasing, while some TMAO-peptide hydrogen bonds are formed (figure 3.21 a). The total number of hydrogen bonds is, however, smaller than in pure water, so that peptide-solvent hydrogen bonds are lost. A slightly larger number of water-peptide hydrogen bonds is generally observed at higher pressure. While water is pushed into the first solvation shell upon applied pressure, resulting in a slight increase in the number of peptide-water hydrogen bonds, TMAO acts to reduce the number of peptide-water hydrogen bonds at higher pressures. This is in line with suggestions that TMAO acts by decreasing the stability of the unfolded state of proteins by decreasing the strength of water-peptide hydrogen bonds[11] and also supports that TMAO rather acts on water in the first solvation shell than directly on the peptide.

We also calculated the tetrahedral order parameter as a function of the distance from the peptide surface. As shown in figure 3.7 b), the order parameter close to the peptide increases with pressure at all TMAO concentrations, which can be attributed to the increase in local water density and the number of peptide-water hydrogen bonds with pressure. It can be observed that at large distances (in the bulk) the order parameter decreases in pure water when pressure is applied as the close packing leads to the disruption of tetrahedrality. This effect becomes smaller when TMAO is added. It is best examined at 4 M as seen in figure 3.7 b), where the pressure effect on the bulk value $\langle q \rangle$ nearly disappears. This might be explained by increasing number of TMAO-water hydrogen bonds with pressure, for which the Hölzl model has been parametrised.[43] Close to the peptide TMAO also slightly reduces the effect of pressure. Overall, TMAO decreases the pressure effects on the tetrahedral order of the solvent.

In summary, TMAO remains depleted from peptide surfaces even at elevated pressures and reduces

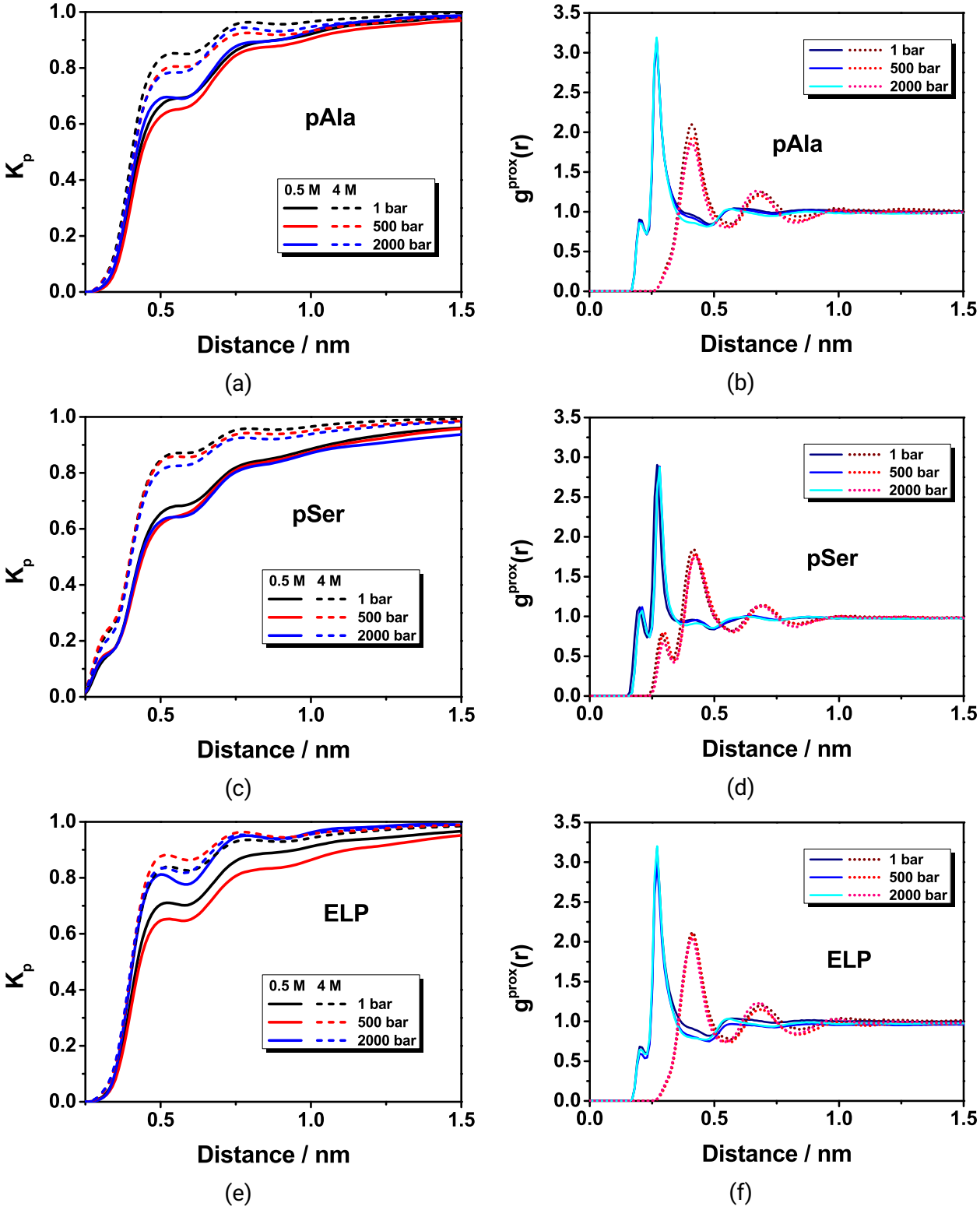

Figure 3.6: Local/bulk partition coefficient at 0.5 and 4 M and at different pressures for a) pAla, c) pSer and e) ELP (system VII). Proximal peptide-TMAO (red) and peptide-water (blue) rdfs at 4 M TMAO concentration for b) pAla, d) pSer, and f) ELP (system VII).

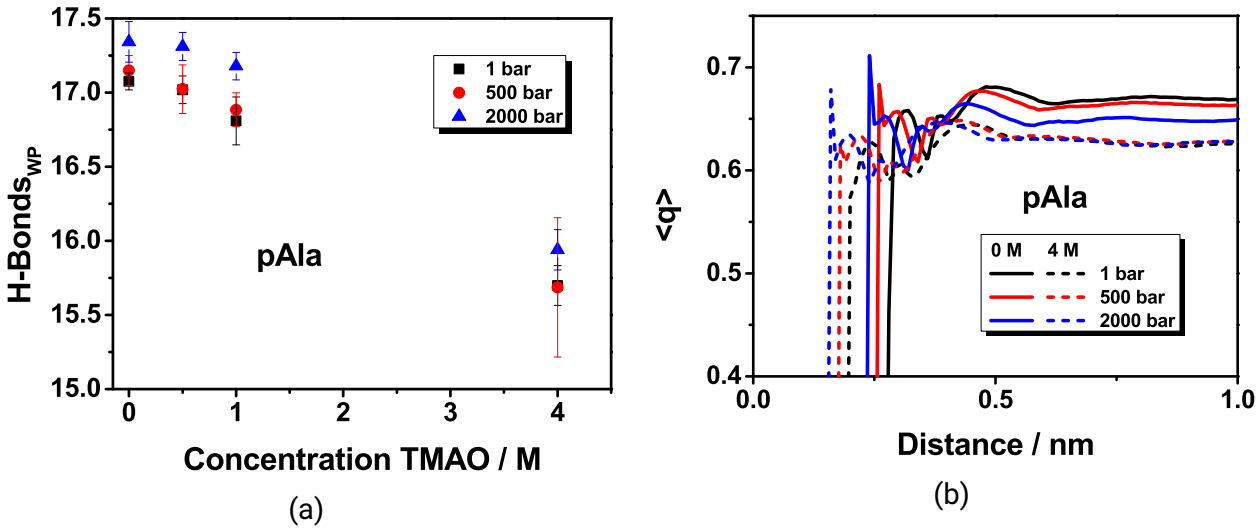

Figure 3.7: a) Number of water-peptide (WP) hydrogen bonds at different pressures as a function of the TMAO bulk concentration (system VII). b) Effect of pressure on the tetrahedral order parameter in water and in 4 M TMAO concentration as a function of the proximal distance from the peptide surface. All graphs except from the one at 0 M and 2000 bar are shifted along the horizontal axis to facilitate the comparison.

solvent-peptide hydrogen bonds at ambient and elevated pressure. Moreover, at higher concentrations TMAO counteracts the effect of pressure on the water structure, i.e. on the tetrahedral order in bulk, and reduces the effect close to the peptide.

5 Conclusion

We have found experimentally that TMAO decreases the solubility of pAla at neutral and basic pH. Thus, TMAO is depleted from the pAla surface. Our simulations match the experimental trends, although we see that the Hölzl and Kast model overestimate the experimental decrease of pAla's water solubility in the presence of TMAO. The simulations furthermore revealed that there exists a second solvation shell, where TMAO is enriched. This local accumulation, however, cannot overcome the net TMAO depletion. Changing the state of the pAla termini from zwitterionic to neutral revealed that at low concentrations TMAO shows slight preferential binding to the short neutral-terminated peptide. Nevertheless, we observe that increasing the peptide chain length to a 15-mer spanned across the periodic boundaries of the simulation box leads to net TMAO depletion. Thus, for pAla the zwitterionic end groups keep TMAO depleted at low concentration, but for longer peptides a the importance of the TMAO depletion from the internal peptide groups comes into play, so that TMAO remains depleted at all concentrations. Only in the case of small, neutral peptides at low TMAO concentration, slight preferential binding of TMAO is found.
The choice of peptides results only in small differences in the magnitude of the TMAO effects.

Qualitatively, TMAO is depleted from the peptide-water interface for the different peptide primary structures studied herein (pAla, pSer, ELP). When pressure is applied, TMAO remains depleted, independent of the peptide. In terms of solutions structure, TMAO counteracts the pressure effect on the tetrahedral order parameter in the bulk, but also reduces the pressure effect on the tetrahedral order parameter close to the peptide and reduces solvent-peptide hydrogen bonds. In the case of proteins, the reduction of solvent-peptide hydrogen bonds might be responsible for a stronger destabilization of the unfolded state, compared to the folded state. This might be the prevailing mechanism as also described by Ma et al.[11] As only small peptides have been studied in this work, the effect/role of TMAO interactions on larger bio-molecular (length scales)/surfaces cannot be unequivocally ruled out. Furthermore, we have not looked into the effect of TMAO on charged residues, which can form salt bridges. Similar to our observation of strong depletion of TMAO from the charged end groups, it has been reported that TMAO is depleted from charged sidechains that can form salt bridges.[7,36,69] The stabilization of salt bridges adds another way to the above mentioned mechanism, studied herein, for TMAO to stabilize the folded protein state. To summarise, our study hints towards a generic TMAO stabilizing effect of protein folded states, which operates via depletion and a destabilization of the unfolded state through a decrease of peptide-solvent hydrogen bonding. Mechanistically, our findings suggest that TMAO interacts with the first hydration shell of the peptide backbone, instead of with the backbone directly. This type of interactions is insensitive to TMAO concentration, primary peptide sequence and pressure.

Acknowledgement

J.P. and J.H. acknowledges the financial support from specific university research (MSMT No 21-SVV/2019). J.H. thanks the Czech Science Foundation (grant 20-24155S) for support. The authors thank Swaminath Bharadwaj for fruitful discussions. MD simulations were performed on the Lichtenberg HighPerformance Computer of the Technische Universität Darmstadt, Germany.

Bibliography

[1] Yancey, P. H.; Fyfe-Johnson, A. L.; Kelly, R. H.; Walker, V. P.; Aun, M. T. Trimethylamine oxide counteracts effects of hydrostatic pressure on proteins of deep-sea teleosts. *J. Exp. Zool.* **2001**, *289*, 172–176.

[2] Julius, K.; Al-Ayoubi, S. R.; Paulus, M.; Tolan, M.; Winter, R. The effects of osmolytes and crowding on the pressure-induced dissociation and inactivation of dimeric LADH. *Phys. Chem. Chem. Phys.* **2018**, *20*, 7093–7104.

[3] Yancey, P.; Siebenaller, J. Trimethylamine oxide stabilizes teleost and mammalian lactate dehydrogenases against inactivation by hydrostatic pressure and trypsinolysis. *J. Exp. Biol.* **1999**, *202*, 3597–3603.

[4] Yancey, P. H.; Gerringer, M. E.; Drazen, J. C.; Rowden, A. A.; Jamieson, A. Marine Fish May Be Biochemically Constrained from Inhabiting the Deepest Ocean Depths. *Proc. Natl. Acad. Sci. U.S.A.* **2014**, *111*, 4461–4465.

[5] Schroer, M. A.; Michalowsky, J.; Fischer, B.; Smiatek, J.; Grübel, G. Stabilizing effect of TMAO on globular PNIPAM states: preferential attraction induces preferential hydration. *Phys. Chem. Chem. Phys.* **2016**, *18*, 31459–31470.

[6] Cho, S. S.; Reddy, G.; Straub, J. E.; Thirumalai, D. Entropic stabilization of proteins by TMAO. *J. Phys. Chem. B* **2011**, *115*, 13401–13407.

[7] Su, Z.; Mahmoudinobar, F.; Dias, C. L. Effects of Trimethylamine-*N*-oxide on the Conformation of Peptides and its Implications for Proteins. *Phys. Rev. Lett.* **2017**, *119*, 108102.

[8] Liao, Y.-T.; Manson, A. C.; DeLyser, M. R.; Noid, W. G.; Cremer, P. S. Trimethylamine-N-oxide stabilizes proteins via a distinct mechanism compared with betaine and glycine. *Proc. Natl. Acad. Sci. U.S.A.* **2017**, *114*, 2479–2484.

[9] Mondal, J.; Stirnemann, G.; Berne, B. J. When Does Trimethylamine N-Oxide Fold a Polymer Chain and Urea Unfold It? *J. Phys. Chem. B* **2013**, *117*, 8723–8732.

[10] Anand, G.; Jamadagni, S. N.; Garde, S.; Belfort, G. Self-Assembly of TMAO at Hydrophobic Interfaces and Its Effect on Protein Adsorption: Insights from Experiments and Simulations. *Langmuir* **2010**, *26*, 9695–9702.

[11] Ma, J.; Pazos, I. M.; Gai, F. Microscopic insights into the protein-stabilizing effect of trimethylamine N-oxide (TMAO). *Proc. Natl. Acad. Sci. U.S.A.* **2014**, *111*, 8476–8481.

[12] Kokubo, H.; Hu, C. Y.; Pettitt, B. M. Peptide conformational preferences in osmolyte solutions: Transfer free energies of decaalanine. *J. Am. Chem. Soc.* **2011**, *133*, 1849–1858.

[13] Schummel, P. H.; Haag, A.; Kremer, W.; Kalbitzer, H. R.; Winter, R. Cosolvent and Crowding Effects on the Temperature and Pressure Dependent Conformational Dynamics and Stability of Globular Actin. *J. Phys. Chem. B* **2016**, *120*, 6575–6586.

[14] Patra, S.; Anders, C.; Schummel, P. H.; Winter, R. Antagonistic effects of natural osmolyte mixtures and hydrostatic pressure on the conformational dynamics of a DNA hairpin probed at the single-molecule level. *Phys. Chem. Chem. Phys.* **2018**, *20*, 13159–13170.

[15] Cinar, S.; Cinar, H.; Chan, H. S.; Winter, R. Pressure-Sensitive and Osmolyte-Modulated Liquid-Liquid Phase Separation of Eye-Lens γ-Crystallins. *J. Am. Chem. Soc.* **2019**, *141*, 7347–7354.

[16] Jaworek, M. W.; Schuabb, V.; Winter, R. The effects of glycine, TMAO and osmolyte mixtures on the pressure dependent enzymatic activity of α-chymotrypsin. *Phys. Chem. Chem. Phys.* **2018**, *20*, 1347–1354.

[17] Auton, M.; Bolen, D. W. Additive Transfer Free Energies of the Peptide Backbone Unit That Are Independent of the Model Compound and the Choice of Concentration Scale. *Biochemistry* **2004**, *43*, 1329–1342.

[18] Qu, Y.; Bolen, C. L.; Bolen, D. W. Osmolyte-driven contraction of a random coil protein. *Proc. Natl. Acad. Sci. U.S.A.* **1998**, *95*, 9268–9273.

[19] Courtenay, E. S.; Capp, M. W.; Anderson, C. F.; Record, M. T. Vapor Pressure Osmometry Studies of Osmolyte Protein Interactions: Implications for the Action of Osmoprotectants in Vivo and for the Interpretation of Osmotic Stress Experiments in Vitro. *Biochemistry* **2000**, *39*, 4455–4471.

[20] Wang, A.; Bolen, D. W. A naturally occurring protective system in urea-rich cells: Mechanism of osmolyte protection of proteins against urea denaturation. *Biochemistry* **1997**, *36*, 9101–9108.

[21] Hong, J.; Xiong, S. TMAO-Protein Preferential Interaction Profile Determines TMAO's Conditional In Vivo Compatibility. *Biophys. J.* **2016**, *111*, 1866 – 1875.

[22] Bru dziak, P.; Adamczak, B.; Kaczkowska, E.; Czub, J.; Stangret, J. Are stabilizing osmolytes preferentially excluded from the protein surface? FTIR and MD studies. *Phys. Chem. Chem. Phys.* **2015**, *17*, 23155–23164.

[23] Auton, M.; Rösgen, J.; Sinev, M.; Holthauzen, L. M. F.; Bolen, D. W. Osmolyte effects on protein stability and solubility: A balancing act between backbone and side-chains. *Biophys. Chem.* **2011**, *159*, 90 – 99.

[24] Auton, M.; Bolen, D. W. Predicting the energetics of osmolyte-induced protein folding/unfolding. *Proc. Natl. Acad. Sci. U.S.A.* **2005**, *102*, 15065–15068.

[25] Bolen, D. W.; Rose, G. D. Structure and Energetics of the Hydrogen-Bonded Backbone in Protein Folding. *Annu. Rev, of Biochem.* **2008**, *77*, 339–362.

[26] Rösgen, J.; Jackson-Atogi, R. Volume Exclusion and H-Bonding Dominate the Thermodynamics and Solvation of Trimethylamine-N-oxide in Aqueous Urea. *J. Am. Chem. Soc.* **2012**, *134*, 3590–3597.

[27] Xie, W. J.; Cha, S.; Ohto, T.; Mizukami, W.; Mao, Y.; Wagner, M.; Bonn, M.; Hunger, J.; Nagata, Y. Large Hydrogen-Bond Mismatch between TMAO and Urea Promotes Their Hydrophobic Association. *Chem* **2018**, *4*, 2615 – 2627.

[28] Hunger, J.; Tielrooij, K. J.; Buchner, R.; Bonn, M.; Bakker, H. J. Complex formation in aqueous trimethylamine-N-oxide (TMAO) solutions. *J. Phys. Chem. B* **2012**, *116*, 4783–4795.

[29] Nayar, D.; van der Vegt, N. F. A. Cosolvent Effects on Polymer Hydration Drive Hydrophobic Collapse. *J. Phys. Chem. B* **2018**, *122*, 3587–3595.

[30] Canchi, D. R.; Jayasimha, P.; Rau, D. C.; Makhatadze, G. I.; Garcia, A. E. Molecular mechanism for the preferential exclusion of TMAO from protein surfaces. *J. Phys. Chem. B* **2012**, *116*, 12095–12104.

[31] Athawale, M. V.; Dordick, J. S.; Garde, S. Osmolyte Trimethylamine-N-Oxide Does Not Affect the Strength of Hydrophobic Interactions: Origin of Osmolyte Compatibility. *Biophys. J.* **2005**, *89*, 858 – 866.

[32] Hu, C. Y.; Lynch, G. C.; Kokubo, H.; Pettitt, B. M. Trimethylamine N-oxide influence on the backbone of proteins: An oligoglycine model. *Proteins* **2010**, *78*, 695–704.

[33] Markthaler, D.; Zeman, J.; Baz, J.; Smiatek, J.; Hansen, N. Validation of Trimethylamine-N-oxide (TMAO) Force Fields Based on Thermophysical Properties of Aqueous TMAO Solutions. *J. Phys. Chem. B* **2017**, *121*, 10674–10688.

[34] Rodríguez-Ropero, F.; Rötzscher, P.; van der Vegt, N. F. A. Comparison of Different TMAO Force Fields and Their Impact on the Folding Equilibrium of a Hydrophobic Polymer. *J. Phys. Chem. B* **2016**, *120*, 8757–8767.

[35] Su, Z.; Ravindhran, G.; Dias, C. L. Effects of Trimethylamine-N-oxide (TMAO) on Hydrophobic and Charged Interactions. *J. Phys. Chem. B* **2018**, *122*, 5557–5566.

[36] Su, Z.; Dias, C. L. Individual and combined effects of urea and trimethylamine N-oxide (TMAO) on protein structures. *Journal of Molecular Liquids* **2019**, *293*, 111443.

[37] Celinski, S. A.; Scholtz, J. M. Osmolyte effects on helix formation in peptides and the stability of coiled-coils. *Protein Sci.* **2002**, *11*, 2048–2051.

[38] Rani, A.; Jayaraj, A.; Jayaram, B.; Venkatesu, P. Trimethylamine-N-oxide switches from stabilizing nature: A mechanistic outlook through experimental techniques and molecular dynamics simulation. *Sci. Rep.* **2016**, *6*, 1–14.

[39] Imoto, S.; Forbert, H.; Marx, D. Water structure and solvation of osmolytes at high hydrostatic pressure: pure water and TMAO solutions at 10 kbar versus 1 bar. *Phys. Chem. Chem. Phys.* **2015**, *17*, 24224–24237.

[40] Higuchi, T.; Connors, K. Phase Solubility Techniques. *Adv. Anal. Chem. Instrum.* **1965**, *4*, 117 – 212.

[41] Kubota, T.; Yamakawa, M.; Tanaka, I. Ultraviolet absorption spectra of trimethylamine N-oxide. *J. Mol. Spectrosc.* **1966**, *20*, 226 – 232.

[42] Saidel, L. J.; Lieberman, H. Ultraviolet absorption spectra of peptides. IV. Alanine residue. *Arch. Biochem. Biophys* **1958**, *76*, 401 – 409.

[43] Hölzl, C.; Kibies, P.; Imoto, S.; Frach, R.; Suladze, S.; Winter, R.; Marx, D.; Horinek, D.; Kast, S. M. Design principles for high-pressure force fields: Aqueous TMAO solutions from ambient to kilobar pressures. *J. Chem. Phys.* **2016**, *144*, 1–4.

[44] Kast, K. M.; Brickmann, J.; Kast, S. M.; Berry, R. S. Binary phases of aliphatic N-oxides and water: Force field development and molecular dynamics simulation. *J. Phys. Chem. A* **2003**, *107*, 5342–5351.

[45] Schneck, E.; Horinek, D.; Netz, R. R. Insight into the molecular mechanisms of protein stabilizing osmolytes from global force-field variations. *J. Phys. Chem. B* **2013**, *117*, 8310–8321.

[46] Sorin, E. J.; Pande, V. S. Exploring the helix-coil transition via all-atom equilibrium ensemble simulations. *Biophys. J.* **2005**, *88*, 2472–2493.

[47] Bjelkmar, P.; Larsson, P.; Cuendet, M. A.; Hess, B.; Lindahl, E. Implementation of the CHARMM Force Field in GROMACS: Analysis of Protein Stability Effects from Correction Maps, Virtual Interaction Sites, and Water Models. *J. Chem. Theory Comput.* **2010**, *6*, 459–466.

[48] Shen, Y.; Maupetit, J.; Derreumaux, P.; Tufféry, P. Improved PEP-FOLD Approach for Peptide and Miniprotein Structure Prediction. *J. Chem. Theory Comput.* **2014**, *10*, 4745–4758.

[49] Abascal, J. L. F.; Vega, C. A general purpose model for the condensed phases of water: TIP4P/2005. *J. Chem. Phys.* **2005**, *123*, 234505.

[50] Beauchamp, K. A.; Lin, Y.-S.; Das, R.; Pande, V. S. Are Protein Force Fields Getting Better? A Systematic Benchmark on 524 Diverse NMR Measurements. *Journal of Chemical Theory and Computation* **2012**, *8*, 1409–1414.

[51] Berendsen, H. J.; Grigera, J. R.; Straatsma, T. P. The missing term in effective pair potentials. *J. Phys. Chem.* **1987**, *91*, 6269–6271.

[52] Berendsen, H. J.; van der Spoel, D.; van Drunen, R. GROMACS: A message-passing parallel molecular dynamics implementation. *Comput. Phys. Commun.* **1995**, *91*, 43–56.

[53] Abraham, M. J.; Murtola, T.; Schulz, R.; Páll, S.; Smith, J. C.; Hess, B.; Lindah, E. Gromacs: High performance molecular simulations through multi-level parallelism from laptops to supercomputers. *SoftwareX* **2015**, *1-2*, 19–25.

[54] Hess, B. P-LINCS: A parallel linear constraint solver for molecular simulation. *J. Chem. Theory Comput.* **2008**, *4*, 116–122.

[55] Berendsen, H. J.; Postma, J. P.; Van Gunsteren, W. F.; Dinola, A.; Haak, J. R. Molecular dynamics with coupling to an external bath. *J. Chem. Phys.* **1984**, *81*, 3684–3690.

[56] Nosé, S. A molecular dynamics method for simulations in the canonical ensemble. *Mol. Phys.* **1984**, *52*, 255–268.

[57] Parrinello, M.; Rahman, A. Polymorphic transitions in single crystals: A new molecular dynamics method. *J. Appl. Phys.* **1981**, *52*, 7182–7190.

[58] Darden, T.; York, D.; Pedersen, L. Particle mesh Ewald: An N·log(N) method for Ewald sums in large systems. *J. Chem. Phys.* **1993**, *98*, 10089–10092.

[59] Lin, B.; Pettitt, B. M. Note: On the universality of proximal radial distribution functions of proteins. *J. Chem. Phys.* **2011**, *134*, 106101.

[60] Ben-Naim, A. Standard thermodynamics of transfer. Uses and misuses. *J. Phys. Chem.* **1978**, *82*, 792–803.

[61] Wyman, J. Linked Functions and Reciprocal Effects in Hemoglobin: A Second Look. *Adv. Prot. Chem.* **1964**, *19*, 223 – 286.

[62] Tanford, C. Extension of the theory of linked functions to incorporate the effects of protein hydration. *J. Mol. Biol.* **1969**, *39*, 539–544.

[63] Kirkwood, J. G.; Buff, F. P. The Statistical Mechanical Theory of Solutions. I. *J. Chem. Phys.* **1951**, *19*, 774–777.

[64] Pierce, V.; Kang, M.; Aburi, M.; Weerasinghe, S.; Smith, P. E. Recent Applications of Kirkwood–Buff Theory to Biological Systems. *Cell Biochem. Biophys.* **2008**, *50*, 1–22.

[65] Canchi, D. R.; García, A. E. Backbone and Side-Chain Contributions in Protein Denaturation by Urea. *Biophysical Journal* **2011**, *100*, 1526 – 1533.

[66] Nayar, D.; Agarwal, M.; Chakravarty, C. Comparison of Tetrahedral Order, Liquid State Anomalies, and Hydration Behavior of mTIP3P and TIP4P Water Models. *J. Chem. Theory. Comput.* **2011**, *7*, 3354–3367.

[67] Errington, J. R.; Debenedetti, P. Relationship between strcutural order and the anomalies of liquid water. *Nature* **2001**, *409*, 318–321.

[68] Felitsky, D. J.; Record, M. T. Application of the Local-Bulk Partitioning and Competitive Binding Models to Interpret Preferential Interactions of Glycine Betaine and Urea with Protein Surface. *Biochemistry* **2004**, *43*, 9276–9288.

[69] Ganguly, P.; Boserman, P.; van der Vegt, N. F. A.; Shea, J.-E. Trimethylamine N-oxide Counteracts Urea Denaturation by Inhibiting Protein–Urea Preferential Interaction. *Journal of the American Chemical Society* **2018**, *140*, 483–492.

[70] Mondal, J.; Halverson, D.; Li, I. T. S.; Stirnemann, G.; Walker, G. C.; Berne, B. J. How osmolytes influence hydrophobic polymer conformations: A unified view from experiment and theory. *Proc. Natl. Acad. Sci. U.S.A.* **2015**, *112*, 9270–9275.

[71] Mukherjee, M.; Mondal, J. Osmolyte-Induced Macromolecular Aggregation Is Length-Scale Dependent. *The Journal of Physical Chemistry B* **2019**, *123*, 8697–8703.

[72] Roche, J.; Caro, J. A.; Norberto, D. R.; Barthe, P.; Roumestand, C.; Schlessman, J. L.; Garcia, A. E.; García-Moreno E., B.; Royer, C. A. Cavities determine the pressure unfolding of proteins. *Proc. Natl. Acad. Sci. U.S.A.* **2012**, *109*, 6945–6950.

[73] Sirotkin, V. A.; Winter, R. Volume Changes Associated with Guanidine Hydrochloride, Temperature, and Ethanol Induced Unfolding of Lysozyme. *J. Phys. Chem. B* **2010**, *114*, 16881–16886.

[74] Record, M. T.; Guinn, E.; Pegram, L.; Capp, M. Introductory lecture: interpreting and predicting Hofmeister salt ion and solute effects on biopolymer and model processes using the solute partitioning model. *Faraday Discuss.* **2013**, *160*, 9–44.

[75] Yancey, P. H.; Blake, W. R.; Conley, J. Unusual organic osmolytes in deep-sea animals: adaptations to hydrostatic pressure and other perturbants. *Comp. Biochem. Phys. A* **2002**, *133*, 667 – 676.

6 Supporting Information

Experimental solubilities are determined through titration and UV/VIS (see figure 3.8, table 3.4). Here, figure S2 illustrates the intensity of cloudiness of the pAla solution with decreasing TMAO concentration. While the solubilities in the titration experiments are given in molality, solubilities in the UV/VIS experiment are proportional to the molarity concentration of the solute. Accordingly, the Setschenow coefficient can be determined as being dependent on the molal (k_m) or molar (k_s) solubilities. The formula to calculate molar concentrations of the peptide c_2 from molal concentrations m_2 in pure water (0) and water-cosolute mixtures are

$$c_{2,0} = \frac{\rho_0 m_{2,0}}{1 + M_2 m_{2,0}} \tag{16}$$

$$c_2 = \frac{\rho m_2}{1 + M_2 m_2 + M_3 m_3} \tag{17}$$

Here M_α is the molar mass of component α, m_α is the molal concentration of component α, ρ is the density of the mixture containing TMAO and ρ_0 the density in the mixture without TMAO. The Setschenow coefficients k_s and k_m are related according to

$$\begin{aligned} k_s \cdot c_3 &= k_m \cdot m_3 + \log\left(\frac{\rho_0(1 + M_2 m_{2,\mathrm{TMAO}} + M_3 m_3)}{\rho_{\mathrm{TMAO}}(1 + M_2 m_{2,0})}\right) \\ &= k_m \cdot m_3 + C \end{aligned} \tag{18}$$

We have calculated the correction factor C using densities of water-TMAO mixtures to obtain the molar scale quantities.

Table 3.4: Solubility of pAla at pH=13.5 and solubility of pAla at pH=7, absorbance of pAla (A_{pAla}) is recalculated back to the original concentration, i.e., prior the dilution. All concentrations are in mol kg^{-1}, densities of binary mixtures are given in kg L^{-1}

pH=13.5			**pH=7**		
m_{TMAO}	ρ	m_{pAla}	m_{TMAO}	ρ	A_{Ala}
0	0.997	0.138	0	0.997	0.467
0.734	0.999	0.086	0.502	0.998	0.372
0.759	0.999	0.089			0.357
2.004	1.002	0.056	1.005	0.999	0.279
3.304	1.006	0.030			0.284
4.541	1.010	0.014			0.261
5.500	1.014	0.011	1.992	1.002	0.177
					0.196

We want to relate experimental solubility changes to preferential binding coefficients from simulations according to equation 10 of the theory. Therefore, Γ_{23} is taken at 1.1 nm distance from

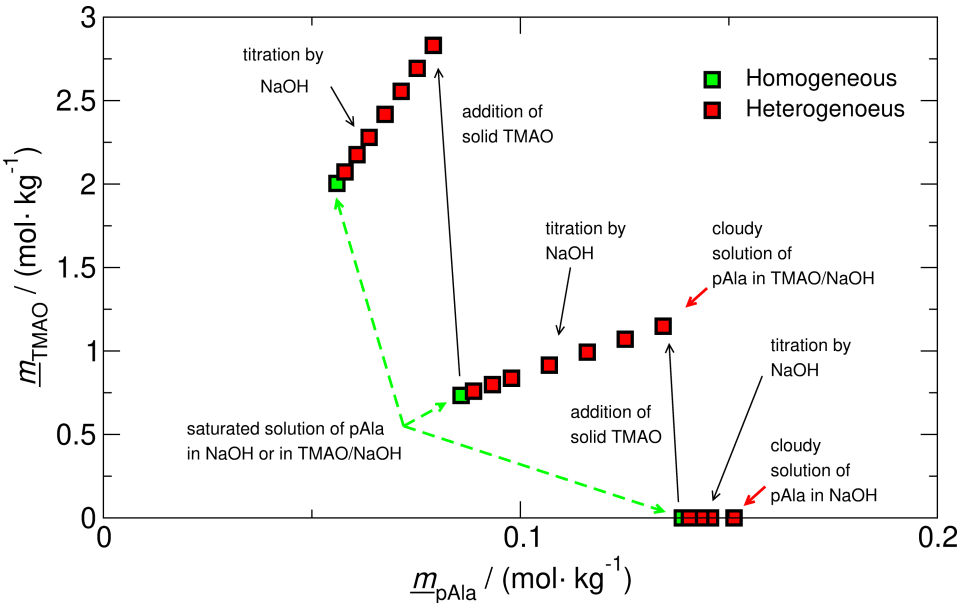

Figure 3.8: Illustration of the back and forth titration experiment performed on the quaternary solution water:NaOH:TMAO:pAla in the vicinity of the pAla saturated solution. The system repeatedly goes from heterogeneous to homogeneous phase and back (see the legend), as small volumes of NaOH solution, or of solid TMAO·2H_2O are added to the solution (see descriptions).

Figure 3.9: Photos of the ternary TMAO-peptide-water mixtures, showing the progress of cloudiness with TMAO concentration. Concentrations of TMAO are given below in molality. Blank stands for the destile water reference.

Table 3.5: KBI values and corrections (activity derivative, a_{cc}) for TMAO activity as shown in equation 20 taken at R=1.25 nm for TMAO-TMAO (G_{33}) and R=1 nm for TMAO-Water (G_{31}) for the Hölzl (left) and Kast (right) force field in L mol^{-1}. Experimental values given in parenthesis are taken from Rösgen et al.[4]

Conc.	G_{33}	G_{31}	a_{cc}	G_{33}	G_{31}	a_{cc}
1 M	–0.60 (-0.39)	–0.10 (–0.04)	1.43 (1.54)	–0.23	–0.06	1.21
2 M	–0.48 (-0.30)	–0.07 (–0.03)	1.99 (2.19)	–0.20	–0.05	1.44
3 M	–0.41	–0.05	2.80	–0.18	–0.04	1.77
4 M	–0.35	–0.04	3.90	–0.17	–3.3	2.14

the peptide. KBIs, defined in equation 14, have been calculated from 100 ns simulations of binary systems using the same number of molecules as described in table 4.1 of the methods section and using the run parameters as described in the method section.

$$G_{\alpha\beta} = \int_0^R dr \left(g_{\alpha\beta}(r) - 1 \right) 4\pi r^2 \tag{19}$$

Radial distribution functions (RDF) have been corrected using the Ganguly correction[1] and then KBIs calculated using the Krüger correction.[2,3] Corrections for the nonideality of TMAO-water solution up to 4 M TMAO concentration, activity derivatives a_{cc} defined according to equation 20, are summarized in table 3.5 for the Hölzl and Kast model.

$$a_{cc} = \frac{1}{1 + c_3(G_{33} - G_{31})} \tag{20}$$

Furthermore, the surface tension has been calculated by enhancing the z-direction of equilibrated boxes to 155 nm and running NVT simulations for 50 ns. The last 40 ns have been used to calculate the surface tension using equation 21.[5] Similar to Feng et al., we have not used any tail corrections since we are mainly interested in the change of surface tension with cosolute concentration[6].

$$\gamma = -\frac{L_z}{2} \cdot \left(\frac{P_{xx} + P_{yy}}{2} - P_{zz} \right) \tag{21}$$

Here γ is the surface tension, L_z the box length in z-direction and $P_{\alpha\alpha}$ the pressure tensor component α=x,y,z. The surface tension shown in figure 3.10 decreases with increasing TMAO concentration, which further validates the Hölzl TMAO force field.

6.1 Additional Analysis of System I and II

We are interested in the change in TMAO preferential binding due to the choice of peptide force field. Therefore, we calculate the solubility ratio from the preferential binding coefficient (figure

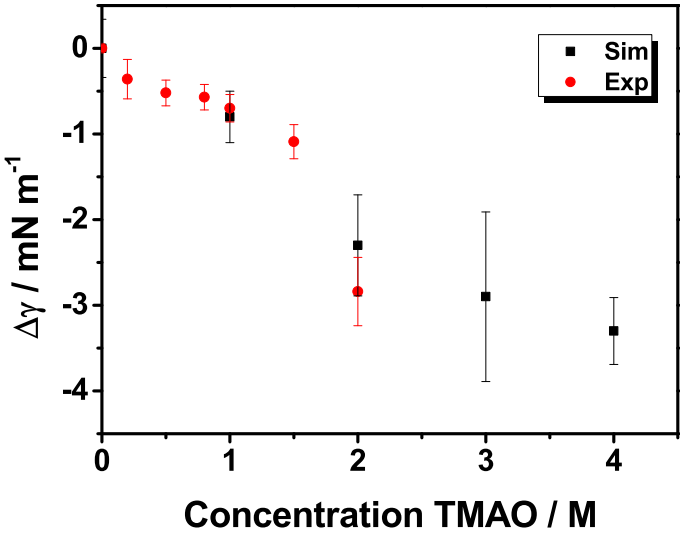

Figure 3.10: Difference in surface tension of TMAO/water mixtures to water calculated from binary systems and the pure water system using equation 21 as a function of TMAO concentration. Experimental surface tension data for TMAO effects have been taken from Liao et al.[7] The surface tension of pure water has been taken from Vargaftik et al.[8]

Table 3.6: SASA of the internal peptide parts and termini as defined in the partial preferential binding coefficient for System Ia and System IV in units of nm^2 at different TMAO concentrations.

Conc.	System Ia			System IV		
	Internal	COO^-	NH_3^+	Internal	COOH	NH_2
1 M	5.18 ± 0.04	1.23 ± 0.00	0.82 ± 0.00	5.04 ± 0.00	1.25 ± 0.00	0.81 ± 0.00
2 M	5.18 ± 0.04	1.23 ± 0.00	0.82 ± 0.00	5.04 ± 0.00	1.25 ± 0.00	0.81 ± 0.00
3 M	5.19 ± 0.04	1.23 ± 0.00	0.82 ± 0.00	5.04 ± 0.00	1.25 ± 0.00	0.81 ± 0.00
4 M	5.15 ± 0.06	1.23 ± 0.00	0.82 ± 0.00	5.04 ± 0.00	1.25 ± 0.00	0.81 ± 0.00

3.12 a) using the Amber and Charmm force field for the peptide (System I). We observe slightly less TMAO depletion when we use the Charmm force field. Therefore the Setschenow coefficient is closer to the experimental value.

The preferential binding coefficient can be split up into contributions as described in the result section. In figure 3.13., we present additional concentration of the partial preferential binding coefficient for the zwitterionic and neutral-terminated pAla. Figure 3.14 shows the partial preferential binding coefficient weighted by the SASA of the corresponding functional group. It can be seen that the charged termini have a big influence on the TMAO binding compared to the internal part, while the influence of the neutral termini is in the same range as the internal part. Table **??** sums up the solvent accessible surface area of the internal peptide parts. It can be seen that the differences of internal peptide-SASA when changing concentrations or the peptide are small. In experiment, the local/bulk partition coefficient can be calculated from the preferential binding coefficient by:[9]

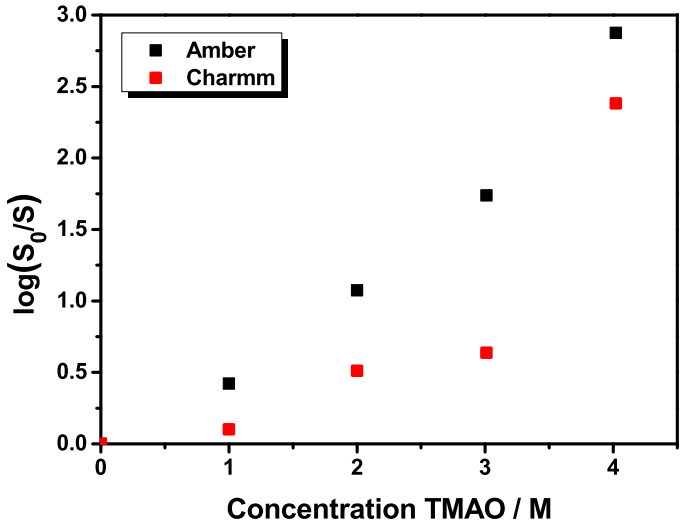

Figure 3.11: Solubility ratio calculated with the zwitterionic peptide (pAla) using the Charmm and Amber force field (System I).

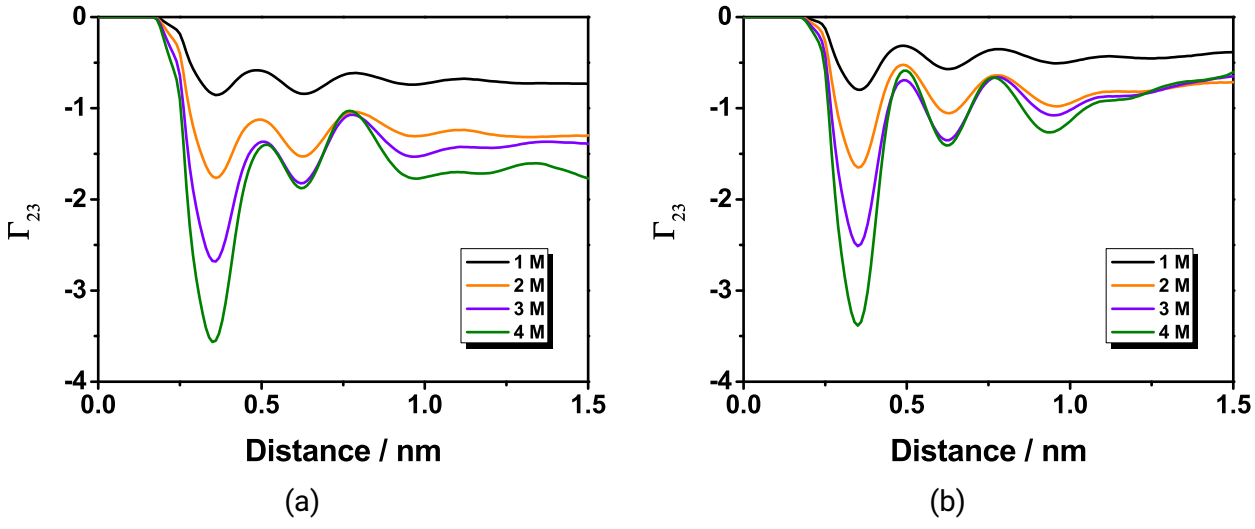

Figure 3.12: Preferential Binding Coefficient of pAla at different concentrations of TMAO and at a) pH=7 (System Ia) b) and pH=13 (System II).

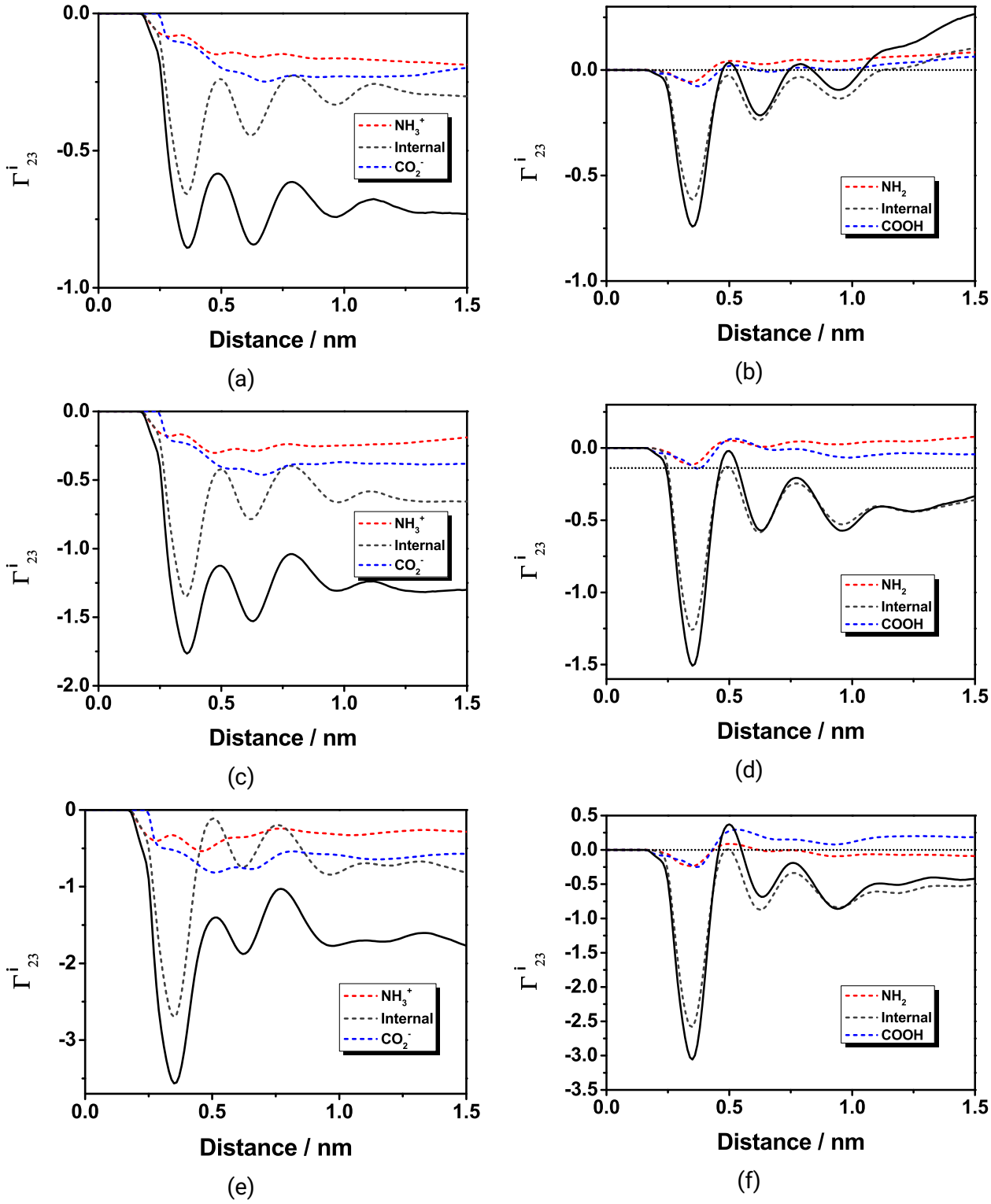

Figure 3.13: Partial preferential binding coefficient Γ^i_{23} for pAla with charged termini (zwitterionic, system Ia) at a) 1 M, c) 2 M and e) 4 M TMAO concentration and pAla with neutral termini (system IV) at b) 1 M, d) 2 M and f) 4 M TMAO concentration. The part of the molecule that does not contain the end groups is referred to as the internal part. The full preferential binding coefficient is shown as the solid line.

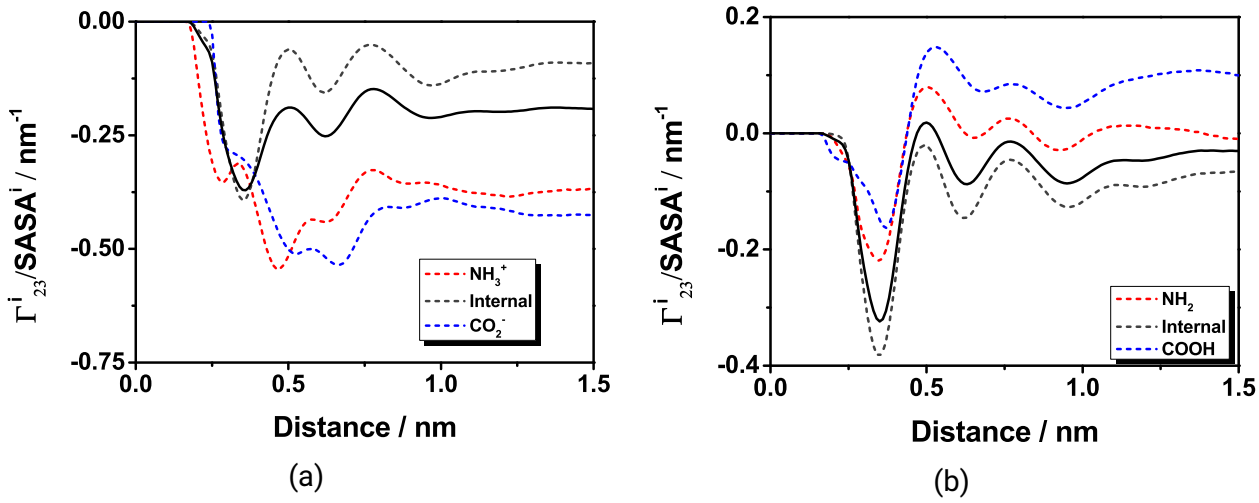

Figure 3.14: Partial preferential binding coefficient Γ^i_{23} for a) pAla with charged termini (zwitterionic, system Ia) and b) pAla with neutral termini (system IV) at 3 M TMAO concentration weighted by the SASA. The part of the molecule that does not contain the end groups is referred to as the internal part. The full preferential binding coefficient is shown as the solid line.

$$K_p = \frac{\Gamma_{23} m_1^o m_3^{-1} + B_1^o}{B_1^o - S_{13}\Gamma_{23}} \tag{22}$$

Here, m_1^o =55 mol H_2O/kg, m_3 is the molal co-solute concentration, B_1^o is the number of water molecules in the local peptide solvation shell in water and S_{13} is the cumulative stochiometry of exchange when adding the co-solute.

Knowledge of the local/bulk partition coefficient gives the local co-solute concentration and thereby the non-ideality in the solvation shell of the peptide can be compared to the bulk non-ideality using equation 23.[9]

$$\alpha = \frac{a_{cc}^{\text{local}}}{a_{cc}^{\text{bulk}}} \frac{c^{\text{local}}}{c^{\text{bulk}}} \tag{23}$$

The local/bulk partition coefficient is also used in experiments, where it is determined indirectly from the preferential binding coefficient. We have calculated the local/bulk partition coefficient as described by Felitsky et al. from our preferential binding coefficients according to equation 22 and obtained the property α which describes the ratio of non-ideality in the local vicinity of the peptide and the bulk in figure 3.15 from equation 23.[9] Similar to the preferential binding coefficient, the local/bulk partition coefficient reveals the non-linear behavior of TMAO preferential binding at low concentrations for System IV. The local non-ideality, as characterized by α, also shows this non-linear trend. In general, the local non-ideality is stronger reduced for the peptide with zwitterionic end groups (System Ia) compared to the neutral-terminated peptide (System IV). The magnitude of α for the peptide with neutral termini is similar to the one determined for glycine betaine with the lacI HTH DNA binding domain (0.92).[9] This difference for our systems stems from the difference in

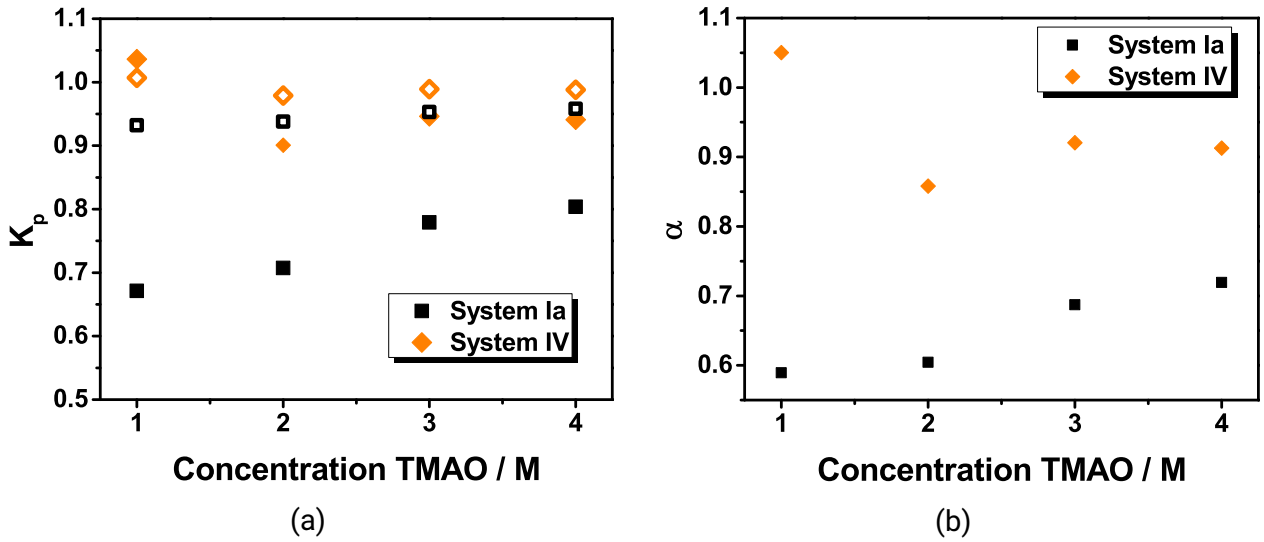

Figure 3.15: a) Closed symbols: Local/bulk partition coefficient of System Ia and System IV obtained from the preferential binding coefficient according to equation 22. The solvation shell is taken at the first minimum of the peptide-water(oxygen) rdf at 0.54 nm. Open symbols: Local/bulk partition coefficient as taken from simulations at 1.1 nm distance (equation 12; 1.1 nm is where the value for the preferential binding coefficient has been taken) b) The local non-ideality parameter α as a function of TMAO concentration for System Ia and System IV.

solute-peptide interactions for both systems. Nevertheless, both TMAO and glycine betaine, which have a similar amphiphilic structure, reduce local non-ideality. This means for both co-solutes, the non-ideality close to the peptide is less dependent on the co-solute concentration than the bulk non-ideality. The exception is the peptide with neutral termini at low concentrations, where the TMAO-TMAO interactions are strengthened close to the peptide compared to the bulk.[9]

We are also interested in the orientation of TMAO in the solvation shell, where we observe local TMAO accumulation. From figure 3.16 b) we might deduce that TMAO slightly prefers to face its methyl groups towards the peptide, as these are closer in the rdf than the nitrogen and oxygen. The contour plot (figure 3.16 a) reveals that very close to the peptide there is a higher probability (cos $\theta \approx 1$) to find TMAO facing its oxygen atom towards the peptide. These are the hydrogen bonded TMAO molecules. There is also a higher probability to find TMAO facing the oxygen away from the peptide (cos $\theta \approx$ -1) a bit farther away from the peptide, so that the methyl groups are facing with the peptide. Nevertheless, in general, also at the distance corresponding to the first peak in the TMAO-peptide proximal rdf, there is an even probability distribution and therefore the TMAO orientation can be described as random.

We also studied quasi-infinite chains of pAla and ELP and are interested in the distribution of TMAO around these chains compared to the pentamers. The local/bulk partition coefficient (figure 3.17 a) shows depletion of TMAO from the chain surface and when looking at the locally resolved K_p^{local} (figure 3.17 b) the local TMAO accumulation can be seen. Comparing the Charmm and Amber force field for the quasi-infinite chains (figure 3.18) again shows that there is less TMAO depletion

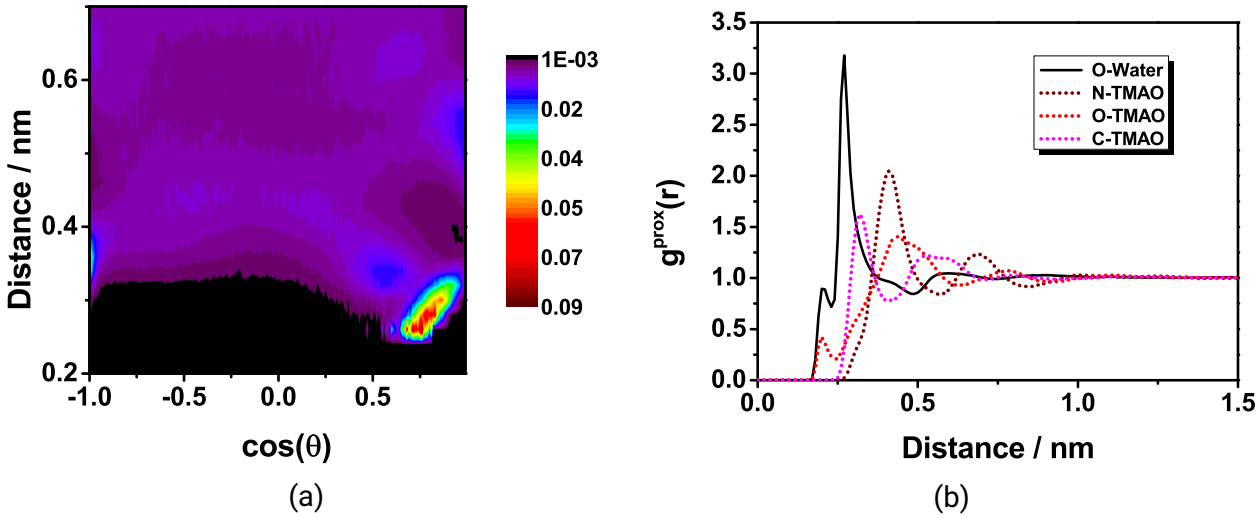

Figure 3.16: a) Probability (color coded) of the orientation of TMAO towards the closest peptide atom (System I). The angle θ is between the vectors of proximal peptide atom to N(TMAO) and oxygen(TMAO) to N(TMAO). The probability distribution has been taken in intervals of distance $\pm$ 0.02 nm. Note that the enhanced probabilty around $\cos\theta \approx 1$ resembles few TMAO molecules, which are close to the peptide at around 0.3 nm. The majority of TMAO molecules are at a distance of around 0.4 nm and are randomly oriented. b) Proximal rdf of water oxygen, TMAO-nitrogen, TMAO-oxygen and TMAO-carbon as a function of peptide-distance.

when using the Charmm force field compared to the Amber force field.

6.2 Peptide Comparison

We summarise further analysis on hydrogen bonds and the tetrahedral order parameter in the following sections.

Peptides lose hydrogen bonds at high TMAO concentration

We investigated the change of the number of hydrogen bonds with increasing TMAO concentration. Especially pSer might show a different behavior since its side chain is able to form hydrogen bonds. Nevertheless, we see that in all cases, the number of hydrogen bonds between the peptide and water decrease when high concentrations of TMAO is added, while it remains nearly constant at low concentrations. The low amount of peptide-TMAO hydrogen bonds formed at high concentrations of TMAO cannot compensate for the loss of peptide-water hydrogen bonds, so that the total number of hydrogen bonds decreases. Comparing peptides, it is observable that pSer forms more hydrogen bonds with TMAO as TMAO prefers to form hydrogen bonds with the side chains instead of the backbone or the end groups, but the trends remain the same.

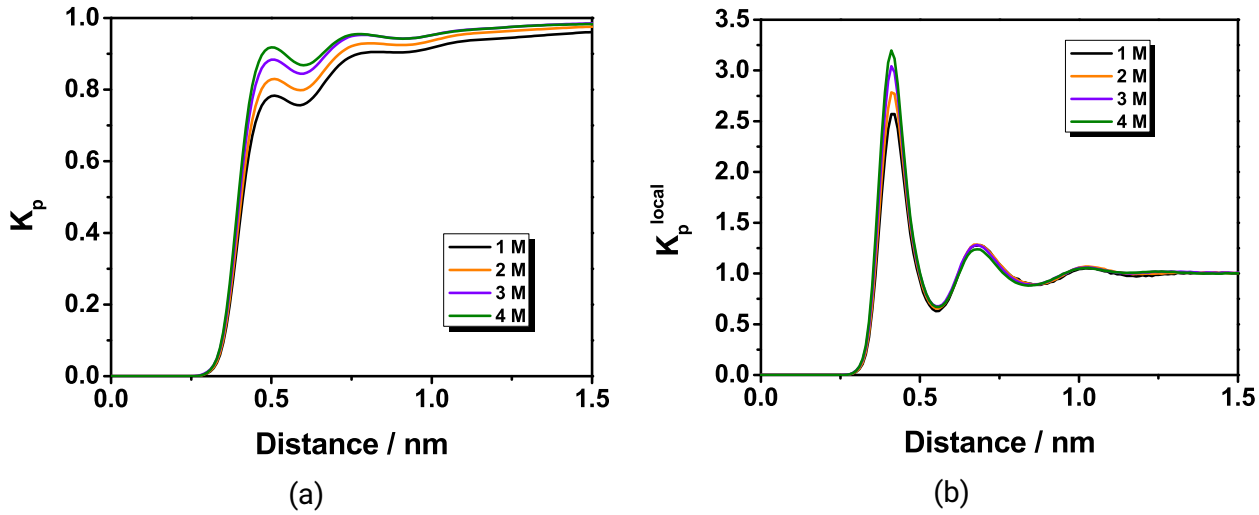

Figure 3.17: Local/bulk partition coefficient of a stretched (quasi-infinite) Ala-15-mer at different concentrations (System Va) a) from the cumulative number and b) locally resolved.

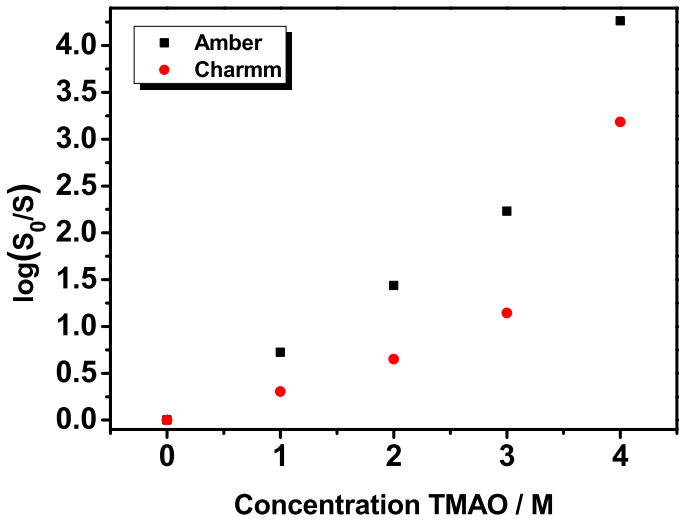

Figure 3.18: Comparison of the solubility ratio of different force fields of the stretched (quasi-infinite) Ala-15-mer (System V) through equation 6.

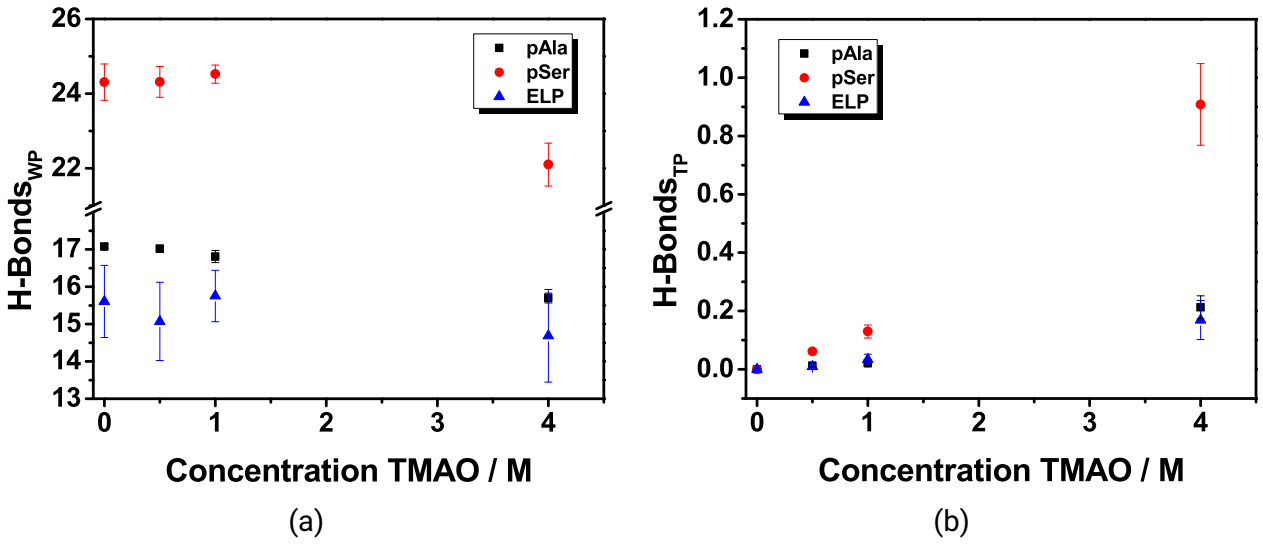

Figure 3.19: Number of hydrogen bonds as a function of TMAO concentration for pAla, pSer and ELP (System VII) at pH = 7 a) between the peptide and water b) and between the peptide and TMAO.

The tetrahedral order reduces when TMAO is added

We see that the tetrahedral structure is not disturbed much by TMAO at low concentrations. Only at a very large concentration, namely 4 M, do the bulky methyl groups of TMAO disrupt the network, both far away and close to the peptide. This does not depend on the chosen peptide. Nevertheless, there are visible differences in tetrahedral order parameter $\langle q \rangle$, between the peptides. These differences disappear quickly beyond 0.5 nm. A higher tetrahedrality observed close to pSer compared to other peptides is due to formation of more hydrogen bonds which allow water to keep its structure. pAla and ELP show very similar behavior although the tetrahedrality close to ELP is slightly smaller. This is due to the smaller number of formed hydrogen bonds between ELP and water as shown in figure 3.19.

6.3 Pressure Effects

(High) Pressure increases the number of peptide-solvent hydrogen bonds

The effect of pressure on the number of hydrogen bonds has been investigated. In figure 3.21 we can observe the changes in hydrogen bonds between peptide and TMAO/water. We see that there is no significant difference in the number of TMAO-peptide hydrogen bonds due to a pressure change. The number of peptide-water hydrogen bonds on the other hand increases when the pressure is increasing as is hinted at by the increased number of water molecules around the peptide. Pressure has no influence on the reduction of the total number of hydrogen bonds with increasing TMAO concentration.

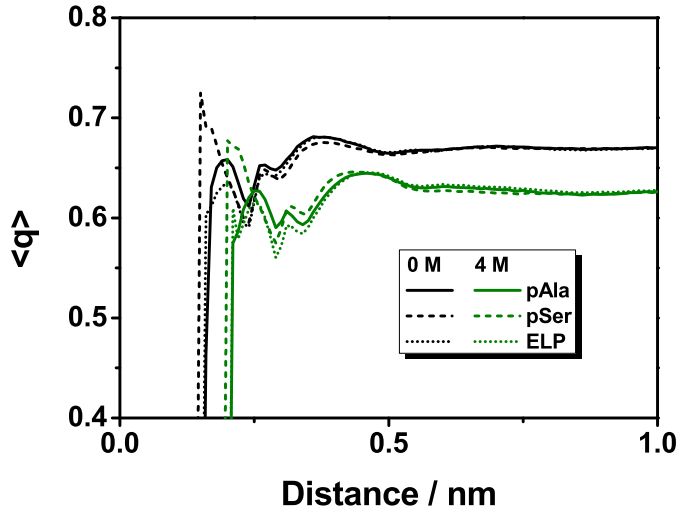

Figure 3.20: Effect of the peptide chemistry on the tetrahedral order parameter in water and in 4 M TMAO as a function of distance from the peptide surface (System VII). Data at 4 M has been shifted by x+0.05 nm to allow a better view.

Pressure increases number of water molecules around the peptide, but decreases tetrahedrality.

The influence of pressure on the number of water and TMAO molecules around pAla can be observed in figure 3.22. While the number of water molecules increases at higher pressure, the change in the number of TMAO molecules with pressure is more complex. The tetrahedral order parameter (figure 3.23) for ELP and pSer shows no different behavior than previously described for pAla. Namely, pressure shows less influence on the tetrahedral order parameter upon addition of TMAO.

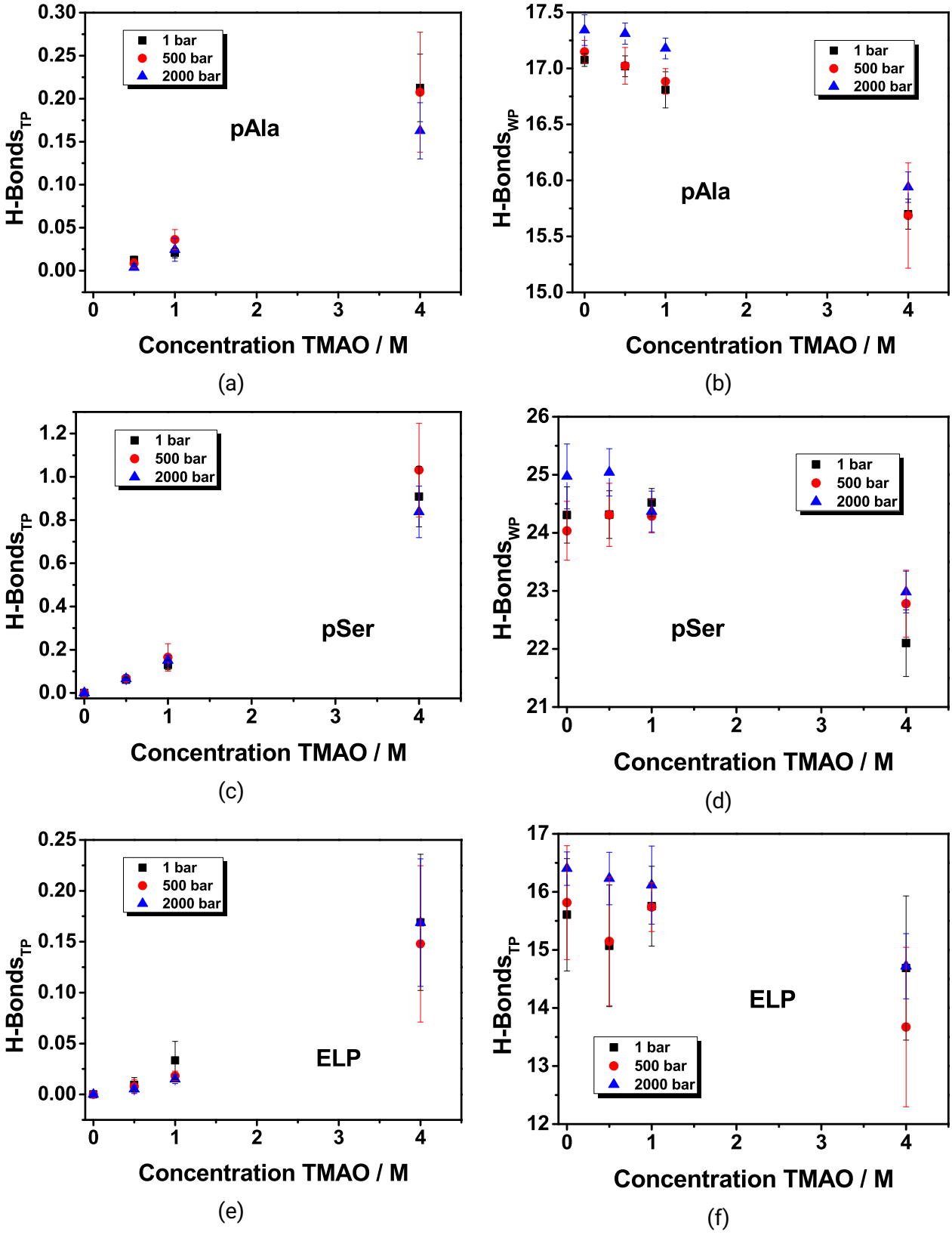

Figure 3.21: Hydrogen Bonds between peptide and TMAO (TP) for a) pAla, c) pSer and e) ELP (System VII) at different pressure. Hydrogen Bonds between peptide and water (WP) for b) pAla, d) pSer and f) ELP (System VII) at different pressure.

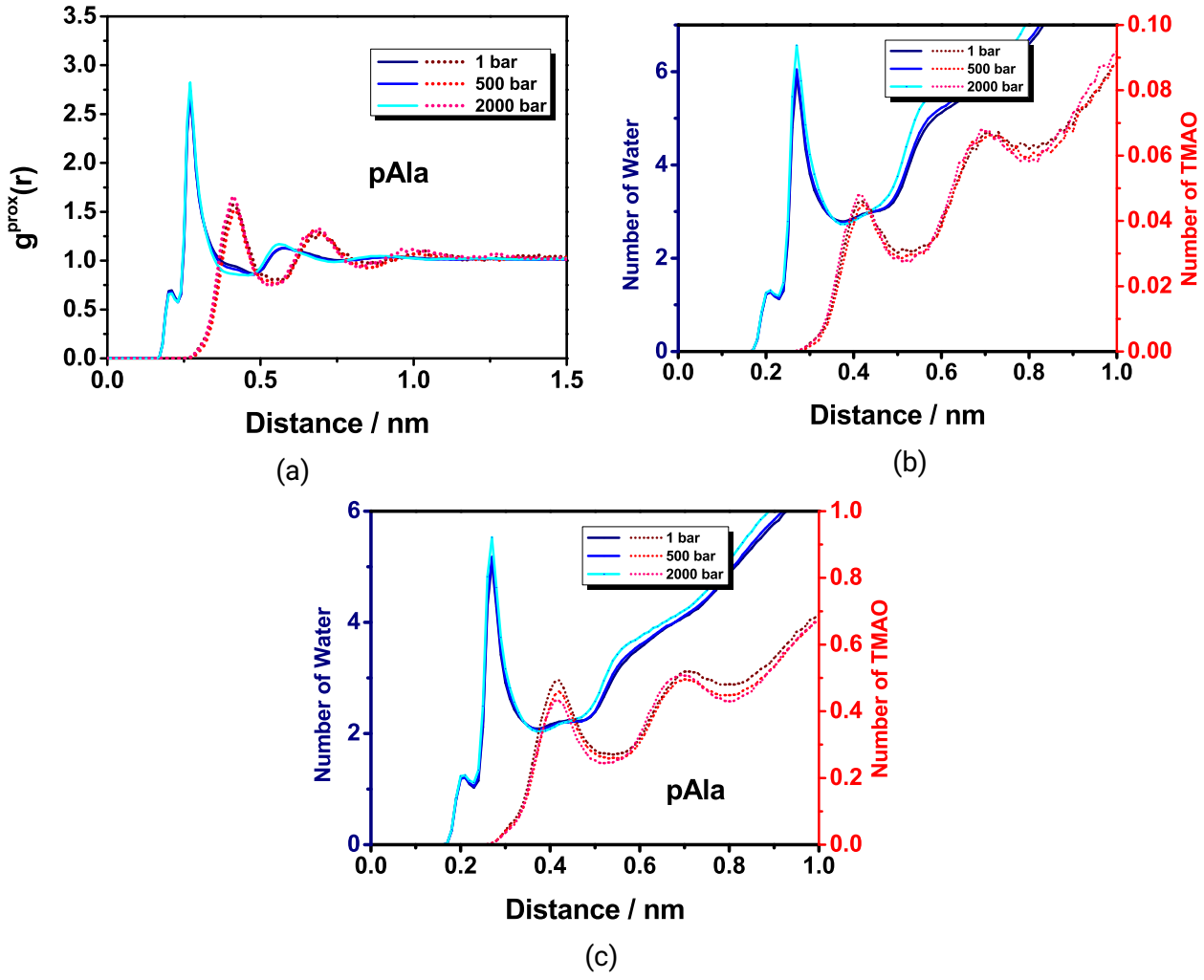

Figure 3.22: a) Proximal rdf of water (blue) and TMAO (red) around pAla at 0.5 M TMAO concentration (System VII). b) Number of Molecules counted in bins of 0.01 nm around the peptide at b) 0.5 M TMAO concentration and c) 4 M TMAO concentration as a function of distance from pAla (System VII).

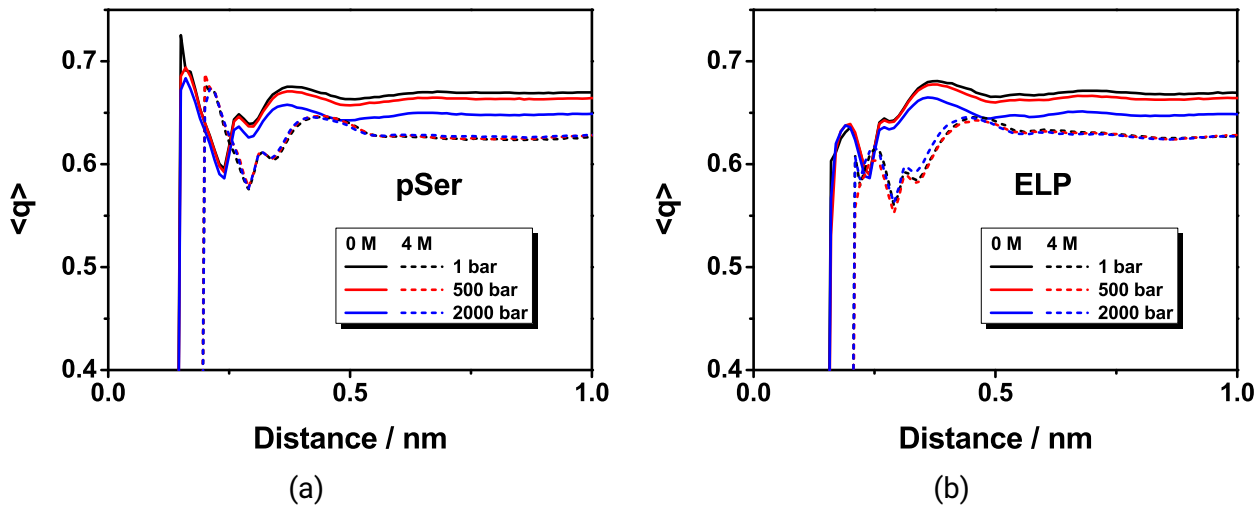

Figure 3.23: Effect of pressure on the tetrahedral order parameter in water and in 4 M TMAO concentration as a function of distance from the peptide surface for a) pSer and b) ELP. Graphs at 4 M are shifted by x+0.05 nm for clarity.

Bibliography

[1] Ganguly, P.; van der Vegt, N. F. A. Convergence of Sampling Kirkwood–Buff Integrals of Aqueous Solutions with Molecular Dynamics Simulations. *J. Chem. Theory Comput.* **2013**, *9*, 1347–1355.

[2] Krüger, P.; Schnell, S. K.; Bedeaux, D.; Kjelstrup, S.; Vlugt, T. J. H.; Simon, J.-M. Kirkwood–Buff Integrals for Finite Volumes. *J. Phys. Chem. Lett.* **2013**, *4*, 235–238.

[3] Milzetti, J.; Nayar, D.; van der Vegt, N. F. A. Convergence of Kirkwood–Buff Integrals of Ideal and Nonideal Aqueous Solutions Using Molecular Dynamics Simulations. *The Journal of Physical Chemistry B* **2018**, *122*, 5515–5526.

[4] Rösgen, J.; Jackson-Atogi, R. Volume Exclusion and H-Bonding Dominate the Thermodynamics and Solvation of Trimethylamine-N-oxide in Aqueous Urea. *J. Am. Chem. Soc.* **2012**, *134*, 3590–3597.

[5] van Buuren, A. R.; Marrink, S. J.; Berendsen, H. J. C. A molecular dynamics study of the decane/water interface. *J. Phys. Chem.* **1993**, *97*, 9206–9212.

[6] Chen, F.; Smith, P. E. Theory and Computer Simulation of Solute Effects on the Surface Tension of Liquids. *J. Phys. Chem. B* **2008**, *112*, 8975–8984.

[7] Liao, Y.-T.; Manson, A. C.; DeLyser, M. R.; Noid, W. G.; Cremer, P. S. Trimethylamine-N-oxide stabilizes proteins via a distinct mechanism compared with betaine and glycine. *Proc. Natl. Acad. Sci. U.S.A.* **2017**, *114*, 2479–2484.

[8] Vargaftik, N. B.; Volkov, B. N.; Voljak, L. D. International Tables of the Surface Tension of Water. *J. Phys. Chem. Ref. Data* **1983**, *12*, 817–820.

[9] Felitsky, D. J.; Record, M. T. Application of the Local-Bulk Partitioning and Competitive Binding Models to Interpret Preferential Interactions of Glycine Betaine and Urea with Protein Surface. *Biochemistry* **2004**, *43*, 9276–9288.

4 Temperature Induced Change of TMAO Effects On Hydrophobic Hydration

This chapter to and is reproduced with permission from

Folberth, A.; van der Vegt, N. F. A; Temperature Induced Change of TMAO Effects On Hydrophobic Hydration. J. Phys. Chem., 2022 with permission from AIP Publishing

Abstract

The effect of trimethylamine-N-oxide (TMAO) on hydrophobic solvation and hydrophobic interactions of methane have been studied with Molecular Dynamics (MD) simulations in the temperature range between 280 K and 370 K at 1 bar ambient pressure. We observe a temperature transition in the effect of TMAO on the aqueous solubility of methane. At low temperature (280 K), methane is preferentially hydrated, causing TMAO to reduce its solubility in water, while above 320 K, methane preferentially interacts with TMAO, causing TMAO to promote its solubility in water. Based on a statistical-mechanical analysis of the excess chemical potential of methane, we find that the reversible work of creating a repulsive methane cavity opposes the solubility of methane in TMAO/water solution more than in pure water. Below 320 K, this solvent-excluded volume effect overcompensates the contribution of methane-TMAO van der Waals interactions, which promote the solvation of methane and are observed at all temperatures. These van der Waals interactions with the methyl groups of TMAO tip the balance above 320 K where the effect of TMAO on solvent-excluded volume is smaller. We furthermore find that the effective attraction between dissolved methane solutes increases with increasing TMAO concentration. This observation correlates with a reduction in the methane solubility below 320 K, but with an increase in methane solubility at higher temperatures.

1 Introduction

Trimethylamine-N-oxide (TMAO) is an organic compound well known as an osmolyte that counteracts the protein-destabilizing effects of pressure. Owing to its large dipole moment, TMAO is a highly water-soluble molecule which forms stable TMAO·2H_2O and TMAO·3H_2O complexes at atmospheric pressure with very long lifetimes exceeding 50 ps at 25 °C.[1] The addition of TMAO to water leads to an increase of the density[2] and to a correspondingly stronger solvent-excluded

volume effect,[3–5] which causes an increase of the chemical potential, and a decrease in solubility, of amino acids.[6,7]

The properties of TMAO are not only determined by its large dipole moment, but also by the hydrophobic groups attached to the positively charged end of the molecule. Computer simulation studies based on all-atom force fields have provided indications that TMAO interacts with, and affects conformational equilibria of, a hydrophobic polymer.[8–11] Interactions of TMAO with hydrophobic regions of the Trpcage mini protein have been reported as well.[12,13] These computer simulations studies indicate that TMAO affects the thermodynamics of hydration of large nonpolar solutes and many-body hydrophobic interactions.

Hydrophobic interactions of TMAO with nonpolar solutes are however comparatively weak. Other amphiphilic organic compounds such as acetone or alcohols bind considerably stronger to hydrophobic polymers[11,14] and to small nonpolar solutes.[15] In particular, this is also observed when the attractive solute-solvent van der Waals forces are neglected in the simulations to examine the role of repulsive excluded-volume interactions. In this respect, TMAO behaves differently, being repelled by small (methane-sized) repulsive solutes but binding weakly to large repulsive solutes.[16] This solute size-dependent binding of TMAO resembles the behavior of weakly hydrated anions which bind to polymers but not to monomers in aqueous solution.[17] This occurs because the local water hydrogen-bonding network is disrupted by large nonpolar solutes but not by small nonpolar solutes. As such, the desolvation of nonpolar groups on polymers occurs at a smaller free-energy cost than the desolvation of the corresponding free monomers, facilitating the binding of weakly hydrated ions.

Based on these considerations, we expect that the binding of TMAO to small nonpolar solutes will be observed only if attractive van der Waals interactions compensate for the desolvation of these solutes and the hydrophobic groups of TMAO. It should be further noted that the local hydrogen-bonding network of water around small nonpolar solutes, and the hydrophobic groups of TMAO, is less tetrahedrally ordered at elevated temperatures, as indicated by the large hydration heat capacity of small nonpolar solutes.[18] We therefore anticipate that the TMAO binding to small nonpolar solutes is temperature dependent.

To further examine this question, we herein study the methane solubility in TMAO/water mixtures as a function of temperature. Such a simple model system, with methane as a hydrophobic solute, allows to make use of computationally efficient test-particle insertions[19] based on which the separate roles of attractive van der Waals interactions and repulsive solvent-excluded volume effects can readily be examined. It will herein be shown that methane-TMAO van der Waals interactions make a critical difference at temperatures above 320 K. Below this temperature, solvent-excluded volume opposes the solvation of methane. While it almost perfectly balances the effect of attractive van der Waals interactions in 1 M TMAO solution, it overcompensates it in 4 M TMAO solution causing a reduction in methane solubility. Above this temperature, methane-TMAO van der Waals interactions however make the critical difference and promote the solvation of methane.

In section II, we discuss the statistical-mechanical approach used in this work to examine the separate roles of repulsive excluded-volume interactions and attractive van der Waals interactions in the excess chemical potential of the solute. Details of the simulations and calculations performed are provided in section III. The results are presented and discussed in section IV and the conclusions are summarized in the final section V.

2 Statistical mechanical analysis of the excess chemical potential

The potential distribution theorem (PDT)[20,21] relates the excess chemical potential of the solute, μ_s^*, and the solute-solvent interaction energy, ψ, according to

$$e^{-\beta\mu_s^*} = \frac{\int e^{-\beta\psi(\mathbf{X})} e^{-\beta U_0(\mathbf{X})} \mathrm{d}\mathbf{X}}{\int e^{-\beta U_0(\mathbf{X})} \mathrm{d}\mathbf{X}} \tag{1}$$

Here, $\beta = \left(k_B T\right)^{-1}$, with k_B the Boltzmann constant and T the temperature. The variable $\mathbf{X}$ refers to the vector of the x, y, z coordinates of all atoms of the solvent (water and TMAO in this work), $U_0(\mathbf{X})$ is the potential energy of solvent configuration $\mathbf{X}$, and $\psi(\mathbf{X})$ refers to the interaction energy of the inserted solute (methane in this work) with the solvent molecules in configuration $\mathbf{X}$. This interaction energy is evaluated at an arbitrary but fixed position of the solute. In shorthand notation, we write

$$e^{-\beta\mu_s^*} = \langle e^{-\beta\psi} \rangle_0 \tag{2}$$

where the subscript 0 attached to the configurational average $\langle ... \rangle_0$ reminds us that equilibrium configurations of the pure solvent are considered (without solute). The test particle insertion method,[19] used to compute μ_s^* in computer simulations, probes $\psi(\mathbf{X})$ with a test particle which does not affect the equilibrium probability density function $e^{-\beta U_0(\mathbf{X})} / \int \mathrm{d}\mathbf{X}\, \mathrm{e}^{-\mathrm{U}_0(\mathbf{X})}$ according to which the solvent configurations are sampled.

The excess chemical potential can be split into contributions originating from the solute-solvent excluded volume repulsion and solute-solvent cohesive attraction. To this end, we write

$$\psi = \psi_R + \psi_A \tag{3}$$

where ψ_R and ψ_A are the contributions of repulsive and attractive solute-solvent interactions to ψ. For nonpolar solutes such as methane, ψ can be expressed as a pairwise additive sum of Lennard-Jones interactions of the solute with all solvent atoms in configuration $\mathbf{X}$. The contributions ψ_R and ψ_A are herein obtained by writing the Lennard-Jones potential, u_{LJ}, as $u_{LJ} = u_R + u_A$ with

$$u_R(r) = \begin{cases} 4\epsilon \left[\left(\frac{\sigma}{r}\right)^{12} - \left(\frac{\sigma}{r}\right)^{6} \right] + \epsilon, & r < 2^{1/6}\sigma \\ 0, & r \geq 2^{1/6}\sigma \end{cases} . \tag{4}$$

and

$$u_A(r) = \begin{cases} -\epsilon, & r < 2^{1/6}\sigma \\ 4\epsilon\left[\left(\frac{\sigma}{r}\right)^{12} - \left(\frac{\sigma}{r}\right)^{6}\right], & r \geq 2^{1/6}\sigma \end{cases} . \tag{5}$$

Here, u_R is the Weeks-Chandler-Andersen (WCA) potential,[22] which accounts for the short-range excluded volume repulsion. The potential u_A accounts for cohesive attraction between the solute and the solvent. We introduce Eq. (3) in Eq. (1) to obtain

$$e^{-\beta\mu_s^*} = \frac{\int e^{-\beta\psi_A(\mathbf{X})} e^{-\beta\left[U_0(\mathbf{X})+\psi_R(\mathbf{X})\right]} d\mathbf{X}}{\int e^{-\beta\left[U_0(\mathbf{X})+\psi_R(\mathbf{X})\right]} d\mathbf{X}} \cdot \frac{\int e^{-\beta\psi_R(\mathbf{X})} e^{-\beta U_0(\mathbf{X})} d\mathbf{X}}{\int e^{-\beta U_0(\mathbf{X})} d\mathbf{X}} \tag{6}$$

where we have divided by and multiplied with $\int d\mathbf{X}\, e^{-\left[U_0(\mathbf{X}) + {}_R(\mathbf{X})\right]}$ in order to write

$$e^{-\beta\mu_s^*} = \langle e^{-\beta\psi_A}\rangle_R \cdot \langle e^{-\beta\psi_R}\rangle_0 \tag{7}$$

In Eq. (7), the term $\langle e^{-\beta\psi_R}\rangle_0$ defines the excess chemical potential, μ_{cav}, of a repulsive (WCA) solute, i.e. according to the PDT (Eq. (1)) we can write $\exp(-\beta\mu_{\text{cav}}) = \langle e^{-\beta\psi_R}\rangle_0$. Notably, μ_{cav}, calculated in computer simulations with test-particle insertions of WCA solutes, corresponds to the reversible work of cavity formation, i.e. to the process of depleting all solvent molecules from a fixed region in space defined by the size and shape of the WCA solute. We therefore refer to μ_{cav} as the cavity contribution to the excess chemical potential, μ_s^*, of the real solute. We further note that local solvent-density fluctuations give rise to spontaneous formation of transient cavities. The ones that are large enough to host the solute at an arbitrary position in the solvent are observed with a probability equal to $\exp(-\beta\mu_{\text{cav}})$. The analysis of μ_{cav} therefore provides information on how the "flexibility" of the solvent medium to open cavities affects the chemical potential of the solute, independent of the effects of cohesive solute-solvent interactions. The term $\langle e^{-\beta\psi_A}\rangle_R$ in Eq. (7) accounts for the cohesive van der Waals interactions of the solute with the pre-formed cavity. We use Eq. (3) to rewrite this term as

$$\langle e^{-\beta\psi_A}\rangle_R = \frac{\int e^{-\beta\left[U_0(\mathbf{X})+\psi(\mathbf{X})\right]} d\mathbf{X}}{\int e^{\beta\psi_A(\mathbf{X})} e^{-\beta\left[U_0(\mathbf{X})+\psi(\mathbf{X})\right]} d\mathbf{X}} = \langle e^{\beta\psi_A}\rangle^{-1} \tag{8}$$

where the configurational averaging $\langle ...\rangle$ is performed using the equilibrium probability density function $e^{-\beta U(\mathbf{X})}/\int d\mathbf{X}\, e^{-U(\mathbf{X})}$ in which $U(\mathbf{X}) = U_0(\mathbf{X}) + \psi(\mathbf{X})$ is the potential energy of solvent configuration $\mathbf{X}$ including the solute molecule located at an arbitrary fixed position. Combining Eq. (7) and Eq. (8) we obtain

$$\mu_s^* = \mu_{\text{cav}} + k_B T \ln\langle e^{\beta\psi_A}\rangle \tag{9}$$

which, upon defining $\delta\psi_A = \psi_A - \langle\psi_A\rangle$, can be written as

Table 4.1: System details: TMAO concentrations, number of water and TMAO molecules, average density and average box volumes (300 K, 1 bar).

TMAO Conc. (M)	# TMAO	# Water	ρ (kg m^{-3})	V (nm^3)
0	0	4000	996.94	120.03
1	73	3715	1000.10	120.23
4	289	2845	1015.94	119.25

$$\mu_s^* = \mu_{\text{cav}} + \langle \psi_A \rangle - Ts_A \tag{10}$$

in which $\langle \psi_A \rangle$ is the average energy corresponding to cohesive solute-solvent attractions and

$$s_A \equiv -k_B \ln \langle e^{\beta \delta \psi_A} \rangle \tag{11}$$

is the fluctuation entropy determined by their fluctuations.[23] The fluctuation entropy is always negative and grows in absolute magnitude with the strength of the "attractive bonds" that cause a biasing of the configuration space of the solvent.[4,24,25] It has been studied in computer simulations of water hydrogen bonding with the π-electron system of benzene,[26] hydrophobic interactions in urea/water solution,[27] water at hydrophobic surfaces[28–30] and polymers in water/cosolvent solutions.[31,32]

3 Methods and Simulation Details

Molecular Dynamics (MD) simulations of TMAO/water and methane/TMAO/water mixtures were performed with the Gromacs package version 4.6.7.[33,34] The cut-off distance for van der Waals interactions was set to 1.0 nm and was combined with long range dispersion corrections applied to pressure and energy. Electrostatic interactions were treated using Particle-Mesh-Ewald (PME)[35] with a real-space cut-off of 1.0 nm, a PME order of 4 and a grid spacing of 0.12. All covalent bonds involving hydrogen atoms were constrained using the LINCS algorithm.[36] We used a united atom force field for methane developed by Ashbaugh et al.[37] Water was described with TIP4P/2005 model,[38] combined with the Hölzl force field[39] for TMAO. This TMAO force field has been proven well in reproducing binary mixture properties.[40] The parameters for cross interactions (TMAO-water, methane-water, methane-TMAO) were determined by the Lorentz-Berthelot combining rules.[41] A cubic box was used with varying amounts of water and TMAO molecules, where the equilibrated box volumes, densities and compositions of the systems investigated with MD are summarized in Table 4.1 for the different TMAO concentrations considered.

Energy minimization was done using the steepest descent algorithm for 10,000 steps and a step size of 0.001 nm. Subsequently, the system was equilibrated in a constant volume-temperature

simulation using the Berendsen thermostat ($\tau_T = 1.0\,\mathrm{ps}$).[42] The temperature ranged from 280 K to 370 K in 10 K increments. The constant volume temperature equilibration was followed by a constant pressure-temperature equilibration using the Berendsen barostat ($\tau_P = 2.0\,\mathrm{ps}$, $p = 1\,\mathrm{bar}$, $\kappa_T = 5 \cdot 10^{-5}\,\mathrm{bar}^{-1}$) for 2.5 ns. The production runs using the Nosé-Hoover thermostat ($\tau_T = 1\,\mathrm{ps}$)[43] and Parrinello-Rahman barostat ($\tau_P = 2.0\,\mathrm{ps}$, $p = 1\,\mathrm{bar}$, $\kappa_T = 5 \cdot 10^{-5}\,\mathrm{bar}^{-1}$)[44] were performed for 100 ns. The first 5 ns were discarded. The integration time step used was 2 fs. Configurations were saved every 1 ps.

The excess chemical potential was calculated with the test-particle insertion (TPI) method. The *NpT* ensemble average corresponding to the canonical ensemble average in Eq. (2) is given by[19]

$$\exp\left(-\mu_s^*/k_\mathrm{B}T\right) = \frac{\langle V \exp\left(-\psi/k_\mathrm{B}T\right)\rangle_0}{\langle V\rangle_0} \tag{12}$$

Note that with this definition of μ_s^*, the ideal gas reference state and the solution have the same solute number density and temperature. The volume, V, that multiplies the exponent in Eq. (12) accounts for volume fluctuations in the *NpT* ensemble. The excess chemical potential was calculated based on 400,000 methane trial insertions per time frame (100,000 frames). An interaction cut off of 1.0 nm was applied together with a long range dispersion correction. To obtain μ_cav, this procedure was repeated using the WCA potential (Eq. (4)) with the parameters of the methane model.

The mean solute-solvent interaction energy, $\langle\psi\rangle$, and the mean attractive solute-solvent interaction energy, $\langle\psi_A\rangle$, were computed from 100 ns constant pressure-temperature simulations based on the systems of Table 4.1 in which one methane solute was introduced. The contributions of the average methane-water and methane-TMAO interaction energy to $\langle\psi\rangle$ were also extracted from these simulations together with the methane-water and methane-TMAO radial distribution functions (RDF).

Methane-methane potentials of mean force, $w(r) = -k_B T \ln g(r)$, were calculated from the methane-methane RDF, $g(r)$, based on the systems of Table 4.1 in which 40 methanes were introduced. The RDFs were corrected using the method of Ganguly to ensure the correct asymptotic tail behavior.[45,46] The MD trajectories with 40 methane solutes in 1 M TMAO and 4 M TMAO solution were furthermore used to determine the methane-water and methane-TMAO Kirkwood-Buff Integrals (KBIs).[47] The KBIs for the solvent components (water-water, TMAO-TMAO, TMAO-water) were obtained from the simulations of the binary solvent (without methane solute). The Krüger and Ganguly corrections[45,48,49] were used to account for finite-size/ensemble effects in the KBIs. Spatial water density distribution functions around TMAO have been calculated using the program Travis.[50] All error bars reported were calculated through block averaging over 5 blocks.

Additionally, we calculated the average tetrahedral order parameter, q, defined as[51–53]

$$q = 1 - \frac{3}{8} \sum_{j=1}^{3} \sum_{k=j+1}^{4} \left(\cos \Psi_{jk} + \frac{1}{3} \right)^2 \tag{13}$$

where Ψ_{jk} is the angle formed by a central oxygen atom on a water molecule or a TMAO molecule and its nearest neighbor oxygen atoms j and k on another water molecule or a TMAO molecule. A tetrahedral order parameter of 1 describes a perfect tetrahedral structure (ice, clathrate), while an order parameter of 0 describes an uncorrelated structure. The tetrahedral order parameter was calculated for the solvent molecules in the solvation shell of methane, the methyl groups of TMAO and for the bulk solution. The cut-off distance used to define the spatial extension of the solvation shell was based on the first minimum of the methane and water(oxygen) RDF (0.54 nm). For the methyl groups of TMAO, this cut-off distance was 0.46 nm.

4 Results

4.1 Force Field Validation

In this work, we use the TIP4P/2005 water model combined with the methane model of Ashbaugh et al.[37] This model reproduces experimental solubilities of methane in water in the same temperature range considered in this work. The remarkable accuracy of this model in describing the methane hydration thermodynamics is linked to the accuracy of the TIP4P/2005 water model in describing the aqueous equation of state. Notably, the reversible work of methane cavity formation is determined by properties of the solvent only, in particular by its density.[3,54–57] In Fig. 4.1, we compare experimental densities of aqueous TMAO mixtures to the densities predicted based on the simulations performed with the Hölzl force field for TMAO.[39] The simulation data are in satisfactory agreement with the experimental data. We therefore expect that the methane cavity thermodynamics is represented well by this force field model. While the methane-water cohesive van der Waals interaction is accurately represented by the methane model selected, we rely on the Lorentz-Berthelot combining rule in describing methane-TMAO cohesive van der Waals interactions. To the best of our knowledge, there exists no experimental data on methane solubility in TMAO-water solutions.

4.2 TMAO's effect on the aqueous solubility of methane is temperature dependent

Figure 4.2(a) shows the excess chemical potential of methane as a function of temperature in water and in two water/TMAO solutions with 1 M and 4 M TMAO. The methane solubility coefficient,

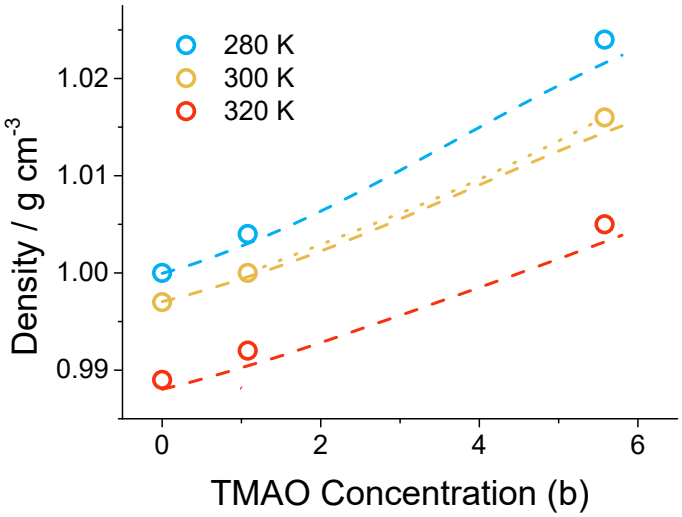

Figure 4.1: The density of binary water/TMAO mixtures as a function of TMAO concentration in molality b taken from experiments and simulations. Dashed lines represent experimental data taken from Ref 2. The data is extrapolated from 4.3 m TMAO concentration onward. The dotted line represents experimental data taken from Ref. 58. Simulation data is shown as symbols.

denoted Σ, is related to the excess chemical potential according to $\Sigma = \exp\left(-\mu_s^*/k_BT\right)$ and is shown in Fig. 4.2(b). This quantity is also referred to as the Ostwald coefficient of gas solubility and is equal to the ratio of the molar concentration, $\rho^{\text{sol}}_{\text{CH}_4}$, of methane gas dissolved in the solution and the molar concentration, $\rho^{\text{gas}}_{\text{CH}_4}$, of methane gas in the gas phase at equilibrium with the solution, i.e. $\Sigma = (\rho^{\text{sol}}_{\text{CH}_4}/\rho^{\text{gas}}_{\text{CH}_4})_{\text{eq}}$. The calculation of μ_s^* was performed for ten different temperatures in the range between 280 K and 370 K at constant 1 bar pressure. The data in Fig. 4.2(a) show a negative concavity, and therefore a positive solvation heat capacity $c_p^* = -T\left(\partial^2\mu_s^*/\partial T^2\right)_p$, characteristic for hydrophobic hydration at all TMAO concentrations. At temperatures below 320 K, the methane solubility in water is not significantly affected by introducing 1 M TMAO. The methane solubility however decreases in this temperature range upon increasing the TMAO concentration to 4 M. Above 320 K, the dependence of the methane solubility on TMAO concentration is inverted, i.e. the presence of TMAO leads to an increased solubility of methane gas.

To rationalize these observations in terms of thermodynamic affinities between the solution components, we make use preferential binding theory.[59] We use the standard convention and refer to the solvent (water) as component 1, the solute (methane) as component 2 and the cosolvent (TMAO) as component 3. In the dilute solute limit $\rho_2 \to 0$, the dependence of $\mu_2^*(=\mu_s^*)$ on the molar concentration ρ_3 of TMAO can be expressed as

$$\left(\frac{\partial\mu_2^*}{\partial\rho_3}\right)_{T,p} = \frac{-k_BT\left(G_{23}-G_{21}\right)}{1+\rho_3\left(G_{33}-G_{31}\right)} \tag{14}$$

in which the G_{ij}s are the KBIs which quantify the thermodynamic affinities between the solution

components. If $(G_{23} - G_{21}) > 0$, methane (2) preferentially attracts TMAO (3) in its solvation shell; if $(G_{23} - G_{21}) < 0$, methane (2) preferentially attracts water (1) in its solvation shell. In the former case, the methane gas solubility increases (μ_2^* decreases) when the concentration of TMAO is increased. In the latter case, the methane gas solubility decreases (μ_2^* increases) when the concentration of TMAO is increased. Note that the denominator on the right hand side of Eq. (14) is positive for stable solvent/cosolvent mixtures. Returning to the data in Fig. 4.2(a), we thus conclude that methane is preferentially hydrated (contains excess water in its solvation shell) when TMAO is present (> 1 M) in the solution at low temperatures (dark grey area). Conversely, methane preferentially interacts with TMAO at high temperatures (white area). Furthermore, a transition region region is observed (Fig. 4.2, light grey area) where TMAO displays a nonlinear influence on the methane solubility, moderately raising it in 1 M TMAO, but decreasing it in 4 M TMAO compared to water. The comparison of the data in pure water and in 1 M TMAO however only show small differences, indicating that the difference between the methane-TMAO and methane-water affinities, $(G_{23} - G_{21})$, is small at low TMAO concentration.

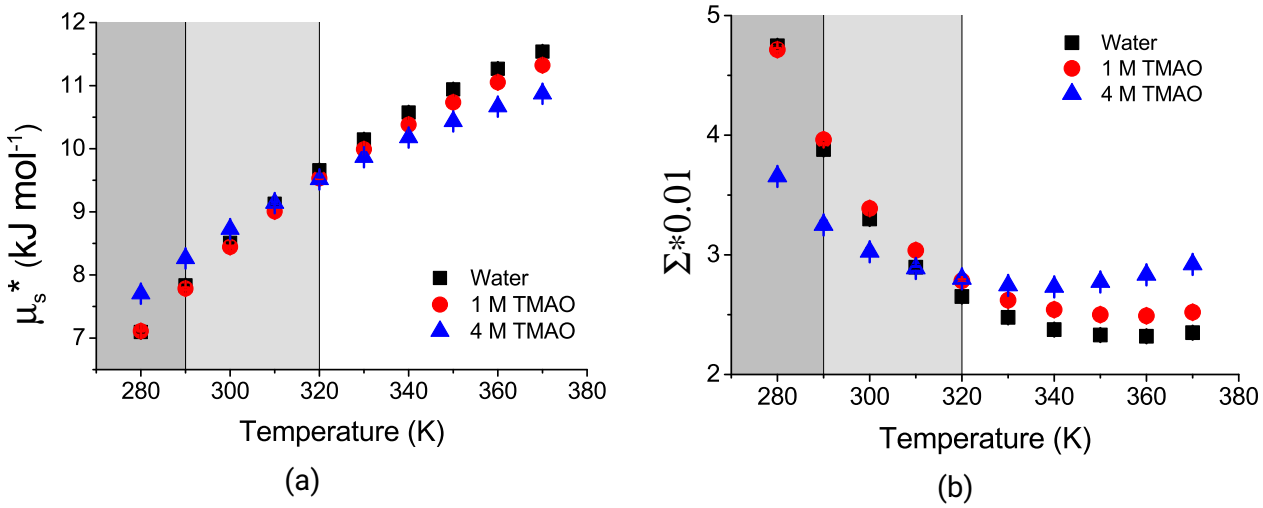

Figure 4.2: a) The excess chemical potential μ_s^* of methane in water/TMAO mixtures as a function of temperature. b) The solubility coefficient Σ of methane in TMAO/water mixtures as a function of temperature. The methane solubility is reduced by TMAO in the dark grey region, increased in the white region and nonlinearly affected in the light grey region.

At low temperatures, the data in Fig. 4.2 indicate that in 4 M TMAO the methane-water affinity exceeds the methane-TMAO affinity. We confirmed this by calculating the methane-water (G_{21}) and methane-TMAO (G_{23}) KBIs from the corresponding RDFs obtained from MD trajectories in which, contrary to the infinitely dilute limit of the solute in Fig. 4.2, 40 methanes were contained in simulation boxes. Fig. 4.3 (a) and (b) show G_{21} and G_{23} in 1 M and 4 M TMAO solutions, respectively, as a function of the temperature. The data corroborate the conclusions that methane preferentially interacts with water at low temperatures while it preferentially interacts with TMAO at high temperatures. Note that the crossover in this behavior is observed at a lower temperature in

Figs. 4.3 (a) and (b) than in Fig. 4.2 which is probably caused by the higher methane concentration.

At high temperatures, methane preferentially interacts with TMAO, i.e. $G_{23} > G_{21}$. This correlates with the observation that the water hydrogen bonded network around methane becomes less tetrahedrally ordered above 320 K, as will be shown below. Moreover, TMAO is less strongly hydrated at higher temperatures, facilitating its interaction with methane. This is observed in Fig. 4.3 (c) and (d), which shows the water-water (G_{11}), TMAO-water (G_{31}) and TMAO-TMAO (G_{33}) KBIs as a function of temperature. While the G_{31} decreases as a function of the temperature, G_{11} stays constant (1 M) or moderately increases (4 M). The water affinity of TMAO (G_{31}) therefore reduces with increasing temperature while the water-water self-affinity (G_{11}) increases, consistent with the observation that methane preferentially interacts with TMAO at higher temperatures. Note that also the TMAO-TMAO self-affinity (G_{33}) increases as a function of the temperature, in particular in the system with 1 M TMAO.

Figure 4.4 shows TMAO-water RDFs at different temperatures. The TMAO(oxygen)-water(oxygen) RDF in Fig. 4.4(a) has a sharp first peak indicating that TMAO-water hydrogen bonds are observed at all temperatures. By taking the integral over the first peak we find that the corresponding average number of TMAO-water hydrogen bonds changes from 2.9 at 280 K to 2.8 at 370 K in the 4 M aqueous TMAO solution (3.0 to 2.97 in 1 M aqueous TMAO solution). The spatial water density distribution functions shown in the inset of Fig. 4.4(a) indicate that the density of water around the methyl groups of TMAO is lower at higher temperatures. This is confirmed by the TMAO(carbon)-water(oxygen) RDFs shown in Fig. 4.4(b).

Figure 4.5 shows the methane-water (a,c) and methane-TMAO (b,d) RDFs as a function of temperature for the 1 M (a,b) and 4 M TMAO (c,d) solutions. We first discuss the system with 1 M TMAO in Figs. 4.5(a) and (b). Interestingly, methane interacts with TMAO at all temperatures. Therefore, a microscopic picture that assumes methane to be repelled by the strongly bound hydration shells of TMAO does not apply. It can further be observed that the first peak of the methane-water RDF decreases with increasing temperature (Fig. 4.5(a)) while the first peak in the methane-TMAO RDF increases (Fig. 4.5(b)). Accordingly, the methane-TMAO affinity (G_{23}) increases while the methane-water affinity (G_{21}) decreases, leading to preferential interaction with TMAO ($G_{23} - G_{21} > 0$) and an increasing methane gas solubility at high temperatures as observed in Fig. 4.2. Microscopically, the insertion of methane in the hydration shell of TMAO is facilitated by the weaker TMAO-water affinity (Fig. 4.3) and the partial dehydration of the TMAO methyl groups (inset in Fig. 4.4(a)) at higher temperatures. In the system with 4 M TMAO, shown in Figs. 4.5(c) and (d), the first peak of the methane-water RDF also decreases with increasing temperature, while the first peak in the methane-TMAO RDF is hardly affected by changes in temperature. This again shows that methane interacts with TMAO but temperature variations do not significantly affect this interaction. At this high TMAO concentration, the observed methane-TMAO contacts may be due to strong TMAO crowding effects which do not significantly depend on the temperature. Therefore, the transition from preferential hydration of methane at low temperatures ($G_{23} - G_{21} < 0$), as implied by the data

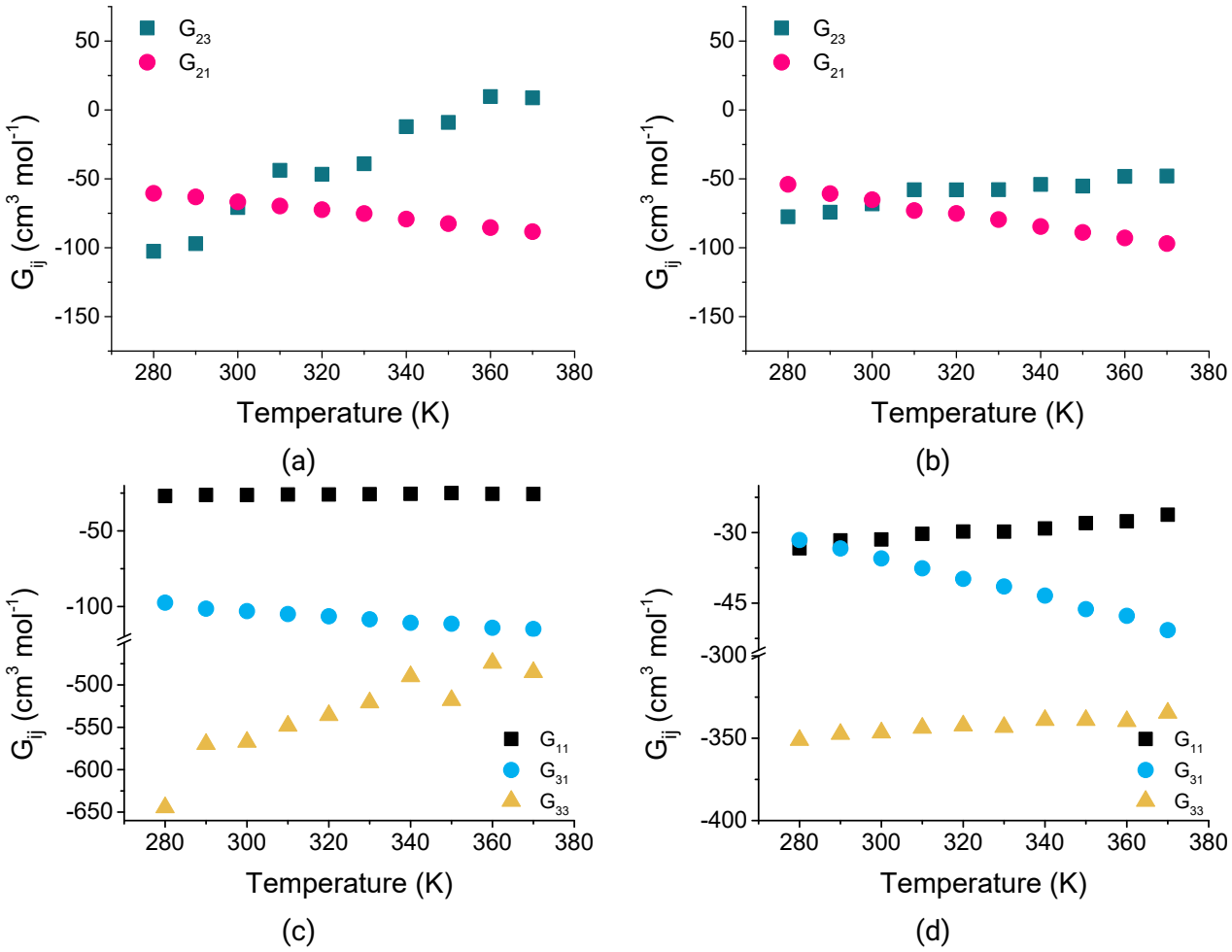

Figure 4.3: Temperature dependence of methane-water (G_{21}) and methane-TMAO (G_{23}) Kirkwood-Buff integrals in (a) 1 M and (b) 4 M aqueous TMAO solution calculated from simulation boxes containing 40 methane molecules. Water-water (G_{11}), TMAO-water (G_{31}) and TMAO-TMAO (G_{33}) Kirkwood-Buff integrals as a function of temperature in (c) 1 M and (d) 4 M aqueous TMAO solution.

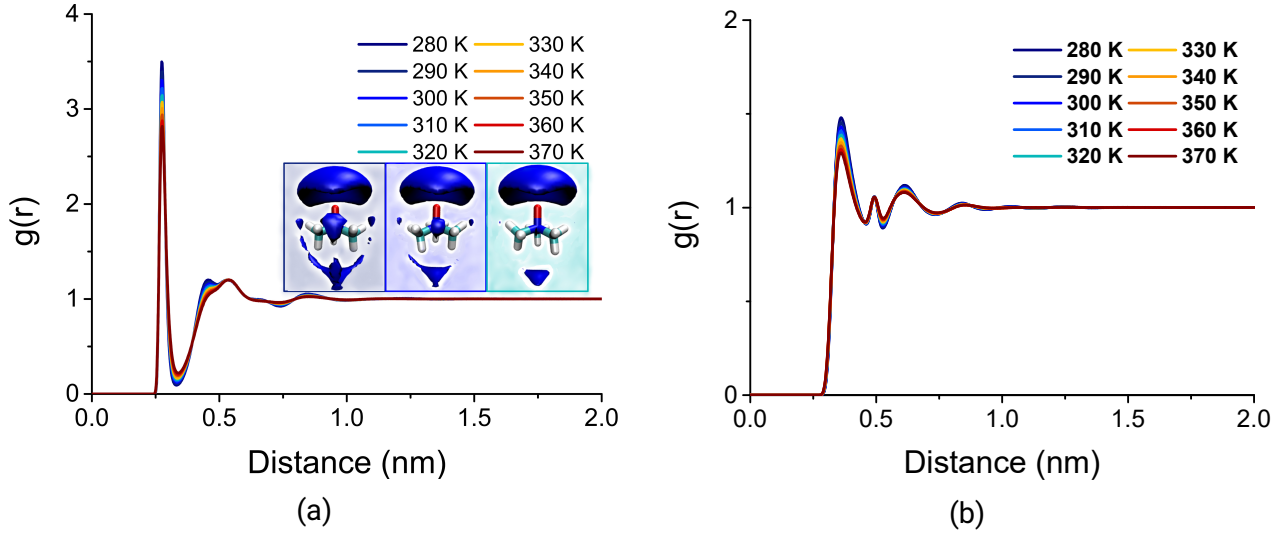

Figure 4.4: a) RDF between the water oxygen and TMAO oxygen at different temperatures in 1 M TMAO solution. Insets show spatial water density maps around a TMAO molecule at 280 K (left), 300 K (middle) and 320 K (right) using an isovalue corresponding to ∼ 4 times the density of bulk water b) RDF between the water oxygen and TMAO carbon atoms.

in Fig. 4.2, to preferential interaction with TMAO at high temperatures ($G_{23} - G_{21} > 0$) is caused by a decrease in methane-water affinity (G_{21}) only. This correlates with the decrease in TMAO-water affinity (Fig. 4.3) because methane and TMAO share their solvation shells in a crowded 4 M TMAO solution.

4.3 Enthalpy-entropy and cavity decomposition of the excess chemical potential

We start by considering temperature derivatives of μ_s^* which provide information on the excess partial enthalpy, $h_s^* = -T^2 \left(\partial(\mu_s^*/T)/\partial T\right)_p$, excess partial entropy, $s_s^* = -\left(\partial \mu_s^*/\partial T\right)_p$, and excess partial heat capacity, $c_p^* = -T \left(\partial^2 \mu_s^*/\partial T^2\right)_p$, of the solute. Note that at constant pressure these quantities are local, i.e. they quantify the properties of the solvation shell in excess to the bulk solvent far away from the inserted solute.[60] Below, we will refer to them as the solvation enthalpy, solvation entropy and solvation heat capacity, respectively. To determine these properties, we fitted the excess chemical potential using the function

$$\mu_s^* = aT + bT\rho^2 - c\rho \tag{15}$$

which was previously used by Ashbaugh et al.[37] and is based on an information theory model.[61,62] The constants a, b and c in Eq. (15) are temperature independent fitting parameters and ρ is

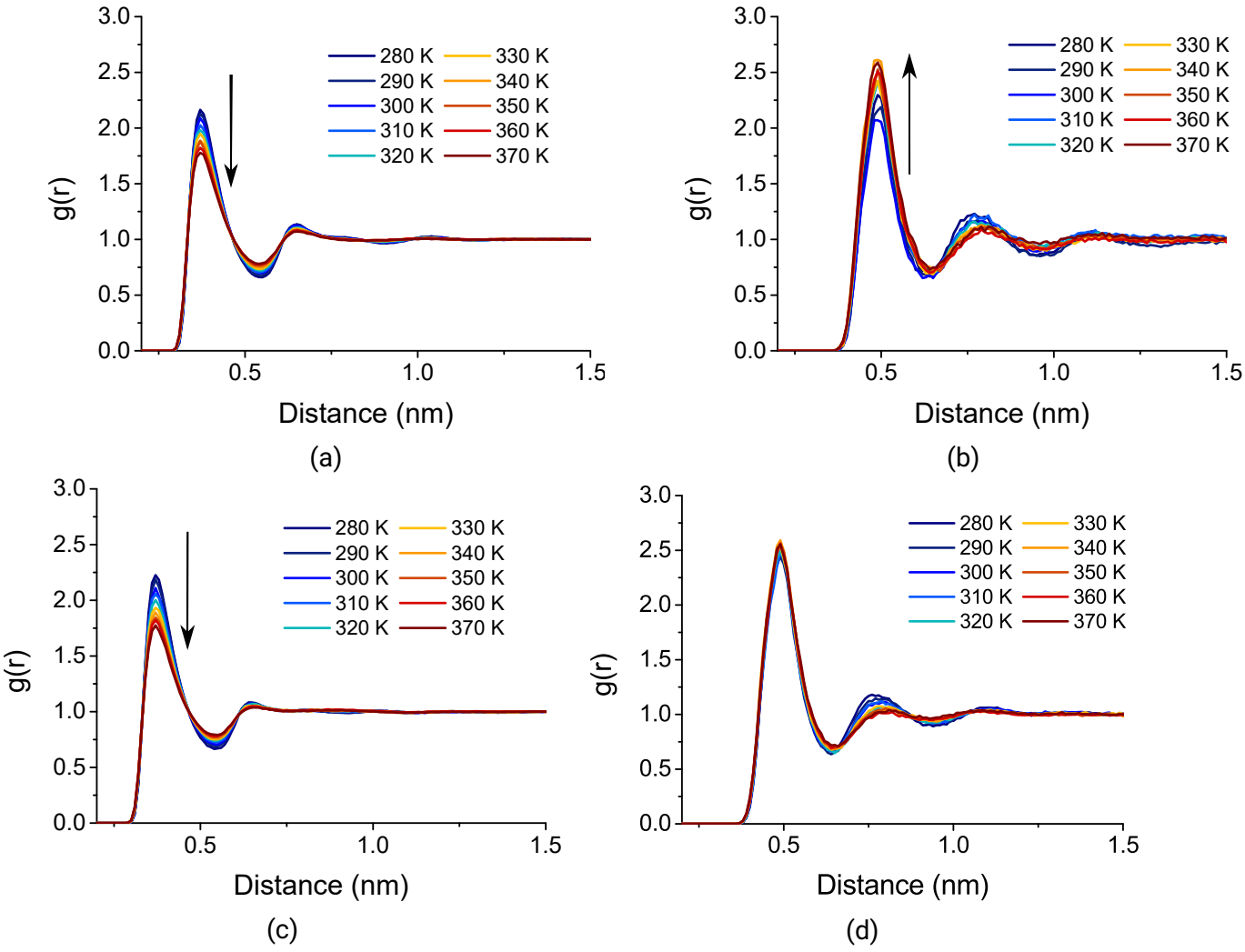

Figure 4.5: a) The methane-water(oxygen) RDF and b) the methane-TMAO(nitrogen) RDF at different temperatures in 1 M aqueous TMAO solution. c) The methane-water(oxygen) RDF and d) the methane-TMAO(nitrogen) RDF at different temperatures in 4 M aqueous TMAO solution. Arrows indicate the direction of change in first peak heights with increasing temperature.

Table 4.2: Fitting parameters γ_i for the Laurent polynomial (units kg m^{-3} K^{2-i}) to obtain the density and fitting parameters a, b, c to obtain the chemical potential from Eq. (15).

TMAO Conc. (M)	γ_0	γ_1	γ_2	γ_3
0	-296602000	4245120	-23793.80333	73.86357
1	-11868500	-50383.56132	2237.00227	-5.21065
4	-269574000	4233910	-25525.3324	83.61322

TMAO Conc. (M)	γ_4	γ_5	a (kJ mol^{-1} K^{-1})
0	-0.11093	$6.51984\cdot10^{-5}$	-0.031 (0.00105)
1	0.00937	$-8.03339\cdot10^{-6}$	-0.03161 (0.00179)
4	-0.13128	$8.05476\cdot10^{-5}$	-0.03375 (0.0031)

TMAO Conc. (M)	b (kJ mol^{-1} K^{-1} kg^{-2} m^6)	c (kJ mol^{-1} kg^{-1} m^3)
0	$1.10069\cdot10^{-7}$ ($1.5\cdot10^{-9}$)	0.01505 ($1.34\cdot10^{-4}$)
1	$1.07579\cdot10^{-7}$ ($2.53\cdot10^{-9}$)	0.01439 ($2.30\cdot10^{-4}$)
4	$9.88682\cdot10^{-8}$ ($4.51\cdot10^{-9}$)	0.01154 ($4.65\cdot10^{-4}$)

the solvent mass density which is temperature dependent. The dependence of ρ on the temperature was obtained by fitting ρ, obtained from the simulations, with a Laurent polynomial $\rho = (\sum_{i=0}^{5} \gamma_i T^i)/T^n$, where γ_i are temperature independent fitting parameters and $n = 2$ for TIP4P/2005 water.[37] The parameters of this fit are summarized in Table 4.2.

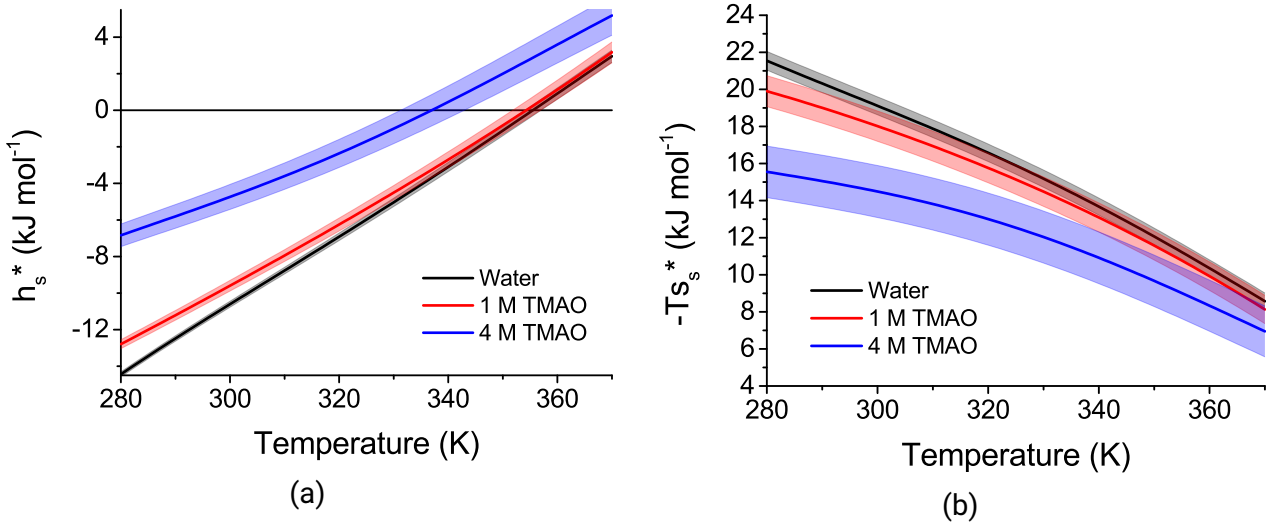

Figure 4.6: Contributions of a) the solvation enthalpy (h_s^*) and b) the solvation entropy ($-Ts_s^*$) to the excess chemical potential, $\mu_s^* = h_s^* - Ts_s^*$, of methane in water and in TMAO/mixtures as a function of temperature.

Fig. 4.6 shows the methane solvation enthalpy and entropy obtained using this procedure as a function of the temperature for pure water and the 1 M and 4 M aqueous TMAO solutions. The data obtained at 298 K are compared to experimental values in Table 4.3. The experimental and

Table 4.3: Solvation thermodynamic properties of methane in water and in 1 M and 4 M aqueous TMAO solution at 298 K and 1 bar. Experimental values for water are taken from References 37, 63, 64.

	μ_s^* (kJ mol^{-1})	h_s^* (kJ mol^{-1})	s_s^* (J mol^{-1} K^{-1})	c_p^* (J mol^{-1} K^{-1})
Exp.	8.37	–11.38	–66.52	204.18
0 M	8.37	–11.0 (0.2)	–65.0 (1.6)	185.7 (3.2)
1 M	8.30	–9.9 (0.3)	–61.2 (2.8)	158.6 (4.6)
4 M	9.66	–5.0 (0.5)	–49.0 (0.7)	108.1 (5.5)

simulation data for methane solvation in water are in almost quantitative agreement. Note that the temperature derivatives of μ_s^*, rather than μ_s^* itself, depend strongly on the water model,[65] in particular on its coefficient of thermal expansion,[65,66] which varies considerably from one water model to another, but is in close agreement with the experimental value for the TIP4P/2005 model.[38] At room temperature, methane solvation in water is accompanied with a negative solvation enthalpy. This is due to favorable water-methane van der Waals interactions that overcompensate the positive enthalpy change associated with solvent reorganization (changes in solvent-solvent interactions).[65,67] The presence of TMAO in the solution causes a positive shift in h_s^* and s_s^* relative to the values in neat water (Fig. 4.6). This is expected for aqueous solvation of nonpolar gaseous solutes in the presence of strongly hydrated cosolvents.[68] It is caused by a positive solvent reorganization enthalpy, which affects both quantities (h_s^* and s_s^*) and is larger in the water/cosolvent mixture than in neat water.[69] Accordingly, solvent-solvent interactions in the solvation shell of methane are more significantly perturbed in the water/TMAO mixture than in neat water. This is confirmed by comparing the difference in the tetrahedral order, Δq, between the solvation shell of methane and the bulk solution in Fig. 4.7(a). With increasing TMAO concentration, Δq shifts to larger negative values, indicating that the solvation shell of methane in water/TMAO solution is less ordered than the bulk. Note that Δq is positive in neat water below 320 K, indicating that in this system the hydration shell of methane has stronger tetrahedral order than bulk water. Above 320 K, the hydrogen bonds in the hydration shell of methane are less tetrahedral and therefore weaker. This observation is in agreement with experimental observations[70] and correlates with the larger solvation heat capacity (c_p^*, see Table 4.3) of the solvation shell of methane in neat water as compared with the water/TMAO solutions. It furthermore correlates with the observation that preferential methane-TMAO interactions and a corresponding increase in methane gas solubility occurs above 320 K (Fig. 4.2). Contrary to methane, the tetrahedral order in the solvation shell of the methyl groups of TMAO, shown in Fig. 4.7(b), is reduced compared to the bulk at all temperatures and has a weaker temperature dependence.

We proceed by considering the statistical mechanical quantities that contribute to the excess chemical potential. Fig. 4.8(a) shows the mean solute-solvent energy, $\langle\psi\rangle$, obtained from the averaged solute-solvent Lennard-Jones interactions in the simulations with methane in a 4 M aqueous TMAO solution, as a function of the temperature. The data show that the mean methane-TMAO

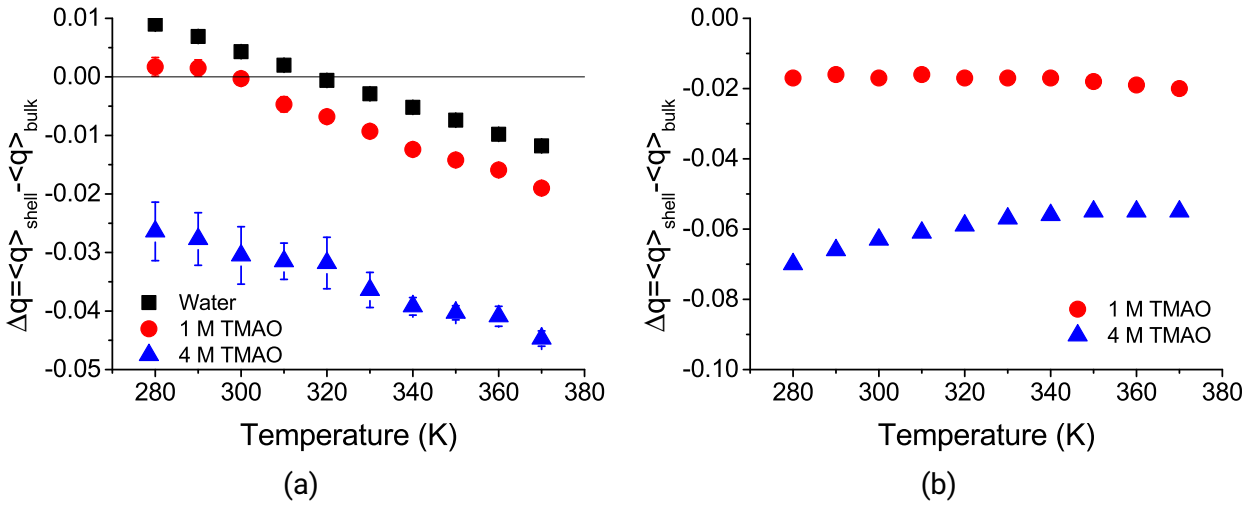

Figure 4.7: Tetrahedral order parameter of (a) the solvation shell of methane (defined up to 0.54 nm from the methane molecule) relative to its bulk value in water, 1 M and 4 M TMAO solution as a function of temperature (b) the solvation shell of methyl groups on TMAO (defined up to 0.46 nm from the methyl group) relative to its bulk value in 1 M and 4 M TMAO solution as a function of temperature.

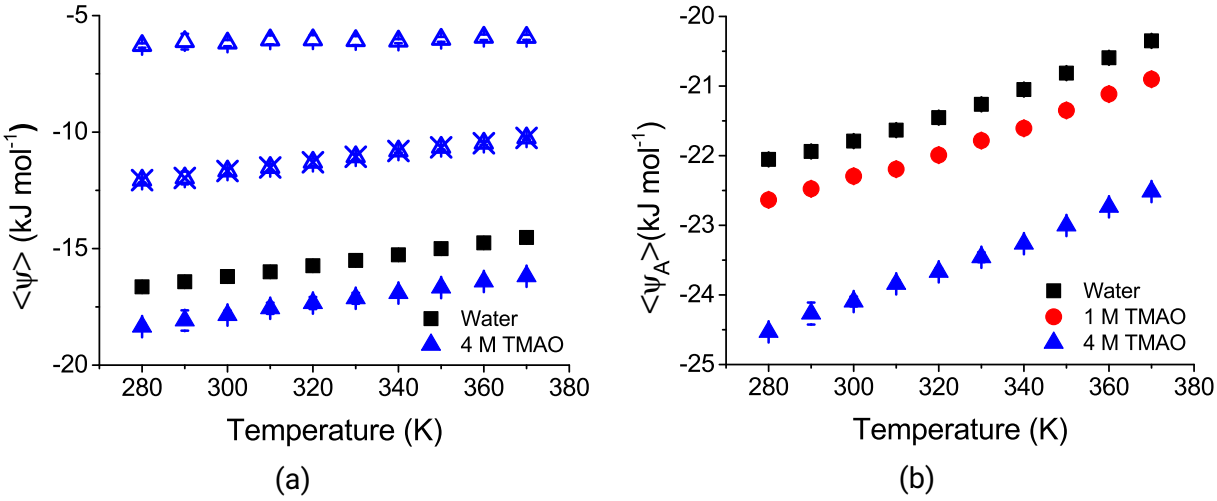

Figure 4.8: a) The average methane-solvent energy $\langle\psi\rangle$ (closed symbols) and its contributions from methane-TMAO (open symbols) and methane-water (open crossed symbols) interactions in water and 4 M TMAO solution as a function of temperature. b) The average attractive interaction energy $\langle\psi_A\rangle$ of methane with the solvent in water, 1 M TMAO and 4 M TMAO solution as a function of temperature.

interaction energy is negative and constant across the entire temperature range. Consistent with the observations made in Fig. 4.5(d) this indicates that favorable methane-TMAO van der Waals interactions occur at all temperature considered. The average methane-water interaction energy is also negative but its absolute value decreases as a function of the temperature. A correspondingly weaker methane-water interaction is also observed in Fig. 4.5(c) for the higher temperatures. Fig. 4.8(b) shows the mean attractive solute-solvent energy, $\langle \psi_A \rangle$, related to the attractive part of the Lennard-Jones interaction defined by Eq. (5). This quantity corresponds to the cohesive energy component in Eq. (10) for the excess chemical potential of the solute. The cohesive interaction of methane with the solvent in the solutions with TMAO is stronger than in neat water at all temperatures. This is again indicative of favorable methane-TMAO interactions. It however furthermore indicates that the transition from preferential hydration of methane at low temperatures to preferential interaction of methane with TMAO at high temperatures (Fig. 4.2) cannot be explained solely based on changes in the mean attractive solute-solvent interactions.

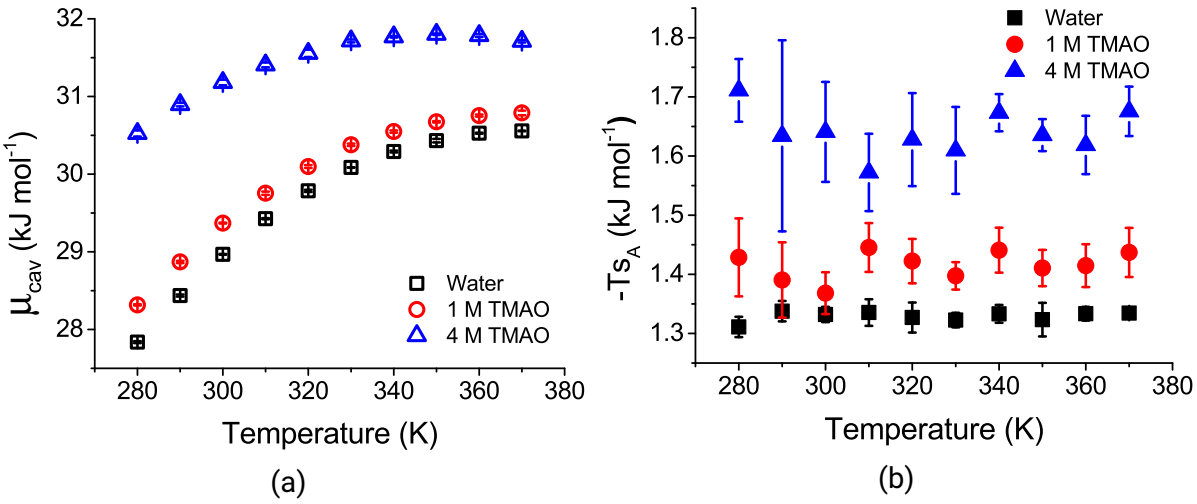

Figure 4.9: a) The cavity contribution to the excess chemical potential of methane molecule in TMAO/water mixtures as a function of temperature. b) The fluctuation entropy contribution to the excess chemical potential of methane in TMAO/water mixtures as a function of temperature.

Fig. 4.9(a) shows the excess chemical potential, μ_{cav}, of WCA methane solutes in water and TMAO/water solutions as a function of temperature. In contrast to the excess chemical potential of methane in Fig. 4.2(a), the curves of $\mu_{\text{cav}}(T)$ for the different TMAO concentrations do not intersect. Therefore, the transition from preferential hydration of methane to preferential interaction of methane with TMAO, implied by the data in Fig. 4.2(a), does not occur for the repulsive WCA solute. The data in Fig. 4.9(a) further show that μ_{cav} increases not only as a function of the temperature but also as a function of the TMAO concentration at all temperatures. Based on Eq. (14), applied to the WCA solute, we thus conclude that the repulsive WCA solute has a larger affinity for water than for TMAO and is therefore preferentially hydrated. This effect is most pronounced at low temperatures where changes in TMAO concentration have the largest effect on μ_{cav}. This

result can be viewed from another angle by noting that $\exp(-\beta\mu_{\text{cav}})$ corresponds to the probability of observing an empty cavity at an arbitrary location in a solvent configuration $\mathbf{X}$ of the water/TMAO system that is large enough to accommodate the solute. These cavities are produced by local solvent-density fluctuations and are herein probed with test-particle insertions. The above observed affinity of the WCA solute for water over TMAO therefore provides information on the local solvent environment in which cavities form: in TMAO/water mixtures empty cavities preferentially open in regions of excess water. We note that similar observations have been reported for mixtures of dimethylsulfoxide (DMSO) and water.[15] Below 320 K, methane preferentially occupies these "wet" cavities, while above 320 K, methane preferentially occupies cavities formed in environments with excess TMAO. This transition occurs because the difference between the probabilities of "wet" cavities and "TMAO-surrounded" cavities decreases as a function of the temperature and the van der Waals interaction with TMAO-surrounded cavities is stronger.

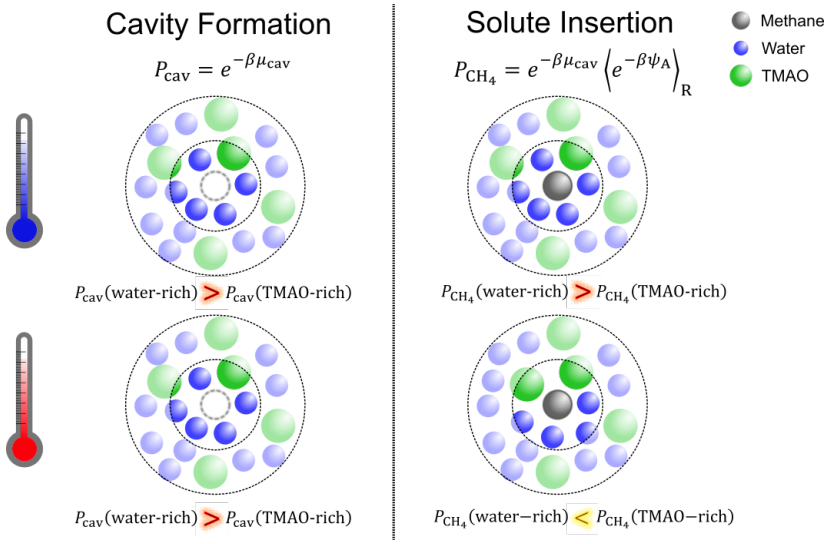

Figure 4.10: Schematic illustration of the local solvent environment of transient cavities and methane occupied cavities at low and at high temperatures. P(water – rich) and P(TMAO – rich) refer to the probability of the cavity (cav) or methane (CH_4) being in a water-rich or TMAO-rich environment, respectively.

The above microscopic picture is shown in Fig. 4.10. It implies that the insertion of methane in spontaneously formed cavities is biased by attractions. As such, fluctuations in the attractive energy ($\delta\psi_A$) are expected to occur, giving rise to a fluctuation entropy, $Ts_A < 0$ (Eq. (11)), contributing to the excess chemical potential of methane. Specifically, methane samples spontaneously formed cavities non-randomly, biased with a weighting factor $e^{-\beta\psi_A}$ as expressed by Eq. (8). The cohesive van der Waals interaction, ψ_A, of methane with cavities in TMAO-rich environments exceeds the interaction with cavities in water-rich environments. Particularly at low temperatures, less probable cavities close to TMAO molecules are therefore weighted stronger than "wet" cavities formed with larger probability. The fluctuation entropy ($-Ts_A$) is shown in Fig. 4.9(b). It is small in abso-

lute magnitude compared with μ_{cav} and $\langle\psi_A\rangle$, but not in comparison to μ_S^*, and therefore cannot be ignored. Its contribution increases with the concentration of TMAO in solution and shows no significant dependence on temperature. Note that $-s_A/k_B$ is determined by the magnitude of the energy fluctuations relative to k_BT and therefore decreases as a function of the temperature. To emphasize the role of the fluctuation entropy, a comparison with a mean field model can be made in which μ_S^* is approximated as $\mu_S^* \approx \mu_{\text{cav}} + \langle\psi_A\rangle$. When this approximation is applied, μ_S^* shows no significant dependence on the TMAO concentration below 320 K, while above 320 K, μ_S^* decreases with increasing TMAO concentration (not shown).

The properties of the WCA cavity described above change for larger-sized cavities. While small cavities in water/TMAO mixtures are preferentially wet, larger cavities attract TMAO, consistent with the effect of TMAO on the surface tension of the air-water interface.[16]

4.4 Hydrophobic interactions of methane

We studied hydrophobic interactions between methane solutes by examining the methane-methane potential of mean force $w(r)$ as a function of temperature and the TMAO concentration. In Fig. 4.11 we present the depth of first minimum in $w(r)$ for the different systems investigated. The data

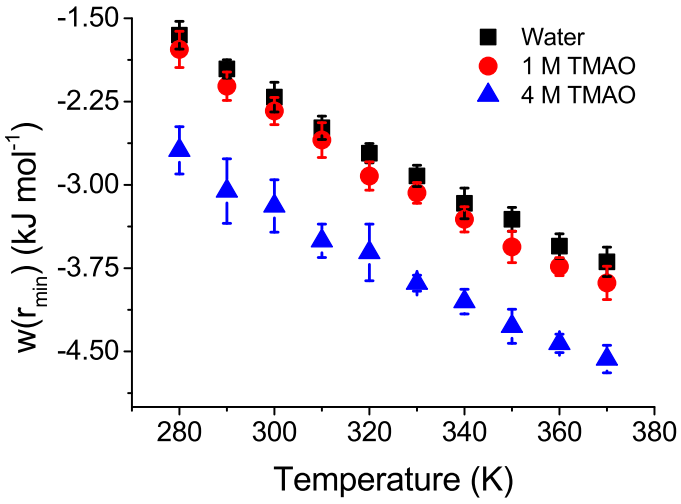

Figure 4.11: Contact free energy for the pair interaction of methane in water, 1 M and 4 M aqueous TMAO solution as a function of temperature.

show that the solvent-induced pair attraction between methane solutes is only marginally affected by TMAO in 1 M TMAO/water solution in agreement with earlier work.[71,72] In the system with 4 M TMAO, the methane pair attraction is stronger than in neat water. Contrary to the observation made in Fig. 4.2, no temperature crossover is observed. We thus see that in 4 M TMAO at low temperatures (< 320 K), the effective attraction between methane solutes increases as the solubility of methane in aqueous solution decreases. This correlation has also been observed by Koga et al.

for aqueous solutions containing NaCl.[73] Conversely, the observed increase in methane solubility (Fig. 4.2) correlates with a stronger solvent-induced pair attraction between methane solutes at higher temperatures (> 320 K). Interestingly, this shows that preferential TMAO interaction with methane at high temperatures does not weaken hydrophobic association but strengthens it instead. The data in Fig. 4.11 in fact correlate better with the dependency of μ_{cav} on TMAO concentration (Fig. 4.9(a)) suggesting that solvent-excluded volume is the dominant effect in the hydrophobic methane-methane interactions. Note however that, in water/cosolvent solutions, the fluctuation entropy may drive the hydrophobic association as well.[4,27]

5 Conclusion

The simulation data presented here show that while methane interacts with TMAO in aqueous solutions, below 320 K it interacts preferentially with water. At higher temperatures, the hydrogen bonds in the hydration shell of methane are weaker and less tetrahedral, while the affinity of TMAO for water decreases. This leads to preferential interaction of methane with TMAO above 320 K, the temperature at which the solvation shell of methane switches from being more to being less tetrahedrally ordered than neat water in the bulk, far away from the nonpolar solute. Accordingly, TMAO helps to solubilize methane at high temperatures, while it forces methane out of solution at low temperatures. In contrast to this observation, TMAO interacts preferentially with hydrophobic surfaces of large nonpolar solutes at room temperature.[8–11,16] This interaction occurs even when there are no attractive van der Waals interactions between TMAO and the nonpolar solute.[16] This is likely due to the fact that large nonpolar solutes, unlike methane, disrupt the hydrogen bonding network of water in their solvation shells,[17] creating an environment where local density fluctuation are larger and the probability of cavities is greater than in bulk water, facilitating the interaction with TMAO. While the decrease in tetrahedral order of the hydrogen bonding network around methane observed in this work promotes the interaction between methane and TMAO at high temperatures, a preferential interaction with methane is observed only when attractive van der Waals interactions are present. Moreover, we find that this preferential interaction, just like TMAO depletion at low temperatures, leads to a stronger solvent-induced pairwise attraction between the dissolved methane solutes rather than a weaker one.

Acknowledgement

Helpful discussions with Swaminath Bharadwaj are gratefully acknowledged. The MD simulations were performed on the Lichtenberg High Performance Computer of the Technische Universität Darmstadt, Germany.

Conflict of Interest

The authors have no conflict to disclose.

Bibliography

[1] Hunger, J.; Tielrooij, K. J.; Buchner, R.; Bonn, M.; Bakker, H. J. Complex formation in aqueous trimethylamine-N-oxide (TMAO) solutions. *J. Phys. Chem. B* **2012**, *116*, 4783–4795.

[2] Makarov, D. M.; Egorov, G. I.; Kolker, A. M. Density and Volumetric Properties of Aqueous Solutions of Trimethylamine N-Oxide in the Temperature Range from (278.15 to 323.15) K and at Pressures up to 100 MPa. *J. Chem. Eng. Data* **2015**, *60*, 1291–1299.

[3] Graziano, G. How does trimethylamine N-oxide counteract the denaturing activity of urea? *Phys. Chem. Chem. Phys.* **2011**, *13*, 17689–17695.

[4] van der Vegt, N. F. A.; Nayar, D. The Hydrophobic Effect and the Role of Cosolvents. *J. Phys. Chem. B* **2017**, *121*, 9986–9998.

[5] Bruce, E. E.; van der Vegt, N. F. A. Molecular Scale Solvation in Complex Solutions. *J. Am. Chem. Soc.* **2019**, *141*, 12948–12956.

[6] Wang, A.; Bolen, D. W. A naturally occurring protective system in urea-rich cells: Mechanism of osmolyte protection of proteins against urea denaturation. *Biochemistry* **1997**, *36*, 9101–9108.

[7] Folberth, A.; Polák, J.; Heyda, J.; van der Vegt, N. F. A. Pressure, Peptides, and a Piezolyte: Structural Analysis of the Effects of Pressure and Trimethylamine-N-oxide on the Peptide Solvation Shell. *J. Phys. Chem. B* **2020**, *124*, 6508–6519.

[8] Mondal, J.; Stirnemann, G.; Berne, B. J. When Does Trimethylamine N-Oxide Fold a Polymer Chain and Urea Unfold It? *J. Phys. Chem. B* **2013**, *117*, 8723–8732.

[9] Mondal, J.; Halverson, D.; Li, I. T. S.; Stirnemann, G.; Walker, G. C.; Berne, B. J. How osmolytes influence hydrophobic polymer conformations: A unified view from experiment and theory. *Proc. Natl. Acad. Sci. U.S.A.* **2015**, *112*, 9270–9275.

[10] Rodríguez-Ropero, F.; Rötzscher, P.; van der Vegt, N. F. A. Comparison of Different TMAO Force Fields and Their Impact on the Folding Equilibrium of a Hydrophobic Polymer. *J. Phys. Chem. B* **2016**, *120*, 8757–8767.

[11] Nayar, D.; van der Vegt, N. F. A. Cosolvent Effects on Polymer Hydration Drive Hydrophobic Collapse. *J. Phys. Chem. B* **2018**, *122*, 3587–3595.

[12] Su, Z.; Mahmoudinobar, F.; Dias, C. L. Effects of Trimethylamine-N-oxide on the Conformation of Peptides and its Implications for Proteins. *Phys. Rev. Lett.* **2017**, *119*, 108102.

[13] Mukherjee, M.; Mondal, J. Unifying the Contrasting Mechanisms of Protein-Stabilizing Osmolytes. *J. Phys. Chem. B* **2020**, *124*, 6565–6574.

[14] Bharadwaj, S.; Nayar, D.; Dalgicdir, C.; van der Vegt, N. F. A. A cosolvent surfactant mechanism affects polymer collapse in miscible good solvents. *Commun. Chem.* **2020**, *3*, 165.

[15] van der Vegt, N. F. A.; van Gunsteren, W. F. Entropic contributions in cosolvent binding to hydrophobic solutes in water. *J. Phys. Chem. B* **2004**, *108*, 1056–1064.

[16] Folberth, A.; Bharadwaj, S.; van der Vegt, N. F. A. Small-to-Large Length Scale Transition of TMAO Interaction with Hydrophobic Solutes. *Phys. Chem. Chem. Phys.* **2022**, *24*, 2080–2087.

[17] Rogers, B. A.; Okur, H. I.; Yan, C.; Yang, T.; Heyda, J.; Cremer, P. S. Weakly hydrated anions bind to polymers but not monomers in aqueous solutions. *Nat. Chem.* **2022**, *14*, 40–45.

[18] Southall, N. T.; Dill, K. A.; Haymet, A. D. J. A View of the Hydrophobic Effect. *J. Phys. Chem. B* **2002**, *106*, 521–533.

[19] Frenkel, D.; Smit, B. *Understanding Molecular Simulation - From Algorithms to Applications*; Academic Press: San Diego, 2002.

[20] Widom, B. Some Topics in the Theory of Fluids. *J. Chem. Phys.* **1963**, *39*, 2808–2812.

[21] Widom, B. Potential-distribution theory and the statistical mechanics of fluids. *J. Phys. Chem.* **1982**, *86*, 869–872.

[22] Weeks, J. D.; Chandler, D.; Andersen, H. C. Role of Repulsive Forces in Determining the Equilibrium Structure of Simple Liquids. *J. Chem. Phys.* **1971**, *54*, 5237–5247.

[23] Ben-Amotz, D.; Widom, B. Generalized Solvation Heat Capacities. *J. Phys. Chem. B* **2006**, *110*, 19839–19849.

[24] Dunitz, J. D. Win some, lose some: enthalpy-entropy compensation in weak intermolecular interactions. *Chem. Biol.* **1995**, *2*, 709 – 712.

[25] Sanchez, I. C.; Truskett, T. M. a. Configurational Properties and Corresponding States in Simple Fluids and Water. *J. Phys. Chem. B* **1999**, *103*, 5106–5116.

[26] Schravendijk, P.; van der Vegt, N. F. A. From Hydrophobic to Hydrophilic Solvation: An Application to Hydration of Benzene. *J. Chem. Theory Comput.* **2005**, *1*, 643–652.

[27] van der Vegt, N. F. A.; Lee, M.-E.; Trzesniak, D.; van Gunsteren, W. F. Enthalpy–Entropy Compensation in the Effects of Urea on Hydrophobic Interactions. *J. Phys. Chem. B* **2006**, *110*, 12852–12855.

[28] Underwood, R.; Ben-Amotz, D. Communication: Length scale dependent oil-water energy fluctuations. *J. Chem. Phys.* **2011**, *135*, 201102.

[29] Taherian, F.; Leroy, F.; van der Vegt, N. F. A. Interfacial Entropy of Water on Rigid Hydrophobic Surfaces. *Langmuir* **2013**, *29*, 9807–9813.

[30] Bharadwaj, S.; Jabes, S. B.; van der Vegt, N. F. A. Direct Calculation of Entropic Components in Cohesive Interaction Free Energies. *J. Phys. Chem. B* **2021**, *125*.

[31] Rodríguez-Ropero, F.; van der Vegt, N. F. A. Mechanism of polymer collapse in miscible good solvents. *J. Phys. Chem. B* **2015**, *119*, 15780–14788.

[32] Rodríguez-Ropero, F.; van der Vegt, N. F. A. On the urea induced hydrophobic collapse of a water soluble polymer. *Phys. Chem. Chem. Phys.* **2015**, *17*, 8491–8498.

[33] Berendsen, H. J.; van der Spoel, D.; van Drunen, R. GROMACS: A message-passing parallel molecular dynamics implementation. *Comput. Phys. Commun.* **1995**, *91*, 43–56.

[34] Abraham, M. J.; Murtola, T.; Schulz, R.; Páll, S.; Smith, J. C.; Hess, B.; Lindahl, E. Gromacs: High performance molecular simulations through multi-level parallelism from laptops to supercomputers. *SoftwareX* **2015**, *1-2*, 19–25.

[35] Darden, T.; York, D.; Pedersen, L. Particle mesh Ewald: An N·log(N) method for Ewald sums in large systems. *J. Chem. Phys.* **1993**, *98*, 10089–10092.

[36] Hess, B. P-LINCS: A parallel linear constraint solver for molecular simulation. *J. Chem. Theory Comput.* **2008**, *4*, 116–122.

[37] Ashbaugh, H. S.; Collett, N. J.; Hatch, H. W.; Staton, J. A. Assessing the thermodynamic signatures of hydrophobic hydration for several common water models. *J. Chem. Phys.* **2010**, *132*, 124504.

[38] Abascal, J. L. F.; Vega, C. A general purpose model for the condensed phases of water: TIP4P/2005. *J. Chem. Phys.* **2005**, *123*, 234505.

[39] Hölzl, C.; Kibies, P.; Imoto, S.; Frach, R.; Suladze, S.; Winter, R.; Marx, D.; Horinek, D.; Kast, S. M. Design principles for high-pressure force fields: Aqueous TMAO solutions from ambient to kilobar pressures. *J. Chem. Phys.* **2016**, *144*, 1–4.

[40] Markthaler, D.; Zeman, J.; Baz, J.; Smiatek, J.; Hansen, N. Validation of Trimethylamine-N-oxide (TMAO) Force Fields Based on Thermophysical Properties of Aqueous TMAO Solutions. *J. Phys. Chem. B* **2017**, *121*, 10674–10688.

[41] Allen, M. P.; Tildesley, D. J. *Computer Simulation of Liquids*; Oxford University Press, 1987.

[42] Berendsen, H. J.; Postma, J. P.; Van Gunsteren, W. F.; Dinola, A.; Haak, J. R. Molecular dynamics with coupling to an external bath. *J. Chem. Phys.* **1984**, *81*, 3684–3690.

[43] Nosé, S. A molecular dynamics method for simulations in the canonical ensemble. *Mol. Phys.* **1984**, *52*, 255–268.

[44] Parrinello, M.; Rahman, A. Polymorphic transitions in single crystals: A new molecular dynamics method. *J. Appl. Phys.* **1981**, *52*, 7182–7190.

[45] Ganguly, P.; van der Vegt, N. F. A. Convergence of Sampling Kirkwood-Buff Integrals of Aqueous Solutions with Molecular Dynamics Simulations. *J. Chem. Theory Comput.* **2013**, *9*, 1347–1355.

[46] Koga, K. Osmotic Second Virial Coefficient of Methane in Water. *J. Phys. Chem. B* **2013**, *117*, 12619–12624.

[47] Kirkwood, J. G.; Buff, F. P. The Statistical Mechanical Theory of Solutions. I. *J. Chem. Phys.* **1951**, *19*, 774–777.

[48] Krüger, P.; Schnell, S. K.; Bedeaux, D.; Kjelstrup, S.; Vlugt, T. J. H.; Simon, J.-M. Kirkwood–Buff Integrals for Finite Volumes. *J. Phys. Chem. Lett.* **2013**, *4*, 235–238.

[49] Milzetti, J.; Nayar, D.; van der Vegt, N. F. A. Convergence of Kirkwood–Buff Integrals of Ideal and Nonideal Aqueous Solutions Using Molecular Dynamics Simulations. *J. Phys. Chem. B* **2018**, *122*, 5515–5526.

[50] Brehm, M.; Thomas, M.; Gehrke, S.; Kirchner, B. TRAVIS—A free analyzer for trajectories from molecular simulation. *J. Chem. Phys.* **2020**, *152*, 164105.

[51] Errington, J. R.; Debenedetti, P. Relationship between structural order and the anomalies of liquid water. *Nature* **2001**, *409*, 318–321.

[52] Nayar, D.; Agarwal, M.; Chakravarty, C. Comparison of Tetrahedral Order, Liquid State Anomalies, and Hydration Behavior of mTIP3P and TIP4P Water Models. *J. Chem. Theory. Comput.* **2011**, *7*, 3354–3367.

[53] Wu, X.; Lu, W.; Streacker, L. M.; Ashbaugh, H. S.; Ben-Amotz, D. Temperature-Dependent Hydrophobic Crossover Length Scale and Water Tetrahedral Order. *J. Phys. Chem. Lett.* **2018**, *9*, 1012–1017.

[54] Hummer, G.; Garde, S.; García, A. E.; Pohorille, A.; Pratt, L. R. An information theory model of hydrophobic interactions. *Proc. Natl. Acad. Sci. U.S.A.* **1996**, *93*, 8951–8955.

[55] Ashbaugh, H. S.; Pratt, L. R. Colloquium: Scaled particle theory and the length scales of hydrophobicity. *Rev. Mod. Phys.* **2006**, *78*, 159–178.

[56] Stillinger, F. H. *The Physical Chemistry of Aqueous System*; Springer, 1973; pp 43–60.

[57] Garde, S.; Khare, R.; Hummer, G. Microscopic density fluctuations and solvation in polymeric fluids. *J. Chem. Phys* **2000**, *112*, 1574–1578.

[58] Zou, Q.; Bennion, B. J.; Daggett, V.; Murphy, K. P. The Molecular Mechanism of Stabilization of Proteins by TMAO and Its Ability to Counteract the Effects of Urea. *J. Am. Chem. Soc.* **2002**, *124*, 1192–1202.

[59] Pierce, V.; Kang, M.; Aburi, M.; Weerasinghe, S.; Smith, P. E. Recent Applications of Kirkwood–Buff Theory to Biological Systems. *Cell Biochem. Biophys.* **2008**, *50*, 1–22.

[60] Matubayasi, N.; Gallicchio, E.; Levy, R. M. On the local and nonlocal components of solvation thermodynamics and their relation to solvation shell models. *J. Chem. Phys.* **1998**, *109*, 4864–4872.

[61] Garde, S.; Hummer, G.; García, A. E.; Paulaitis, M. E.; Pratt, L. R. Origin of Entropy Convergence in Hydrophobic Hydration and Protein Folding. *Phys. Rev. Lett.* **1996**, *77*, 4966–4968.

[62] Garde, S.; García, A. E.; Pratt, L. R.; Hummer, G. Temperature dependence of the solubility of non-polar gases in water. *Biophys. Chem.* **1999**, *78*, 21 – 32.

[63] Garrido, N. M.; Queimada, A. J.; Jorge, M.; Macedo, E. A.; Economou, I. G. 1-Octanol/Water Partition Coefficients of n-Alkanes from Molecular Simulations of Absolute Solvation Free Energies. *J. Chem. Theory Comput.* **2009**, *5*, 2436–2446.

[64] Wagner, W.; Pruß, A. The IAPWS Formulation 1995 for the Thermodynamic Properties of Ordinary Water Substance for General and Scientific Use. *J. Phys. Chem. Ref. Data* **2002**, *31*, 387–535.

[65] Hess, B.; van der Vegt, N. F. A. Hydration Thermodynamic Properties of Amino Acid Analogues - A Systematic Comparison of Biomolecular Force Fields and Water Models. *J. Phys. Chem. B* **2006**, *110*, 17616–17626.

[66] Peter, C.; van der Vegt, N. F. A. Solvent Reorganization Contributions in Solute Transfer Thermodynamics: Inferences from the Solvent Equation of State. *J. Phys. Chem. B* **2007**, *111*, 7836–7842.

[67] Lee, M.-E.; van der Vegt, N. F. A. Molecular Thermodynamics of Methane Solvation in tert-Butanol-Water Mixtures. *J. Chem. Theory Comput.* **2007**, *3*, 194–200.

[68] Symons, E. A. Hydrogen Gas Solubility in the Dimethyl Sulfoxide – Water System: A Further Clue to Solvent Structure in These Media. *Can. J. Chem.* **1971**, *49*, 3940–3947.

[69] Ozal, T. A.; van der Vegt, N. F. A. Confusing Cause and Effect: Energy-Entropy Compensation in the Solvation of a Nonpolar Solute in Dimethyl Sulfoxide/water Mixtures. *J. Phys. Chem. B* **2006**, *110*, 12104–12112.

[70] Wu, X.; Lu, W.; Streacker, L. M.; Ashbaugh, H. S.; Ben-Amotz, D. Methane Hydration-Shell Structure and Fragility. *Angew. Chem. Int. Ed.* **2018**, *57*, 15133–15137.

[71] Athawale, M. V.; Dordick, J. S.; Garde, S. Osmolyte Trimethylamine-N-Oxide Does Not Affect the Strength of Hydrophobic Interactions: Origin of Osmolyte Compatibility. *Biophys. J.* **2005**, *89*, 858 – 866.

[72] Sarma, R.; Paul, S. Association of Small Hydrophobic Solute in Presence of the Osmolytes Urea and Trimethylamine-N-oxide. *J. Phys. Chem. B* **2012**, *116*, 2831–2841.

[73] Koga, K.; Yamamoto, N. Hydrophobicity Varying with Temperature, Pressure, and Salt Concentration. *J. Phys. Chem. B* **2018**, *122*, 3655–3665.

5 Small-to-Large Length Scale Transition of TMAO Interaction with Hydrophobic Solutes

This chapter has been reproduced from:

Folberth, A.; Bharadwaj, S.; van der Vegt, N. F. A; Small-to-Large Length Scale Transition of TMAO Interaction with Hydrophobic Solutes. Phys. Chem. Chem. Phys., **2022***, 24, 2080–2087*
with permission from the Royal Society of Chemistry

Abstract

We report the effect of trimethylamine N-oxide (TMAO) on the solvation of nonpolar solutes in water studied with molecular dynamics (MD) simulations and free-energy calculations. The simulation data indicate the occurrence of a length scale crossover in the TMAO interaction with repulsive Weeks-Chandler-Andersen (WCA) solutes: while TMAO is depleted from the hydration shell of a small WCA solute (methane) and increases the free-energy cost of solute-cavity formation, it preferentially binds to a large WCA solute (α-helical polyalanine), reducing the free-energy cost of solute-cavity formation via a surfactant-like mechanism. Significantly, we show that this surfactant-like behaviour of TMAO reinforces the solvent-mediated attraction between large WCA solutes by means of an entropic force linked to the interfacial accumulation of TMAO. Specifically, this entropic force arises from the natural tendency of adsorbed TMAO molecules to mix back into the bulk. It therefore favours solute-solute contact states that minimise the surface area exposed to the solvent and have a small overall number of TMAO molecules adsorbed. In contrast to the well-known depletion force, its effect is compensated by enthalpic solute-solvent interactions. Correspondingly, the hydrophobic association free energy of the large α-helical solutes passes through a minimum at low TMAO concentration when cohesive solute-solvent van der Waals interactions are considered. The observations reported herein are reminiscent to cosolvent effects on hydrophobic polymer coil-globule collapse free energies (Bharadwaj et al. *Commun. Chem.* **2020**, 3, 165) and may be of general significance in systems whose properties are determined by hydrophobic self-assembly.

1 Introduction

The solvation mechanisms that determine the thermodynamic characteristics of small and large nonpolar solutes in water are remarkably different. While solvation of small nonpolar solutes is dictated by solvent density fluctuations and can qualitatively be described with bulk-water properties such as its density and isothermal compressibility,[1] an interfacial thermodynamics description is required for large solutes thus indicating a length scale transition from a "microscopic" to a "macroscopic" hydration behaviour.[2–4] Early studies on this subject have investigated the free-energy cost of inserting hard-sphere solutes (equivalent to the reversible work of creating a hard-sphere cavity) in aqueous solutions.[3,5,6] In these studies, a transition length scale close to 1 nm was identified where the reversible work of cavity formation per unit surface area, $\Delta G_R/4\pi r^2$, changes from a volume, $\Delta G_R/4\pi r^2 \sim r$, to an interfacial, $\Delta G_R/4\pi r^2 \sim 1$, dependence.

Accordingly, one may rationalise the effect of cosolutes (or cosolvents) on the solvation free energy of small and large nonpolar solutes in terms of their impact on the density and surface tension of aqueous solutions.[6] Usually, cosolutes influence the density and surface tension in a similar way. Examples of this behaviour include salts such as sodium chloride, which increase both the density[7] and the surface tension of water,[8] and amphiphilic cosolvents such as alcohols and acetone, which reduce both the density[9] and surface tension.[10,11] In line with these observations, computer simulations of the solvation of Weeks-Chandler-Andersen (WCA)[12] solutes have shown that $\Delta G_R/4\pi r^2$ increases (decreases) for, both, small and large WCA solutes with the addition of NaCl (ethanol) though the increment (decrement) is different in the two regimes.[6] In terms of a preferential binding picture,[13] this means that NaCl depletes away from the solvation shell of nonpolar solutes, in analogy to its depletion from the air-water interface. Conversely, amphiphilic cosolvents tend to preferentially adsorb to nonpolar solutes,[14] in analogy to their adsorption to the air-water interface. These observations demonstrate that cosolutes have a qualitatively similar effect on the solvation thermodynamics of small and large nonpolar solutes in water. As such, one expects that understanding the effects of cosolutes at small scales provides insight on large-scale behaviour, too.

Trimethylamine N-oxide (TMAO) is a strongly hydrated organic cosolute which increases the density of aqueous solutions.[15,16] Proteins are preferentially hydrated in its presence, i.e. TMAO is depleted from protein surfaces.[17–19] Based on these two observations, it has been assumed that TMAO increases the solvation free energy of large hydrophobic solutes and repulsive hard-sphere cavities.[20,21] In this work, we show that TMAO-solute interactions exhibit a length scale crossover where it preferentially depletes from small (repulsive) solutes and preferentially adsorbs on large (repulsive) solutes. This occurs as TMAO, due to its large dipole moment and hydrophobic groups, increases the density of aqueous solutions but simultaneously reduces the air-water surface tension.[22–24] As a result, TMAO reduces the solubility (increases the solvation free energy) of small nonpolar solutes through its effect on the solvent density and solvent density fluctuations.[1] It how-

ever increases the solubility of large nonpolar solutes via a surfactant-like mechanism.

To understand this length scale crossover, we herein consider a methane molecule to study the small solute regime and a polyalanine α-helix to study the large solute regime. Similar to earlier efforts involving WCA solute-solvent interactions,[6,25,26] we first study the effect of TMAO on the solvation free energy of the WCA-solute cavities of methane and α-helical polyalanine. Our results show that TMAO preferentially depletes from the methane cavity and monotonically increases its solvation free energy with TMAO concentration. On the other hand, TMAO preferentially adsorbs on the polyalanine α-helical cavity via a surfactant-like mechanism and monotonically reduces its solvation free energy with TMAO concentration. We furthermore study the effect of TMAO on the hydrophobic interaction free energy of two α-helical polyalanine cavities, and α-helical polyalanine cavities augmented with cohesive van der Waals interactions with the solvent. Based on these calculations, we show that the above surfactant-like mechanism leads to an effective attraction, strengthening the hydrophobic association of these large WCA and van-der-Waals solutes through a novel entropic mechanism recently reported for the polymer coil-globule transition.[27] We find that this, TMAO induced, entropic attraction is compensated by enthalpic interactions of the helices with the solvent at high TMAO concentrations, thus leading to a minimum in their association free energy at 1 M TMAO concentration.

Table 5.1: System details: TMAO concentrations, number of water and TMAO molecules, average density (300 K, 1 bar) and box volume.

# helices	TMAO conc. / M	# TMAO	# water	$\langle\rho\rangle$ / kg m^{-3}	$\langle V\rangle$ / nm^3
0	0	0	10635	997.5	343.6
	1	207	10635	1000.7	343.7
	2	414	9789	1005.1	342.7
	3	620	8951	1010.5	341.5
1	0	0	4408	994.0	136.9
	1	81	4128	997.3	138.2
	2	163	3809	1001.5	138.3
	3	244	3495	1006.5	138.3
2	0	0	8562	993.7	266.3
	1	158	8042	996.6	269.6
	2	317	7421	1001.0	269.7
	3	475	6810	1006.0	269.8

2 Methods

2.1 Molecular Dynamics simulation details

We analysed the assembly of two polyalanine α-helices (36-mers) at different TMAO concentrations. The Amber99sb-ildn force field[28] was used for the polypeptide, the Hölzl force field[29] for TMAO, and the TIP4P/2005 model[30] for water. The Hölzl force field, in combination with the TIP4P/2005 water model, has been proven to reproduce the properties of binary systems at ambient pressure well.[15] The compositions, equilibrated box volumes and densities of the systems investigated with MD are summarised in Table 6.1 for the different TMAO concentrations considered.

The starting configuration of a single helix was created with PEPFOLD3.[31] The head and tail groups of the helix were connected across the periodic boundary conditions to resemble a quasi-infinite chain. The intramolecular hydrogen bonds stabilising the helix were restrained using a harmonic potential with a force constant of strength 10^3 kJ mol^{-1} nm^{-1}. All simulations were performed with the GROMACS package version 2019.4.[32,33] The LINCS algorithm[34] was used to restrain all bonds involving a hydrogen atom. Coulomb interactions were treated using particle mesh Ewald (PME)[35] with a real-space cut off of 1 nm, a PME order of 4 and a grid spacing of 0.12 nm. The van der Waals interaction cut off length was set at 1 nm with long range dispersion corrections applied to the pressure and energy. The neighbour list was updated every five time steps. Energy minimization was done using the steepest descent algorithm with 50000 steps and a step size of 0.001 nm. Subsequently, the system was equilibrated for 0.3 ns in a constant volume-temperature simulation using the Berendsen thermostat (τ_T=1.0 ps, $T = 300$ K),[36] followed by a 1 ns constant pressure-temperature simulation using the Berendsen barostat (τ_P=2.0 ps, $\kappa_T = 5 \cdot 10^{-5}$ bar^{-1}, $P = 1$ bar). In all simulations containing the quasi-infinite helix, semi-isotropic pressure coupling was used to ensure that the box dimension in z-direction remains constant by setting the compressibility to 0 in the z-direction. The time step was fixed at 2 fs. All production runs

were done using the Nose-Hoover thermostat[37] at 300 K (τ_T=1.0 ps) and the Parrinello-Rahman barostat at 1 bar (τ_P=2.0 ps)[38] with a compressibility of $5 \cdot 10^{-5}$ bar^{-1}.

2.2 Umbrella sampling

Umbrella sampling simulations were performed to calculate the potential of mean force (PMF) between two polyalanine helices.[39,40] The distance between the two helices in the associated state was identified from the first minimum in the PMF. The starting configurations for the umbrella sampling simulations were created by using pulling simulations with the setting of the *NpT* equilibration mentioned above. The polypeptides were pulled apart in the x-y-direction using an umbrella potential (k =10^3 kJ mol^{-1} nm^{-2}). Each umbrella window was again equilibrated in a constant pressure-temperature simulation for 1 ns (k =$5 \cdot 10^3$ kJ mol^{-1} nm^{-2}). Then the production runs were performed for 30 ns (k =10^4 kJ mol^{-1} nm^{-2}) using the settings described above. The first 5 ns were discarded and the PMF (see Fig. S1 in Sec. S1) was obtained using the weighted histogram analysis method.[41] A configuration in the first minimum of the PMF was chosen randomly and was restrained for the subsequent simulations. Hereafter, we refer to this configuration the associated state.

2.3 Free energy calculations

The free energy perturbation (FEP) and thermodynamic integration (TI) methods were used to calculate the solvation free energy, ΔG, of the polyalanine α-helices. A stochastic dynamics integrator has been used in all FEP simulations. The λ-coupling parameter values are summarised in Sec. S2 of the SI. A soft-core potential with soft-core parameters α = 0.5, p = 1 and σ = 0.28 nm was used to avoid singularities at the (uncoupled) end state in the TI calculations.[42] The BAR algorithm was used for the FEP calculations.[43,44] We note that all free-energy data pertaining to the α-helical solutes presented below were computed with, both, FEP and TI. Below, the FEP data are reported. The comparison of the TI and FEP data is discussed in the SI (see Fig. S2 in Sec. S3).

We herein split the solvation free energy into three contributions

$$\Delta G = \Delta G_{\mathrm{vdW,R}} + \Delta G_{\mathrm{vdW,A}} + \Delta G_{\mathrm{Elec}} , \tag{1}$$

where $\Delta G_{\mathrm{vdW,R}}$, $\Delta G_{\mathrm{vdW,A}}$ and ΔG_{Elec} are the respective free energies associated with introducing repulsive (excluded volume) solute-solvent interactions, attractive solute-solvent van der Waals (vdW) interactions, and electrostatic solute-solvent interactions in stages. We note that these definitions apply to sequentially introducing the different parts of the full solute-solvent interaction using FEP/TI in this order.[45]

All following procedures were performed for the associated state, taken from the minimum of the umbrella sampling simulations, and a single helix. Free energies of the dissociated state (two

helices at infinite distance) were obtained by doubling the single helix free energy. Here we define relative (with respect to pure water) solvation free energies $\Delta\Delta G_{\mathrm{j}}$

$$\Delta\Delta\, G_{\mathrm{j}}(c_{\mathrm{TMAO}}) \;= \Delta\, G_{\mathrm{j}}(c_{\mathrm{TMAO}}) - \Delta\, G_{\mathrm{j}}(0\,\mathrm{M}), \tag{2}$$

where the index j represents the different contributions (eqn 1) to the solvation free energy. The values of these different contributions to the solvation free energy in pure water are given in table S1 in Sec. S4 of the SI.

Calculation of $\Delta G_{\mathrm{vdW,R}}$

To calculate $\Delta G_{\mathrm{vdW,R}}$, the WCA potential[12]

$$\psi_R = \begin{cases} 4\epsilon\left[\left(\frac{\sigma}{r}\right)^{12} - \left(\frac{\sigma}{r}\right)^{6}\right] + \epsilon, & r < 2^{1/6}\sigma \\ 0, & r \geq 2^{1/6}\sigma \end{cases} . \tag{3}$$

was used. Here, ϵ and σ are the Lennard-Jones parameters and r is the distance between the interacting particles. In the FEP/TI calculations, position restraints ($k = 10^5\,\mathrm{kJ\,mol^{-1}\,nm^{-1}}$) were applied to the polyalanine α-helix atoms in the associated and dissociated states. The α-helix remains stable without position restraints, but they are necessary to keep them intact when using the WCA potential. At each λ-value, constant volume-temperature equilibrations were performed for 0.4 ns and constant pressure-temperature equilibrations for 0.5 ns. The production runs lasted 5 ns and the last 4.5 ns were used for analysis. Below, we will use the terminology "solvation free energy" and "free-energy cost of cavity formation" interchangeably when referring to $\Delta G_{\mathrm{vdW,R}}$. In line with previous simulations on repulsive cavities,[6] we have studied the dependence of $\Delta G_{\mathrm{vdW,R}}$/SASA on TMAO concentration, where SASA is the solvent accessible surface area (see Sec. S5 in the SI for more details).

Calculation of $\Delta G_{\mathrm{vdW,A}}$ and ΔG_{Elec}

The attractive solute-solvent potential, ψ_A, is defined as

$$\psi_A = \begin{cases} -\epsilon, & r < 2^{1/6}\sigma \\ 4\epsilon\left[\left(\frac{\sigma}{r}\right)^{12} - \left(\frac{\sigma}{r}\right)^{6}\right], & r \geq 2^{1/6}\sigma \end{cases} . \tag{4}$$

and may be used to obtain $\Delta G_{\mathrm{vdW,A}}$ from a FEP/TI calculation performed between two end states ($\lambda = 0$ and $\lambda = 1$) corresponding to the solute-solvent potentials $\psi = \psi_R$ and $\psi = \psi_R + \psi_A$. As $\psi_R + \psi_A$ corresponds to the Lennard-Jones potential, a FEP/TI calculation performed with solute-solvent potentials $\psi = \psi_R + \psi_A$ as one end state, and $\psi = 0$ as another, provides the solvation free energy ΔG_{vdW} of a vdW solute, which, with the above decomposition in repulsive and attractive

terms, can be written as $\Delta G_{\mathrm{vdW}} = \Delta G_{\mathrm{vdW,R}} + \Delta G_{\mathrm{vdW,A}}$. We herein used FEP/TI to calculate $\Delta G_{\mathrm{vdW,R}}$ and ΔG_{vdW}, and obtained $\Delta G_{\mathrm{vdW,A}}$ by subtraction. The electrostatic component, ΔG_{Elec}, was obtained separately from an additional FEP/TI calculation in which the electrostatic solute-solvent interactions were introduced starting from the vdW solute. In the FEP/TI calculations, constant volume-temperature equilibrations were done for 0.4 ns and constant pressure-temperature equilibrations for 0.5 ns at each λ-value. The production runs lasted 5 ns and the last 4.5 ns were used for analysis.

2.4 Test particle insertion

Simulation boxes containing TMAO-water binary mixtures (Table 6.1) were equilibrated in a constant volume-temperature simulation for 2.5 ns, followed by a constant pressure-temperature simulation for 2.5 ns. The subsequent production run was 100 ns. The simulation settings were the same as described above, using isotropic pressure coupling and therefore with equal compressibility in all directions. We employed a united-atom methane model[46] to calculate ΔG with test-particle insertion,[47]

$$\exp\left(-\Delta G/k_{\mathrm{B}}T\right) = \frac{\langle V \exp\left(-\Delta U/k_{\mathrm{B}}T\right)\rangle}{\langle V\rangle} \tag{5}$$

performing the NpT ensemble averaging, $\langle ...\rangle$, based on 400,000 insertions per frame using a total of 100,000 frames stored in the 100 ns production runs (k_{B} is the Boltzmann constant and T the temperature). A cutoff distance of 1 nm was used to calculate the test-particle energy, ΔU, combined with a long range dispersion correction. To calculate $\Delta G_{\mathrm{vdW,R}}$ of the corresponding repulsive methane cavity, the WCA potential, eqn (3), was used based on the united atom LJ parameters of methane.

3 Results and Discussion

The solvation process is herein considered in stages (eqn (1)) where, first, a repulsive WCA cavity, with the same shape and size as the solute, is created to host the solute and, subsequently, the cohesive interactions between the molecules of the solvent and this pre-formed cavity are introduced. This decomposition allows to examine how repulsive and attractive components of the solute-solvent interaction contribute to the solvation free energy and to the hydrophobic interaction of nonpolar solutes. Below, contributions of attractive solute-solvent van der Waals forces and solute-solvent electrostatic forces to the cohesive solute-solvent interaction are considered separately.

3.1 The repulsive cavity contribution

The free energy of solvating repulsive solutes depends on the solute's excluded volume and on the interactions among the molecules comprising the cosolute-solvent mixture. To study this property, we consider repulsive WCA cavities which have the exact shape and size of a methane and a α-helical polyalanine molecule. Hereafter, they will be referred to as "methane cavity" and "polyalanine-helix cavity".

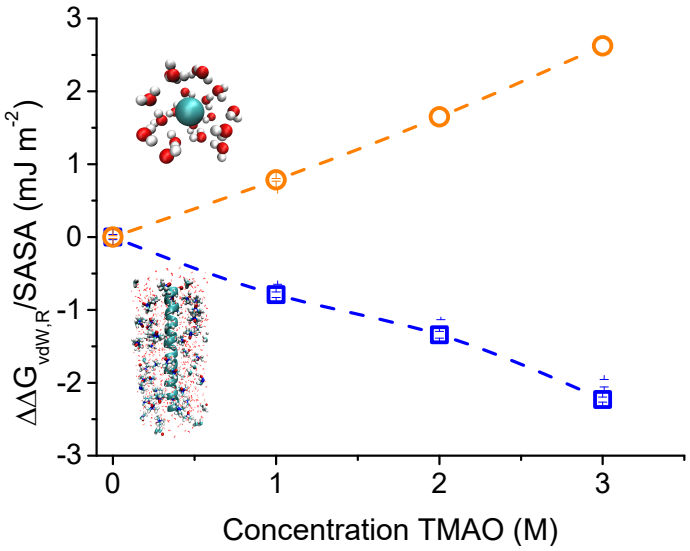

Figure 5.1: Dependence of the free-energy cost of solute cavity formation on TMAO concentration. The relative solvation free energy per unit solvent-accessible surface area (SASA), $\Delta\Delta G_{\mathrm{vdW,R}}/\mathrm{SASA} = \left[\Delta G_{\mathrm{vdW,R}}(\text{TMAO solution}) - \mathrm{G}_{\mathrm{vdW,R}}(\text{water})\right]/\mathrm{SASA}$, is shown for methane (orange symbols) and polyalanine-helix (blue symbols) cavities in dependence on the TMAO concentration.

The data in Fig. 5.1 show that the relative (with respect to pure water) free-energy cost of cavity formation, $\Delta\Delta G_{\mathrm{vdW,R}}$, increases monotonically with TMAO concentration for the methane cavity. The observation that TMAO increases the free-energy cost of cavity formation in water indicates that TMAO is depleted from the methane cavity-water interface (i.e. the methane cavity is preferentially hydrated).[13,48] The increase of $\Delta G_{\mathrm{vdW,R}}$ can be understood in terms of the influence of TMAO on solvent density fluctuations. TMAO progressively increases the density of water-TMAO mixtures and suppresses solvent density fluctuations required for cavity formation in analogy to the effect of NaCl on water density fluctuations.[1] Interestingly, the data in Fig. 5.1 further shows that the relative free-energy cost of polyalanine-helix cavity formation decreases linearly with TMAO concentration. Accordingly, TMAO preferentially adsorbs to the polyalanine-helix cavity, reflecting the amphiphilic nature of TMAO that gives rise to a weak surfactant-like effect which also leads to a mild reduction of the (macroscopic) surface tension of water.[22,49] Significantly, these results show that the interaction of TMAO with WCA solutes in water exhibits a length scale transition. While

being expelled from the hydration shell of the small methane-sized WCA solute, TMAO is weakly attracted into the hydration shell of the α-helical WCA solute.

In Fig. 5.2(a), we compare the free energy of solvating two independent (i.e. spatially separated) α-helical WCA solutes with the free energy of solvating two α-helical WCA solutes in their associated state, as a function of the TMAO concentration. The solvation free energies decrease with the concentration of TMAO in solution, indicating that TMAO preferentially adsorbs to the associated and dissociated WCA solutes (also see preferential binding coefficients Γ_{23} in Fig. S3 in Sec. S6 of the SI). Intriguingly, the data for the associated state fall below the data for the dissociated state to an extent that becomes larger with increasing TMAO concentration. Therefore, the associated state progressively becomes more favourably solvated than the dissociated state as the TMAO concentration increases, indicating that preferential TMAO binding to the α-helical WCA solutes drives their association. This striking observation is at odds with the expectation that surfactant-like cosolutes which preferentially adsorb to nonpolar substances should instead aid their solvation and dissolution in water. Fig. 5.2(b) shows the relative association free energy, $\Delta\Delta G^{\mathrm{D}\to\mathrm{A}}_{\mathrm{vdW,R}} (= \Delta\Delta G^{\mathrm{A}}_{\mathrm{vdW,R}} - \Delta\Delta G^{\mathrm{D}}_{\mathrm{vdW,R}})$, versus the TMAO concentration of the solution. Clearly, association of the α-helical WCA solutes in TMAO solution leads to a favourable gain in free energy compared to their association in pure water.

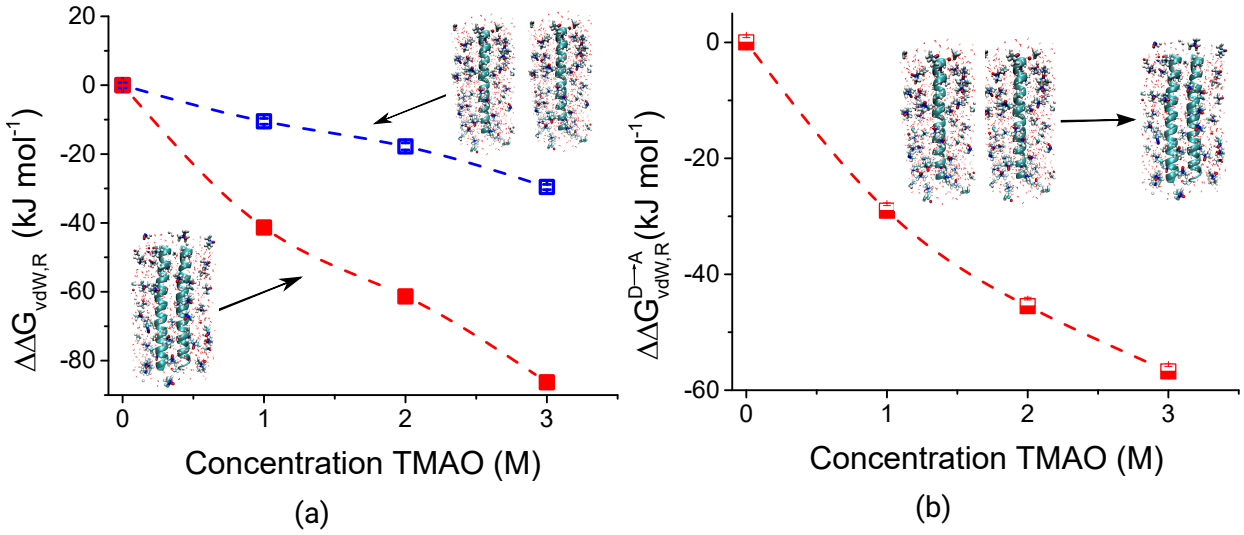

Figure 5.2: (a) Dependence of the relative free-energy cost of cavity formation on TMAO concentration for associated ($\Delta\Delta G^{\mathrm{A}}_{\mathrm{vdW,R}}$, red symbols) and dissociated ($\Delta\Delta G^{\mathrm{D}}_{\mathrm{vdW,R}}$, blue symbols) WCA polyalanine-helix cavities. (b) The relative free energy change upon association, $\Delta\Delta G^{\mathrm{D}\to\mathrm{A}}_{\mathrm{vdW,R}} = \Delta\Delta G^{\mathrm{A}}_{\mathrm{vdW,R}} - \Delta\Delta G^{\mathrm{D}}_{\mathrm{vdW,R}}$. The negative slopes in (a) indicate that TMAO preferentially adsorbs at the cavity-water interfaces of the associated and dissociated polyalanine helices, therefore reducing the free-energy cost of cavity formation via a surfactant-like mechanism. The association free energy of the polyalanine-helix cavities in (b) decreases, progressively favouring helix-cavity association with increasing TMAO concentration due to stronger TMAO adsorption to the associated state with the smaller SASA than to the dissociated state with the larger SASA.

The stabilisation of the associated state induced by TMAO adsorption can be explained in terms of a (bulk-interface) cosolute partitioning equilibrium: The loss in the translational entropy of the cosolute, due to its accumulation at the solute-water interface, is small when the interfacial area to which the cosolute adsorbs is small.[50–52] Therefore, the preferential binding of TMAO to the associated state is larger than to the dissociated state which exposes a larger SASA. This effect in turn shifts the dissociation-association equilibrium ($D \rightleftharpoons A$) of the α-helical WCA solutes towards the associated state, i.e. the cosolute shifts the $D \rightleftharpoons A$ equilibrium to the side to which it preferentially binds. This mechanism, occurring on the account of TMAO's surfactant-like behaviour, has also been recently reported to play an important role in the alcohol-induced collapse of thermoresponsive polymers.[27] This mechanism requires extended macromolecular surfaces, and is generic in systems with preferentially adsorbing cosolutes, but may be offset or reinforced by cohesive solute-solvent interactions.[27]

3.2 Cohesive van der Waals interactions

Cohesive solute-solvent interactions are described with eqn (4). The introduction of these attractive interactions between the α-helical WCA solute and the water and TMAO molecules of the solvent is accompanied with a change in free energy, $\Delta G_{\mathrm{vdW,A}}$. Fig. 5.3(a) shows the relative solvation free energy, $\Delta\Delta G_{\mathrm{vdW}} = \Delta\Delta G_{\mathrm{vdW,R}} + \Delta\Delta G_{\mathrm{vdW,A}}$, of the associated and dissociated α-helical vdW solutes as a function of the TMAO concentration. It can be observed that $\Delta\Delta G_{\mathrm{vdW}}$ decreases with TMAO concentration as was also observed for $\Delta\Delta G_{\mathrm{vdW,R}}$ (Fig. 5.2(a)). In fact, the decrease of $\Delta\Delta G_{\mathrm{vdW}}$ with TMAO concentration is larger than the decrease of $\Delta\Delta G_{\mathrm{vdW,R}}$, indicating that attractive van der Waals interactions lead to enhanced TMAO preferential binding to the solute. This is in line with previous experiments and MD simulations that have shown that TMAO adsorbs to hydrophobic surfaces and also to nonpolar residues on proteins.[53–57]

Figure S4 (Sec. S7 of the SI) shows $\Delta\Delta G_{\mathrm{vdW,A}}$ calculated for the associated and dissociated states of the two α-helical solutes. For, both, the dissociated and associated states of the α-helical vdW solutes, $\Delta\Delta G_{\mathrm{vdW,A}}$ decreases if the TMAO concentration is raised. This effect is however larger for the dissociated state due to its larger SASA. Therefore, the data ($\Delta\Delta G_{\mathrm{vdW,A}}$) for the dissociated state fall below the data for the associated state, as opposed to the data ($\Delta\Delta G_{\mathrm{vdW,R}}$) in Fig. 5.2(a). Due to the opposing trends in $\Delta\Delta G_{\mathrm{vdW,A}}$ and $\Delta\Delta G_{\mathrm{vdW,R}}$, the decrease in $\Delta\Delta G_{\mathrm{vdW}}$ of the associated and dissociated state is nearly equal as can be observed in Fig. 5.3(a). This leads to a non-monotonic trend in $\Delta G_{\mathrm{vdW}}^{D\rightarrow A}$ with increase in TMAO concentration shown in Fig. 5.3(b). At low concentrations, TMAO stabilises the associated state as the surfactant-like mechanism is dominant. Above 1 M TMAO concentration, the effect reverses due to the domination of attractive polyalanine-TMAO van der Waals interactions, leading to the destabilisation of the associated state upon increasing the TMAO concentration further. This non-monotonic effect has also been reported for the coil-globule collapse transition of a hydrophobic polymer in water.[53]

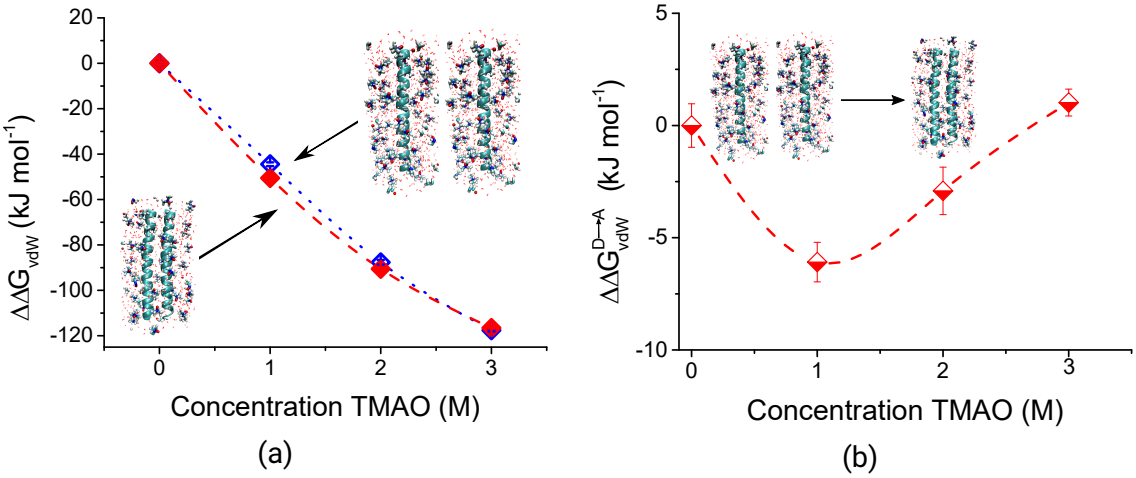

Figure 5.3: Solvation and association free energies of polyalanine vdW solutes. (a) Dependence of the relative solvation free energy of the associated ($\Delta\Delta G^{\mathrm{A}}_{\mathrm{vdW}}$) and dissociated ($\Delta\Delta G^{\mathrm{D}}_{\mathrm{vdW}}$) states of the vdW solutes. (b) Relative solvation free energy change of association, $\Delta\Delta G^{\mathrm{D}\to\mathrm{A}}_{\mathrm{vdW}} = \Delta\Delta G^{\mathrm{A}}_{\mathrm{vdW}} - \Delta\Delta G^{\mathrm{D}}_{\mathrm{vdW}}$, on the TMAO concentration.

3.3 Electrostatic interaction

Electrostatic interactions of the polyalanine α-helix with water and TMAO mostly involve the polar peptide backbone and therefore contribute to ΔG (eqn (1)) in addition to the van der Waals interactions discussed above. While TMAO adsorbs to extended hydrophobic surfaces,[54,57] it is depleted from the hydration shell of proteins which has been attributed to thermodynamically unfavourable TMAO interactions with the polar backbone.[17] Therefore, the preferential TMAO interaction with the α-helical vdW solute discussed above may be affected after introducing the electrostatic interactions with water and TMAO. Fig. 5.4 shows $\Delta\Delta G_{\mathrm{vdW,A}}$ and $\Delta\Delta G_{\mathrm{Elec}}$ versus TMAO concentration. The negative slope of $\Delta\Delta G_{\mathrm{vdW,A}}$ indicates that introducing attractive van der Waals interactions aids preferential TMAO binding. The positive slope of $\Delta\Delta G_{\mathrm{Elec}}$ however indicates that the subsequent introduction of electrostatic interactions counteracts TMAO binding. Therefore, competing electrostatic interactions of TMAO and water with the polar peptide backbone lead to weaker TMAO binding to α-helical polyalanine in comparison to systems in which these interactions are absent. This result corroborates conclusions obtained previously based on transfer free energy experiments.[17] From Fig. 5.4 it can be seen that the contributions to the relative solvation free energy from electrostatic and cohesive van der Waals interactions nearly compensate each other. At low TMAO concentrations, the trends in $\Delta\Delta G$ (see Sec. S8 in the SI) are governed by $\Delta\Delta G_{\mathrm{vdW,R}}$, leading to preferential TMAO binding. At TMAO concentrations above 2 M the electrostatic interactions dominate, leading to an increase in $\Delta\Delta G$ and therefore TMAO depletion (also see Fig. S3 of the SI).

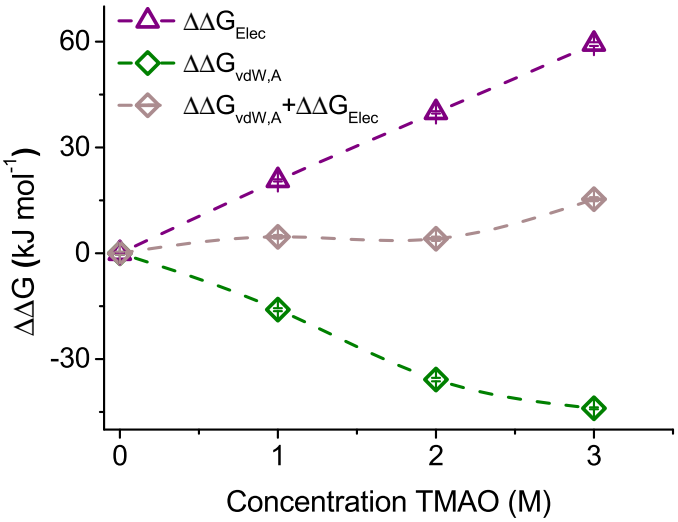

Figure 5.4: Dependence of the solute-solvent cohesive interaction free energies $\Delta\Delta G_{\mathrm{vdW,A}}$, $\Delta\Delta G_{\mathrm{Elec}}$ and $\Delta\Delta G_{\mathrm{vdW,A}} + \Delta\Delta G_{\mathrm{Elec}}$ on TMAO concentration. The introduction of attractive van der Waals solute-solvent interactions is free energy favourable and leads to stronger preferential TMAO adsorption on the vdW solute than on the corresponding WCA cavity. The subsequent introduction of electrostatic solute-solvent interactions is free energy unfavourable (relative to pure water) and leads to weaker preferential TMAO adsorption on the polyalanine α-helix than on the corresponding vdW solute. At TMAO concentrations below 2 M, the contribution to the solvation free energy from the solute-solvent electrostatic and cohesive van der Waals interactions nearly compensate each other.

4 Conclusions

We have shown that TMAO interactions with nonpolar solutes in water are length scale dependent and change from repulsive at small scales to attractive at large scales. This length-scale transition, discovered by studying Weeks-Chandler-Andersen (WCA) solutes that represent the molecular-sized cavities of methane and α-helical polyalanine, is linked to the dipolar/hydrophobic characteristic[58] of TMAO that causes an increase of the density but a decrease of the surface tension of the aqueous solution. Interestingly, this length scale transition may be similar to the one recently observed in ion binding of weakly hydrated anions with polymers.[59]

The MD simulations performed in this work showed that this surfactant-like property of TMAO causes an attenuating effect on the free-energy cost of cavity formation while it, counterintuitively, reinforces the water-mediated attraction between two α-helical polyalanine cavities. The same observation was made for the corresponding α-helical van der Waals (vdW) solutes, which, in addition to WCA core repulsion, interact with water and TMAO through attractive vdW forces (modelled by a Lennard-Jones potential).

The observed TMAO-reinforcement of the hydrophobic interaction can neither be described with ”macroscopic” surface tension models nor with ”microscopic” scaled-particle-theory (SPT) models. The surface tension model, which has been applied in protein folding/stability problems,[22] predicts

that TMAO attenuates cavity-cavity attraction and should lead to protein unfolding in contrast to what is experimentally observed. The SPT model correctly predicts that TMAO reinforces cavity-cavity attraction, but for the wrong reason as it assumes that the free-energy cost of cavity formation increases because the density of aqueous TMAO solutions exceeds the density of pure water.[20,60]

The TMAO stabilisation mechanism reported in this work involves a coupling between the interface-bulk partitioning of TMAO and the dissociation-association ($D \rightleftharpoons A$) equilibrium of the nonpolar solutes. Because interfacial partitioning of TMAO is entropically penalised, TMAO preferentially binds to the side of the equilibrium that exposes the smallest solvent-accessible surface area. Accordingly, the $D \rightleftharpoons A$ equilibrium is shifted towards the right side, which, for the systems studied herein, corresponds to the associated α-helical solutes. We have furthermore found that, at sufficiently high TMAO concentrations, TMAO-solute vdW interactions overcompensate this effect and shift the $D \rightleftharpoons A$ equilibrium back to the left. As such, TMAO affects hydrophobic interactions in a concentration dependent manner, reminiscent to previously reported cosolvent effects on the polymer coil-globule equilibrium in aqueous solutions.[27,53,61]

In summary, the results reported in this work have implications for a fundamental understanding of solvation. We anticipate that the mechanism proposed herein is relevant to biomolecular self-assembly driven by hydrophobic interactions and phase behaviour in aqueous TMAO solutions.[62,63]

Conflicts of interest

There are no conflicts of interest.

Acknowledgement

The MD simulations were performed on the Lichtenberg HighPerformance Computer of the Technische Universität Darmstadt, Germany. SB and NvdW thank the DFG for funding through the Collaborative Research Center Transregio TRR 146 Multiscale Simulation Methods for Soft Matter Systems.

Bibliography

[1] Hummer, G.; Garde, S.; García, A. E.; Paulaitus, M. E.; Pratt, L. R. Hydrophobic Effects on a Molecular Scale. *J. Phys. Chem. B* **1998**, *102*, 10469–10482.

[2] Lum, K.; Chandler, D.; Weeks, J. D. Hydrophobicity at Small and Large Length Scales. *J. Phys. Chem. B* **1999**, *103*, 4570–4577.

[3] Huang, D. M.; Chandler, D. Temperature and length scale dependence of hydrophobic effects and their possible implications for protein folding. *Proc. Natl. Acad. Sci. U.S.A.* **2000**, *97*, 8324–8327.

[4] Chandler, D. Interfaces and the driving force of hydrophobic assembly. *Nature* **2005**, *437*, 640–647.

[5] Huang, D. M.; Geissler, P. L.; Chandler, D. Scaling of Hydrophobic Solvation Free Energies. *J. Phys. Chem. B* **2001**, *105*, 6704–6709.

[6] Rajamani, S.; Truskett, T. M.; Garde, S. Hydrophobic hydration from small to large length-scales: Understanding and manipulating the crossover. *Proc. Natl. Acad. Sci. U.S.A.* **2005**, *102*, 9475–9480.

[7] Rogers, P. S. Z.; Pitzer, K. S. Volumetric Properties of Aqueous Sodium Chloride Solutions. *J. Phys. Chem. Ref. Data* **1982**, *11*, 15–81.

[8] Marcus, Y. Surface Tension of Aqueous Electrolytes and Ions. *J. Chem. Eng. Data* **2010**, *55*, 3641–3644.

[9] Mikhail, S. Z.; Kimel, W. R. Densities and Viscosities of Methanol-Water Mixtures. *J. Chem. Eng. Data* **1961**, *6*, 533–537.

[10] Vazquez, G.; Alvarez, E.; Navaza, J. M. Surface Tension of Alcohol Water + Water from 20 to 50 .degree.C. *J. Chem. Eng. Data* **1995**, *40*, 611–614.

[11] Lide, D. R. *CRC handbook of chemistry and physics, 89th edition, edited by David R. Lide*, 89th ed.; Boca Raton, 2008.

[12] Weeks, J. D.; Chandler, D.; Andersen, H. C. Role of Repulsive Forces in Determining the Equilibrium Structure of Simple Liquids. *J. Chem. Phys.* **1971**, *54*, 5237–5247.

[13] Pierce, V.; Kang, M.; Aburi, M.; Weerasinghe, S.; Smith, P. E. Recent Applications of Kirkwood–Buff Theory to Biological Systems. *Cell Biochem. Biophys.* **2008**, *50*, 1–22.

[14] van der Vegt, N. F. A.; van Gunsteren, W. F. Entropic contributions in cosolvent binding to hydrophobic solutes in water. *J. Phys. Chem. B* **2004**, *108*, 1056–1064.

[15] Markthaler, D.; Zeman, J.; Baz, J.; Smiatek, J.; Hansen, N. Validation of Trimethylamine-N-oxide (TMAO) Force Fields Based on Thermophysical Properties of Aqueous TMAO Solutions. *J. Phys. Chem. B* **2017**, *121*, 10674–10688.

[16] Makarov, D. M.; Egorov, G. I.; Kolker, A. M. Density and Volumetric Properties of Aqueous Solutions of Trimethylamine N-Oxide in the Temperature Range from (278.15 to 323.15) K and at Pressures up to 100 MPa. *J. Chem. Eng. Data* **2015**, *60*, 1291–1299.

[17] Auton, M.; Rösgen, J.; Sinev, M.; Holthauzen, L. M. F.; Bolen, D. W. Osmolyte effects on protein stability and solubility: A balancing act between backbone and side-chains. *Biophys. Chem.* **2011**, *159*, 90 – 99.

[18] Shimizu, S.; Smith, D. J. Preferential hydration and the exclusion of cosolvents from protein surfaces. *J. Chem. Phys.* **2004**, *121*, 1148–1154.

[19] Davis-Searles, P. R.; Saunders, A. J.; Erie, D. A.; Winzor, D. J.; Pielak, G. J. Interpreting the effects of small uncharged solutes on protein-folding equilibria. *Annu. Rev. Biophys. Biomol. Struct.* **2001**, *30*, 271–306.

[20] Cozzolino, S.; Oliva, R.; Graziano, G.; Del Vecchio, P. Counteraction of denaturant-induced protein unfolding is a general property of stabilizing agents. *Phys. Chem. Chem. Phys.* **2018**, *20*, 29389–29398.

[21] Graziano, G. How does trimethylamine N-oxide counteract the denaturing activity of urea? *Phys. Chem. Chem. Phys.* **2011**, *13*, 17689–17695.

[22] Auton, M.; Ferreon, A. C. M.; Bolen, D. W. Metrics that Differentiate the Origins of Osmolyte Effects on Protein Stability: A Test of the Surface Tension Proposal. *J. Mol. Biol.* **2006**, *361*, 983 – 992.

[23] Sagle, L. B.; Cimatu, K.; Litosh, V. A.; Liu, Y.; Flores, S. C.; Chen, X.; Yu, B.; Cremer, P. S. Methyl Groups of Trimethylamine N-Oxide Orient Away from Hydrophobic Interfaces. *J. Am. Chem. Soc.* **2011**, *133*, 18707–18712.

[24] Liao, Y.-T.; Manson, A. C.; DeLyser, M. R.; Noid, W. G.; Cremer, P. S. Trimethylamine-N-oxide stabilizes proteins via a distinct mechanism compared with betaine and glycine. *Proc. Natl. Acad. Sci. U.S.A.* **2017**, *114*, 2479–2484.

[25] Mochizuki, K.; Koga, K. Cononsolvency behavior of hydrophobes in water + methanol mixtures. *Phys. Chem. Chem. Phys.* **2016**, *18*, 16188–16195.

[26] Koga, K.; Yamamoto, N. Hydrophobicity Varying with Temperature, Pressure, and Salt Concentration. *J. Phys. Chem. B* **2018**, *122*, 3655–3665, PMID: 29357255.

[27] Bharadwaj, S.; Nayar, D.; Dalgicdir, C.; van der Vegt, N. F. A. A cosolvent surfactant mechanism affects polymer collapse in miscible good solvents. *Commun. Chem.* **2020**, *3*, 165.

[28] Sorin, E. J.; Pande, V. S. Exploring the helix-coil transition via all-atom equilibrium ensemble simulations. *Biophys. J.* **2005**, *88*, 2472–2493.

[29] Hölzl, C.; Kibies, P.; Imoto, S.; Frach, R.; Suladze, S.; Winter, R.; Marx, D.; Horinek, D.; Kast, S. M. Design principles for high-pressure force fields: Aqueous TMAO solutions from ambient to kilobar pressures. *J. Chem. Phys.* **2016**, *144*, 1–4.

[30] Abascal, J. L. F.; Vega, C. A general purpose model for the condensed phases of water: TIP4P/2005. *J. Chem. Phys.* **2005**, *123*, 234505.

[31] Shen, Y.; Maupetit, J.; Derreumaux, P.; Tufféry, P. Improved PEP-FOLD Approach for Peptide and Miniprotein Structure Prediction. *J. Chem. Theory Comput.* **2014**, *10*, 4745–4758.

[32] Berendsen, H. J.; van der Spoel, D.; van Drunen, R. GROMACS: A message-passing parallel molecular dynamics implementation. *Comput. Phys. Commun.* **1995**, *91*, 43–56.

[33] Abraham, M. J.; Murtola, T.; Schulz, R.; Páll, S.; Smith, J. C.; Hess, B.; Lindah, E. Gromacs: High performance molecular simulations through multi-level parallelism from laptops to supercomputers. *SoftwareX* **2015**, *1-2*, 19–25.

[34] Hess, B. P-LINCS: A parallel linear constraint solver for molecular simulation. *J. Chem. Theory Comput.* **2008**, *4*, 116–122.

[35] Darden, T.; York, D.; Pedersen, L. Particle mesh Ewald: An N·log(N) method for Ewald sums in large systems. *J. Chem. Phys.* **1993**, *98*, 10089–10092.

[36] Berendsen, H. J.; Postma, J. P.; Van Gunsteren, W. F.; DiNola, A.; Haak, J. R. Molecular dynamics with coupling to an external bath. *J. Chem. Phys.* **1984**, *81*, 3684–3690.

[37] Nosé, S. A molecular dynamics method for simulations in the canonical ensemble. *Mol. Phys.* **1984**, *52*, 255–268.

[38] Parrinello, M.; Rahman, A. Polymorphic transitions in single crystals: A new molecular dynamics method. *J. Appl. Phys.* **1981**, *52*, 7182–7190.

[39] Torrie, G.; Valleau, J. Nonphysical sampling distributions in Monte Carlo free-energy estimation: Umbrella sampling. *J. Comput. Phys.* **1977**, *23*, 187–199.

[40] Kästner, J. Umbrella sampling. *WIREs Comput. Mol. Sci.* **2011**, *1*, 932–942.

[41] Kumar, S.; Rosenberg, J. M.; Bouzida, D.; Swendsen, R. H.; Kollman, P. A. THE weighted histogram analysis method for free-energy calculations on biomolecules. I. The method. *J. Comput. Chem.* **1992**, *13*, 1011–1021.

[42] Pham, T. T.; Shirts, M. R. Identifying low variance pathways for free energy calculations of molecular transformations in solution phase. *J. Chem. Phys.* **2011**, *135*, 034114.

[43] Bennett, C. H. Efficient estimation of free energy differences from Monte Carlo data. *J. Comput. Phys.* **1976**, *22*, 245–268.

[44] Shirts, M. R.; Chodera, J. D. Statistically optimal analysis of samples from multiple equilibrium states. *J. Chem. Phys.* **2008**, *129*, 124105.

[45] Smith, P. E.; van Gunsteren, W. F. When are free energy components meaningful? *J. Phys. Chem.* **1994**, *98*, 13735–13740.

[46] Ashbaugh, H. S.; Collett, N. J.; Hatch, H. W.; Staton, J. A. Assessing the thermodynamic signatures of hydrophobic hydration for several common water models. *J. Chem. Phys.* **2010**, *132*, 124504.

[47] Frenkel, D.; Smit, B. *Understanding Molecular Simulation - From Algorithms to Applications*; Academic Press: San Diego, 2002.

[48] Timasheff, S. N. Protein-solvent preferential interactions, protein hydration, and the modulation of biochemical reactions by solvent components. *Proc. Natl. Acad. Sci. U.S.A.* **2002**, *99*, 9721–9726.

[49] Kita, Y.; Arakawa, T.; Lin, T.-Y.; Timasheff, S. N. Contribution of the surface free energy perturbation to protein-solvent interactions. *Biochemistry* **1994**, *33*, 15178–15189.

[50] Rodríguez-Ropero, F.; van der Vegt, N. F. A. Direct Osmolyte–Macromolecule Interactions Confer Entropic Stability to Folded States. *J. Phys. Chem. B* **2014**, *118*, 7327–7334.

[51] van der Vegt, N. F. A.; Nayar, D. The Hydrophobic Effect and the Role of Cosolvents. *J. Phys. Chem. B* **2017**, *121*, 9986–9998, PMID: 28921974.

[52] van der Vegt, N. F. A. Length-Scale Effects in Hydrophobic Polymer Collapse Transitions. *J. Phys. Chem. B* **2021**, *125*, 5191–5199.

[53] Nayar, D.; van der Vegt, N. F. A. Cosolvent Effects on Polymer Hydration Drive Hydrophobic Collapse. *J. Phys. Chem. B* **2018**, *122*, 3587–3595.

[54] Anand, G.; Jamadagni, S. N.; Garde, S.; Belfort, G. Self-Assembly of TMAO at Hydrophobic Interfaces and Its Effect on Protein Adsorption: Insights from Experiments and Simulations. *Langmuir* **2010**, *26*, 9695–9702.

[55] Su, Z.; Mahmoudinobar, F.; Dias, C. L. Effects of Trimethylamine-*N*-oxide on the Conformation of Peptides and its Implications for Proteins. *Phys. Rev. Lett.* **2017**, *119*, 108102.

[56] Su, Z.; Ravindhran, G.; Dias, C. L. Effects of Trimethylamine-N-oxide (TMAO) on Hydrophobic and Charged Interactions. *J. Phys. Chem. B* **2018**, *122*, 5557–5566.

[57] Mondal, J.; Halverson, D.; Li, I. T. S.; Stirnemann, G.; Walker, G. C.; Berne, B. J. How osmolytes influence hydrophobic polymer conformations: A unified view from experiment and theory. *Proc. Natl. Acad. Sci. U.S.A.* **2015**, *112*, 9270–9275.

[58] Schneck, E.; Horinek, D.; Netz, R. R. Insight into the molecular mechanisms of protein stabilizing osmolytes from global force-field variations. *J. Phys. Chem. B* **2013**, *117*, 8310–8321.

[59] Rogers, B. A.; Okur, H. I.; Yan, C.; Yang, T.; Heyda, J.; Cremer, P. S. Weakly hydrated anions bind to polymers but not monomers in aqueous solutions. *Nat. Chem.* **2021**, 1755–4349.

[60] Vigorita, M.; Cozzolino, S.; Oliva, R.; Graziano, G.; Del Vecchio, P. Counteraction ability of TMAO toward different denaturing agents. *Biopolymers* **2018**, *109*, e23104.

[61] Bharadwaj, S.; Nayar, D.; Dalgicdir, C.; van der Vegt, N. F. A. An interplay of excluded-volume and polymer–(co)solvent attractive interactions regulates polymer collapse in mixed solvents. *J. Chem. Phys.* **2021**, *154*, 134903.

[62] Cinar, H.; Fetahaj, Z.; Cinar, S.; Vernon, R. M.; Chan, H. S.; Winter, R. Temperature, Hydrostatic Pressure, and Osmolyte Effects on Liquid–Liquid Phase Separation in Protein Condensates: Physical Chemistry and Biological Implications. *Chem. Eur. J.* **2019**, *25*, 13049–13069.

[63] Cinar, S.; Cinar, H.; Chan, H. S.; Winter, R. Pressure-Sensitive and Osmolyte-Modulated Liquid-Liquid Phase Separation of Eye-Lens γ-Crystallins. *J. Am. Chem. Soc.* **2019**, *141*, 7347–7354.

5 Supporting Information

5.1 Association of polyalanine helices

The potential of mean force (PMF) between two polyalanine-helices is shown in Fig. 6.4. The configuration of the associated helices at around 0.85 nm was randomly taken from the first minimum of the PMF, where the helices are in contact and mainly interact via van der Waals interactions. The second minimum at around 1.05 nm corresponds to a solvent-shared helix pair, where one layer of water molecules separates the solutes.

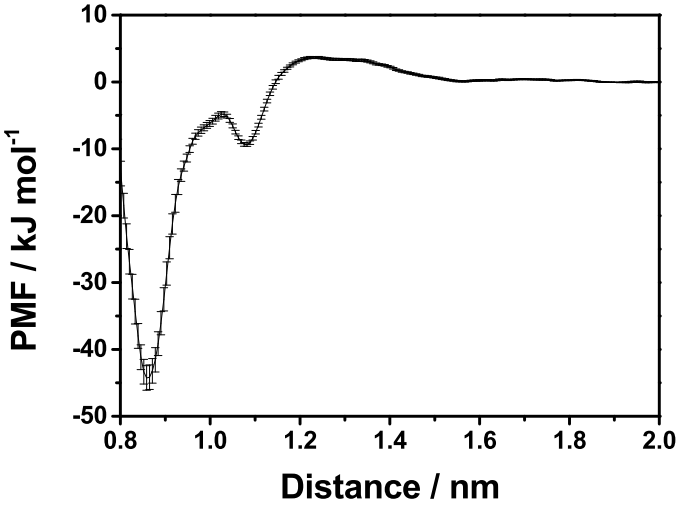

Figure 5.5: PMF between the center of mass of two polyalanine-helices in water obtained via umbrella sampling.

5.2 Free energy calculations

The solvation free energy ΔG of the polyalanine-helices in water-TMAO mixtures was computed using free energy perturbation (FEP) and thermodynamic integration (TI). The solvation process can be considered as a two step thermodynamic process where a repulsive cavity is created to host the solute and subsequently solute-solvent cohesive interactions are introduced. The contribution to the solvation free energy from the solute-solvent cohesive interactions can be further subdivided into contributions from cohesive solute-solvent van der Waals interactions and solute-solvent electrostatic interactions. The solvation free energy is then

$$\begin{aligned} \Delta G &= \Delta G_{\mathrm{vdW,R}} + \Delta G_{\mathrm{vdW,A}} + \Delta G_{\mathrm{Elec}} \\ \Delta G_{\mathrm{vdW}} &= \Delta G_{\mathrm{vdW,R}} + \Delta G_{\mathrm{vdW,A}} \end{aligned} \tag{6}$$

where $\Delta G_{\mathrm{vdW,R}}$ is the reversible work of creating a repulsive cavity which has the same shape and size as the solute, $\Delta G_{\mathrm{vdW,A}}$ is the reversible work associated with subsequently introducing cohesive solute-solvent van der Waals interactions with the preformed cavity, and ΔG_{Elec} is the reversible work associated with the final introduction of solute-solvent electrostatic interactions. Note that these contributions to the solvation free energy are dependent on the sequence in which the different solute-solvent interactions are introduced. ΔG_{vdW} is the reversible work associated with introducing solute-solvent van der Waals interactions. In this work, the solute-solvent van der Waals interactions are modelled through the Lennard-Jones (LJ) potential and the solute-solvent repulsive interactions are modelled through the Weeks-Chandler-Andersen (WCA) potential.[1] The cohesive solute-solvent van der Waals interaction energy ψ_A is then given by the following expression,

$$\psi_A = \begin{cases} -\epsilon, & r < 2^{1/6}\sigma \\ 4\epsilon\left[\left(\frac{\sigma}{r}\right)^{12} - \left(\frac{\sigma}{r}\right)^{6}\right], & r \geq 2^{1/6}\sigma \end{cases} . \tag{7}$$

In this work, the different contributions to ΔG were computed from a combination of two sets of simulations. From the first set of simulations, $\Delta G_{\mathrm{vdW,R}}$ was calculated. $\Delta G_{\mathrm{vdW,R}}$ can be computed by gradually introducing the solute-solvent WCA interactions. Equivalently, one can also compute $\Delta G_{\mathrm{vdW,R}}$ by gradually decoupling the solute-solvent WCA interactions through a set of $\lambda_{\mathrm{vdW,R}}$ values. The latter approach was employed in this work to compute $\Delta G_{\mathrm{vdW,R}}$. Here, $\lambda_{\mathrm{vdW,R}} = 0$ is the state where the solute-solvent WCA interactions are coupled and $\lambda_{\mathrm{vdW,R}} = 1$ is the state where solute-solvent WCA interactions are decoupled.

The second set of simulations involves two steps where first the solute-solvent LJ interactions were gradually introduced to compute ΔG_{vdW}. Subsequently, the solute-solvent electrostatic interactions were gradually introduced to compute ΔG_{Elec}. Equivalently, one can also compute these free energies by gradually decoupling the different solute-solvent interactions. Note that the solute-solvent electrostatic interactions are decoupled first and then the solute-solvent LJ interactions are decoupled. In this work, the solute-solvent electrostatic interactions were gradually decoupled to obtain ΔG_{Elec} through a set of λ_{Elec} values where $\lambda_{\mathrm{Elec}} = 0$ refers to the state where both solute-solvent LJ and electrostatic interactions are coupled and $\lambda_{\mathrm{Elec}} = 1$ is the state where only solute-solvent LJ interactions are coupled. Subsequently, ΔG_{vdW} was computed by gradually decoupling the solute-solvent LJ interactions through a set of λ_{vdW} values where $\lambda_{\mathrm{vdW}} = 0$ refers to the state where the solute-solvent LJ interactions are coupled and $\lambda_{\mathrm{vdW}} = 1$ is the state where solute-solvent LJ interactions are decoupled. ΔG and $\Delta G_{\mathrm{vdW,A}}$ were then computed from the following expressions,

$$\begin{aligned} \Delta G &= \Delta G_{\mathrm{vdW}} + \Delta G_{\mathrm{Elec}} \\ \Delta G_{\mathrm{vdW,A}} &= \Delta G_{\mathrm{vdW}} - \Delta G_{\mathrm{vdW,R}} \end{aligned} \tag{8}$$

The open source python tool “Alchemical Analysis” (AA) was employed to compute the solvation

free energy and the different contributions to it.[2] The AA tool computes the solvation free energy through TI, and FEP methods such as Bennett Acceptance Ratio (BAR), Deletion Exponential Averaging (DEXP) and Insertion Exponential Averaging (IEXP).[3] The set of $\lambda_{\mathrm{vdW,R}}$, λ_{vdW} and λ_{Elec} values were chosen in a manner which ensures that the solvation free energies calculated from these four methods were in quantitative agreement (see Sec. 5.3). This also ensures that the errors in the computed solvation free energies are very small (see Fig. 5.6(a)). Note that such an approach leads to unevenly spaced $\lambda_{\mathrm{vdW,R}}$, λ_{vdW} and λ_{Elec} values in this work. The values of the $\lambda_{\mathrm{vdW,R}}$, λ_{vdW} and λ_{Elec} for polyalanine-helix cavities at different TMAO concentrations are listed in the subsequent sections.

5.5.2.1 Calculation of $\Delta G_{\mathrm{vdW,R}}$ for the polyalanine-helix cavity

Single helix

All concentrations (51 parameters)

$\lambda_{\mathrm{vdW,R}}$ = 0.000 0.050 0.100 0.150 0.250 0.300 0.350 0.400 0.450 0.500 0.550 0.580 0.600 0.630 0.650 0.680 0.700 0.715 0.730 0.750 0.760 0.770 0.780 0.790 0.800 0.810 0.820 0.825 0.830 0.834 0.837 0.840 0.844 0.847 0.850 0.855 0.860 0.865 0.870 0.880 0.884 0.887 0.890 0.900 0.910 0.920 0.930 0.950 0.980 1.000

Associated helices

All concentrations (64 parameters)

$\lambda_{\mathrm{vdW,R}}$ = 0.000 0.050 0.100 0.150 0.200 0.250 0.300 0.350 0.400 0.450 0.500 0.550 0.575 0.600 0.625 0.650 0.675 0.700 0.710 0.720 0.730 0.740 0.750 0.760 0.770 0.780 0.790 0.800 0.810 0.820 0.830 0.840 0.845 0.850 0.855 0.860 0.865 0.870 0.872 0.874 0.876 0.878 0.880 0.885 0.890 0.895 0.900 0.905 0.910 0.915 0.920 0.930 0.940 0.945 0.950 0.955 0.960 0.965 0.970 0.975 0.980 0.985 0.990 1.000

5.5.2.2 Calculation of ΔG_{vdW} for the polyalanine-helix

Single helix

0 M (56 parameters)

λ_{vdW} = 0.000 0.050 0.100 0.150 0.200 0.250 0.300 0.350 0.400 0.450 0.475 0.500 0.525 0.550 0.575 0.600 0.625 0.650 0.670 0.690 0.700 0.710 0.720 0.730 0.740 0.750 0.760 0.765 0.770 0.775 0.778 0.780 0.782 0.784 0.786 0.788 0.790 0.795 0.800 0.805 0.810 0.820 0.830 0.840 0.850 0.860 0.870 0.880 0.890 0.900 0.910 0.925 0.940 0.950 0.970 1.000

1 M (57 parameters)

λ_{vdW} = 0.000 0.050 0.100 0.150 0.200 0.250 0.300 0.350 0.400 0.450 0.475 0.500 0.525 0.550 0.575 0.600 0.625 0.650 0.670 0.690 0.700 0.710 0.720 0.730 0.740 0.750 0.760 0.765

0.770 0.773 0.775 0.778 0.780 0.783 0.787 0.790 0.793 0.797 0.800 0.803 0.807 0.810 0.815 0.820 0.830 0.840 0.850 0.860 0.870 0.880 0.890 0.900 0.910 0.925 0.940 0.950 0.970 1.000

2 M (57 parameters)

λ_{vdW} = 0.000 0.050 0.100 0.150 0.200 0.250 0.300 0.350 0.400 0.450 0.475 0.500 0.525 0.550 0.575 0.600 0.625 0.650 0.670 0.690 0.700 0.710 0.720 0.730 0.740 0.750 0.760 0.765 0.770 0.775 0.780 0.782 0.784 0.786 0.788 0.790 0.800 0.810 0.813 0.817 0.820 0.825 0.830 0.840 0.850 0.860 0.870 0.880 0.890 0.900 0.910 0.925 0.940 0.950 0.960 0.970 0.980 1.000

3 M (54 parameters)

λ_{vdW} = 0.000 0.050 0.100 0.150 0.200 0.250 0.300 0.350 0.400 0.450 0.475 0.500 0.525 0.550 0.575 0.600 0.625 0.650 0.670 0.690 0.700 0.710 0.720 0.730 0.740 0.750 0.760 0.765 0.770 0.775 0.780 0.790 0.800 0.805 0.810 0.813 0.817 0.820 0.825 0.830 0.840 0.850 0.860 0.870 0.880 0.890 0.900 0.910 0.925 0.940 0.950 0.960 0.970 0.980 1.000

Associated helices

0 M (61 parameters)

λ_{vdW} = 0.000 0.050 0.075 0.100 0.125 0.150 0.175 0.200 0.225 0.250 0.275 0.300 0.325 0.350 0.375 0.400 0.425 0.450 0.475 0.500 0.525 0.550 0.575 0.600 0.625 0.650 0.675 0.700 0.720 0.740 0.750 0.760 0.765 0.770 0.772 0.774 0.776 0.778 0.780 0.782 0.784 0.786 0.788 0.790 0.795 0.800 0.805 0.810 0.815 0.820 0.830 0.840 0.850 0.870 0.890 0.900 0.920 0.940 0.950 0.960 0.980 1.000

1 M (55 parameters)

λ_{vdW} = 0.000 0.050 0.075 0.100 0.125 0.150 0.175 0.200 0.225 0.250 0.275 0.300 0.325 0.350 0.375 0.400 0.425 0.450 0.475 0.500 0.525 0.550 0.575 0.600 0.625 0.650 0.675 0.700 0.720 0.740 0.750 0.760 0.770 0.775 0.780 0.790 0.800 0.810 0.815 0.820 0.825 0.830 0.835 0.840 0.850 0.860 0.870 0.880 0.890 0.900 0.920 0.940 0.950 0.960 0.980 1.000

2 M (60 parameters)

λ_{vdW} = 0.000 0.050 0.075 0.100 0.125 0.150 0.175 0.200 0.225 0.250 0.275 0.300 0.325 0.350 0.375 0.400 0.425 0.450 0.475 0.500 0.525 0.550 0.575 0.600 0.625 0.650 0.675 0.700 0.720 0.740 0.750 0.760 0.770 0.775 0.780 0.790 0.795 0.800 0.810 0.815 0.820 0.825 0.830 0.835 0.840 0.850 0.860 0.870 0.880 0.890 0.900 0.910 0.920 0.930 0.940 0.950 0.960 0.970 0.980 0.990 1.000

3 M (71 parameters)

λ_{vdW} = 0.000 0.050 0.075 0.100 0.125 0.150 0.175 0.200 0.225 0.250 0.275 0.300 0.325 0.350

0.375 0.400 0.425 0.450 0.475 0.500 0.525 0.550 0.575 0.600 0.625 0.650 0.675 0.690 0.700 0.710 0.720 0.730 0.740 0.750 0.760 0.770 0.775 0.780 0.790 0.795 0.800 0.805 0.810 0.813 0.817 0.820 0.823 0.827 0.830 0.835 0.840 0.845 0.850 0.855 0.860 0.865 0.870 0.875 0.880 0.885 0.890 0.900 0.910 0.920 0.930 0.940 0.950 0.960 0.970 0.980 0.990 1.000

5.5.2.3 Calculation of $\Delta G_{\mathbf{Elec}}$ for the polyalanine-helix

Single helix

0 M (20 parameters)

λ_{Elec} = 0.000 0.050 0.100 0.150 0.200 0.250 0.300 0.350 0.400 0.450 0.475 0.500 0.550 0.600 0.650 0.700 0.750 0.800 0.850 0.900 1.000

1 M (30 parameters)

λ_{Elec} = 0.000 0.025 0.050 0.075 0.100 0.125 0.150 0.175 0.200 0.225 0.250 0.275 0.300 0.325 0.350 0.375 0.400 0.425 0.450 0.475 0.500 0.550 0.600 0.650 0.700 0.750 0.800 0.850 0.900 1.000

2 M (39 parameters)

λ_{Elec} = 0.000 0.010 0.025 0.040 0.050 0.060 0.075 0.090 0.100 0.110 0.125 0.140 0.150 0.160 0.175 0.190 0.200 0.210 0.225 0.250 0.275 0.300 0.325 0.350 0.375 0.400 0.425 0.450 0.475 0.500 0.550 0.600 0.650 0.700 0.750 0.800 0.850 0.900 1.000

3 M (23 parameters)

λ_{Elec} = 0.000 0.050 0.100 0.150 0.200 0.220 0.240 0.250 0.300 0.350 0.400 0.450 0.475 0.500 0.550 0.600 0.650 0.700 0.750 0.800 0.850 0.900 1.000

Associated helices

0 M (33 parameters)

λ_{Elec} = 0.000 0.025 0.050 0.070 0.100 0.120 0.150 0.170 0.200 0.220 0.250 0.270 0.300 0.350 0.400 0.450 0.500 0.520 0.550 0.570 0.600 0.620 0.650 0.670 0.700 0.720 0.750 0.770 0.800 0.850 0.900 0.950 1.000

1 M (41 parameters)

λ_{Elec} = 0.000 0.010 0.020 0.030 0.040 0.050 0.070 0.085 0.100 0.120 0.150 0.170 0.200 0.220 0.250 0.270 0.300 0.325 0.350 0.375 0.400 0.425 0.450 0.475 0.500 0.520 0.550 0.570 0.600 0.620 0.650 0.670 0.700 0.720 0.750 0.770 0.800 0.850 0.900 0.950 1.000

2 M (40 parameters)

λ_{Elec} = 0.000 0.010 0.020 0.030 0.040 0.050 0.070 0.100 0.120 0.150 0.170 0.200 0.220 0.250 0.270 0.300 0.325 0.350 0.375 0.400 0.425 0.450 0.475 0.500 0.520 0.550 0.570 0.600 0.620 0.650 0.670 0.700 0.720 0.750 0.770 0.800 0.850 0.900 0.950 1.000

3 M (32 parameters)

λ_{Elec} = 0.000 0.050 0.070 0.100 0.120 0.150 0.170 0.200 0.220 0.250 0.270 0.300 0.350 0.400 0.450 0.500 0.520 0.550 0.570 0.600 0.620 0.650 0.670 0.700 0.720 0.750 0.770 0.800 0.850 0.900 0.950 1.000

5.3 Comparison of TI and BAR

We compare the results obtained from thermodynamic integration (TI)[4] and the BAR algorithm.[3,5] We have calculated $\Delta\Delta G^{\mathrm{A}}_{\mathrm{vdW}}$ and $\Delta\Delta G^{\mathrm{D}}_{\mathrm{vdW}}$ and then obtained the association solvation free energy through $\Delta\Delta G^{\mathrm{D}\to\mathrm{A}}_{\mathrm{vdW}} = \Delta\Delta G^{\mathrm{A}}_{\mathrm{vdW}} - \Delta\Delta G^{\mathrm{D}}_{\mathrm{vdW}}$. $\Delta\Delta G^{\mathrm{D}\to\mathrm{A}}_{\mathrm{vdW}}$ is an order of magnitude smaller than $\Delta\Delta G_{\mathrm{vdW}}$ and therefore very susceptible to errors in $\Delta\Delta G_{\mathrm{vdW}}$. $\Delta\Delta G^{\mathrm{D}\to\mathrm{A}}_{\mathrm{vdW,R}}$ and $\Delta\Delta G^{\mathrm{D}\to\mathrm{A}}_{\mathrm{vdW,A}}$ on the other hand are on a similar order of magnitude compared to the respective solvation free energies from which they are calculated. Therefore, the influence of the algorithm on the quantitative results can be best estimated from $\Delta\Delta G^{\mathrm{D}\to\mathrm{A}}_{\mathrm{vdW}}$. It can be seen in Fig. 5.6(a) that the relative solvation free energies $\Delta\Delta G_{\mathrm{vdW}}$ obtained from different algorithms are in quantitative agreement. Nevertheless, as shown in Fig. 5.6(b) there are still some small differences in $\Delta\Delta G^{\mathrm{D}\to\mathrm{A}}_{\mathrm{vdW}}$ obtained from TI and BAR. However, the trends remain the same.

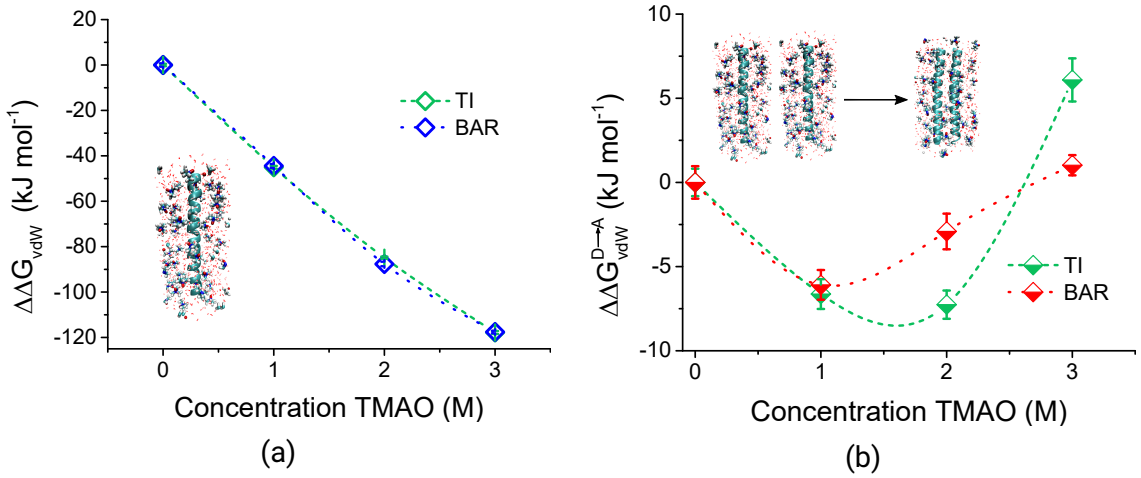

Figure 5.6: a) Change in the relative solvation free energy $\Delta\Delta G_{\mathrm{vdW}}$ as a function of TMAO concentration for the single helix using TI and BAR. It can be seen that the results obtained by either analysis are in quantitative agreement. Errors are in order of the symbol size. b) Change in the relative solvation free energy $\Delta\Delta G^{\mathrm{D}\to\mathrm{A}}_{\mathrm{vdW}}$ as a function of TMAO concentration for TI and BAR. It can be seen that the trends remain the same, but there are small differences in absolute values.

5.4 Solvation free energies in pure water

We have reported all solvation free energies in reference to the solvation free energy in pure water. Table 5.2 summarizes the different contributions to the solvation free energy in pure water.

5.5 Solvent accessible surface area (SASA)

The SASA has been calculated using the double cubic lattice method developed by Eisenhaber et al. as implemented in GROMACS.[6] The SASA for the single helix is 24.13 nm^2 and the one of

Table 5.2: Solvation free energies ΔG, ΔG_{vdW}, $\Delta G_{\mathrm{vdW,R}}$, $\Delta G_{\mathrm{vdW,A}}$ and ΔG_{Elec} in pure water for the dissociated (D) and associated (A) states. Solvation free energies of the dissociated state were obtained by doubling the solvation free energy of a single helix. The solvation free energies are expressed in kJ mol^{-1}.

	Dissociated state	Associated state
ΔG	-429.2 ± 0.8	-341.0 ± 0.5
ΔG_{vdW}	105.1 ± 0.7	131.9 ± 0.2
$\Delta G_{\mathrm{vdW,R}}$	1475.0 ± 0.8	1113.2 ± 0.3
$\Delta G_{\mathrm{vdw,A}}$	-1369.9 ± 1.5	-981.3 ± 0.4
ΔG_{Elec}	-534.2 ± 0.4	-472.9 ± 0.4

the associated helices is 37.72 nm^2. Therefore, 10.54 nm^2 of the solute surface area becomes inaccessible to the solvent upon association.

5.6 Preferential binding coefficient Γ_{23}

The preferential binding coefficient Γ_{23} is defined by the following expression,

$$\Gamma_{23} = \rho_3 \left(G_{23} - G_{21} \right), \tag{9}$$

where the index $i = 1$ stands for water, $i = 2$ for the solute and $i = 3$ for TMAO. ρ_3 is the molar concentration of TMAO, G_{23} and G_{21} are the solute-TMAO and solute-water Kirkwood-Buff integrals. TMAO is preferentially adsorbed on the solute for $\Gamma_{23} > 0$. On the other hand, the solute is preferentially hydrated for $\Gamma_{23} < 0$, i.e. TMAO is depleted from the solute. Γ_{23} can also be written in terms of the number of TMAO and water molecules in the following way,[7]

$$\Gamma_{23}(r) = \left\langle n_3(r) - \frac{N_3 - n_3(r)}{N_1 - n_1(r)} n_1(r) \right\rangle, \tag{10}$$

where $n_3(r)$ and $n_1(r)$ are the number of TMAO and the number of water molecules within a proximal distance of r from the solute surface, respectively. N_3 and N_1 are the total number of TMAO and water molecules in the system, respectively. The preferential binding coefficients were calculated using the expression in eqn 3. The dependence of the solvation free energy, of the associated or the dissociated state, on the TMAO concentration can be related to the corresponding preferential binding coefficients through the Wyman-Tanford relations,[8,9]

$$\frac{\partial \Delta G^{\mathrm{j}}}{\partial \rho_3} = -\frac{\Gamma_{23}^{\mathrm{j}}}{\rho_3 \left(1 + \rho_3 \left(G_{33} - G_{31} \right) \right)} \tag{11}$$

where the index j=A,D represents the associated or dissociated state, G_{33} and G_{31} are the Kirkwood-Buff integrals corresponding to the TMAO-TMAO interaction and the TMAO-water interaction, re-

spectively. Note that the factor $1+\rho_3\left(G_{33}-G_{31}\right)$ is positive at all TMAO concentrations as TMAO and water form stable mixtures.[10] Preferential adsorption of TMAO ($\Gamma_{23}>0$) leads to a decrease in the solvation free energy with increase in TMAO concentration. On the other hand, the solvation free energy increases with increase in TMAO concentration when TMAO is depleted from the solute surface, $\Gamma_{23}<0$. Then, for the dissociation-association equilibrium, $D \rightleftharpoons A$, the dependence of the free energy change upon association, $\Delta G^{D\to A}$, on the TMAO concentration concentration can be related to the preferential binding coefficients of the associated and dissociated states in the following way

$$\left(\frac{\partial \Delta G^{\mathrm{D}\to\mathrm{A}}}{\partial \rho_3}\right)_{p,T} = -\frac{\Gamma_{23}^{\mathrm{A}}-\Gamma_{23}^{\mathrm{D}}}{\rho_3\left(1+\rho_3\left(G_{33}-G_{31}\right)\right)} = -\frac{\Delta\Gamma_{23}^{\mathrm{D}\to\mathrm{A}}}{\rho_3\left(1+\rho_3\left(G_{33}-G_{31}\right)\right)} \tag{12}$$

$\Delta G^{\mathrm{D}\to\mathrm{A}}$ increases with the increase in the TMAO concentration when TMAO preferentially adsorbs on the dissociated state, i.e. $\Delta\Gamma_{23}^{\mathrm{D}\to\mathrm{A}}<0$. This shifts the $D \rightleftharpoons A$ equilibrium towards the dissociated state. On the other hand, TMAO shifts the $D \rightleftharpoons A$ equilibrium towards the associated state when it preferentially adsorbs on the associated state ($\Delta\Gamma_{23}^{\mathrm{D}\to\mathrm{A}}>0$), i.e. $\Delta G^{\mathrm{D}\to\mathrm{A}}$ decreases with increase in TMAO concentration.

The dissociated (single helix) and associated state have been simulated starting from 10 different random initial configurations for 150 ns. The random initial configurations were taken from an initial 100 ns production run using the settings described in section 2.2 of the main manuscript at 3 M TMAO concentration. Errors were calculated using block averaging over 10 preferential binding coefficients obtained from each run. Preferential binding coefficients of the single helix have been doubled to obtain the preferential binding coefficient of the dissociated state. The preferential binding coefficients of TMAO for the helices interacting through WCA, vdW and, vdW and electrostatic (Full) interactions are shown in Fig. 5.7. TMAO preferentially binds ($\Gamma_{23}>0$) to the repulsive helix cavity, which would lead to a decrease of $\Delta\Delta G_{\mathrm{vdW,R}}$ (see eqn 11). The preferential TMAO binding increases with the introduction of attractive van der Waals interactions. On the other hand, TMAO is depleted from the fully interacting helix (van der Waals (vdW) and electrostatics, $\Gamma_{23}<0$), which would lead to an increase of $\Delta\Delta G$ at high TMAO concentrations. These qualitative predictions, which are based on the results in Fig. 5.7 and eqn 11, are in agreement with the solvation free energy calculations (Fig. 2, 3, 5.8, 5.10).

5.7 Contribution to the solvation free energy from cohesive van der Waals interactions $\Delta\Delta G_{\mathrm{vdW,A}}$

Figure 5.8(a) shows the dependence of $\Delta\Delta G_{\mathrm{vdW,A}}$ on the TMAO concentration for the associated and dissociated states. $\Delta\Delta G_{\mathrm{vdW,A}}$ decreases at a faster rate for the dissociated state than for the associated state, which in turn shifts the $D \rightleftharpoons A$ equilibrium towards the dissociated state i.e.

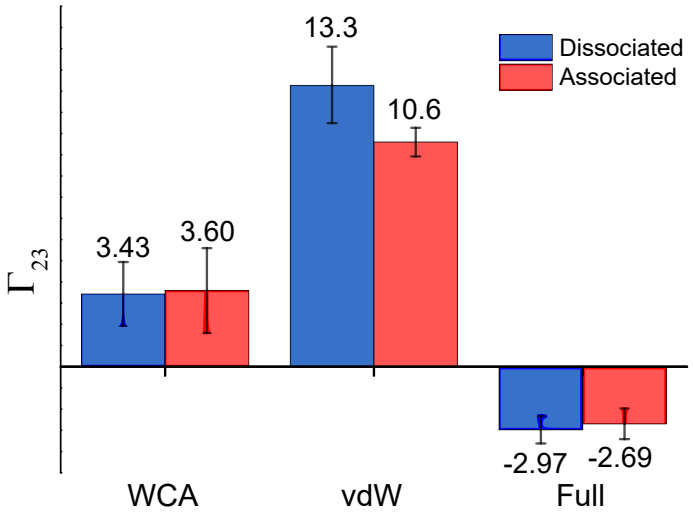

Figure 5.7: Preferential binding coefficient Γ_{23} of TMAO at 3 M TMAO concentration for the associated and dissociated polyalanine helices. The preferential binding coefficient of TMAO for the helices interacting via WCA interactions is positive, showing preferential TMAO binding, as also indicated by the negative slope of $\Delta\Delta G_{\mathrm{vdW,R}}$. The introduction of attractive van der Waal interactions lead to an increase in the preferential binding coefficient (vdW). The preferential binding coefficient of TMAO for the helices interacting via van der Waals and electrostatic (full interactions) interactions is negative, showing TMAO depletion, as indicated by the positive slope of $\Delta\Delta G$ at high TMAO concentrations.

$\Delta\Delta G^{\mathrm{D}\to\mathrm{A}}_{\mathrm{vdW,A}}$ increases with increase in TMAO concentration (Figure 5.8(b)). This occurs due to the larger SASA of the dissociated state, as compared to the associated state, which leads to a larger number of favorable polyalanine-TMAO contacts.

5.8 Free energies of introducing van der Waals and electrostatic interactions

From Figs. 2(a), 4 in the main text and Fig. 5.8, it can be seen that, with increase in TMAO concentration, the solvation free energies decrease when only solute-solvent van der Waals interactions are considered. The solute-solvent electrostatic interactions however counteract this favorable decrease in the solvation free energies as can be seen in Fig. 5.9.

This observation applies for, both, the associated and dissociated states. Therefore, the dependence of the relative solvation free energy of the fully interacting solute (van der Waals and electrostatic interactions), $\Delta\Delta G$, on the TMAO concentration is governed by the interplay of these two contributions that show compensating behaviors.

The effect of this interplay can be seen in Fig. 5.10(a) where $\Delta\Delta G$, for both the associated and dissociated states, exhibits a non-monontonic dependence on the TMAO concentration. At low TMAO concentrations, $\Delta\Delta G$ decreases with increase in TMAO concentration indicating that the contribution from the solute-solvent van der Waals interactions is dominant (TMAO is preferentially adsorbed). On the other hand, at high TMAO concentrations, $\Delta\Delta G$ increases with increase

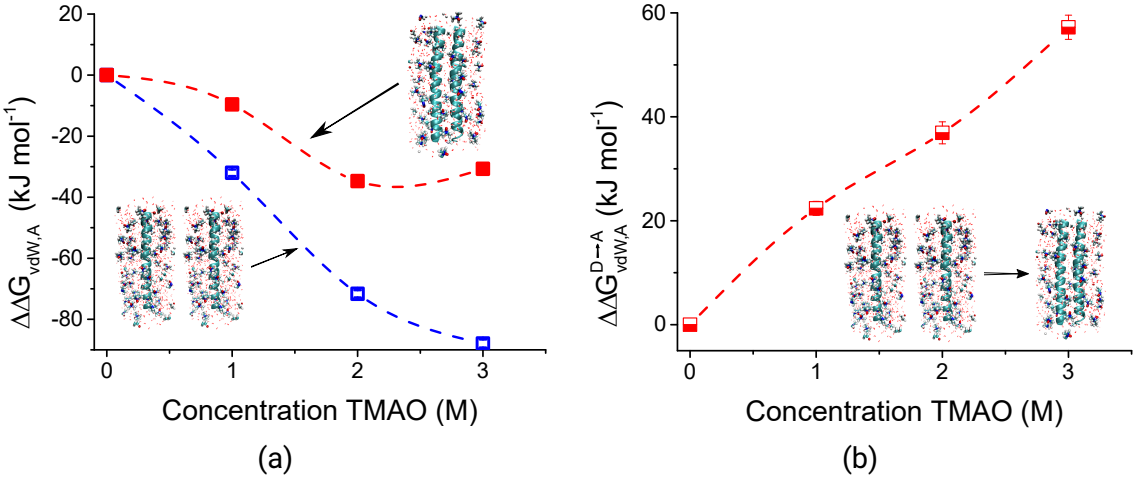

Figure 5.8: a) Relative solvation free energy $\Delta\Delta G_{\mathrm{vdW,A}}$ as a function of TMAO concentration for the dissociated state ($\Delta\Delta G^{\mathrm{D}}_{\mathrm{vdW,A}}$, blue symbols) and the associated state ($\Delta\Delta G^{\mathrm{A}}_{\mathrm{vdW,A}}$, red symbols). The addition of TMAO has a bigger influence on $\Delta\Delta G^{\mathrm{D}}_{\mathrm{vdW,A}}$ due to its larger SASA. b) Dependence of the relative solvation free energy $\Delta\Delta G^{\mathrm{D}\to\mathrm{A}}_{\mathrm{vdW,A}}$, the attractive van der Waals interactions, on the TMAO concentration.

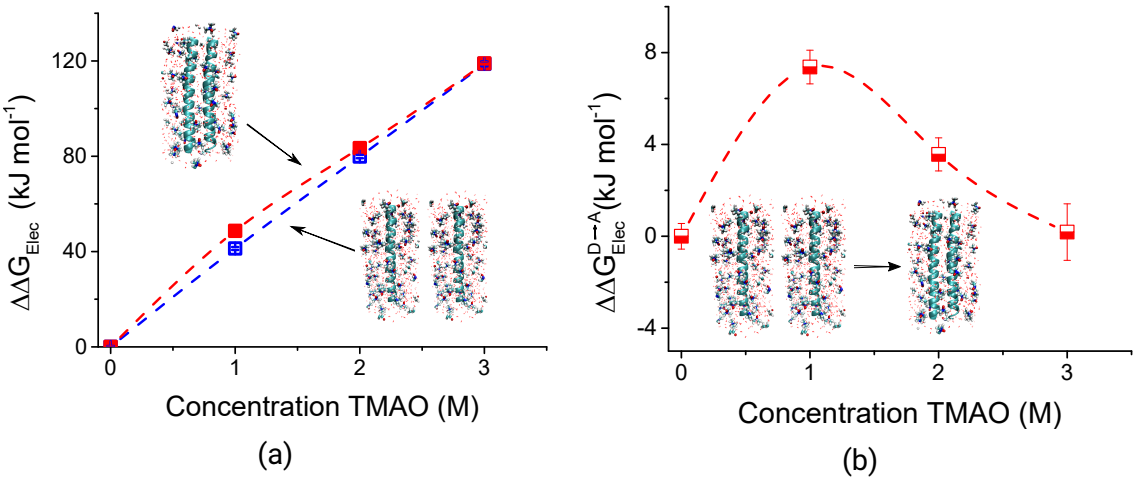

Figure 5.9: a) Dependence of the relative solvation electrostatic free energy $\Delta\Delta G_{\mathrm{Elec}}$ on TMAO concentration for the associated ($\Delta\Delta G^{\mathrm{A}}_{\mathrm{Elec}}$, red symbols) and dissociated ($\Delta\Delta G^{\mathrm{D}}_{\mathrm{Elec}}$, blue symbols) state. b) The relative solvation free energy of association $\Delta\Delta G^{\mathrm{D}\to\mathrm{A}}_{\mathrm{Elec}} = \Delta\Delta G^{\mathrm{A}}_{\mathrm{Elec}} - \Delta\Delta G^{\mathrm{D}}_{\mathrm{Elec}}$ as a function of TMAO concentration. The positive slope in (a) indicates that TMAO accumulation is reduced by electrostatic interactions. The free energy of association in (b) reversely mirrors the trend in the free energy of solvation of van der Waals solutes (see Fig. 3(b)), leading to compensations between these two quantities.

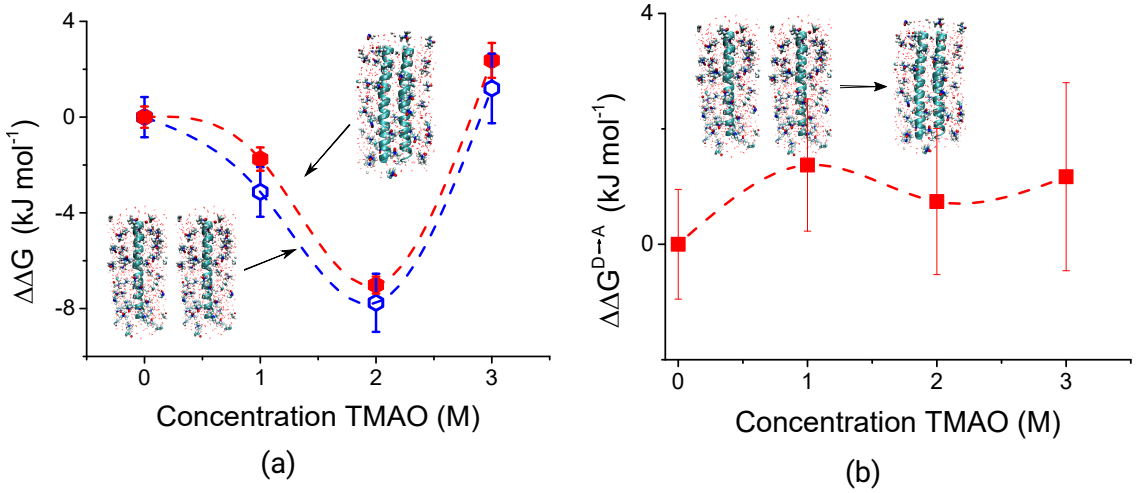

Figure 5.10: a) Dependence of the relative solvation free energy $\Delta\Delta G$ on TMAO concentration for the associated ($\Delta\Delta G^{\mathrm{A}}$, red symbols) and dissociated ($\Delta\Delta G^{\mathrm{D}}$, blue symbols) polyalanine helices interacting through van der Waals and electrostatic interactions. b) The relative solvation free energy of association $\Delta\Delta G^{\mathrm{D}\to\mathrm{A}} = \Delta\Delta G^{\mathrm{A}} - \Delta\Delta G^{\mathrm{D}}$ as a function of TMAO concentration. The slope in a) is concentration dependent. The negative slope at low concentrations indicates preferential TMAO binding, while the positive slope indicates that at higher TMAO concentration, TMAO is depleted. The relative free energy of association for polyalanine does not display a clear trend but rather seems to remain constant.

in TMAO concentration which indicates that the contribution from the solute-solvent electrostatic interactions overcompensates the contribution from the solute-solvent van der Waals interactions (TMAO is depleted). From the dependence of $\Delta\Delta G^{\mathrm{D}\to\mathrm{A}}$ on the TMAO concentration in Fig. 5.10(b), it can be seen that the introduction of solute-solvent electrostatic interactions leads to the disappearance of the non-monotonic trends in $\Delta\Delta G^{\mathrm{D}\to\mathrm{A}}_{\mathrm{vdW}}$ (see Fig. 3(b) of the main text).

Bibliography

[1] Weeks, J. D.; Chandler, D.; Andersen, H. C. Role of Repulsive Forces in Determining the Equilibrium Structure of Simple Liquids. *J. Chem. Phys.* **1971**, *54*, 5237–5247.

[2] Klimovich, P. V.; Shirts, M. R.; Mobley, D. L. Guidelines for the analysis of free energy calculations. *J. Comput. Aided Mol. Des.* **2015**, *29*, 397–411.

[3] Bennett, C. H. Efficient estimation of free energy differences from Monte Carlo data. *J. Comput. Phys.* **1976**, *22*, 245–268.

[4] Straatsma, T. P.; McCammon, J. A. Multiconfiguration thermodynamic integration. *J. Chem. Phys.* **1991**, *95*, 1175–1188.

[5] Shirts, M. R.; Chodera, J. D. Statistically optimal analysis of samples from multiple equilibrium states. *J. Chem. Phys.* **2008**, *129*, 124105.

[6] Eisenhaber, F.; Lijnzaad, P.; Argos, P.; Sander, C.; Scharf, M. The double cubic lattice method: Efficient approaches to numerical integration of surface area and volume and to dot surface contouring of molecular assemblies. *J. Comput. Chem.* **1995**, *16*, 273–284.

[7] Pierce, V.; Kang, M.; Aburi, M.; Weerasinghe, S.; Smith, P. E. Recent Applications of Kirkwood–Buff Theory to Biological Systems. *Cell Biochem. Biophys.* **2008**, *50*, 1–22.

[8] Wyman, J. Linked Functions and Reciprocal Effects in Hemoglobin: A Second Look. *Adv. Prot. Chem.* **1964**, *19*, 223 – 286.

[9] Tanford, C. Extension of the theory of linked functions to incorporate the effects of protein hydration. *J. Mol. Biol.* **1969**, *39*, 539–544.

[10] Ben-Naim, A. *Molecular theory of solutions*; Oxford University Press: Oxford, 2006.

6 A unique piezolyte mechanism of TMAO: Hydrophobic interactions under extreme pressure conditions

Abstract

We report a computer simulation study of the effect of trimethylamine N-oxide (TMAO) on the pressure stability of the hydrophobic contact interaction of two polyalanine-based helices. We found that TMAO counterbalanced the disruptive effect of pressure denaturation on the account of an earlier reported electronic polarization effect that led to an increased TMAO dipole moment under compression of the solvent. This direct stabilization mechanism became ineffective when the dipole polarization of TMAO was not considered and was linked to nonspecific van der Waals interactions of TMAO with the nonpolar surfaces of the two helices which became weaker as TMAO became stronger polarized at high pressure. The corresponding thermodynamic driving forces are discussed and should be generic for hydrophobic interactions under high pressure. The proposed mechanism suggests that TMAO stands out as a piezolyte among stabilizing osmolytes, potentially protecting biological assemblies formed by hydrophobic interactions under extreme pressure conditions.

Around 16% of Earth species are found in the deep sea,[1] the potential birth place of life, where lack of light and increased pressure force these creatures to adapt. High pressure forces proteins to unfold and thereby disrupts vital functions, such as enzymatic reactions and sub-cellular transport.[2–6] It also destabilizes functional biocondensates which are formed by liquid-liquid-phase separation (LLPS), a process important for membrane-less compartmentalization in the cell.[7–11] The question is: How are these organisms, called piezophiles because they have adapted to high pressure, able to counteract the high pressure conditions?

The adaption can either occur by attuned piezophilic proteins or by the presence of small organic cosolutes referred to as osmolytes. It has been found that deep sea creatures have a high concentration of certain osmolytes, such as methylamines, in their cells that alongside of pressure increases linearly with depth.[12] Based on this observation, these osmolytes, in particular trimethylamine N-oxide (TMAO), are thought to be specialized in their counteractions of pressure denaturation and have therefore been termed ”piezolytes”.[13–15] TMAO has been found to increase the pressure

stability of proteins and stabilize biomolecular condensates formed by LLPS under high pressure conditions,[7–11,16] but until now there are no indications that piezolytes are distinct from other osmolytes. In this regard, especially their effect on hydrophobic parts of proteins is of interest, since the hydrophobic core formation is crucial in protein folding and hydrophobic interactions are important in LLPS, e.g. the elastine-like peptide (ELP), which exhibits pressure- and osmolyte-dependent LLPS, is made up of nearly 80% of hydrophobic amino acids.[10]

The effect of pressure on any chemical equilibrium is determined by the volume difference between reactants and products according to Le-Chateliers principle. For example, in protein folding, the unfolded state has a smaller volume than the folded state, resulting in protein denaturation upon pressure increase.[4] On the other hand, the effect of cosolutes on a chemical equilibrium (e.g. protein folding or protein association in solution) is determined by the preferential binding of the cosolutes to the reactants and products.[17,18] Correspondingly, the dependence of the Gibbs energy, $\Delta G_2(p, c_3)$, of folding a protein on pressure, p, and cosolute concentration, c_3, at a fixed temperature, T, can be written as:

$$\mathrm{d}\Delta G_2(p, c_3) = \Delta\overline{V}_2 \mathrm{d}p - RT\Delta\Gamma_{23}\frac{a_{33}}{c_3}\mathrm{d}c_3 \tag{1}$$

where we used the standard convention and refer to water as component 1, the protein as component 2, and the cosolute as component 3. In Eq. 1, ΔG_2 is the difference in Gibbs energy of the folded (F) and unfolded (U) states of the protein, $\Delta\overline{V}_2 = \overline{V}_2^{\mathrm{F}} - \overline{V}_2^{\mathrm{U}}$ the volume difference upon folding, $\Delta\Gamma_{23} = \Gamma_{23}^{\mathrm{F}} - \Gamma_{23}^{\mathrm{U}}$ the difference in cosolute preferential binding coefficient upon folding,[17] R is the gas constant, and $a_{33} = \left[1 + c_3(G_{33} - G_{31})\right]^{-1}$ an activity enhancement factor (> 1 for strong water-binding osmolytes) in which G_{33} and G_{31} are the Kirkwood-Buff integrals related to the components water and cosolute of the bulk solvent.

One hypothesis regarding how piezophiles have adapted to high pressure is based on the first part of the above expression: Proteins from piezophiles have a smaller volume change upon unfolding or the volume change upon unfolding is reduced due to the addition of piezolytes. However, the adaption of proteins has been disproven by Avagyan et al. who studied several proteins of piezophiles and non-piezophiles.[19] Papini et al. measured the effects of protecting osmolytes and denaturants on $\Delta\overline{V}_2$ of bovine ribonuclease and egg white lysozyme with differential scanning calorimetry and pressure perturbation calorimetry.[20] However, these authors found that there was nothing special about osmolytes that have been termed piezolytes, as all protecting osmolytes considered in their work had no direct effect on $\Delta\overline{V}_2$ and the pressure denaturation of proteins. They therefore dismissed the term "piezolyte". We note that, because $\Delta\overline{V}_2$ is independent of c_3,[20] Eq. 1 implies that $RT\Delta\Gamma_{23}a_{33}/c_3$ does not depend on pressure.

Although TMAO cannot be distinguished as a piezolyte in pressure stabilization of proteins, its hydration properties are pressure dependent and, by contrast to other cosolutes like urea,[21] determined by changes in electronic polarization at high pressure.[15,22,23] TMAO has a large dipole

moment, which increases by nearly a factor of two when transferred from the gas phase to water.[23] Due to its zwitterionic nature it is able to tightly bind water molecules with its negatively charged oxygen.[24] This property leads to the depletion of TMAO from many protein surfaces with a corresponding increase in their thermal stability[25] and an indirect effect on pressure stabilization.[20] At ambient pressure, TMAO binds around 3 water molecules. At high hydrostatic pressure, the compression of the solvent however leads to electronic polarization effects that further enhance the dipole moment of TMAO.[23] Interestingly, at 10 kbar it has been found that TMAO increases its water binding to a partial fourfold coordination of the oxygen atom.[15] Although this change in TMAO-water interaction has an insignificant direct effect on the pressure stability of proteins,[20] it potentially affects hydrophobic interactions[26] and may therefore play a role in biomolecular LLPS and the pressure stability of functional biomolecular condensates which are more susceptible to pressure than the folding of proteins.[9,10]

To explore this question, we herein report a computer simulation study combined with free-energy calculations that quantify the effect of pressure-induced changes in TMAO polarization on the hydrophobic interaction of two nonpolar polyalanine-α-helices. This model system was chosen in order to isolate the potential role of piezolytic effects on hydrophobic interactions relevant in biomolecular systems. The calculations reported below revealed that TMAO counterbalanced the pressure denaturation of hydrophobic interactions due to its enhanced dipole polarization at high pressure. We found that this pressure-stabilizing effect disappeared when ignoring the polarization of the TMAO dipole and found indications that this newly-discovered effect was controlled by thermodynamic driving forces that should be generic for hydrophobic interactions in TMAO/water solutions under extreme pressure conditions.

We used the nonpolarizable, pressure-dependent TMAO force field (FF) of Hölzl et al..[23] This force field assigns adjustable partial charges to TMAO which model the increased dipole polarization at high pressure. To explore the implications of this polarization effect on the hydrophobic interaction of the two polyalanine-α-helices under high-pressure conditions (2 kbar) we performed umbrella sampling molecular dynamics (MD) simulations using two different approaches: 1) MD simulations were performed that used the polarized TMAO model with an increased dipole moment, from hereon called high-dipole FF, 2) MD simulations were performed that used the non-polarized TMAO model, parameterized for ambient pressure conditions, from hereon called low-dipole FF. We further calculated the volume difference between the associated and dissociated states of the two α-helices and the preferential binding coefficient, Γ_{23}, of the single helix with these two approaches. The technical details on the force fields and umbrella sampling simulations are provided in the SI.

Ambient Pressure. Fig. 6.1 (a) reports the Gibbs energy of association, $w(r_{\mathrm{min}})$, corresponding to the minimum of the potential of mean force (PMF) obtained with umbrella sampling (see SI Fig. S1 for the PMF), as a function of the TMAO concentration (c_3) in solution. These data are in qualitative agreement with previously reported calculations based on the free-energy perturba-

tion method.[26] The Gibbs energy of association displays a non-monotonic dependence on c_3 and has a minimum at $c_3 = 1$ M where the hydrophobic association is strongest. As was previously reported,[26] preferential TMAO binding gives rise to two opposing thermodynamic driving forces that lead to such a non-monotonic dependence: An entropy loss associated with the accumulation of excess TMAO in the hydration shells of the two helices drives their association (i.e. drives a decrease of the overall nonpolar solvent-accessible surface area) at low bulk concentrations ($c_3 < 1$ M). However, when the bulk TMAO concentration is further increased, this effect is overcompensated by cohesive van der Waals interactions of TMAO with the two nonpolar solutes, leading to their dissociation. The concentration (c_3) where the hydrophobic association is strongest thus depends on a delicate energy-entropy balance linked to the weak binding of TMAO to nonpolar surfaces. This energy-entropy balance changes under varying environmental conditions such as pressure.

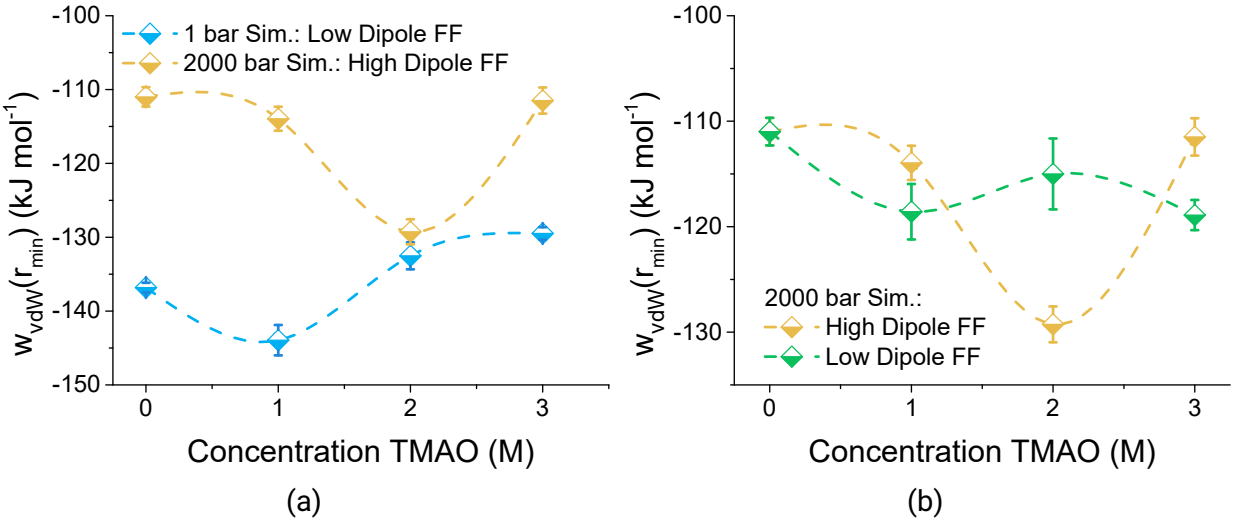

Figure 6.1: (a) Dependence of the Gibbs energy upon helix association at $T = 300$ K, taken from the minimum of the PMF, on TMAO concentration at 1 bar (blue data points) and 2000 bar (yellow data points). (b) Dependence of the Gibbs energy change upon helix association at $T = 300$ K, taken from the minimum of the PMF, on TMAO concentration at 2000 bar obtained using the low-dipole FF (green data points) and high-dipole FF (yellow data points).

High Pressure. In pure water, pressure shifted the helix-association equilibrium towards the dissociated state as indicated by the increase of the Gibbs energy of association (Fig. 6.1 (a) at $c_3 = 0$ M). Interestingly, at 2 kbar, the Gibbs energy of association also depended non-monotonically on c_3, but the minimum at $c_3 = 2$ M was deeper and shifted to a larger value of c_3 as compared to the data obtained at 1 bar. This observation is linked to the high-pressure polarization of the TMAO dipole that leads to stronger TMAO hydration and a correspondingly weaker preferential binding of TMAO to the two α-helical solutes as will be demonstrated below. Therefore, a higher TMAO bulk concentration was required to reach the turning point where cohesive van der Waals interactions of

TMAO with the two nonpolar solutes overcompensated the entropic driving force for their association. The shift of the Gibbs energy minimum caused by this mechanism led to the remarkable observation that at $c_3 = 2\,\mathrm{M}$ the two data points in Fig. 6.1 (a) almost merged, i.e. at this concentration TMAO almost fully counteracted the pressure-induced destabilization of the hydrophobic interaction. Fig. 6.2 summarizes the mechanism.

We repeated the high-pressure MD simulations using the low-dipole FF for TMAO. The corresponding data are shown in Fig. 6.1 (b) together with the data obtained with the high-dipole FF. The TMAO stabilization effect observed with the high-dipole FF disappeared when the low-dipole FF was employed in the simulations at 2 kbar. Comparison of the data in Figs. 6.1 (a) and 6.1 (b) showed that the data obtained with the low-dipole FF at 2 kbar were shifted up along the vertical axis as compared to the data obtained with the low-dipole FF at 1 bar while maintaining qualitatively the same non-monotic dependence on c_3. This indicated that the high-pressure polarization of the TMAO dipole was essential in achieving pressure stability of hydrophobic contacts.

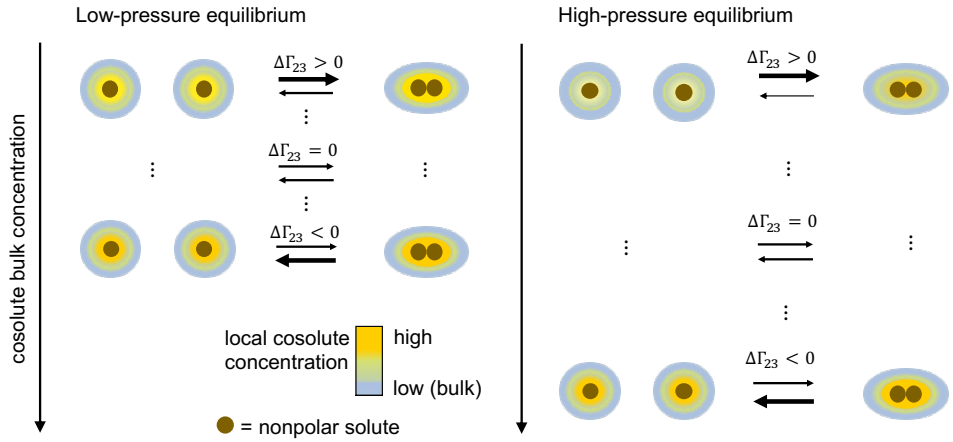

Figure 6.2: Direct interaction mechanism: (left) Partitioning of TMAO in the hydration shells of the nonpolar solutes enhances the forward association reaction and strengthens the hydrophobic contact interaction. The forward reaction is entropy-driven, i.e. it reduces the entropically unfavorable, non-uniform spatial distribution of solvent components due to bulk-interface partitioning of TMAO.[27] Cohesive van der Waals interactions between TMAO and the nonpolar solutes drive the reverse reaction and enhance it at high bulk concentrations of TMAO. (right) Polarization of the TMAO dipole under compression of the solvent at high pressure leads to weaker partitioning of TMAO in the hydration shells of the nonpolar solutes. Accordingly, TMAO-solute van der Waals interactions are weaker as compared to the low-pressure scenario and the forward reaction dominates the reverse reaction to a greater extent over a wider range of TMAO bulk concentrations.

The observations made with the high- and low-dipole FFs, alternatively to the above explanation based on preferential binding, could stem from their effects on the volume difference, $\Delta\overline{V}_2$, upon

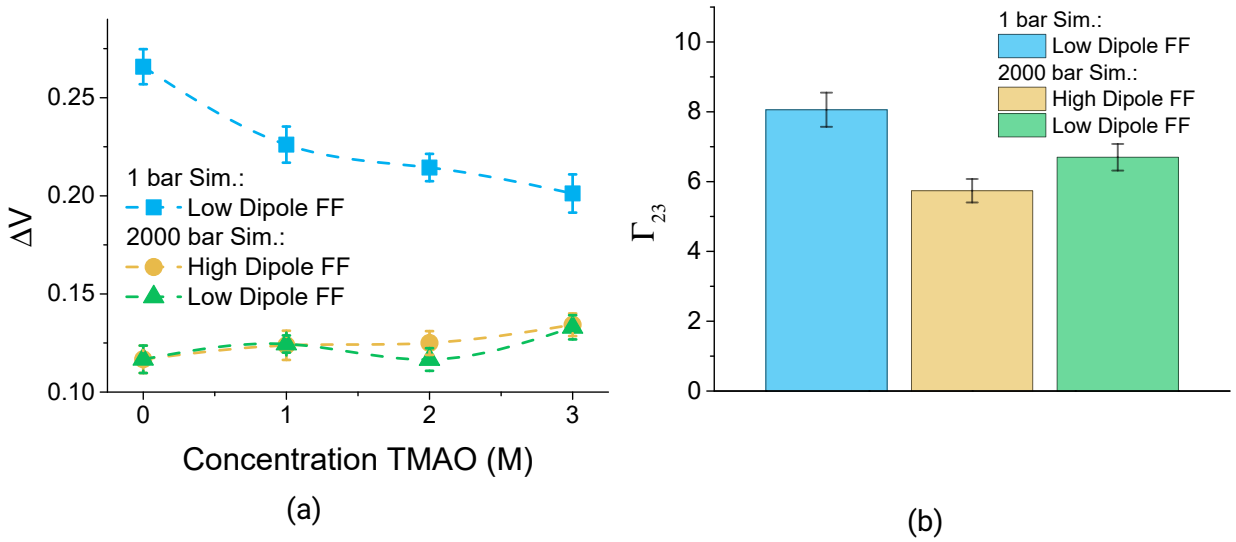

Figure 6.3: (a) Volume difference, $\Delta\overline{V}_2$, between the associated and dissociated state as a function of TMAO concentration (b) Preferential binding coefficient, Γ_{23}, of TMAO to the nonpolar α-helix at 2 M TMAO concentration obtained from solvation free energy data (Fig. S2) using Eqn. S3 reported in the SI.

helix association. Fig. 6.3 (a) reports the data obtained for $\Delta\overline{V}_2$ as a function of c_3 for the low-dipole FF and the high-dipole FF at 1 bar and 2 kbar. The low-pressure data indicated that $\Delta\overline{V}_2$ decreased as c_3 increased, i.e. at 1 bar, TMAO increased the pressure stability of the hydrophobic contact between the two α-helices. By contrast, this dependence disappeared at 2 kbar independent of whether the high-dipole FF or low-dipole FF was used. Because $\Delta\overline{V}_2$ did not depend on the TMAO dipole, the differences in the Gibbs energies of association (Fig. 6.1 (b)) obtained at high pressure with the high- and low-dipole FFs originated from differences in preferential binding of TMAO to the α-helices.

The preferential binding coefficient (Γ_{23}) is shown in Fig. 6.3 (b) and confirms this conclusion. When pressure was raised from 1 bar to 2 kbar, Γ_{23} decreased. While this occurred with both the high- and low-dipole FFs, Γ_{23} decreased more with the high-dipole FF as expected based on stronger TMAO-water binding of the high-dipole model. Note that the data in Fig. 6.3 (b) furthermore show that $\Gamma_{23} > 0$, i.e. TMAO accumulated in the hydration shell of the α-helix and stabilized the hydrophobic contact interaction of the two helices through direct interactions as indicated in Fig. 6.2.

In summary, the present work showed that the term ”piezolyte” aptly captures the effect of TMAO in terms of high-pressure stability of hydrophobic interactions. We proposed a stabilization mechanism, which, by contrast to indirect depletion effects on protein stability, involves the role of weak van der Waals interactions. This direct interaction mechanism is based on two opposing thermodynamic driving forces: (1) an entropic force that strengthens the hydrophobic attraction between the extended nonpolar α-helices due to the natural tendency of adsorbed TMAO molecules

to be assimilated by the bulk solution, (2) an enthalpic driving force that weakens the hydrophobic attraction between the extended nonpolar α-helices due to their cohesive van der Waals interaction with TMAO. The equilibrium of these two forces resulted in a minimum in the Gibbs energy of hydrophobic association upon changing the concentration of TMAO at low and high pressure. The high-pressure minimum occurred due to electronic polarization of TMAO and was deeper and shifted to a higher concentration of TMAO, indicating that an increased concentration of TMAO at high pressure provided a stabilizing environment for hydrophobic interactions.

The piezolyte effect described herein resulted from nonspecific van der Waals interactions of TMAO with nonpolar surfaces and should therefore be generic for hydrophobic interactions under extreme pressure conditions.

Acknowledgement

The authors offer special thanks to Dr. Swaminath Bharadwaj for fruitful discussions. The MD simulations were performed on the Lichtenberg High-Performance Computer of the Technische Universität Darmstadt, Germany.

Bibliography

[1] Costello, M. J.; Chaudhary, C. Marine Biodiversity, Biogeography, Deep-Sea Gradients, and Conservation. *Curr. Biol.* **2017**, *27*, R511–R527.

[2] Grigera, J. R.; McCarthy, A. N. The behavior of the hydrophobic effect under pressure and protein denaturation. *Biophys. J.* **2010**, *98*, 1626–1631.

[3] Garcia, A. E.; Paschek, D. Simulation of the pressure and temperature folding/unfolding equilibrium of a small RNA hairpin. *J. Am. Chem. Soc.* **2008**, *130*, 815–817.

[4] Mozhaev, V. V.; Heremans, K.; Frank, J.; Masson, P.; Balny, C. High pressure effects on protein structure and function. *Proteins* **1996**, *24*, 81–91.

[5] Luong, T. Q.; Kapoor, S.; Winter, R. Pressure—A gateway to fundamental insights into protein solvation, dynamics, and function. *ChemPhysChem* **2015**, *16*, 3555–3571.

[6] Arsiccio, A.; Shea, J.-E. Pressure Unfolding of Proteins: New Insights into the Role of Bound Water. *J. Phys. Chem. B* **2021**, *125*, 8431–8442.

[7] Möller, J.; Grobelny, S.; Schulze, J.; Bieder, S.; Steffen, A.; Erlkamp, M.; Paulus, M.; Tolan, M.; Winter, R. Reentrant liquid-liquid phase separation in protein solutions at elevated hydrostatic pressures. *Phys. Rev. Lett.* **2014**, *112*, 028101.

[8] Cinar, H.; Cinar, S.; Chan, H. S.; Winter, R. Pressure-Induced Dissolution and Reentrant Formation of Condensed, Liquid–Liquid Phase-Separated Elastomeric α-Elastin. *Chem. Eur. J.* **2018**, *24*, 8286–8291.

[9] Cinar, S.; Cinar, H.; Chan, H. S.; Winter, R. Pressure-Sensitive and Osmolyte-Modulated Liquid-Liquid Phase Separation of Eye-Lens γ-Crystallins. *J. Am. Chem. Soc.* **2019**, *141*, 7347–7354.

[10] Cinar, H.; Fetahaj, Z.; Cinar, S.; Vernon, R. M.; Chan, H. S.; Winter, R. H. Temperature, hydrostatic pressure, and osmolyte effects on liquid–liquid phase separation in protein condensates: physical chemistry and biological implications. *Chem. Eur. J.* **2019**, *25*, 13049–13069.

[11] Cinar, H.; Winter, R. The effects of cosolutes and crowding on the kinetics of protein condensate formation based on liquid–liquid phase separation: a pressure-jump relaxation study. *Sci. Rep.* **2020**, *10*, 1–16.

[12] Yancey, P. H.; Fyfe-Johnson, A. L.; Kelly, R. H.; Walker, V. P.; Aun, M. T. Trimethylamine oxide counteracts effects of hydrostatic pressure on proteins of deep-sea teleosts. *J. Exp. Zool.* **2001**, *289*, 172–176.

[13] Martin, D.; Bartlett, D.; Roberts, M. Solute accumulation in the deep-sea bacterium Photobacterium profundum. *Extremophiles : life under extreme conditions* **2003**, *6*, 507–14.

[14] Yancey, P. H.; Gerringer, M. E.; Drazen, J. C.; Rowden, A. A.; Jamieson, A. Marine Fish May Be Biochemically Constrained from Inhabiting the Deepest Ocean Depths. *Proc. Natl. Acad. Sci. U.S.A.* **2014**, *111*, 4461–5.

[15] Imoto, S.; Kibies, P.; Rosin, C.; Winter, R.; Kast, S. M.; Marx, D. Toward Extreme Biophysics: Deciphering the Infrared Response of Biomolecular Solutions at High Pressures. *Angew. Chem. Int. Ed.* **2016**, *55*, 9534–9538.

[16] Cinar, H.; Fetahaj, Z.; Cinar, S.; Vernon, R. M.; Chan, H. S.; Winter, R. Temperature, Hydrostatic Pressure, and Osmolyte Effects on Liquid–Liquid Phase Separation in Protein Condensates: Physical Chemistry and Biological Implications. *Chem. Eur. J.* **2019**, *25*, 13049–13069.

[17] Pierce, V.; Kang, M.; Aburi, M.; Weerasinghe, S.; Smith, P. E. Recent Applications of Kirkwood–Buff Theory to Biological Systems. *Cell Biochem. Biophys.* **2008**, *50*, 1–22.

[18] Timasheff, S. N. Water as ligand: preferential binding and exclusion of denaturants in protein unfolding. *Biochemistry* **1992**, *31*, 9857–9864.

[19] Avagyan, S.; Vasilchuk, D.; Makhatadze, G. I. Protein adaptation to high hydrostatic pressure: Computational analysis of the structural proteome. *Proteins* **2020**, *88*, 584–592.

[20] Papini, C. M.; Pandharipande, P. P.; Royer, C. A.; Makhatadze, G. I. Putting the piezolyte hypothesis under pressure. *Biophys. J.* **2017**, *113*, 974–977.

[21] Hölzl, C.; Kibies, P.; Imoto, S.; Noetzel, J.; Knierbein, M.; Salmen, P.; Paulus, M.; Nase, J.; Held, C.; Sadowski, G., *et al.* Structure and thermodynamics of aqueous urea solutions from ambient to kilobar pressures: From thermodynamic modeling, experiments, and first principles simulations to an accurate force field description. *Biophys. Chem.* **2019**, *254*, 106260.

[22] Imoto, S.; Forbert, H.; Marx, D. Water structure and solvation of osmolytes at high hydrostatic pressure: pure water and TMAO solutions at 10 kbar versus 1 bar. *Phys. Chem. Chem. Phys.* **2015**, *17*, 24224–24237.

[23] Hölzl, C.; Kibies, P.; Imoto, S.; Frach, R.; Suladze, S.; Winter, R.; Marx, D.; Horinek, D.; Kast, S. M. Design principles for high-pressure force fields: Aqueous TMAO solutions from ambient to kilobar pressures. *J. Chem. Phys.* **2016**, *144*, 1–4.

[24] Hunger, J.; Tielrooij, K. J.; Buchner, R.; Bonn, M.; Bakker, H. J. Complex formation in aqueous trimethylamine-N-oxide (TMAO) solutions. *J. Phys. Chem. B* **2012**, *116*, 4783–4795.

[25] Ma, J.; Pazos, I. M.; Gai, F. Microscopic insights into the protein-stabilizing effect of trimethylamine N-oxide (TMAO). *Proc. Natl. Acad. Sci. U.S.A.* **2014**, *111*, 8476–8481.

[26] Folberth, A.; Bharadwaj, S.; van der Vegt, N. F. Small-to-large length scale transition of TMAO interaction with hydrophobic solutes. *Phys. Chem. Chem. Phys.* **2022**, *24*, 2080–2087.

[27] van der Vegt, N. F. A. Length-Scale Effects in Hydrophobic Polymer Collapse Transitions. *J. Phys. Chem. B* **2021**, *125*, 5191–5199.

1 Supporting Information

1.1 Methods

1.1.1.1 Molecular Dynamics simulation details

We analyzed the assembly of two polyalanine α-helices (36-mers) at different TMAO concentrations at 1 and 2000 bar. The polypeptide was described using the Amber99sb-ildn force field[1], TMAO with the Hölzl force field[2], and water with the TIP4P/2005 model.[3] The Hölzl force field and the TIP4P/2005 water model were optimized to reproduce the properties of binary systems at ambient pressure well.[4] The number of molecules, equilibrated box volumes and densities of the systems at 300 K and 1 bar are summarized in Table 6.1 for 1 to 3 M TMAO concentration. The polyalanine-water and polyalanine-TMAO interactions did not include electrostatic contributions. This choice was made in order to model a nonpolar, model hydrophobic, surface onto which TMAO preferentially adsorbs.

PEPFOLD3 was used to create the starting configuration of a single helix.[5] A quasi-infinite chain was generated by connecting the head and tail groups of the helix across periodic boundary conditions, forming a peptide bond. Intramolecular hydrogen bonds between the backbone atoms of the helix were restrained using a harmonic potential with a force constant of strength 10^3 kJ mol^{-1} nm^{-1} to ensure a stable helix. All simulations were performed with the Gromacs package version 2021.1.[6,7] All chemical bonds involving a hydrogen atom were restrained using the LINCS algorithm.[8] Coulomb interactions were treated using particle mesh Ewald (PME)[9] with a real-space cut off of 1 nm, a PME order of 4 and a grid spacing of 0.12 nm. Long range dispersion corrections were applied to the pressure and energy and the van der Waals interaction cut off length was set at 1 nm. The neighbour list was updated every time step for umbrella sampling simulations and every five time steps for FEP simulations. In the equilibration, energy minimization was first done using the steepest descent algorithm with 50000 steps and a step size of 0.001 nm. Subsequently, the system was equilibrated in a constant volume-temperature simulation using the Berendsen thermostat (τ_T=1.0 ps, T = 300 K).[10] It was followed by a 1 ns constant pressure-temperature simulation using the Berendsen barostat (τ_P=2.0 ps, $\kappa_T = 5 \cdot 10^{-5}$ bar^{-1}, P = 1 bar or 2000 bar). Semi-isotropic pressure coupling was used in simulations with the quasi-infinite helix using a compressibility of 0 in the z-direction to ensure that the box dimension in z-direction remains constant. The time step was fixed at 2 fs in all simulations. All production runs were performed using the Nose-Hoover thermostat[11] at 300 K (τ_T=1.0 ps) and the Parrinello-Rahman barostat at 1 and 2000 bar (τ_P=2.0 ps)[12] with a compressibility of $5 \cdot 10^{-5}$ bar^{-1}.

Table 6.1: System details: TMAO concentrations, number of (No.) water and TMAO molecules, average density (300 K, 1 bar) and box volume for the umbrella sampling simulations.

TMAO conc. / M	No. TMAO	No. water	$\langle\rho\rangle$ / kg m^{-3}	$\langle$V$\rangle$ / nm^3
0	0	8562	1002.6	264.0
1	149	7574	1005.8	252.2
2	298	6989	1009.9	252.3
3	447	6413	1015.2	252.3

1.1.1.2 Umbrella sampling

Umbrella sampling simulations were performed to obtain the potential of mean force (PMF) between two polyalanine helices and thereby get the free energy of association of two helices. Starting configurations for the umbrella sampling simulations were created by using pulling simulations with the setting of the NPT equilibration mentioned above. The polypeptides were both oriented along the z-axis and were pulled apart in the x-y-direction using an umbrella potential (k =10^3 kJ mol^{-1} nm^{-2}). Umbrella windows ranged from 0.65 to 2.00 nm for the van der Waals solutes. The windows were created in steps of 0.05 nm with an additional point at 0.925 nm for all simulations and at 0.825, 0.84 and 0.94 nm ($k = 6 \cdot 10^3$ kJ mol^{-1} nm^{-2}) for the high pressure simulations and 1.00 nm ($k = 6 \cdot 10^3$ kJ mol^{-1} nm^{-2}) for better sampling. Each umbrella window was again equilibrated in a constant pressure-temperature simulation for 1 ns (k =$5 \cdot 10^3$ kJ mol^{-1} nm^{-2}). The production runs were performed for 90 ns (k =10^4 kJ mol^{-1} nm^{-2}, $k = 6{\cdot}10^4$ kJ mol^{-1} nm^{-2} at 0.825, 0.84, 0.94 and 1.00 nm) using the settings described above. The last 85 ns were used for analysis and the PMF was calculated using the weighted histogram analysis method (WHAM).[13] Compared to our study using FEP,[14] positional restraints of the solute atoms were not necessary. High-pressure simulations were performed using the high-pressure FF as well as the low-dipole FF at a simulation pressure of 2000 bar. The free energy of association $w(r_{\min})$ was obtained from the PMF at the distance, $r_{\min}$, of the first minimum.

1.2 Potentials of Mean Force

Fig. 6.4 shows the PMFs as a function of helix distance for different TMAO concentrations at 1 bar (a) and 2000 bar ((b) and (c)). The data in (c) were obtained from simulations performed using the low-dipole FF. The first minimum of the PMF (at around 0.775 nm) was taken as $w(r_{\min})$ to analyze the influence of TMAO on the free energy of helix association.

1.1.2.1 Free energy calculations

The free energy perturbation (FEP) and thermodynamic integration (TI) methods were used to calculate the solvation free energy, ΔG, of a polyalanine α-helix at 1 and 2000 bar. A stochastic

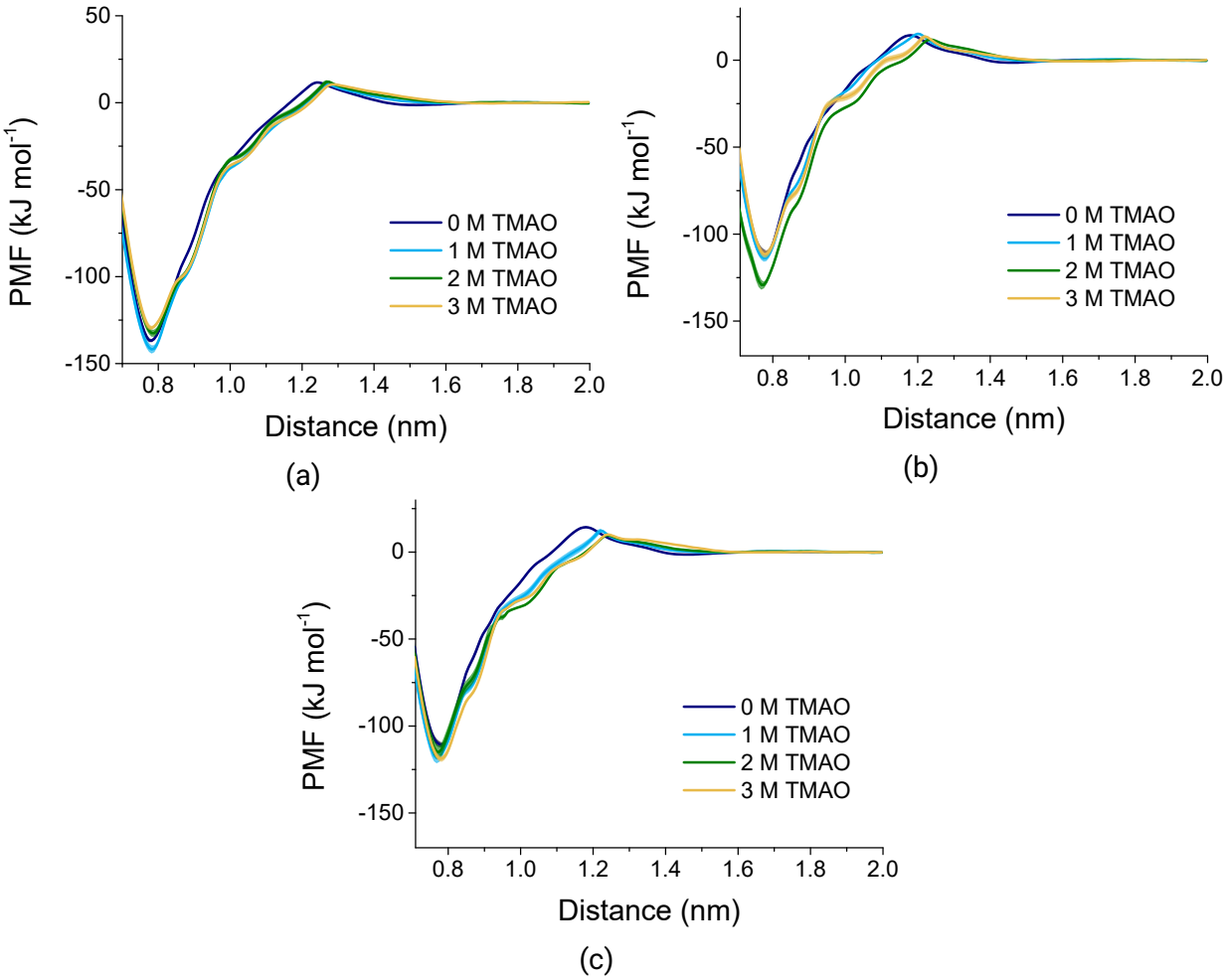

Figure 6.4: (a) PMF of the association of nonpolar helices as a function of distance at different TMAO concentrations at 1 bar. (b) PMF of the association of nonpolar helices as a function of distance at different TMAO concentrations at 2000 bar using the high-dipole FF. (c) PMF of the association of nonpolar helices as a function of distance at different TMAO concentrations at 2000 bar using the low-dipole FF.

dynamics integrator was used in all FEP simulations. The λ-coupling parameter values are summarized in the following subsection. A soft-core potential with soft-core parameters $\alpha = 0.5$, p = 1 and $\sigma = 0.28$ nm was used to avoid singularities at the (uncoupled) end state in the TI calculations.[15] The BAR algorithm was used to analyze the FEP calculations.[16,17] We report the FEP data and refer to our previous calculations[14] to see the agreement between FEP and TI calculations. The preferential binding coefficient, Γ_{23}, was retrieved from the data using an approach described below.

The λ coupling parameters used in the solvation free-energy calculations are:

1 bar

0 M (56 parameters)

Table 6.2: System details for the FEP calculations including a single helix: TMAO concentrations, number of (No.) water and TMAO molecules, average density (300 K, 1 bar) and box volume.

TMAO conc. / M	No. TMAO	No. water	$\langle\rho\rangle$ / kg m^{-3}	$\langle$V$\rangle$ / nm^3
0	0	4408	994.02	136.94
1	81	4128	997.26	138.22
2	163	3809	1001.47	138.32
3	244	3495	1006.51	138.34

λ_{vdW} = 0.000 0.050 0.100 0.150 0.200 0.250 0.300 0.350 0.400 0.450 0.475 0.500 0.525 0.550 0.575 0.600 0.625 0.650 0.670 0.690 0.700 0.710 0.720 0.730 0.740 0.750 0.760 0.765 0.770 0.775 0.778 0.780 0.782 0.784 0.786 0.788 0.790 0.795 0.800 0.805 0.810 0.820 0.830 0.840 0.850 0.860 0.870 0.880 0.890 0.900 0.910 0.925 0.940 0.950 0.970 1.000

1 M (57 parameters)

λ_{vdW} = 0.000 0.050 0.100 0.150 0.200 0.250 0.300 0.350 0.400 0.450 0.475 0.500 0.525 0.550 0.575 0.600 0.625 0.650 0.670 0.690 0.700 0.710 0.720 0.730 0.740 0.750 0.760 0.765 0.770 0.773 0.775 0.778 0.780 0.783 0.787 0.790 0.793 0.797 0.800 0.803 0.807 0.810 0.815 0.820 0.830 0.840 0.850 0.860 0.870 0.880 0.890 0.900 0.910 0.925 0.940 0.950 0.970 1.000

2 M (57 parameters)

λ_{vdW} = 0.000 0.050 0.100 0.150 0.200 0.250 0.300 0.350 0.400 0.450 0.475 0.500 0.525 0.550 0.575 0.600 0.625 0.650 0.670 0.690 0.700 0.710 0.720 0.730 0.740 0.750 0.760 0.765 0.770 0.775 0.780 0.782 0.784 0.786 0.788 0.790 0.800 0.810 0.813 0.817 0.820 0.825 0.830 0.840 0.850 0.860 0.870 0.880 0.890 0.900 0.910 0.925 0.940 0.950 0.960 0.970 0.980 1.000

3 M (54 parameters)

λ_{vdW} = 0.000 0.050 0.100 0.150 0.200 0.250 0.300 0.350 0.400 0.450 0.475 0.500 0.525 0.550 0.575 0.600 0.625 0.650 0.670 0.690 0.700 0.710 0.720 0.730 0.740 0.750 0.760 0.765 0.770 0.775 0.780 0.790 0.800 0.805 0.810 0.813 0.817 0.820 0.825 0.830 0.840 0.850 0.860 0.870 0.880 0.890 0.900 0.910 0.925 0.940 0.950 0.960 0.970 0.980 1.000

2000 bar

λ_{vdW} = 0.000 0.050 0.100 0.150 0.200 0.225 0.250 0.275 0.300 0.325 0.350 0.375 0.400 0.425 0.450 0.475 0.500 0.525 0.550 0.565 0.580 0.590 0.600 0.615 0.630 0.650 0.660 0.670 0.680 0.685 0.690 0.695 0.700 0.705 0.710 0.715 0.720 0.723 0.727 0.730 0.740 0.750 0.758 0.765 0.770 0.775 0.780 0.790 0.800 0.808 0.815 0.830 0.840 0.850 0.858 0.865 0.873 0.880 0.890 0.900 0.908 0.915 0.924 0.930 0.940 0.950 0.965 0.980 1.000

The relative solvation free energies, $\Delta\Delta G(c_3) = \Delta G(c_3) - \Delta G(c_3 = 0)$, are reported in Fig. 6.5

Table 6.3: System details for the KBI calculations: TMAO concentrations, number of (No.) water and TMAO molecules.

TMAO conc. / M	No. TMAO	No. water
0.5	105	11121
1	211	10703
1.5	316	10289
2	422	9875
2.5	527	9469
3	632	9062

(a) as a function of c_3. It can be observed that $\Delta\Delta G < 0$, i.e. solvation of the nonpolar α-helix is aided by thermodynamically favorable TMAO-α-helix interactions. These interactions are weaker at high pressure where $|\Delta\Delta G|$ is smaller.

1.1.2.2 Calculation of Kirkwood-Buff Integrals

TMAO-TMAO (G_{33}) and TMAO-water (G_{31}) KBIs were calculated from binary solvent mixtures using settings described in the umbrella sampling section and in Tab 6.3. The production run was executed for 100 ns. The last 95 ns were used to calculate radial distribution functions (RDFs) and from those the KBIs, which were corrected using the Ganguly and Krüger correction.[18,19] Values are shown in Tab. 6.4.

1.3 Preferential binding coefficient

The preferential binding coefficient is defined as:

$$\Gamma_{23} = c_3(G_{23} - G_{21}), \tag{2}$$

in which c_3 is the molar TMAO concentration and G_{23} and G_{21} are the helix-TMAO and helix-water Kirkwood-Buff integrals, respectively. The cosolute preferentially binds to the solute if $\Gamma_{23} > 0$ and is depleted from the hydration shell of the solute if $\Gamma_{23} < 0$. In computer simulations, Γ_{23} is usually calculated using the expression[20]

$$\Gamma_{23}(r) = \left\langle n_3(r) - \frac{N_3 - n_3(r)}{N_1 - n_1(r)} n_1(r) \right\rangle, \tag{3}$$

where $n_3(r)$ and $n_1(r)$ are the numbers of cosolute and water molecules, respectively, in proximal distance r to the solute (2), and N_3 and N_1 are the total numbers of cosolute and water molecules in the system. The preferential binding coefficient is related to the solvation free energy, ΔG, of a

Table 6.4: Values used to calculate Γ_{23} from Eqn. 4

Pressure (bar)	TMAO Dipole FF	Slope (J L mol^{-2})	G_{33} (cm^{3}mol^{-1})	G_{31} (cm^{3}mol^{-1})
1	Low-Dipole	-19959 $\pm$ 496	-476	-65.5
2000	High-Dipole	-14134 $\pm$ 432	-454	-61.5
2000	Low-Dipole	-16303 $\pm$ 960	-431	-67.1

solute according to[21,22]

$$\left(\frac{\partial \Delta G}{\partial c_3}\right)_{p,T} = -\frac{RT\,\Gamma_{23}}{c_3\left[1 + c_3(G_{33} - G_{31})\right]} = -\frac{RT\,\Gamma_{23}\,a_{33}}{c_3} \tag{4}$$

The activity enhancement factor, $a_{33} = \left[1 + c_3(G_{33} - G_{31})\right]^{-1}$, is positive for stable solutions and is shown in Fig. 6.5 (b) as a function of the TMAO concentration for the low- and high-dipole FF at 1 bar and 2000 bar.

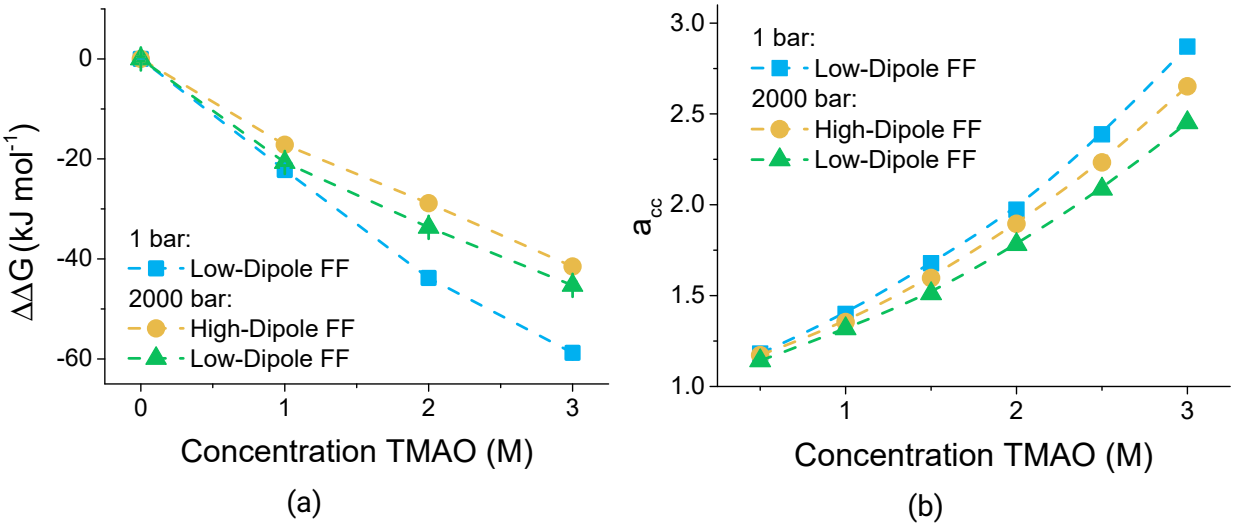

Figure 6.5: (a) Relative solvation free energy of a single non-polar helix (reference: pure water) (b) a_{33} plotted as a function of TMAO concentration for low and high pressure and different TMAO force fields.

Eq. 4 has been used in this work to determine Γ_{23} as it yields smaller error bars than the application of Eq. 3 due to the enhanced sampling provided by the free energy perturbation method. To this end, the solvation free energy of the single helix was fitted by a linear regression, fixing the intercept to 0 and using an instrumental weighting of the given values. Values for the slope, $\left(\partial \Delta G/\partial c_3\right)_{p,T}$, and the Kirkwood-Buff integrals G_{33} and G_{31} at 2 M TMAO concentration are summarized in Tab. 6.4.

Bibliography

[1] Sorin, E. J.; Pande, V. S. Exploring the helix-coil transition via all-atom equilibrium ensemble simulations. *Biophys. J.* **2005**, *88*, 2472–2493.

[2] Hölzl, C.; Kibies, P.; Imoto, S.; Frach, R.; Suladze, S.; Winter, R.; Marx, D.; Horinek, D.; Kast, S. M. Design principles for high-pressure force fields: Aqueous TMAO solutions from ambient to kilobar pressures. *J. Chem. Phys.* **2016**, *144*, 1–4.

[3] Abascal, J. L. F.; Vega, C. A general purpose model for the condensed phases of water: TIP4P/2005. *J. Chem. Phys.* **2005**, *123*, 234505.

[4] Markthaler, D.; Zeman, J.; Baz, J.; Smiatek, J.; Hansen, N. Validation of Trimethylamine-N-oxide (TMAO) Force Fields Based on Thermophysical Properties of Aqueous TMAO Solutions. *J. Phys. Chem. B* **2017**, *121*, 10674–10688.

[5] Shen, Y.; Maupetit, J.; Derreumaux, P.; Tufféry, P. Improved PEP-FOLD Approach for Peptide and Miniprotein Structure Prediction. *J. Chem. Theory Comput.* **2014**, *10*, 4745–4758.

[6] Berendsen, H. J.; van der Spoel, D.; van Drunen, R. GROMACS: A message-passing parallel molecular dynamics implementation. *Comput. Phys. Commun.* **1995**, *91*, 43–56.

[7] Abraham, M. J.; Murtola, T.; Schulz, R.; Páll, S.; Smith, J. C.; Hess, B.; Lindah, E. Gromacs: High performance molecular simulations through multi-level parallelism from laptops to supercomputers. *SoftwareX* **2015**, *1-2*, 19–25.

[8] Hess, B. P-LINCS: A parallel linear constraint solver for molecular simulation. *J. Chem. Theory Comput.* **2008**, *4*, 116–122.

[9] Darden, T.; York, D.; Pedersen, L. Particle mesh Ewald: An N·log(N) method for Ewald sums in large systems. *J. Chem. Phys.* **1993**, *98*, 10089–10092.

[10] Berendsen, H. J.; Postma, J. P.; Van Gunsteren, W. F.; DiNola, A.; Haak, J. R. Molecular dynamics with coupling to an external bath. *J. Chem. Phys.* **1984**, *81*, 3684–3690.

[11] Nosé, S. A molecular dynamics method for simulations in the canonical ensemble. *Mol. Phys.* **1984**, *52*, 255–268.

[12] Parrinello, M.; Rahman, A. Polymorphic transitions in single crystals: A new molecular dynamics method. *J. Appl. Phys.* **1981**, *52*, 7182–7190.

[13] Kumar, S.; Rosenberg, J. M.; Bouzida, D.; Swendsen, R. H.; Kollman, P. A. THE weighted histogram analysis method for free-energy calculations on biomolecules. I. The method. *J. Comput. Chem.* **1992**, *13*, 1011–1021.

[14] Folberth, A.; Bharadwaj, S.; van der Vegt, N. F. Small-to-large length scale transition of TMAO interaction with hydrophobic solutes. *Phys. Chem. Chem. Phys.* **2022**, *24*, 2080–2087.

[15] Pham, T. T.; Shirts, M. R. Identifying low variance pathways for free energy calculations of molecular transformations in solution phase. *J. Chem. Phys.* **2011**, *135*, 034114.

[16] Bennett, C. H. Efficient estimation of free energy differences from Monte Carlo data. *J. Comput. Phys.* **1976**, *22*, 245–268.

[17] Shirts, M. R.; Chodera, J. D. Statistically optimal analysis of samples from multiple equilibrium states. *J. Chem. Phys.* **2008**, *129*, 124105.

[18] Krüger, P.; Schnell, S. K.; Bedeaux, D.; Kjelstrup, S.; Vlugt, T. J. H.; Simon, J.-M. Kirkwood–Buff Integrals for Finite Volumes. *J. Phys. Chem. Lett.* **2013**, *4*, 235–238.

[19] Ganguly, P.; van der Vegt, N. F. A. Convergence of Sampling Kirkwood–Buff Integrals of Aqueous Solutions with Molecular Dynamics Simulations. *J. Chem. Theory Comput.* **2013**, *9*, 1347–1355.

[20] Pierce, V.; Kang, M.; Aburi, M.; Weerasinghe, S.; Smith, P. E. Recent Applications of Kirkwood–Buff Theory to Biological Systems. *Cell Biochem. Biophys.* **2008**, *50*, 1–22.

[21] Wyman, J. Linked Functions and Reciprocal Effects in Hemoglobin: A Second Look. *Adv. Prot. Chem.* **1964**, *19*, 223 – 286.

[22] Tanford, C. Extension of the theory of linked functions to incorporate the effects of protein hydration. *J. Mol. Biol.* **1969**, *39*, 539–544.

7 Influence of TMAO and Pressure on the Folding Equilibrium of TrpCage

Abstract

Trimethylamine-N-oxide (TMAO) is an osmolyte known for its ability to counteract pressure denaturation of proteins. Computational studies addressing molecular mechanisms of TMAOs osmolyte action have however focused exclusively on its protein-stabilizing properties at ambient pressure, neglecting changes that may occur under high-pressure conditions where TMAOs hydration structure changes to that of increased water binding. Here, we present the first study on the combined effect of pressure and TMAO on a miniprotein, TrpCage. The results showed that pressure destabilized the hydrophobic core and the salt bridge of TrpCage. This effect was mitigated by TMAO which was found to be stronger depleted from the protein-water interface at 1 kbar than at 1 bar ambient pressure, thus counterbalancing the thermodynamically unfavorable effect of elevated pressure in the free energy of folding. TMAO was depleted from charged groups, like the salt bridge forming ones, and accumulated around hydrophobic groups. Still, it stabilized both kinds of interactions. Furthermore, enthalpically favorable TrpCage-water hydrogen bonds were reduced in the presence of TMAO, causing a stronger destabilization of the unfolded state than the folded state. This shifted the protein folding equilibrium towards the folded state. Therefore, TMAO showed stabilizing effects on different kinds of groups, which were partially enhanced at high pressure.

1 Introduction

Cellular proteins and biomolecular condensates formed by liquid-liquid phase separation (LLPS) are both crucial in the functioning of the living cell. Their structure however loses stability in high-pressure environments such as the ocean floor. Deep sea creatures have adapted to these environments as their cells contain small organic molecules (osmolytes) such as TMAO that counterbalance the disruptive effects of hydrostatic pressure and osmotic stress.[1–3] Experimentally, it has been found that TMAO counteracts pressure denaturation and prevents the pressure-induced dissolution of LLPS domains.[4–6] The commonly assumed thermodynamic mechanism is based on data obtained with osmometry and dialysis experiments: TMAO is depleted from the protein surface and thereby enhances protein-protein interactions and stabilizes their native structure.[7–10] Recently, this view has been challenged and more detailed microscopic mechanisms have been ex-

amined based on computer simulations. This has led to new insights in the TMAO stabilization mechanism, including the role of different protein functional groups and preferential binding effects of TMAO, hydrophobic interactions, and protein-water hydrogen bonding.

Several recent studies have reported that, as opposed to depletion, preferential binding of TMAO can stabilize the protein folded state, drive hydrophobic polymer collapse, and enhance hydrophobic interactions.[11–14] That preferential TMAO binding can lead to the stabilization of the protein folded state has also been observed based on molecular dynamics (MD) simulations of the mini-protein TrpCage, where preferential TMAO binding to the folded state was found to be stronger than to the unfolded state.[14] It has furthermore been reported that TMAO stabilizes the formation of salt bridges. An indication for this is that TMAO stabilizes the NaCl contact pair in water and can counteract the screening effect of salt on electrostatic interactions.[15,16] The salt bridge of the mini-protein TrpCage has been found to be more stable in solutions with TMAO than in neat water.[17,18] However, of the three salt bridges in the R2 peptides one is stabilized and two are destabilized by TMAO.[19] In addition to these effects on salt bridges, experiments and simulations have provided indications that TMAO shifts the folding equilibrium of proteins to the folded state by reducing the hydrogen bonding ability of water to the unfolded state.[20,21]

As an important driving force for protein folding, hydrophobic interactions may be influenced by TMAO. However, there is no consensus as to whether TMAO strengthens or weakens hydrophobic interactions.[11,13,17,22,23] TMAO adsorbs to hydrophobic surfaces, leading to reduced protein adsorption driven by hydrophobic interactions.[24] Weakening of hydrophobic interactions has also been shown with the mini-protein TrpCage,[17] while another study showed the stabilization of TrpCage through net preferential binding of TMAO caused by TMAO interactions with hydrophobic groups.[14] It has also been found that TMAO has a negligible influence on hydrophobic interactions of small molecules and model hydrophobic molecules,[22,23] while another study reported a strengthening effect.[25] It has been furthermore demonstrated that the effect of TMAO on hydrophobic interactions is often non-monotonic, strengthening them at low TMAO concentrations, while weakening them at high TMAO concentrations.[12,26] This has also been observed experimentally with the protein stem bromelain.[27]

All of the above studies have been conducted at ambient pressure and therefore it is not obvious how TMAO counteracts pressure denaturation. How far the reported observations depend on the force fields used in the simulations furthermore remains incompletely understood. Recent work has provided indications that agreement between predictions based on MD simulations and experimentally probed melting temperatures of TrpCage in TMAO/water solutions at 1 bar ambient pressure can only be achieved under the condition of TMAO depletion.[28] This is confirmed by the work we report below.

There exist several TMAO force fields that can be used to describe TMAO/water solutions.[29–34] The TMAO model by Hölzl et al. has been shown to be superior in the description of binary solvent properties.[33,34] This model has been parameterized at ambient pressure and then adjusted to

represent high-pressure properties correctly. Charge redistribution upon compression at high pressure leads to an increased dipole moment of TMAO and an increase in the number of TMAO-water hydrogen bonds, which is captured in the model by pressure-dependent partial charges.[34–36] Moreover, the Hölzl TMAO force field is combined with the TIP4P/2005 water model, which is excellent in representing the water phase diagram, also at high pressure.[37]

Here, we analyze the combined effect of TMAO and pressure on the folding equilibrium of a miniprotein: TrpCage (PDB: 1L2Y). TrpCage is a small protein with fast folding dynamics. Therefore, it is commonly used as a model system. We examine how TMAO affects the hydrophobic core and salt bridge, the most common features present in TrpCage, and whether high-pressure conditions counteract or reinforce these effects, e.g. due to changes in preferential binding.

2 Methods

2.1 Molecular Dynamics simulation details

The TrpCage sequence (Ac-NLYIQWLKDGGPSSGRPPPS-NME) was generated from the pdb structure (PDB:1L2Y) using GROMACS. N- and C- termini were capped with methyl groups, resulting in a peptide consisting of 313 atoms. TrpCage was solvated in water (4002 molecules) and a 2 M TMAO mixture (146 TMAO molecules and 3425 water molecules). The Amber03w protein force field[38] was used combined with the TIP4P/2005 model for water[37] and the Hölzl model for TMAO.[34]

All simulations were performed with the GROMACS package version 2019.4.[39,40] All bonds involving a hydrogen atom were constrained using the LINCS algorithm[41]. Coulomb interactions were described using the particle mesh Ewald (PME) method[42] with a real-space cut off of 1 nm, a PME order of 4 and a grid spacing of 0.12 nm. Long range dispersion corrections were applied to the pressure and energy and the van der Waals cut-off was set to 1 nm. Reruns to calculate the electrostatic solute-solvent energies were conducted using the reaction-field method. The neighbour list was updated every ten time steps.

The system was energy minimized using the steepest descent algorithm with 50000 steps and a step size of 0.001 nm. Replica exchange MD simulations were performed using 50 temperature windows generated at 280, 283.0, 286.1, 289.2, 292.3, 295.5, 298.7, 301.9, 305.1, 308.4, 311.6, 314.9, 318.3, 321.6, 325.0, 328.5, 331.9, 335.4, 338.9, 342.4, 346.0, 349.6, 353.3, 356.9, 360.6, 364.3, 368.1, 371.9, 375.7, 379.5, 383.4, 387.3, 391.3, 395.3, 399.3, 403.3, 407.4, 411.5, 415.7, 419.8, 424.1, 428.4, 432.7, 437.0, 441.4, 445.8, 450.2, 454.7, 459.2 and 460.0 K which were equilibrated in a constant volume-temperature simulation using the Berendsen thermostat (τ_T=1.0 ps) for 5 ns[43]. Subsequently, a constant pressure-temperature simulation using the Berendsen barostat (τ_P=2.0 ps, $\kappa_T = 5 \cdot 10^{-5}$ bar^{-1}) was performed for 5 ns. Production runs with a sampling time of 1 μs were then carried out using the Nose-Hoover thermostat[44] (τ_T=1.0 ps) and

the Parrinello-Rahman barostat at 1, 500, 1000 and 2000 bar (τ_P=2.0 ps)[45] with a compressibility of $5 \cdot 10^{-5}$ bar^{-1}, discarding the first 400 ns for equilibration. The exchange probability ranged from 20 and 25% (not taking the last, very close pair into account) with exchange attempts every 750 steps.

The RMSD (root-mean-square deviation) was used to calculate the fraction folded x_F by comparing the TrpCage structure to the pdb structure. Structures with a RMSD smaller than 0.22 nm were considered folded.[17,46,47] The free energy of folding was then calculated from the equilibrium folding fraction using $\Delta G^{U\to F} = -RT \ln(x_F/(1-x_F))$. The salt bridge distance was calculated between the center of mass (COM) of the carboxyl group of the aspartic acid residue (D9) and the COM of the guanidinium group of the arginine residue (R16). The radius of gyration R_g of the hydrophobic groups was calculated by taking into account 2LEU (L), 4ILE (I), 6TRP (W), 7LEU (L), 12PRO (P), 17PRO (P), 18PRO (P) and 19PRO (P) residues.

3 Results

We have studied the folding equilibrium of TrpCage in pure water and in a 2 M TMAO mixture, at 1, 500, 1000 and 2000 bar pressure using REMD with 50 temperature windows between 280 and 460 K. Below, we mostly show data obtained at 1000 bar because the protein was mostly denatured at this pressure. Data for other pressure values can be found in the SI.

3.1 Comparison with experiment

We have used a capped TrpCage molecule for our study. Experimental TrpCage melting temperatures were obtained for the uncapped protein.[30,48] However, the end groups should have only marginal effects compared to the backbone and side chains. We calculated the melting temperature of TrpCage from the simulation data by determining the temperature at which the free energy of folding $\Delta G^{U\to F} = 0$ ($x_F = 0.5$). Our simulations predicted the melting temperature in pure water at ambient pressure to be 327 K, based on the fraction folded shown in Fig. 7.1 (a) (experimental melting temperature without capped end groups: 317 K).[48] The data obtained for 1 bar ambient pressure shown in Fig. 7.1 (b) indicate that the melting temperature increased with 4 K (experiment: 3 K $\pm$ 2 K)[30] in the solution with 2 M TMAO. Therefore, TMAO stabilized the protein folded state and the computed melting temperature matched the experimental value. However, the folding equilibrium followed a non-monotonic dependence on pressure, as shown in Fig. 7.1 (b), indicating that several intermediate folded states with different volumes were visited as the pressure was increased. We consider the 1000 bar data for our following analysis as the protein clearly denatured at this pressure. The data indicate that TMAO counteracted pressure denaturation at 1000 bar and stabilized the folded TrpCage structure even further than at 1 bar (no experimental comparison available). Furthermore, it can be observed in Fig. 7.1 (a) that the net effect of TMAO

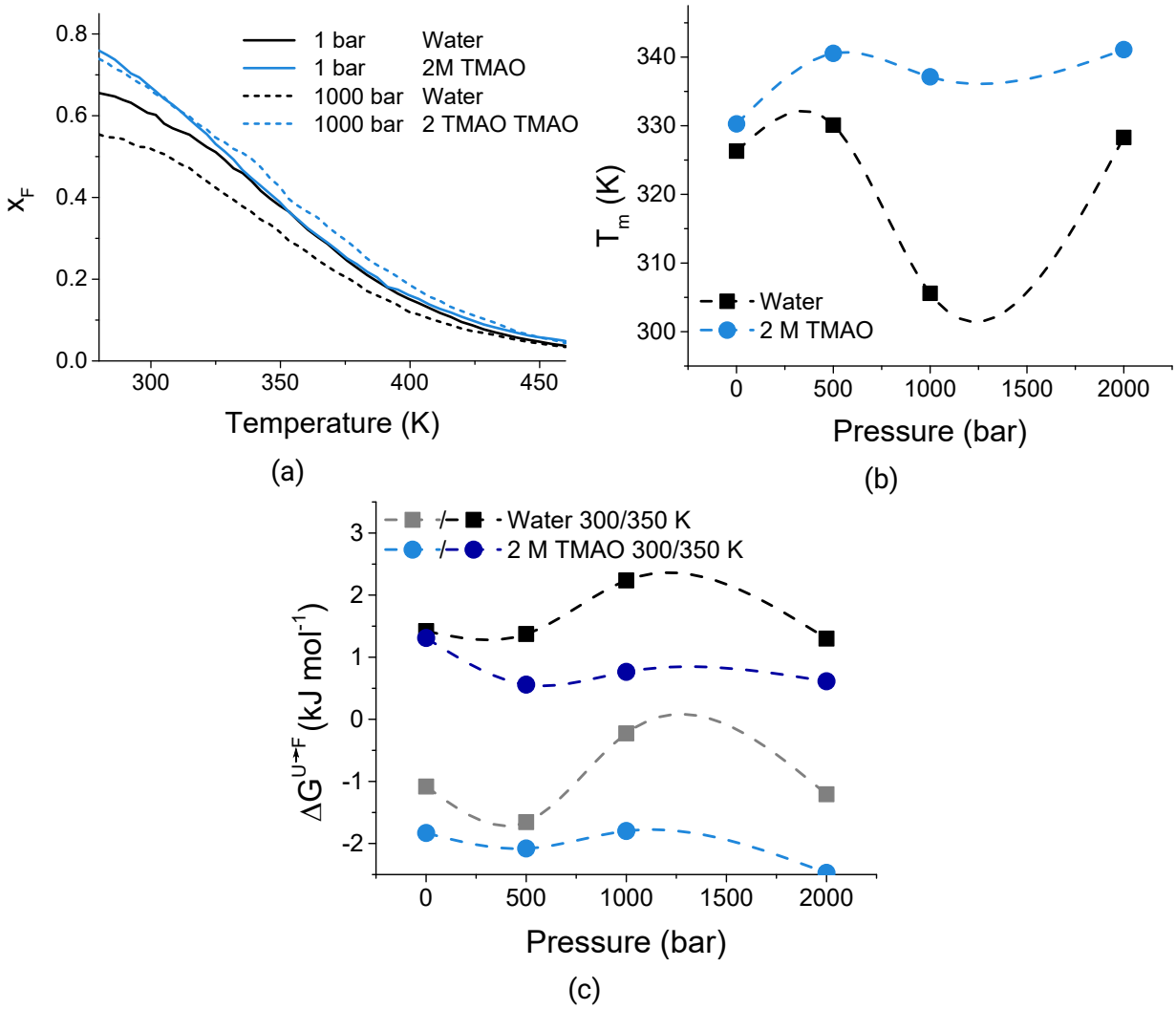

Figure 7.1: a) Fraction folded for the TrpCage molecule in water and 2 M TMAO at 1 and 1000 bar (see Fig. S1 of the SI for other pressure values) (b) Dependence of the melting temperature of TrpCage on pressure. (c) Free energy of folding of TrpCage in water and 2 M TMAO at 300 and 350 K as a function of pressure. Pressure at 1000 bar decreases the fraction folded in water, but increases it in TMAO. TMAO shows a stabilizing effect at both ambient and high pressure. The free energy of folding shows a non-monotonic effect with pressure. Dashed lines are used to guide the eye.

on the fraction folded was larger at increased pressure at all temperatures, i.e. TMAO exerted a larger stabilizing effect at high pressure than at ambient pressure. In general, TMAO lowered the free energy of folding at all temperatures and pressures, shown for two examples (300 K and 350 K) in Fig. 7.1 (c), indicating a stabilizing TMAO effect across the whole pressure-temperature plane (see SI, Fig. S1). To understand the TMAO stabilization mechanism, we investigated the preferential binding of TMAO to TrpCage, and the pressure effect on it, as previous studies have shown contradicting results.

3.2 Preferential Binding

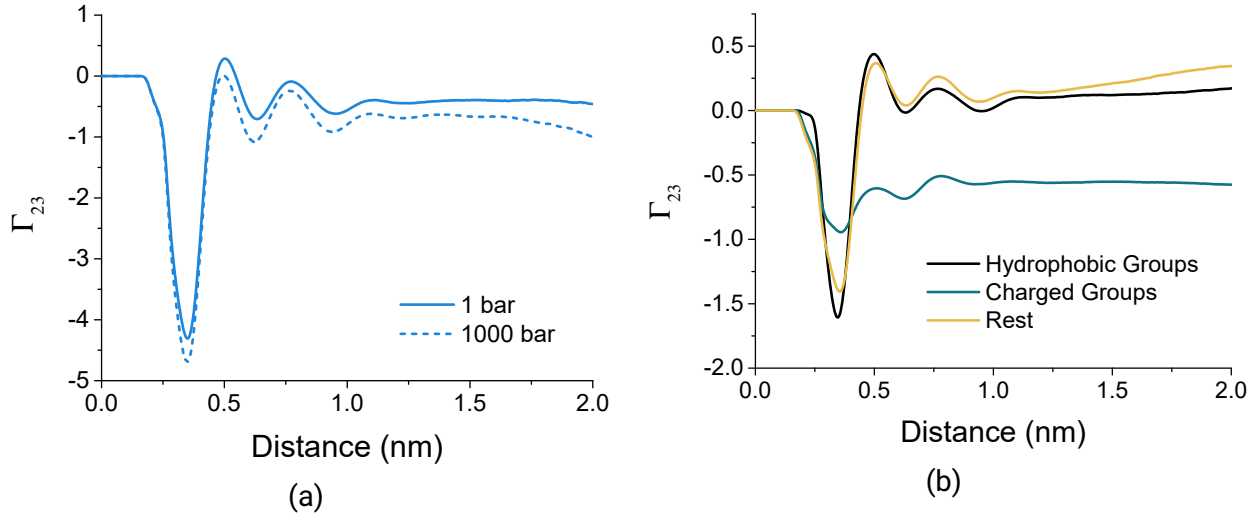

Figure 7.2: Preferential binding coefficient Γ_{23} of TMAO to (a) the whole TrpCage molecule and (b) to the hydrophobic (2L, 4I, 6W, 7L, 12P, 17P, 18P, 19P), charged (8K, D9, R16) and other residues at 1 bar pressure. The negative value of the total preferential binding coefficient in (a) implies TMAO depletion. The depletion increases at high pressure (see Fig. S2 for other pressure values).

The preferential binding coefficient of TMAO to proteins is usually negative, indicating net depletion of TMAO.[7,8,10,49] This measurement is not available for TrpCage, but the preferential binding coefficient is commonly assumed to be negative for this mini-protein as well.[30] The distance-dependent preferential binding coefficient of TMAO obtained from our simulations is shown in Fig. 7.2(a). It shows that TMAO was depleted for most distances, corroborating earlier work.[30] Moreover, the net depletion of TMAO from the protein/water interface was larger at 1000 bar (see Fig. S2 of the SI for pressure values other than 1000 bar). This may be caused by the higher dipole moment of TMAO at higher pressure, leading to enhanced TMAO-water binding.[35] To gain further insight, we decomposed the preferential binding coefficient in Fig. 7.2 (b) by considering only the TMAO and water molecules in proximal distance to hydrophobic, charged and other groups (labelled Rest in Fig. 7.2 (b)) on the protein.[21] This analysis showed that the negative preferential binding coefficient was mostly caused by unfavorable interactions of TMAO with the

charged groups, as was also observed with a penta-peptide in a previous study.[21] It also indicated that charged end groups would further lower the preferential binding coefficient. As expected, the preferential binding coefficient to hydrophobic groups was positive, indicating that TMAO accumulated around the hydrophobic protein groups. Interestingly, TMAO also accumulated ($\Gamma_{23} > 0$) around the rest of the protein, including mostly polar serine and glycine groups. This is unexpected, because the contribution of the backbone (which is the largest in case of glycine) to the preferential binding coefficient is negative according to the transfer model.[50] The observed differences in preferential binding suggests that TMAO may affect distinct protein groups differently. Therefore, we further examined the impact of TMAO on hydrophobic interactions, the formation of salt bridges and protein-solvent hydrogen bonds.

3.3 Hydrophobic interactions, salt bridges and hydrogen bonds

To understand which protein interactions were stabilized or destabilized by TMAO, we considered effects on the salt bridge, the hydrophobic core and protein-solvent hydrogen bonds. Fig. 7.3 (a)

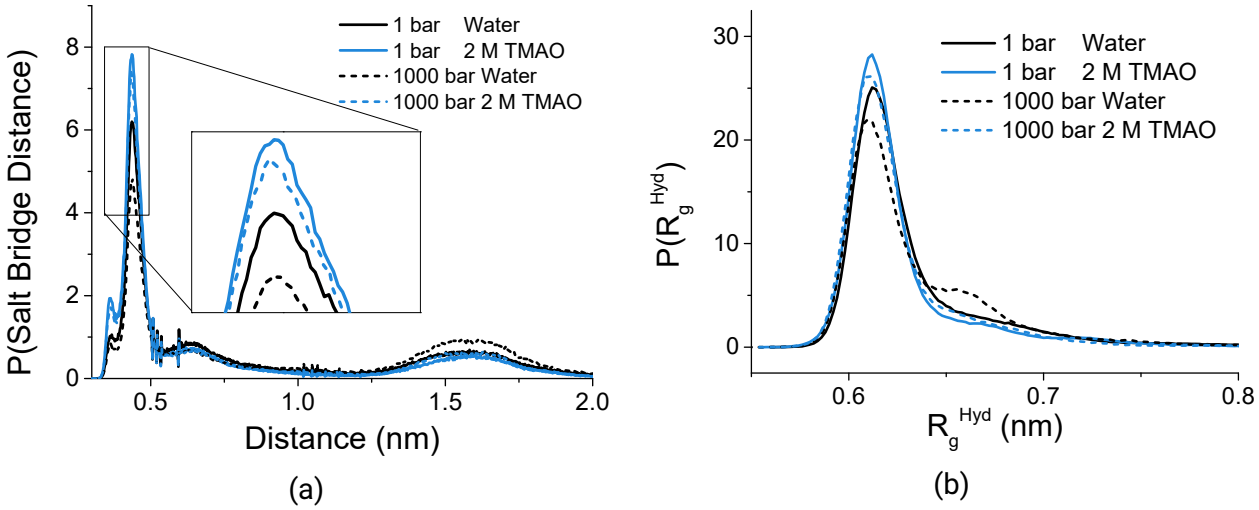

Figure 7.3: (a) Histograms of the salt bridge distance (COM of the carboxyl group of D9 and COM of the guanidinium group of R16) and (b) radius of gyration of the hydrophobic groups of TrpCage. TMAO enhances the probability of salt bridge formation, but pressure lowers it. The compactness of the hydrophobic core shown in (b) is increased in 2 M TMAO. It is decreased due to pressure, but TMAO enhances hydrophobic interactions in a way to compensate for the pressure effect (see Fig. S3 for other pressure values).

shows the histograms of the salt bridge distances at 1 bar and 1000 bar in pure water and 2 M TMAO solution. The probability of salt bridge formation (distance < 0.5 nm) was larger in 2 TMAO solution than in pure water and larger at 1 bar than at 1000 bar. The net TMAO effect was however larger at high pressure, leading to a higher probability of salt bridge formation at high pressure in the system with TMAO than at ambient pressure in water. The compactness of the hydrophobic core, shown in Fig. 7.3 (b) in terms of the radius of gyration of hydrophobic groups, was reduced

by pressure, but increased by TMAO to an extent that 2 M TMAO counteracted the denaturing pressure effect completely. Therefore, although TMAO was preferentially bound to the hydrophobic groups of TrpCage, it enhanced the hydrophobic interactions contributing to stabilizing the folded structure.

Finally, we have calculated the protein-solvent solvation energy (i.e. the average overall van der Waals plus electrostatic energy due to interactions between the protein and the components of the solvent) and the number of hydrogen bonds of TrpCage with TMAO and water. TMAO reduced the protein-solvent solvation energy due to reduced hydrogen bonding of TrpCage with the solvent (Fig. 7.4 (a) and (b)), similar to previously reported observations made for a penta-peptide.[21] Note that in the unfolded state the protein lost more hydrogen bonds with the solvent than in the folded state when TMAO was introduced. Fig. 7.4 (c) shows the change in the number of hydrogen bonds upon folding as a function of TMAO concentration. In the absence of TMAO, the folding of TrpCage led to a loss of around 4 solute-solvent hydrogen bonds. This number increased at high pressure due to a tighter packing of water. Interestingly, the loss of hydrogen bonds upon folding was reduced in the presence of TMAO. This effect is slightly decreased at high pressure. Fig. 7.4 (b) shows the average protein-solvent energies at 1 bar and 1000 bar in pure water and in a 2 M TMAO solution. The presence of TMAO led to a reduction of, both, favorable van der Waals and electrostatic protein-solvent interaction energies. The unfavorable change of protein-solvent energy upon folding shown in Fig. 7.4 (d) was dominated by electrostatic interactions but mitigated by TMAO. This mitigating effect was however slightly weaker at high pressure and therefore does not explain the enhanced stabilizing TMAO effect observed at high pressure in the free energy of folding (7.1 (c)). In summary, we observed that TMAO stabilized the protein folded state at all temperatures and pressures considered. TMAOs direct contribution to stabilizing the folded state of TrpCage occurred through reinforcing protein-internal hydrophobic and electrostatic interactions, while its indirect contribution to stabilizing the folded state of TrpCage occurred through decreasing the hydrogen bonding ability of water to the unfolded state.

4 Conclusions

We have investigated the collective effect of pressure and TMAO concentration on the folding equilibrium of TrpCage using replica exchange molecular dynamics simulations. This is, to the best of our knowledge, the first study that provides molecular interpretations to the effect of both pressure and TMAO concentration on the folding equilibrium of a protein. We observed that TMAO counteracted pressure denaturation and stabilized the folded state of the protein across the whole pressure-temperature space. This has previously only been studied with small hydrophobic molecules using a different TMAO model, where TMAO did not show any effect.[23,51] We observed that TMAO was net depleted from the protein surface, an effect that became stronger at high pressures, mainly due to the unfavorable interactions of TMAO with charged groups as previously observed using penta-

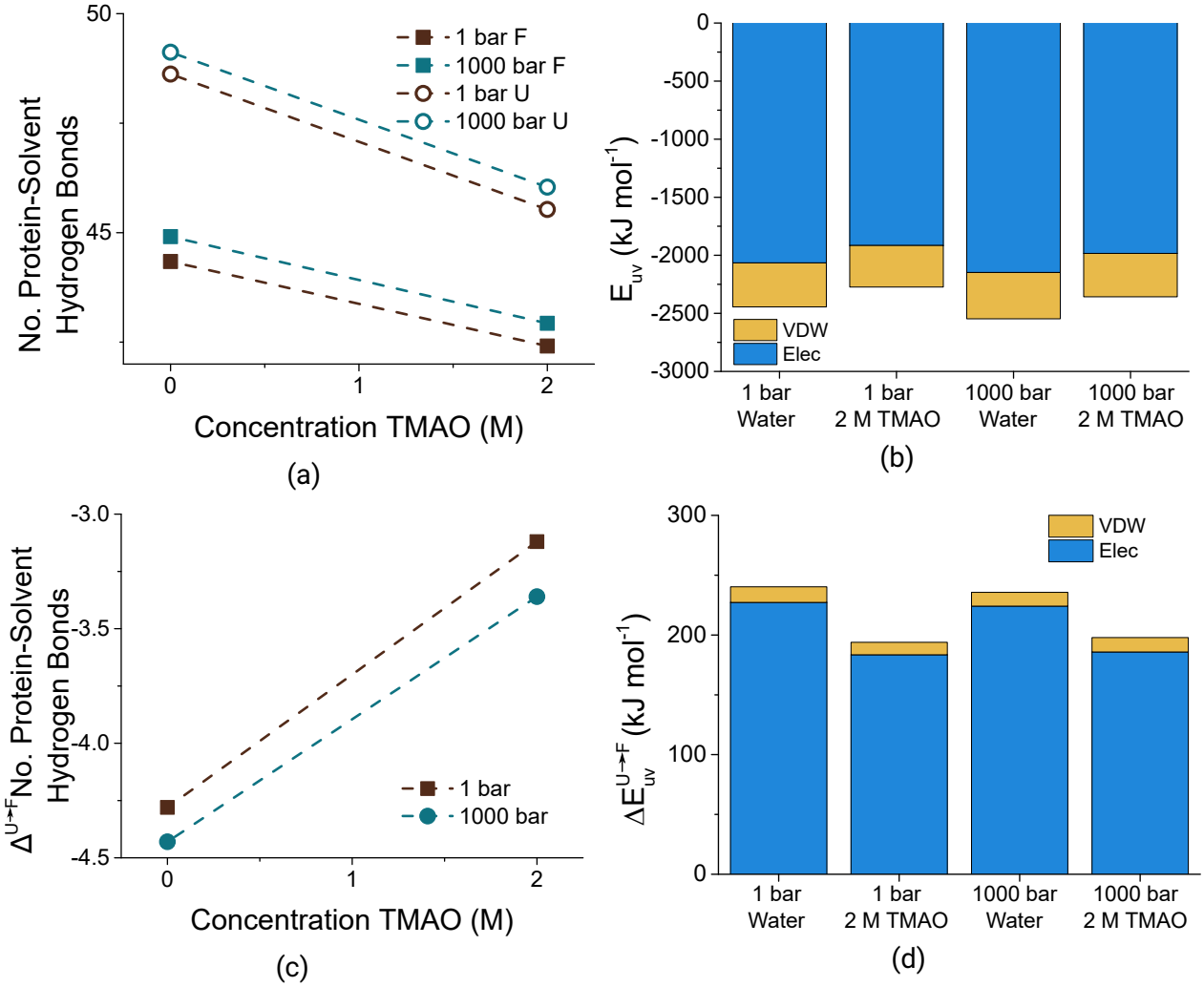

Figure 7.4: (a) Number of protein-solvent hydrogen bonds for the unfolded (U) and folded (F) state (b) Average protein-solvent energy of TrpCage at different TMAO concentrations and pressures. (c) The change of the number of protein-solvent hydrogen bonds upon folding in water and 2 M TMAO at 1 and 1000 bar. (d) The difference in protein-solvent energy upon folding at different TMAO concentrations and pressure. TMAO reduces he protein-solvent energy of TrpCage as seen in (b) and thereby stabilizes the folded state by reducing the unfavorable change upon folding as shown in (d). The change of electrostatic interactions can mainly be attributed by the reduced loss of protein-solvent hydrogen bonds in the TMAO mixture. See Fig. S4 for other pressure values.

peptides.[21] TMAO stabilized the formation of the salt bridge and the extent of this was enhanced at high pressure. This effect has also been reported by Su et al. at ambient pressure, where they suggested that it is the main driving force of protein stabilization in TMAO mixtures.[17] Even though TMAO interacted with hydrophobic groups of the protein, it stabilized its hydrophobic core. This unexpected observation is linked to the previously reported bulk-interface partitioning equilibrium of TMAO that entropically favors the folded state with the smaller hydrophobic solvent-accessible surface area and the smaller number of TMAO molecules adsorbed.[12] The effects of TMAO at high pressure were similar to those at ambient pressure. Furthermore, TMAO reduced the unfavorable increase in protein-solvent energy upon folding as it reduced the number of protein-solvent hydrogen bonds. The reduction in protein-solvent hydrogen bonding was larger for the unfolded state whose solvent-accessible surface area is larger, leading to protein folding.

In summary, we observed a stabilizing effect of TMAO on several interactions relevant for protein folding. At high pressure, some of these interactions were enhanced and correlated with enhanced TMAO depletion. Therefore, the stabilizing effect of TMAO can be manifold, which makes it such a good osmolyte to counteract pressure and even temperature effects.

Acknowledgement

The authors thank Dr. Madhusmita Tripathy and Dr. Pritam Ganguly for fruitful discussions. MD simulations were performed on the Lichtenberg HighPerformance Computer of the Technische Universität Darmstadt, Germany.

Bibliography

[1] Yancey, P. H.; Gerringer, M. E.; Drazen, J. C.; Rowden, A. A.; Jamieson, A. Marine Fish May Be Biochemically Constrained from Inhabiting the Deepest Ocean Depths. *Proc. Natl. Acad. Sci. U.S.A.* **2014**, *111*, 4461–5.

[2] Yancey, P. H.; Blake, W. R.; Conley, J. Unusual organic osmolytes in deep-sea animals: adaptations to hydrostatic pressure and other perturbants. *Comp. Biochem. Physiol.* **2002**, *133*, 667–676.

[3] Yancey, P. H.; Fyfe-Johnson, A. L.; Kelly, R. H.; Walker, V. P.; Aun, M. T. Trimethylamine oxide counteracts effects of hydrostatic pressure on proteins of deep-sea teleosts. *J. Exp. Zool.* **2001**, *289*, 172–176.

[4] Smolin, N.; Voloshin, V. P.; Anikeenko, A. V.; Geiger, A.; Winter, R.; Medvedev, N. N. TMAO and urea in the hydration shell of the protein SNase. *Phys. Chem. Chem. Phys.* **2017**, *19*, 6345–6357.

[5] Cinar, H.; Fetahaj, Z.; Cinar, S.; Vernon, R. M.; Chan, H. S.; Winter, R. Temperature, Hydrostatic Pressure, and Osmolyte Effects on Liquid–Liquid Phase Separation in Protein Condensates: Physical Chemistry and Biological Implications. *Chem. Eur. J.* **2019**, *25*, 13049–13069.

[6] Cinar, S.; Cinar, H.; Chan, H. S.; Winter, R. Pressure-Sensitive and Osmolyte-Modulated Liquid-Liquid Phase Separation of Eye-Lens γ-Crystallins. *J. Am. Chem. Soc.* **2019**, *141*, 7347–7354.

[7] Lin, T.-Y.; Timasheff, S. N. Why do some organisms use a urea-methylamine mixture as osmolyte? Thermodynamic compensation of urea and trimethylamine N-oxide interactions with protein. *Biochemistry* **1994**, *33*, 12695–12701.

[8] Courtenay, E. S.; Capp, M. W.; Anderson, C. F.; Record, M. T. Vapor Pressure Osmometry Studies of Osmolyte Protein Interactions: Implications for the Action of Osmoprotectants in Vivo and for the Interpretation of Osmotic Stress Experiments in Vitro. *Biochemistry* **2000**, *39*, 4455–4471.

[9] Auton, M.; Bolen, D. W.; Rösgen, J. Structural thermodynamics of protein preferential solvation: Osmolyte solvation of proteins, aminoacids, and peptides. *Proteins: Struct. Funct. Genet.* **2008**, *73*, 802–813.

[10] Hong, J.; Xiong, S. TMAO-Protein Preferential Interaction Profile Determines TMAO's Conditional In Vivo Compatibility. *Biophys. J.* **2016**, *111*, 1866 – 1875.

[11] Mondal, J.; Halverson, D.; Li, I. T. S.; Stirnemann, G.; Walker, G. C.; Berne, B. J. How osmolytes influence hydrophobic polymer conformations: A unified view from experiment and theory. *Proc. Natl. Acad. Sci. U.S.A.* **2015**, *112*, 9270–9275.

[12] Folberth, A.; Bharadwaj, S.; van der Vegt, N. F. A. Small-to-large length scale transition of TMAO interaction with hydrophobic solutes. *Phys. Chem. Chem. Phys.* **2022**, *24*, 2080–2087.

[13] Rodríguez-Ropero, F.; Rötzscher, P.; van der Vegt, N. F. A. Comparison of Different TMAO Force Fields and Their Impact on the Folding Equilibrium of a Hydrophobic Polymer. *J. Phys. Chem. B* **2016**, *120*, 8757–8767.

[14] Mukherjee, M.; Mondal, J. Unifying the Contrasting Mechanisms of Protein-Stabilizing Osmolytes. *J. Phys. Chem. B* **2020**, *124*, 6565–6574.

[15] Su, Z.; Ravindhran, G.; Dias, C. L. Effects of Trimethylamine-N-oxide (TMAO) on Hydrophobic and Charged Interactions. *J. Phys. Chem. B* **2018**, *122*, 5557–5566.

[16] Govrin, R.; Tcherner, S.; Obstbaum, T.; Sivan, U. Zwitterionic Osmolytes Resurrect Electrostatic Interactions Screened by Salt. *J. Am. Chem. Soc.* **2018**, *140*, 14206–14210.

[17] Su, Z.; Mahmoudinobar, F.; Dias, C. L. Effects of Trimethylamine-*N*-oxide on the Conformation of Peptides and its Implications for Proteins. *Phys. Rev. Lett.* **2017**, *119*, 108102.

[18] Borgohain, G.; Paul, S. Atomistic level understanding of the stabilization of protein Trp cage in denaturing and mixed osmolyte solutions. *Comput. Theor. Chem.* **2018**, *1131*, 78–89.

[19] Ganguly, P.; Boserman, P.; van der Vegt, N. F. A.; Shea, J.-E. Trimethylamine N-oxide Counteracts Urea Denaturation by Inhibiting Protein–Urea Preferential Interaction. *J. Am. Chem. Soc.* **2018**, *140*, 483–492.

[20] Ma, J.; Pazos, I. M.; Gai, F. Microscopic insights into the protein-stabilizing effect of trimethylamine N-oxide (TMAO). *Proc. Natl. Acad. Sci. U.S.A.* **2014**, *111*, 8476–8481.

[21] Folberth, A.; Polák, J.; Heyda, J.; van der Vegt, N. F. A. Pressure, Peptides, and a Piezolyte: Structural Analysis of the Effects of Pressure and Trimethylamine-N-oxide on the Peptide Solvation Shell. *J. Phys. Chem. B* **2020**, *124*, 6508–6519.

[22] Athawale, M. V.; Dordick, J. S.; Garde, S. Osmolyte Trimethylamine-N-Oxide Does Not Affect the Strength of Hydrophobic Interactions: Origin of Osmolyte Compatibility. *Biophys. J.* **2005**, *89*, 858 – 866.

[23] Sarma, R.; Paul, S. The effect of aqueous solutions of trimethylamine-N-oxide on pressure induced modifications of hydrophobic interactions. *J. Chem. Phys.* **2012**, *137*, 094502.

[24] Anand, G.; Jamadagni, S. N.; Garde, S.; Belfort, G. Self-Assembly of TMAO at Hydrophobic Interfaces and Its Effect on Protein Adsorption: Insights from Experiments and Simulations. *Langmuir* **2010**, *26*, 9695–9702.

[25] Folberth, A.; van der Vegt, N. F. A. Temperature induced change of TMAO effects on hydrophobic hydration. *J. Chem. Phys.* **2022**, *156*, 184501.

[26] Nayar, D.; van der Vegt, N. F. A. Cosolvent Effects on Polymer Hydration Drive Hydrophobic Collapse. *J. Phys. Chem. B* **2018**, *122*, 3587–3595.

[27] Rani, A.; Jayaraj, A.; Jayaram, B.; Pannuru, V. Trimethylamine-N-oxide switches from stabilizing nature: A mechanistic outlook through experimental techniques and molecular dynamics simulation. *Sci. Rep.* **2016**, *6*, 1–14.

[28] Ganguly, P.; Bubák, D.; Polák, J.; Fagan, P.; Dracinsky, M.; van der Vegt, N. F. A.; Heyda, J.; Shea, J.-E. Cosolvent Exclusion Drives Protein Stability in TMAO and Betaine Solutions. **2022**, submitted.

[29] Kast, K. M.; Brickmann, J.; Kast, S. M.; Berry, R. S. Binary phases of aliphatic N-oxides and water: Force field development and molecular dynamics simulation. *J. Phys. Chem. A* **2003**, *107*, 5342–5351.

[30] Canchi, D. R.; Jayasimha, P.; Rau, D. C.; Makhatadze, G. I.; Garcia, A. E. Molecular mechanism for the preferential exclusion of TMAO from protein surfaces. *J. Phys. Chem. B* **2012**, *116*, 12095–12104.

[31] Schneck, E.; Horinek, D.; Netz, R. R. Insight into the molecular mechanisms of protein stabilizing osmolytes from global force-field variations. *J. Phys. Chem. B* **2013**, *117*, 8310–8321.

[32] Larini, L.; Shea, J. E. Double resolution model for studying TMAO/water effective interactions. *J. Phys. Chem. B* **2013**, *117*, 13268–13277.

[33] Imoto, S.; Forbert, H.; Marx, D. Water structure and solvation of osmolytes at high hydrostatic pressure: pure water and TMAO solutions at 10 kbar versus 1 bar. *Phys. Chem. Chem. Phys.* **2015**, *17*, 24224–24237.

[34] Hölzl, C.; Kibies, P.; Imoto, S.; Frach, R.; Suladze, S.; Winter, R.; Marx, D.; Horinek, D.; Kast, S. M. Design principles for high-pressure force fields: Aqueous TMAO solutions from ambient to kilobar pressures. *J. Chem. Phys.* **2016**, *144*, 1–4.

[35] Imoto, S.; Kibies, P.; Rosin, C.; Winter, R.; Kast, S. M.; Marx, D. Toward Extreme Biophysics: Deciphering the Infrared Response of Biomolecular Solutions at High Pressures. *Angew. Chem. Int. Ed.* **2016**, *55*, 9534–9538.

[36] Imoto, S.; Forbert, H.; Marx, D. Aqueous TMAO solutions as seen by theoretical THz spectroscopy: hydrophilic versus hydrophobic water. *Phys. Chem. Chem. Phys.* **2018**, *20*, 6146–6158.

[37] Abascal, J. L. F.; Vega, C. A general purpose model for the condensed phases of water: TIP4P/2005. *J. Chem. Phys.* **2005**, *123*, 234505.

[38] Best, R. B.; Mittal, J. Protein Simulations with an Optimized Water Model: Cooperative Helix Formation and Temperature-Induced Unfolded State Collapse. *J. Phys. Chem. B* **2010**, *114*, 14916–14923.

[39] Berendsen, H. J.; van der Spoel, D.; van Drunen, R. GROMACS: A message-passing parallel molecular dynamics implementation. *Comput. Phys. Commun.* **1995**, *91*, 43–56.

[40] Abraham, M. J.; Murtola, T.; Schulz, R.; Páll, S.; Smith, J. C.; Hess, B.; Lindah, E. Gromacs: High performance molecular simulations through multi-level parallelism from laptops to supercomputers. *SoftwareX* **2015**, *1-2*, 19–25.

[41] Hess, B. P-LINCS: A parallel linear constraint solver for molecular simulation. *J. Chem. Theory Comput.* **2008**, *4*, 116–122.

[42] Darden, T.; York, D.; Pedersen, L. Particle mesh Ewald: An N·log(N) method for Ewald sums in large systems. *J. Chem. Phys.* **1993**, *98*, 10089–10092.

[43] Berendsen, H. J.; Postma, J. P.; Van Gunsteren, W. F.; DiNola, A.; Haak, J. R. Molecular dynamics with coupling to an external bath. *J. Chem. Phys.* **1984**, *81*, 3684–3690.

[44] Nosé, S. A molecular dynamics method for simulations in the canonical ensemble. *Mol. Phys.* **1984**, *52*, 255–268.

[45] Parrinello, M.; Rahman, A. Polymorphic transitions in single crystals: A new molecular dynamics method. *J. Appl. Phys.* **1981**, *52*, 7182–7190.

[46] Paschek, D.; Hempel, S.; García, A. E. Computing the stability diagram of the Trp-cage miniprotein. *Proc. Natl. Acad. Sci. U.S.A.* **2008**, *105*, 17754–17759.

[47] Day, R.; Paschek, D.; Garcia, A. E. Microsecond simulations of the folding/unfolding thermodynamics of the Trp-cage miniprotein. *Proteins: Struct. Funct. Genet.* **2010**, *78*, 1889–1899.

[48] Streicher, W. W.; Makhatadze, G. I. Unfolding Thermodynamics of Trp-Cage, a 20 Residue Miniprotein, Studied by Differential Scanning Calorimetry and Circular Dichroism Spectroscopy. *Biochemistry* **2007**, *46*, 2876–2880.

[49] Auton, M.; Bolen, D. W. Predicting the energetics of osmolyte-induced protein folding/unfolding. *Proc. Natl. Acad. Sci. U.S.A.* **2005**, *102*, 15065–15068.

[50] Auton, M.; Rösgen, J.; Sinev, M.; Holthauzen, L. M. F.; Bolen, D. W. Osmolyte effects on protein stability and solubility: A balancing act between backbone and side-chains. *Biophys. Chem.* **2011**, *159*, 90 – 99.

[51] Sarma, R.; Paul, S. Effect of trimethylamine-N-oxide on pressure-induced dissolution of hydrophobic solute. *J. Chem. Phys.* **2012**, *137*, 114503.

5 Supporting Information

5.1 Fraction folded of TrpCage

We have calculated the fraction folded of TrpCage at 1, 500, 1000 and 2000 bar pressure, in water and a 2 M TMAO mixture and in the temperature range between 280 and 460 K using REMD. The pressure effect is non-monotonic, while an increased temperature always decreased the fraction folded. TMAO increased the fraction folded across the whole pressure-temperature range.

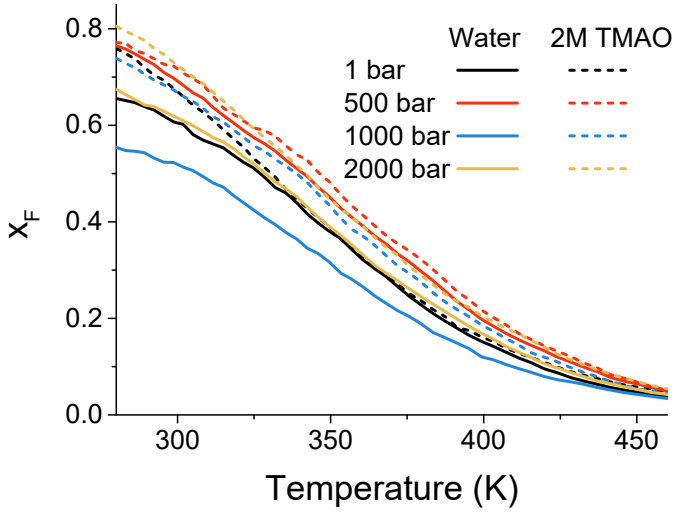

Figure 7.5: a) Fraction folded for the TrpCage molecule in water (solid lines) and 2 M TMAO (dashed lines) at 1, 500, 1000 and 2000 bar pressure. The pure water case is always shown as solid line, the 2 M TMAO case as dashed lines.

5.2 Preferential TMAO Binding

The preferential binding coefficient Γ_{23} of TMAO to the protein provides information about the TMAO distribution around the protein. $\Gamma_{23} > 0$ indicates TMAO accumulation and $\Gamma_{23} < 0$ indicates TMAO depletion. Γ_{23} can be split into different contributions Γ^i_{23}. Therefore, the solvent molecule which is proximal to group i is only counted in the calculation for group i

$$\Gamma^i_{23} = \left\langle n^i_3(r) - \frac{N_3 - n^i_3(r)}{N_1 - n^1_1(r)} n^i_1(r) \right\rangle$$

where $n^i_3(r)$ and $n^i_1(r)$ are the number of TMAO and water molecules in the proximal distance of group i. Solvent molecules are thereby only counted once to a certain group i. We present the preferential binding coefficient of TMAO to the protein at 1, 500, 1000 and 2000 bar pressure in Fig. 7.6. Pressure decreases the preferential binding coefficient.

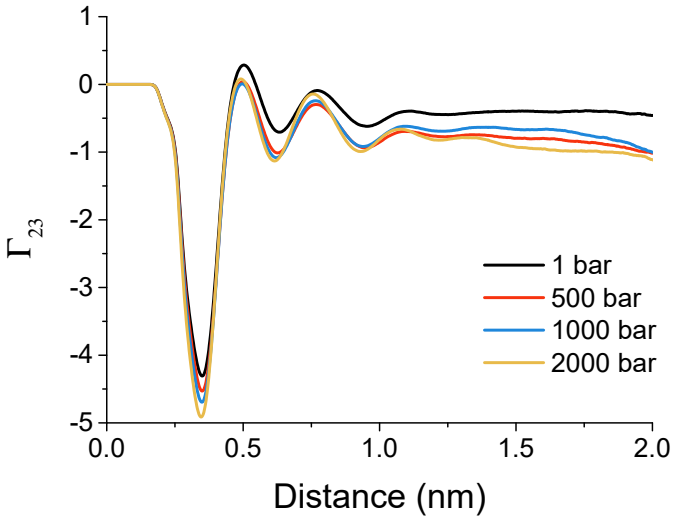

Figure 7.6: Preferential binding coefficient Γ_{23} for TMAO to TrpCage at 1, 500, 1000 and 2000 bar pressure.

5.3 Hydrophobic Interactions, Salt Bridges and Hydrogen Bonds

We have calculated the probability of the distance between the salt bridge forming residues in pure water and a 2 M TMAO mixture and at 1, 500, 1000 and 2000 bar pressure. Fig. 7.7 (a) shows the histogram of the salt bridge distance. It can be seen that TMAO always enhances the likelihood of the salt bridge. Similarly, it can be seen in Fig. 7.7 that TMAO always enhances the compactness of the hydrophobic core.

TMAO lowers the number of hydrogen bonds with the solvent (Fig. 7.8 (a), which the protein loses upon folding (Fig. 7.8 (b). Fig. 7.8 (c) shows that TMAO lowers the protein-solvent energies at 500 and 2000 bar (see the main text for other values). Thereby the loss of favorable protein-solvent energies upon folding is reduced (Fig. 7.8 (d) and therefore the protein folded state stabilized. At 2000 bar the effect is enhanced due to an increase in protein-solvent hydrogen bonds at high pressure.

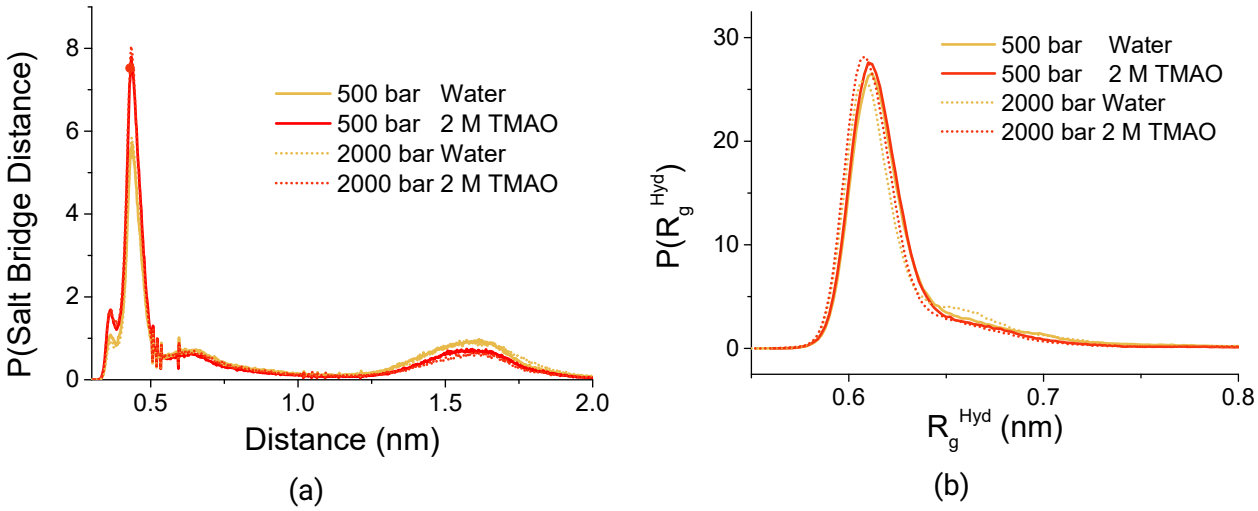

Figure 7.7: (a) Histograms of the salt bridge distance (COM of the carboxyl group of D9 and COM of the guanidinium group of R16). Lines at 500 and 2000 bar are overlapping. (b) Histogram of the radius of gyration of the hydrophobic groups of TrpCage at 500 and 2000 bar. TMAO enhances the probability of salt bridge formation, but pressure lowers it. The compactness of the hydrophobic core shown in (b) is increased in 2 M TMAO. It is decreased due to pressure, but TMAO enhances hydrophobic interactions in a way to compensate for the pressure effect.

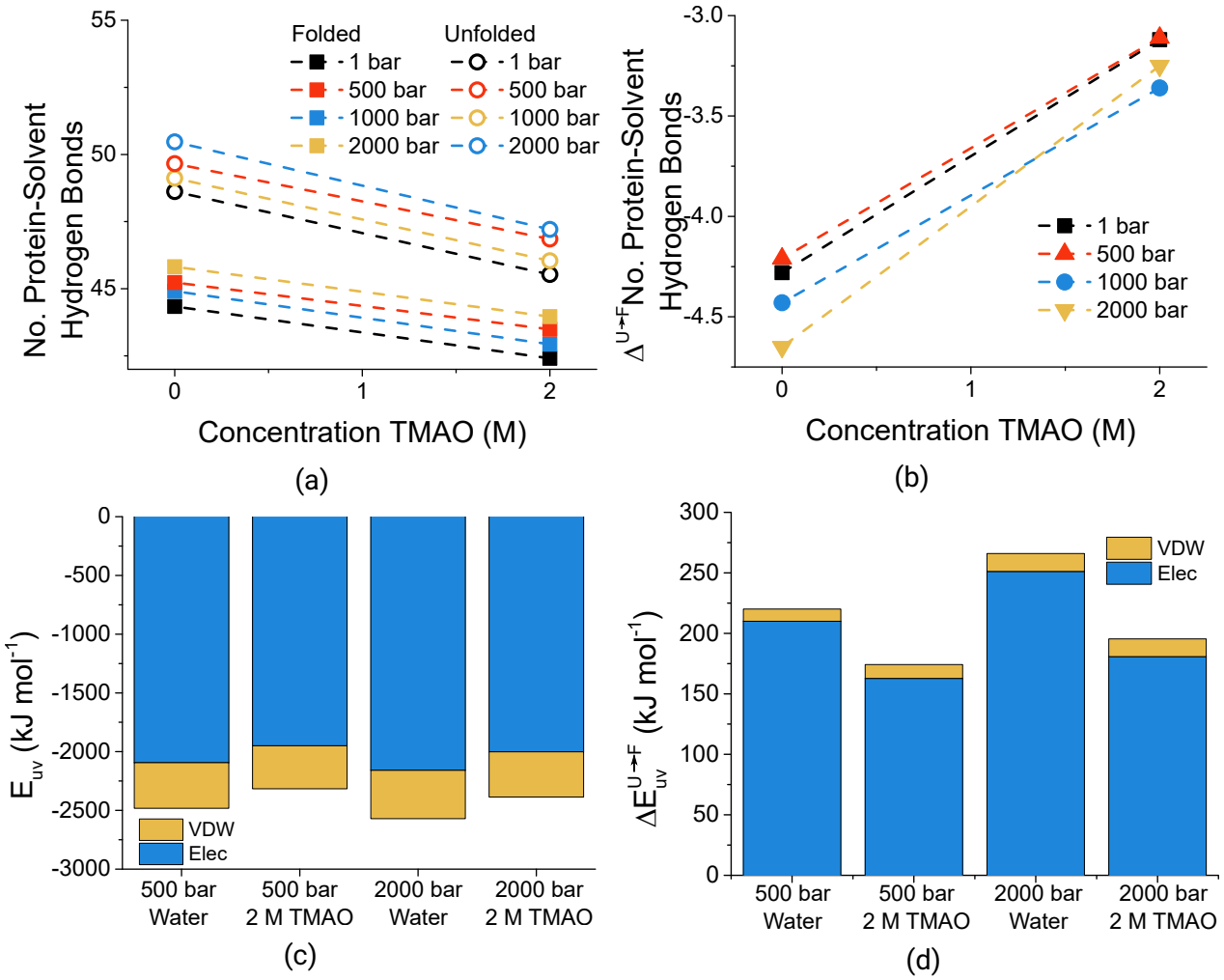

Figure 7.8: (a) The number of protein-solvent hydrogen bonds as a function of TMAO concentration for the protein folded and unfolded state (b) The change of the number of protein-solvent hydrogen bonds upon folding in water and 2 M TMAO at 500 and 2000 bar. (c) Average protein-solvent energy of TrpCage at different TMAO concentrations and a pressure of 500 and 2000 bar. (d) The difference in protein-solvent energy upon folding at different TMAO concentrations and at 500 and 2000 bar pressure. TMAO reduces he protein-solvent energy of TrpCage as seen in (b) and thereby stabilizes the folded state by reducing the unfavorable change upon folding as shown in (c). The change of electrostatic interactions can mainly be attributed by the reduced loss of protein-solvent hydrogen bonds in the TMAO mixture.

8 Conclusion

In the past years, studies on the influence of cosolutes on polymer collapse and protein folding have challenged the explanation that TMAO depletion is the only driving force for its ability to stabilize the protein folded state and polymer collapsed state and looked into more detailed explanations.[1–3] This also enhanced the understanding how other osmolytes can work similarly.[1,4,5] While TMAO is net depleted from proteins, its interactions with hydrophobic parts of the protein are not well understood. Computer simulations have helped to provide a deeper understanding of these effects by granting a molecular picture and the ability to freely manipulate the chemical structure and interactions of molecules in the computational model.

This work enhances the understanding of the interplay of TMAO effects and temperature, pressure and solute size on the association of apolar molecules. TMAO is depleted from the protein backbone due to unfavorable electrostatic interactions, but its interactions with hydrophobic groups has not been studied well. TMAO is an amphiphilic molecule and can interact uniquely with polar, charged and apolar solute groups with its different groups. Effects on either solute group may be influenced by the presence of others and therefore it is not trivial to discover driving forces in complex systems. Therefore, we have focused on apolar groups since hydrophobic interactions are important for phenomena like protein folding, liquid-liquid-phase separation and the collapse of thermoresponsive polymers. Due to the depletion from proteins and model predictions from scaled particle theory it has been assumed that TMAO is depleted from hydrophobic groups.[6,7] However, TMAO decreases the surface tension and therefore it has been proposed that it binds to hydrophobic surfaces.[8] This has lead to the assumption that TMAO decreases hydrophobic interactions.[2,9] Therefore, this thesis challenges the notion that TMAO only enhances solvent-mediated interactions through a depletion mechanism[7,10] and shows that the accumulation of TMAO to hydrophobic surfaces can enhance hydrophobic interactions. Studies on the effect of TMAO on hydrophobic interactions have been inconclusive and mainly pointed out that TMAO may diminish hydrophobic interactions due to its preferential binding.[2,11–14] One problem is the existance of many TMAO force fields, which are not able to capture all binary solvent properties well. Recently, a new force field has been proposed,[15] which is also used with the TIP4P/2005 water model.[16] This water model is known to be able to describe water properties very well and it has been shown that the combination of the new TMAO force field with the TIP4P/2005 water model is able to reproduce binary TMAO-water solvent properties well.[17]

First, it has to be assured that the effect of TMAO on protein solubility is correctly described in the simulations. We wanted to validate the TMAO force field, which has been repeatedly used in this study. We have found good agreement between our force field and experiments. Furthermore, we found that charged end groups of penta-peptides drive TMAO depletion and that TMAO is depleted from long chains, but is accumulated around small, uncharged chains. Despite its net depletion it locally accumulates around peptides independent of peptide chemistry and pressure. The presence of TMAO reduces the peptide-solvent hydrogen bonds. Since the protein unfolded state has a higher solvent accessible surface area, this should destabilise the unfolded protein state more than their folded state, driving protein folding.

Similar to the length scale dependence of TMAO preferential binding found in our previous study, hydrophobic hydration is length scale dependent. TMAO increases the density, but decreases the surface tension. This unusual effect on the solvent property can also affect the length scale transition, as the solvation of small repulsive solutes depends on the density, but that of large solutes depends on the surface tension. Therefore, TMAO preferential binding to repulsive and nonpolar surfaces has been discussed in the literature but studies remain divided. We found a length-scale transition, where TMAO is depleted from the small methane cavity surface, but preferentially binds to large polyalanine cavity surfaces via a surfactant-like mechanism. Furthermore, this surfactant-like mechanism enhances the solvent-mediated interactions of the WCA polyalanine helices. In nonpolar helices, where cohesive van der Waals interactions are present, the surfactant-like mechanism is opposed by favorable TMAO-solute interactions, which drive the dissociation of the helices. The hydrophobic association of the apolar α-helices is dominated by the surfactant-like mechanism at low TMAO concentrations. Enthalpic solute-solvent interactions overcompensate this effect at high TMAO concentrations, leading to a non-monotonic free energy of association between two nonpolar α-helices.

Similarly to the increase of the solute size, which decreases the tetrahedral order of water and thereby can leads to preferential cosolute binding,[18] temperature can decrease the tetrahedral order of the solvation shell. In a second study we investigated the joint effect of temperature and TMAO concentration on the hydrophobic hydration and hydrophobic interactions of small nonpolar molecules, namely methane. We observed that there is a temperature dependent change in TMAO-methane interactions. Methane is preferentially hydrated at low temperatures (TMAO depletion, descrease in solubility), but preferentially interacts with TMAO at high temperatures (increased solubility). TMAO enhances the solvent-excluded volume effect, decreasing the solubility. This is dominant at low temperatures. However, TMAO increases the solubility through favorable TMAO-methane van der Waals interactions. At high temperatures, these favorable interactions overcompensate the solvent-excluded volume effect, leading to an increase of the solubility in TMAO/water mixtures. TMAO strenghtens hydropobic interactions of methane at all temperatures and therefore switches from a depletion mechanism to an adsorption induced mechanism.

Then, we investigated the interplay of high pressure and TMAO concentration on the association

of the apolar helices and TMAOs ability to work as a piezolyte, a subgroup of protecting osmolytes, which are especially useful to counteract pressure denaturation of proteins. It has been discussed that TMAO may not have any piezolytic abilities different from other osmolytes.[19] Therefore, it is not clear why it is preferably used by deep sea creatures and whether it has a piezolytic effect for hydrophobic molecules. Pressure drives the dissociation of apolar helices due to the higher volume of the associated state. At high pressure, TMAO displays the same non-monotonic effect as at ambient pressure. The minimum is shifted towards higher TMAO concentrations and deepens compared to the minimum at ambient pressure, nearly compensating for the pressure effect on helix association. TMAO has an enhanced dipole moment at high pressure, leading to a higher water-coordination. The amplified stabilisation of the helix association at high pressure due to the presence of TMAO disappears if its dipole moment is not enhanced. Therefore, TMAOs piezolytic abilities stem from the enhanced dipole moment at high pressure and the resulting change in preferential binding.

Lastly, we studied the cumulative effect of TMAO and pressure on the folding equilibrium of TrpCage. TMAO is able to enhance the protein stability across the whole pressure-temperature plane. It increases the salt bridge and hydrophobic core stability of TrpCage, counteracting the pressure effect. Furthermore, it reduces the protein-solvent hydrogen bonds. As predicted with the penta-peptides, TMAO shifts the protein folding equilibrium towards the folded state due to this reduction of protein-solvent hydrogen bonds.

9 Outlook

We have found that TMAO can enhance hydrophobic interactions at ambient and high pressure and displays piezolytic features in the case of nonpolar solutes.

However, solvation properties are often not additive, so that surrounding groups of different functionality may change TMAO effects on hydrophobic groups.[20,21] Therefore, it may be beneficial to start introducing only one different kind of functional group (charged groups, polar groups capable of hydrogen bonding or apolar groups). Therefore, the additivity may be tested. This has been done in water with self-assembled monolayers (SAM), where 4 or 7 CH_3 groups have been substituted by OH groups with different patterns.[22] We are able to also analyze the effect of TMAO on other functional groups (which has been done, e.g. in the case of salt bridges modeled as the association of NaCl)[9] and then look at the influence of adding this functional group (e.g. a charged atom) on the already studied hydrophobic interactions (e.g. substituting some of the alanine residues with serine residues). This can also be studied in large protein systems, although the overlap of different effects may be difficult to dissect and may lead to wrong conclusions. The change in dipole moment can also be investigated with these systems and therefore it can be made sure that the piezolytic effect is also present for complex systems.

While we have investigated the effect of TMAO on the association of two molecules, it is not clear how TMAO influences the assembly of several big molecules. This is an important effect in liquid-liquid phase separation (LLPS).[23–25] Proteins, which show LLPS are usually intrinsically disordered proteins, those that do not have a ordered three-dimensional structure. The buried groups of the molecules are not well solvated and the preferential binding of TMAO can change due to this difference in the solvation shell compared to the solvation shell facing the bulk and also due to confinement effects. It has been proposed that TMAO can preferentially bind to different parts of proteins and thereby keep a protein core tight by binding to different hydrophobic patches of the protein.[8] Therefore, it would be interesting to see if the TMAO concentration inside such protein aggregates exceeds the bulk concentration. Additionally, pressure effects influence protein aggregates to a larger extend than the secondary structure of folded proteins. Thus, mechanisms may also vary compared to those discussed in this study. Molecular dynamics simulations can provide additional insight, extending the knowledge obtained from experiments, which is most often phenomenological. To model LLPS it would be necessary to look into big systems containing several proteins and large amounts of solvent. Currently we are not able to simulate LLPS to gain

insight into equilibrium properties. This will change in the next years since computers will become more powerful and provide the necessary tools.[26]

Lastly, mixtures containing several cosolutes may display non-additive effects as has been shown with ions.[27] This becomes important when we want to transfer our knowledge of cosolute effects to the phenomena happening in cells. Urea, a denaturant, is a cosolute that is often found in cells and has been discussed to counteract osmotic pressure in deep sea organism. It has been discussed that TMAO not only offsets the effect of pressure, but also the denaturing effect of urea.[28,29] Therefore, studies have focused on the coaction of TMAO and urea and have found that they mutually exclude each other from amino acids.[30] This can be extended to studies on the effect of TMAO and salts and even studies containing more cosolutes or variations in external stimuli like pressure and temperature. These examinations demand the correct description of not only protein-cosolute and cosolute-water interactions, but also interactions of different cosolutes. This can be done by tuning the force field parameters of the cosolute-cosolute interactions or by creation of new force fields which capture the empirical data of the mixtures.[31] This also points out a major flaw of computer simulations. Force fields are often parameterized in their aqueous mixtures. Therefore, water-protein and water-cosolute interactions are well described, but not those of the cosolute with the protein. The advantage of hydrophobic properties is that they largely depend on the equation of state of the solvent mixtures and therefore are less sensitive to the depiction of cosolute-solute interactions. In case of proteins, which also interact via coulombic interactions and therefore have more complex interactions with the solvent, it would be necessary to tune the protein-cosolute interactions. There exists only a handful of force field studies of ternary mixtures containing TMAO comparing the data to experiments and this should be further explored in the future.[14,32]

Although we have answered a lot of questions in this study, we have also brought up a few new ones, which have been partially mentioned above, but will be repeated for completeness:

1. The fluctuation entropy is a quantity which is far less studied than the cavity contribution or contributons from attractive interactions and also far less understood. Which part in the protein stabilisation does the fluctuation entropy play? We have seen that it is important in the methane solubility effect, but what about bigger systems?

2. The curvature of the solute can change the solvation free energy in water. What is the effect of solute curvature on the length-scale effect? When does the transition exactly occur?

3. The surfactant-like mechanism is important to understand the effect of TMAO on the association of big apolar solutes. How does the surfactant-like mechanism work with additional cosolutes? Does it disappear?

4. Does the surfactant-like mechanism play a role in protein folding, although TMAO is net depleted from proteins? Does TMAO preferentially bind to hydrophobic parts of the protein

and stabilise the folded state or LLPS through the same mechanism as it does the association of two hydrophobic molecules?

5. Transfer models are often used to predict the effect of cosolutes on the free energy of folding of large proteins. That is, experimentally transfer free energies of amino acids are determined and then weighted with their solvent accessible surface area to obtain the tranfer free energy of the protein folded and unfolded state. Are transfer models based on additive effects valid?

Bibliography

[1] Mondal, J.; Halverson, D.; Li, I. T.; Stirnemann, G.; Walker, G. C.; Berne, B. J. How osmolytes influence hydrophobic polymer conformations: A unified view from experiment and theory. *Proc. Natl. Acad. Sci. U.S.A.* **2015**, *112*, 9270–9275.

[2] Su, Z.; Mahmoudinobar, F.; Dias, C. L. Effects of Trimethylamine-*N*-oxide on the Conformation of Peptides and its Implications for Proteins. *Phys. Rev. Lett.* **2017**, *119*, 108102.

[3] Mukherjee, M.; Mondal, J. Unifying the Contrasting Mechanisms of Protein-Stabilizing Osmolytes. *J. Phys. Chem. B* **2020**, *124*, 6565–6574.

[4] Nayar, D.; Folberth, A.; van der Vegt, N. F. A. Molecular origin of urea driven hydrophobic polymer collapse and unfolding depending on side chain chemistry. *Phys. Chem. Chem. Phys.* **2017**, *19*, 18156–18161.

[5] Bharadwaj, S.; Nayar, D.; Dalgicdir, C.; van der Vegt, N. F. A cosolvent surfactant mechanism affects polymer collapse in miscible good solvents. *Comm. Chem.* **2020**, *3*, 1–7.

[6] Hong, J.; Xiong, S. TMAO-Protein Preferential Interaction Profile Determines TMAO's Conditional In Vivo Compatibility. *Biophys. J.* **2016**, *111*, 1866 – 1875.

[7] Cozzolino, S.; Oliva, R.; Graziano, G.; Del Vecchio, P. Counteraction of denaturant-induced protein unfolding is a general property of stabilizing agents. *Phys. Chem. Chem. Phys.* **2018**, *20*, 29389–29398.

[8] Liao, Y.-T.; Manson, A. C.; DeLyser, M. R.; Noid, W. G.; Cremer, P. S. Trimethylamine-N-oxide stabilizes proteins via a distinct mechanism compared with betaine and glycine. *Proc. Natl. Acad. Sci. U.S.A.* **2017**, *114*, 2479–2484.

[9] Su, Z.; Ravindhran, G.; Dias, C. L. Effects of Trimethylamine-N-oxide (TMAO) on Hydrophobic and Charged Interactions. *J. Phys. Chem. B* **2018**, *122*, 5557–5566.

[10] Auton, M.; Rösgen, J.; Sinev, M.; Holthauzen, L. M. F.; Bolen, D. W. Osmolyte effects on protein stability and solubility: a balancing act between backbone and side-chains. *Biophys. Chem.* **2011**, *159*, 90–99.

[11] Athawale, M. V.; Dordick, J. S.; Garde, S. Osmolyte Trimethylamine-N-Oxide Does Not Affect the Strength of Hydrophobic Interactions: Origin of Osmolyte Compatibility. *Biophys. J.* **2005**, *89*, 858–866.

[12] Sarma, R.; Paul, S. The effect of aqueous solutions of trimethylamine-N-oxide on pressure induced modifications of hydrophobic interactions. *J. Chem. Phys.* **2012**, *137*, 094502.

[13] Nayar, D.; van der Vegt, N. F. A. Cosolvent Effects on Polymer Hydration Drive Hydrophobic Collapse. *J. Phys. Chem. B* **2018**, *122*, 3587–3595.

[14] Rodríguez-Ropero, F.; Ro tzscher, P.; van der Vegt, N. F. Comparison of different TMAO force fields and their impact on the folding equilibrium of a hydrophobic polymer. *J. Phys. Chem. B* **2016**, *120*, 8757–8767.

[15] Hölzl, C.; Kibies, P.; Imoto, S.; Frach, R.; Suladze, S.; Winter, R.; Marx, D.; Horinek, D.; Kast, S. M. Design principles for high–pressure force fields: Aqueous TMAO solutions from ambient to kilobar pressures. *J. Chem. Phys.* **2016**, *144*, 144104.

[16] Abascal, J. L. F.; Vega, C. A general purpose model for the condensed phases of water: TIP4P/2005. *J. Chem. Phys.* **2005**, *123*, 234505.

[17] Markthaler, D.; Zeman, J.; Baz, J.; Smiatek, J.; Hansen, N. Validation of Trimethylamine-N-oxide (TMAO) Force Fields Based on Thermophysical Properties of Aqueous TMAO Solutions. *J. Phys. Chem. B* **2017**, *121*, 10674–10688.

[18] Rogers, B. A.; Okur, H. I.; Yan, C.; Yang, T.; Heyda, J.; Cremer, P. S. Weakly hydrated anions bind to polymers but not monomers in aqueous solutions. *Nat. Chem.* **2022**, *14*, 40–45.

[19] Papini, C. M.; Pandharipande, P. P.; Royer, C. A.; Makhatadze, G. I. Putting the Piezolyte Hypothesis under Pressure. *Biophys. J.* **2017**, *113*, 974–977.

[20] Hajari, T.; van der Vegt, N. F. A. Peptide Backbone Effect on Hydration Free Energies of Amino Acid Side Chains. *J. Phys. Chem. B* **2014**, *118*, 13162–13168.

[21] Ben-Naim, A. *Molecular Theory of Water and Aqueous Solutions*; World Scientific Publishing Company, 2011.

[22] Xi, E.; Venkateshwaran, V.; Li, L.; Rego, N.; Patel, A. J.; Garde, S. Hydrophobicity of proteins and nanostructured solutes is governed by topographical and chemical context. *Proc. Natl. Acad. Sci. U.S.A.* **2017**, *114*, 13345–13350.

[23] Cinar, H.; Fetahaj, Z.; Cinar, S.; Vernon, R. M.; Chan, H. S.; Winter, R. H. A. Temperature, Hydrostatic Pressure, and Osmolyte Effects on Liquid–Liquid Phase Separation in Protein Condensates: Physical Chemistry and Biological Implications. *Chem. Eur. J.* **2019**, *25*, 13049–13069.

[24] Cinar, S.; Cinar, H.; Chan, H. S.; Winter, R. Pressure-sensitive and osmolyte-modulated liquid–liquid phase separation of eye-lens γ-crystallins. *J. Am. Chem. Soc.* **2019**, *141*, 7347–7354.

[25] Mozhaev, V. V.; Heremans, K.; Frank, J.; Masson, P.; Balny, C. High pressure effects on protein structure and function. *Proteins* **1996**, *24*, 81–91.

[26] Moore, F., Gordon Cramming more components onto integrated circuits. *Electronics* **1965**, *38*.

[27] Bruce, E. E.; Bui, P. T.; Rogers, B. A.; Cremer, P. S.; van der Vegt, N. F. A. Nonadditive Ion Effects Drive Both Collapse and Swelling of Thermoresponsive Polymers in Water. *J. Am. Chem. Soc.* **2019**, *141*, 6609–6616.

[28] Yancey, P. H.; Somero, G. N. Counteraction of urea destabilization of protein structure by methylamine osmoregulatory compounds of elasmobranch fishes. *Biochem. J.* **1979**, *183*, 317–323.

[29] Yancey, P. H.; Clark, M. E.; Hand, S. C.; Bowlus, R. D.; Somero, G. N. Living with Water Stress: Evolution of Osmolyte Systems. *Science* **1982**, *217*, 1214–1222.

[30] Ganguly, P.; Hajari, T.; Shea, J.-E.; van der Vegt, N. F. A. Mutual Exclusion of Urea and Trimethylamine N-Oxide from Amino Acids in Mixed Solvent Environment. *J. Phys. Chem. Lett.* **2015**, *6*, 581–585.

[31] Ganguly, P.; Polák, J.; van der Vegt, N. F. A.; Heyda, J.; Shea, J.-E. Protein Stability in TMAO and Mixed Urea–TMAO Solutions. *J. Phys. Chem. B* **2020**, *124*, 6181–6197.

[32] Schneck, E.; Horinek, D.; Netz, R. R. Insight into the Molecular Mechanisms of Protein Stabilizing Osmolytes from Global Force-Field Variations. *J. Phys. Chem. B* **2013**, *117*, 8310–8321.

Erklärung zum Eigenanteil an den Veröffentlichung

Im Folgenden ist aufgelistet, mit welchem Anteil ich an den Veröffentlichungen beteiligt war.

Mein Anteil an der folgenden Veröffentlichung beträgt 70%:
Folberth, A.; Polák; J. Heyda, J.; van der Vegt, N. F. A; Pressure, Peptides, and a Piezolyte: Structural Analysis of the Effects of Pressure and Trimethylamine-N-oxide on the Peptide Solvation Shell. J. Phys. Chem. B, **2020**, 124(30), 6508-6519.

Mein Anteil an der folgenden Veröffentlichung beträgt 85%:
Folberth, A.; Bharadwaj, S.; van der Vegt, N. F. A; Small-to-Large Length Scale Transition of TMAO Interaction with Hydrophobic Solutes. Phys. Chem. Chem. Phys., **2022**, 24, 2080–2087

Mein Anteil an der folgenden Veröffentlichung beträgt 100%:
Folberth, A.; van der Vegt, N. F. A; Temperature Induced Change of TMAO Effects On Hydrophobic Hydration. J. Chem. Phys., **2022**, 184501

Mein Anteil an der folgenden Veröffentlichung beträgt 100%:
Folberth, A.; van der Vegt, N. F. A; Influence of TMAO and Pressure on the Folding Equilibrium of TrpCage; submitted

Mein Anteil an der folgenden Veröffentlichung beträgt 100%:
Folberth, A.; van der Vegt, N. F. A; A unique piezolyte mechanism of TMAO: Hydrophobic interactions under extreme pressure conditions, submitted

Erklärung zur Begutachtung der Veröffentlichungen

Datum _____

Referent: Prof. Dr. Nico van der Vegt
Korreferent: Prof. Dr. Florian Müller-Plathe

Weder Referent (Prof. Dr. Nico van der Vegt) noch Korreferent (Prof. Dr. Florian Müller-Plathe) der vorliegenden kumulativen Doktorarbeit waren an der Begutachtung der nachfolgenden Veröffentlichungen beteiligt:

Folberth, A.; Polák; J. Heyda, J.; van der Vegt, N. F. A; Pressure, Peptides, and a Piezolyte: Structural Analysis of the Effects of Pressure and Trimethylamine-N-oxide on the Peptide Solvation Shell. J. Phys. Chem. B, **2020**, 124(30), 6508-6519.

Folberth, A.; Bharadwaj, S.; van der Vegt, N. F. A; Small-to-Large Length Scale Transition of TMAO Interaction with Hydrophobic Solutes. Phys. Chem. Chem. Phys., **2022**, 24, 2080–2087

Folberth, A.; van der Vegt, N. F. A; Temperature Induced Change of TMAO Effects On Hydrophobic Hydration. J. Chem. Phys., **2022**, 184501

Folberth, A.; van der Vegt, N. F. A; Influence of TMAO and Pressure on the Folding Equilibrium of TrpCage; submitted

Folberth, A.; van der Vegt, N. F. A; A unique piezolyte mechanism of TMAO: Hydrophobic interactions under extreme pressure conditions; submitted

Referent
Prof. Dr. Nico van der Vegt

Korreferent
Prof. Dr. Florian Müller-Plathe